SOIL STRUCTURE INTERACTION FOR SHRINK-SWELL SOILS

"A NEW DESIGN PROCEDURE FOR FOUNDATION SLABS ON SHRINK-SWELL SOILS"

A Dissertation

by

REMON I. ABDELMALAK

Submitted to the Office of Graduate Studies of
Texas A&M University
in partial fulfillment of the requirements for the degree of

DOCTOR OF PHILOSOPHY

December 2007

Major Subject: Civil Engineering

SOIL STRUCTURE INTERACTION FOR SHRINK-SWELL SOILS

"A NEW DESIGN PROCEDURE FOR FOUNDATION SLABS ON SHRINK-SWELL SOILS"

A Dissertation

by

REMON I. ABDELMALAK

Submitted to the Office of Graduate Studies of
Texas A&M University
in partial fulfillment of the requirements for the degree of

DOCTOR OF PHILOSOPHY

Approved by:

Chair of Committee,	Jean-Louis Briaud
Committee Members,	Millard Coody
	Giovanna Biscontin
	Joseph Bracci
Head of Department,	David Rosowsky

December 2007

Major Subject: Civil Engineering

ABSTRACT

Soil Structure Interaction for Shrink-Swell Soils
"A New Design Procedure for Foundation Slabs on Shrink-Swell Soils."
(December 2007)
Remon I. Abdelmalak, B.S., El-Minia University;
M.S., El-Minia University
Chair of Advisory Committee: Dr. Jean-Louis Briaud

Problems associated with shrink-swell soils are well known geotechnical problems that have been studied and researched by many geotechnical researchers for many decades. Potentially shrink-swell soils can be found almost anywhere in the world especially in the semi-arid regions of the tropical and temperate climate. Foundation slabs on grade on shrink-swell soils are one of the most efficient and inexpensive solutions for this kind of problematic soil. It is commonly used in residential foundations or any light weight structure on shrink-swell soils.

Many design methods have been established for this specific problem such as Building Research Advisory Board (BRAB), Wire Reinforcement Institute (WRI), Post-Tensioning Institute (PTI), and Australian Standards (AS 2870) design methods. This research investigates most of these methods, and then, proposes a moisture diffusion soil volume change model, a soil-weather interaction model, and a soil-structure interaction model.

The proposed moisture diffusion soil volume change model starts with proposing a new laboratory test to determine the coefficient of unsaturated diffusivity for intact soils. Then, it introduces the development of a cracked soil diffusion factor, provides a chart for it, and explains a large scale laboratory test that verifies the proposed moisture diffusion soil volume change model.

The proposed soil-weather interaction model uses the FAO 56-PM method to simulate a weightless cover performance for six cities in the US that suffer significantly

from shallow foundation problems on shrink-swell soils due to seasonal weather variations. These simulations provide more accurate weather site-specific parameters such as the range of surface suction variations. The proposed weather-site specific parameters will be input parameters to the soil structure models.

The proposed soil-structure interaction model uses Mitchell (1979) equations for moisture diffusion under covered soil to develop a new closed form solution for the soil mound shape under the foundation slab. Then, it presents a parametric study by carrying out several 2D finite elements plane strain simulations for plates resting on a semi-infinite elastic continuum and resting on different soil mounds. The parametric study outcomes are then presented in design charts that end with a new design procedure for foundation slabs on shrink-swell soils.

Finally, based on the developed weather-soil-structure interaction models, this research details two procedures of a proposed new design method for foundation slabs on grade on shrink-swell soils: a suction based design procedure and a water content based design procedure.

DEDICATION

To

My wife and best friend: Nagwa Gali

My sons and love: John and Anthony

My parents, my brother and my sister

ACKNOWLEDGEMENTS

I am deeply grateful to my Ph.D. committee chairman, Dr. Jean-Louis Briaud, for his invaluable guidance and continuous inspiration, support, and his constant confidence in me throughout the course of my stay at Texas A&M University. I am fortunate to have had the opportunity of learning from him, especially his enthusiastic pursuit of practical scientific research. I greatly appreciate his advice, encouragement, supervision, and financial support, which made the completion of this dissertation possible. I am indebted to my advisory committee members, Dr. Joseph Bracci, Dr. Giovanna Biscontin, and Dr. Millard Coody for their helpful suggestions, assistance, and encouragement.

I am also thankful to Dr. James D. Murff, Dr. J.N. Reddy, Dr. Hamn-Ching Chen, Dr. Paolo Gardoni, Dr. Jean-Louis Briaud, and Dr. Giovanna Biscontin for all that they have taught me during my Ph.D. course work which contributed to this dissertation.

I would like to express my sincere gratitude for all the support and assistance from many individuals who made this work possible; I would like to sincerely thank Xiong Zhang, Keunyoung Rhee, Namgyu Park, Mike Linger, and Anand Govindasamy.

Special thanks go to the Spencer J. Buchanan Chair for its sponsorship and continuous support to this research work.

TABLE OF CONTENTS

CHAPTER Page

CHAPTER Page

LIST OF FIGURES

FIGURE Page

FIGURE Page

FIGURE Page

FIGURE Page

FIGURE Page

FIGURE Page

LIST OF TABLES

TABLE Page

CHAPTER I

INTRODUCTION

1.1 Problem description

Soil engineers did not recognize problems associated with shrink-swell soils until 1930, the increasingly extensive use of concrete slab on ground construction, after 1940, have further increased the damage to structures caused by expansive soils. Since the last seven decades there was a world wide interest in expansive clay and shale.

Potentially shrink-swell soils can be found almost anywhere in the world specially in the semi-arid regions of the tropical and temperate climate zones, in countries such as Australia, Argentina, Canada, India, Iran, South Africa, Turkey, U.S.A. and many of other countries.

Foundation slabs on grade of shrink-swell soils is one of the most efficient and inexpensive solutions for this kind of problematic soils. It is commonly used in residential foundations or any light weight structure on shrink-swell soils.

Yet, modeling foundation slabs on shrink-swell soils is a complicated problem. Weather and vegetation constitutes an important portion of the problem's boundary conditions. Precipitation and evapotranspiration are accountable for infiltration to and water loses from the soil continuum around and underneath the slab. Moisture changes in the soil mass develop soil movements, which affect the conditions of the soil support under the foundation slab. Consequently, induced distortions and straining actions on the slab and the super-structure take place. Different weather-soil and soil-structure interaction models have been developed to simulate this problem. Many of those models end in a design procedure, yet research and development of new design methods addressing this problem continues.

The style and format of this dissertation follow the *Journal of Geotechnical and Geoenvironmental Engineering, ASCE.*

There are several design methods that address foundation slabs on shrink-swell soils such as: The BRAB (1968) (Building Research Advisory Board), Lytton slab design procedures (1970, 1972, and 1973), Walsh procedure (1974 and 1978), Fraser and Wardle (1975), Swinburne Method (1980), WRI Method (1981, 1996) (Wire Reinforcement Institute), The Post-Tensioning Institute (PTI) design method (1996, 2004), and Australian Standard AS 2870 method (1990, 1996). The following methods are among the most common methods used to design foundation slabs on shrink-swell soils: 1) BRAB Method (1968); 2) WRI Method (1980, 1996); 3) AS 2870 (1996), 4) PTI Method (1996, 2004).

1.2 Significance of the research

Expansive soils are found through out the United States and in almost all parts of the world. The influence of expansive soil damage on a local, regional, or national scale is considerable. Jones and Holtz (1973) estimated that the annual cost of expansive soil damage in the U.S. is $2.2 billion, which exceeds that caused by earthquakes, hurricanes, and flood combined in an average year. Krohn and Slosson (1980) estimated that the annual cost of expansive soil damage in the US to be $7.billion in 1980. Krohn and Slosson further estimated that damages to single-family and commercial buildings accounted for nearly one-third of the total amount of damage resulting from expansive soils. A damage survey conducted solely in Dallas County, Texas, identified 8,470 residential foundation failures in only one year (1974), 98% of which occurred in expansive soils (Wray, 1989). Huge loss caused by expansive soils and the awareness of the public to the damage caused by expansive soils pose great requirement for the research in the foundation on expansive soils.

1.3. Objective of study

Although there are several available design methods, most of consultant engineers still have some concerns with each of the aforementioned design methods. These concerns differ or conform from one design method to another. Generally, these concerns may be

regarding the following aspects: reliability, simplicity, soundness of scientific bases, practicality, deficiency of site specific parameters, deficiency of experimental verifications, ignorance of the role of some important factors such as soil cracks effects, and usage limitations. The design methods usage limitations may include: applicability limitations to certain regions outside the US, limitations to some design parameters' ranges, or to some types of construction methods. As a result, geotechnical practitioners resort to their own engineering sense to judge the outcomes of these methods; and, they still aspire having a design method that mostly covers their concerns efficiently.

This research shall firstly review the commonly used design methods, point out the scientific bases on which they rely, and compare beam depths as an intrinsic output parameter resulting from using these methods to approximate the range of discrepancy of the methods outcomes.

Then, the research shall focus on proposing a new method for the design of slabs on grade to be built on shrink-swell soils. The proposed method shouldn't be complicated and addresses the basic factors that influence the behavior of the soil and of the structure. The design process shall start by considering the weather tied to the city where the foundation is to be built, the soil parameter shall be obtained from a simple shrink-swell test, and then design charts will be used to obtain the slab cantilever length from which the maximum bending moment is calculated and the needed slab stiffness is obtained.

1.4 Outline of this dissertation

Chapter II summarizes procedures of the commonly used design methods for foundation slabs on grade of shrink-swell soils.

Chapter III discuses the implemented models in BRAB, WRI, PTI, and AS 2870 design methods. And presents a parametric study comparing beam depths resulted from different design methods and another parametric study examining the influence of Texas ASCE guidelines on the resulting beam depths using BRAB 1968 and WRI 1996.

Chapter IV explains the proposed moisture diffusion soil volume change model. First, it details the proposed new laboratory test to determine coefficient of unsaturated diffusivity for intact soils. Second, it introduces a the development of cracked soil diffusion factor, and provides a chart for it. Finally, this chapter explains a large scale laboratory test that verify the proposed moisture diffusion soil volume change model.

Chapter V explains using the FAO 56-PM method to simulate a weightless cover performance for six cities in US that suffer significantly from shallow foundation problems on shrink-swell soils due to seasonal weather variations. These simulations provide more accurate weather site-specific parameters of such as the range of surface suction variations. The proposed weather-site specific parameters will be input parameters to the soil structure models.

Chapter VI presents the development of the implemented soil-structure interaction model by using Mitchell (1979) equations for moisture diffusion under covered soil to develop a new closed form solution for the soil mound shape under the foundation slab. Then, it presents a parametric study by carrying out several 2D finite elements plane strain simulations for plates resting on a semi-infinite elastic continuum, and resting on different soil mounds. The parametric study outcomes are then presented in design charts that end with a new design procedure for foundation slabs on shrink-swell soils.

Chapter VII summarizes the main conclusions of this dissertation and details two procedures of the proposed new design method for foundations slabs on grade on shrink-swell soils; suction based design procedure, and water content based design procedure.

CHAPTER II

LITERATURE REVIEW OF DESIGN METHODS FOR FOUNDATIONS ON SHRINK-SWELL SOILS

2.1 Introduction

As mentioned before, there are several design methods that address foundation slabs on shrink-swell soils. These methods handle this complicated problem using different approaches, hypothesis, weather indices, soil parameters, and soil-structure idealizations. This chapter summarizes procedures of the most commonly used design methods for foundation slabs on grade of shrink-swell soils.

2.2 BRAB (1968)

The first BRAB (Building Research Advisory Board) study of slabs-on-ground, which dealt with structurally related problems dates back to 1955. A final report was published in September 1962. In 1968, a revised version of the 1962 report was published which incorporated further information developed through field studies particularly in shrink-swell soil areas. BRAB 1968 assumes a rectangular mound shape (i.e. the slab stiffness doesn't influence the unsupported distance) and introduces an empirical support index related to climatic rating and soil properties. The procedure can be summarized as follows:

1-Choose the climatic rating index (C_W) for continental United States map Fig.2.1.

2-Determinate the support index (C) using Fig.2.2.

3-The support index can be increased to a modified support index (C_m) or decreased to a reduced support index (C_r) according to the site soil condition and type.

4- Divide slabs of irregular shape into overlapping rectangles of length (L) and width (L').

5-Having a uniformly distributed superstructure load, determine the effective load for each rectangle dimension according to its aspect ratio.

6- Maximum bending moment, shearing force and differential deflection can be calculated from:

$$M_{\max} = \frac{wL^2L'(1-C)}{8},\ V_{\max} = \frac{wLL'(1-C)}{2},\ \text{and}\ \Delta_{\max} = \frac{wL^4L'(1-C)}{48EI} \qquad (2.1)$$

where; Δ is the deflection of the slab.

The required steel ratio for the corresponding design is then calculated by the 1963 ACI Code.

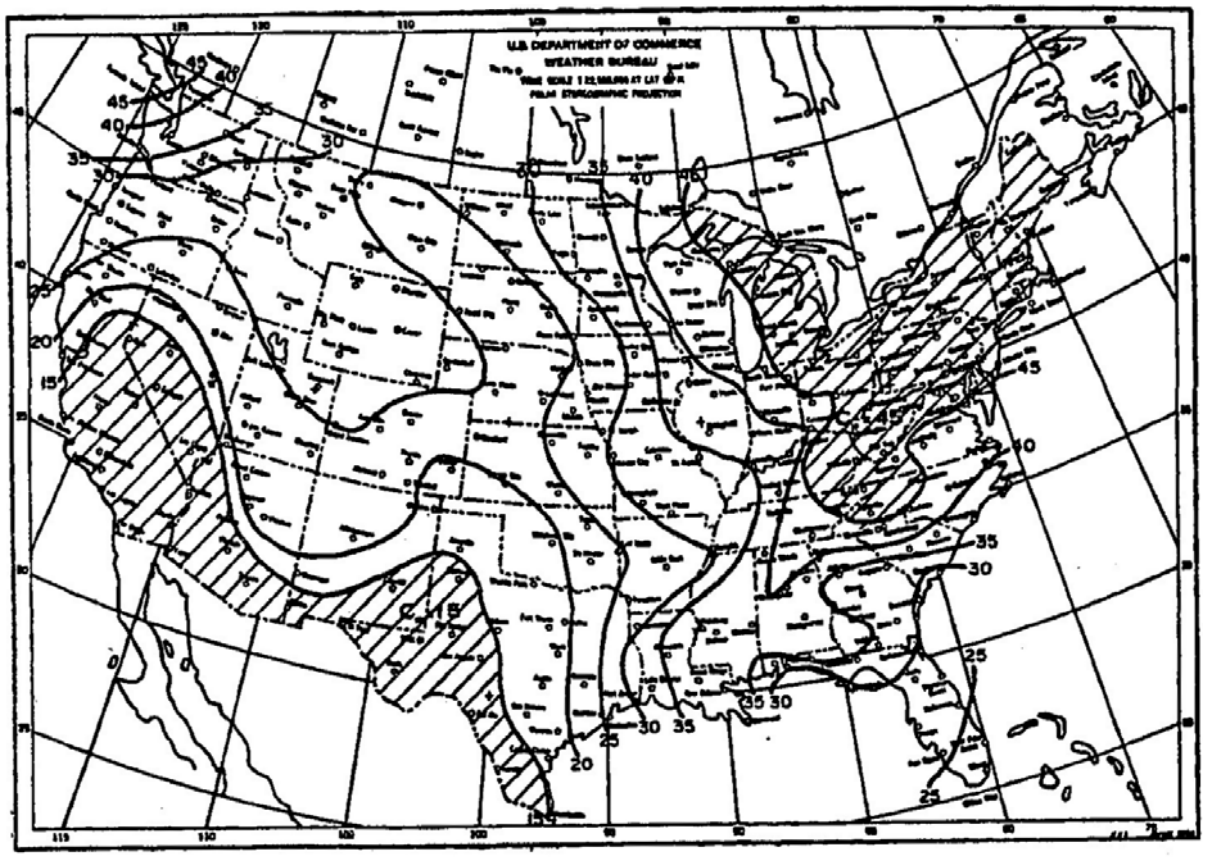

Fig. 2.1 Climate rating, C_w, for continental United States (After BRAB, 1968).

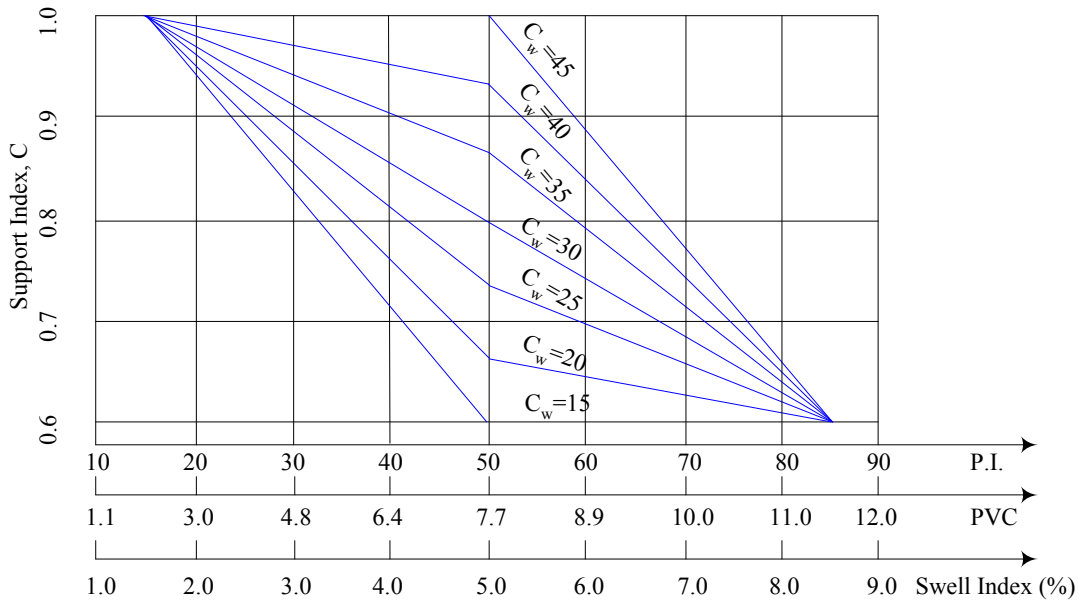

Fig. 2.2 Supporting index, C, based on criterion for soils sensitivity and climatic rating (After BRAB 1968).

2.3 Lytton (1970, 1972, 1973)

Lytton (1970) improved the rationality of the BRAB procedure by proposing elastic mathematical models of beam and slab on a curved mound. Lytton formulated the foundation soil for center lift analysis using the Winkler model and for edge lift analysis using the coupled spring model. The design quantities are then calculated. Lytton modified the general beam equation by including the effects of shearing resistance, which was represented by the couple springs, of the foundation soil. The differential equation, which was put forward to represent a beam on a coupled spring mound, is given by

$$\frac{d^2}{dx^2}\left(EI\frac{d^2w}{dx^2}\right)-\frac{d}{dx}\left(GhB\frac{d}{dx}(w-y)\right)+kB(w-y)=q \qquad (2.2)$$

where:

EI = beam flexural stiffness,

w = transverse deflection of the beam,

y = position of mound,

G = effective soil shear modulus,

h = effective depth within which soil shearing resistance is mobilized,

B = effective width within which soil support for the beam is mobilized,

k = effective subgrade modulus, and

q = distributed load on the beam.

A second equation for the case of an isotropic elastic plate, which includes the effects of the soil shearing resistance, on the same foundation type, is given by

$$D\nabla^4 w - \nabla\left(Gh.\nabla\left(w-y\right)\right) + k\left(w-y\right) = p \tag{2.3}$$

where:

D = flexural rigidity for the plate,

p = distributed load on the plate,

$\nabla = \frac{\partial}{\partial x} + \frac{\partial}{\partial y}$, $\nabla^4 = \frac{\partial^4}{\partial x^4} + 2\frac{\partial^4}{\partial x^2 y^2} + \frac{\partial^4}{\partial y^4}$ Laplace operators.

The shape of the curved mound was chosen fit experimentally determined or observed field shapes and was given in the form

$$y = \beta x^m \tag{2.4}$$

where:

m = the mound exponent,

β = a constant,

x = distance along the beam, and

y = distance below the highest point of the mound.

Lytton proposes that the beam equation can be applied to a slab when the slab is assumed to take a cylindrical deflection pattern, however, it is also pointed out that if two dimensional bending becomes the primary mode of distortion, then the assumption of the cylindrical deflection pattern is not valid. This differential equation applies only in the region where the beam is in contact with the soil, and a second equation, in which kB and GhB are put equal to zero, applies from the points not in contact with the soil. An

iterative process is required to locate these points. A rigid beam solution was also developed to determine maximum moment and shear envelopes. The main benefit gained from these studies is an appreciation of the relative importance of the different design variables and the rational mathematical models of soil-structure interaction.

Lytton (1972) proposed to use line loads around the perimeter and along the centerline of the slab and a uniformly distributed load and live load over the whole slab. The maximum moment is then calculated in each direction, assume both the soil and the slab to be rigid, and then reduced by a correction term to account for soil compressibility. In the case of center lift, the equation for the one-dimensional design moment, M_l in the direction L is given by

$$M_l = \frac{q_e LL'}{2} + \frac{L^2}{8}\left(2q_e + q_c + q_l L'\right) - c\frac{TL}{8} \tag{2.5}$$

where:

q_e = line load acting on the perimeter,

q_c = line load acting through the center of the building,

q_e = uniformly distributed load from dead and live loads,

T = total load on the rectangular,

c = support index,

and for the edge lift case

$$M_l = \frac{q_c LL'}{4} + \frac{L^2}{8}\left(2q_e + q_l L'\right) - c\frac{TL}{8} \tag{2.6}$$

In the case where the one- dimensional, design moment obtained from Eqs. 2.5 and 2.6 are adjusted for the two dimensional plate behavior for the long direction

$$M_L = M_l\left(1.4 - 0.4\frac{L}{L'}\right) \tag{2.7}$$

and for the short direction

$$M_S = M_l\left[1 + 0.9\left(1.2 - c\right)\left(\frac{L}{L'} - c\right)\right] \tag{2.8}$$

the design value for the shear force and deflection are estimated from

$$V = \frac{4M}{L}, \qquad w = \frac{ML^2}{12EI} \tag{2.9}$$

and V is the shear force and w is the deflection.

The support index presented by BRAB depends on experience and empirical consideration of observed site conditions; however Lytton proposed a support index, c, by using the rational analysis of the interaction between the expected swelling profile and the slab. The support index can be obtained from

$$c = \frac{m+1}{m+2}\left[\frac{m+1}{m}\frac{1}{ky_m}\frac{T}{A}\right]^{\frac{1}{m+1}} \tag{2.10}$$

where:

m = mound exponent,

A = slab area,

T = total load acting on the slab,

y_m = maximum differentional heave, and

k = Winkler subgrade modulus.

Lytton (1973) developed more precise methods of determining the differential soil movement, y_m, based on the thermodynamics of the soil moisture and the volume strain theory for swelling soils.

2.4 Walsh (1974, 1978)

Walsh (1974) proposed a design method which is essentially a combination of the BRAB (1968) and Lytton (1970) approaches, yet Walsh attempted to rationalize the determination of the support index. Walsh recommended dividing the foundation slab into overlapping rectangles, similarly to BRAB (1968), and each rectangle is analyzed in both directions assuming the simplified two-dimensional center and edge heave patterns. Walsh (1974) also assumes the dead and live load to be uniformly distributed over the whole slab area, but uses the beam on mound equation (Eq. 2.2) proposed by Lytton (1970) to determine the support index. Then, the design values of moment, shear, and

stiffness can be determined from equations identical to those proposed by BRAB (Eq. 2.1).

Walsh (1978) modified his earlier method by introducing a procedure for the determination of the stiffness constant, k. The mound is assumed to be consisting of a soft mound with stiffness, k_S, underlain by a hard mound with stiffness, k_H, A laboratory or field procedure is outlined to obtain swell pressure curves from which k_S can be determined. In addition, Walsh (1978) proposed a modification to the beam mound equation.

2.5. Fraser and Wardle (1975)

Fraser and Wardle (1975) modified the Lytton and Walsh approaches by using a three-dimensional semi-infinite elastic soil foundation model instead of a Winkler or coupled spring model. Their model was analyzed using the Commonwealth Scientific and Industrial Research Organization (SCIRO) FOCALS computer program as an interacting plate rather than the two-dimensional beams used by Lytton and Walsh. Their approach produced smaller sections than any of the previously described methods; however, they apparently had the same problem as the other methods, i.e. defining the mound shape and edge penetration distance.

Fraser and Wardle (1975) approach, finite element plate resting on a semi-infinite elastic soil, is a sophisticated approach to the problem. However, they stopped short of producing a general design procedure.

2.6 Swinburne (1980)

It was developed by Holland et al. (1980) from an exhaustive analysis of a modified version of Fraser and Wardle (1975) method and the observed behavior of experimental and housing slabs.

The Swinburne design method can be summarized as follows:

1- Divide the slab into overlapping rectangles.

2- Choose 28 day laboratory concrete compressive strength, $F_{c'}$, beam width, b (6 in < b < 16 in), and slab panel thickness, t (3 in < t < 6 in).

3- Select appropriate Δ/L ratio and beam spacing from Table 2.1.

Table 2.1. Allowable curvature deflection ratios (Δ/L) (After Holland et al. 1980).

Code	**Superstructure Type**	**Δ/L**
A	Stucco, Timber and Articulated Brick Veneer	1 in 250
B	Brick Veneer	1 in 500
C	Fully articulated Solid Brick	1 in 1000
D	Solid Brick	1 in 2000

4- Estimate edge distance, e, and mound differential heave, y_m from the following equations:

$$e = (S_F - S_L)^2 \quad \text{in feet} \qquad (2.11)$$

$$y_m = (S_F - S_L) \quad \text{in inches} \qquad (2.12)$$

where:

S_F = calculated potential vertical rise (PVR) in inches based on the free swell test starting with sample in dry condition.

S_L = calculated potential vertical rise (PVR) in inches based on the loaded swell test starting with sample in dry condition (sample allowed to swell under a load of 1000 psf)

5- Determine the moment from Fig. 2.3. Chart I

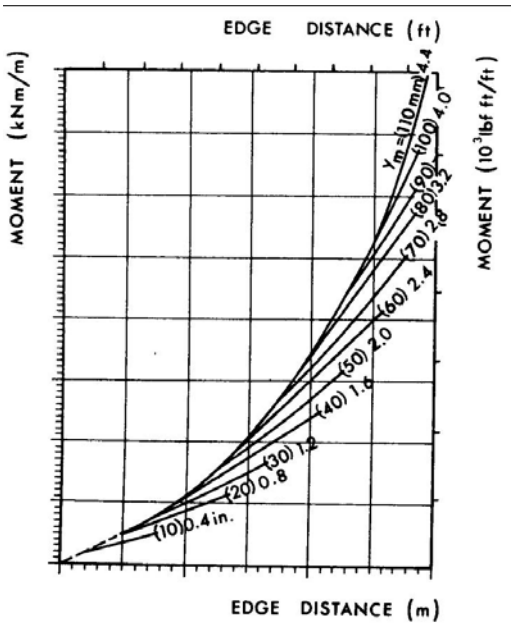

Chart I

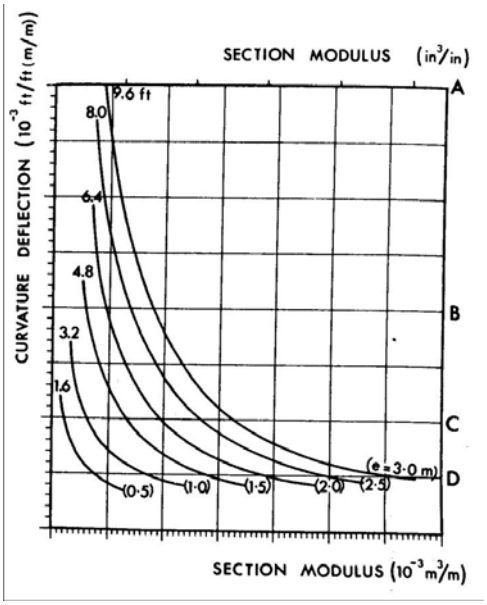

Chart II

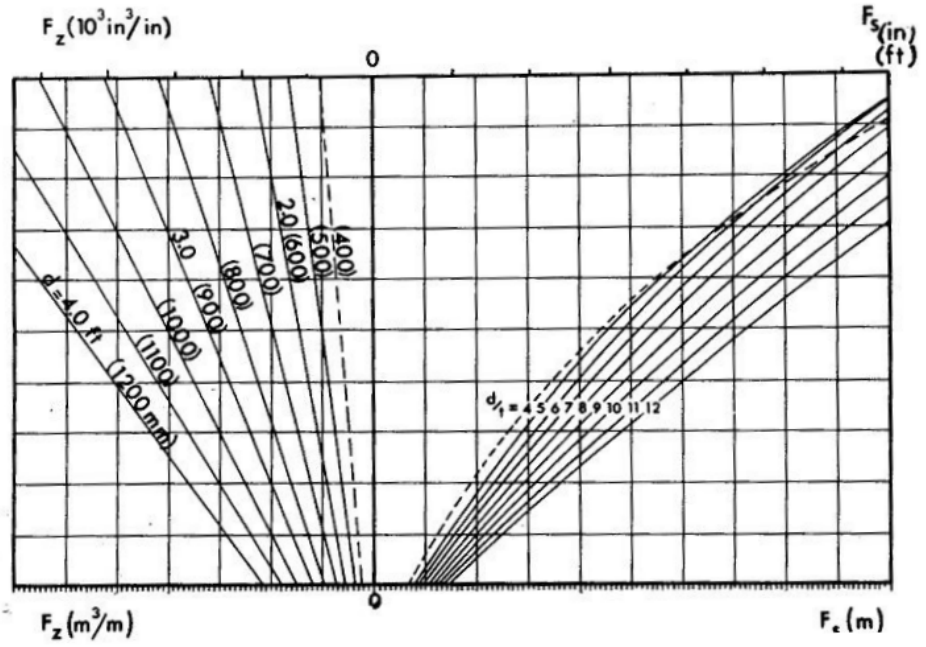

Chart III

Fig. 2.3. Swinburne design charts (After Holland et al. 1980).

6- Calculate the section modulus, Z, as:

$$Z = M / f_t \qquad (2.13)$$

where:

M = moment

f_t = concrete tensile strength

7- Determine actual Δ/L ratio from Fig. 2.3. Chart II. If Δ / L ratio exceeds the allowable Δ / L ratio (estimated in step 3), then increase Z accordingly.

8- Calculate the Width Factor, W, for each rectangle slab –assigned in step 1- as follows:

$$W = L / nb \qquad (2.14)$$

using the number of beams (n) crossing the rectangle dimension (L) –see Table 2.2. for beam spacing-where (b) is the beam width. Use the maximum value for the entire slab design.

9- Calculate factors F_Z and F_S as shown below:

$$F_Z = ZW/0.2 \qquad (in^3/in.) \qquad (2.15)$$

$$F_S = t\,(W-1)/0.2 \qquad (in.) \qquad (2.16)$$

10- Using factors F_Z and F_S values; determine beam depth, d, directly from Fig. 2.3. Chart III as follows:

a) Draw F_Z and F_S lines vertically from the F_Z and F_S axes respectively at the calculated values.
b) Mark the intersections of these lines with the graph lines.
c) Draw two lines (the upper and lower) to connect corresponding points of equal beam depth.
d) These two lines must converge from opposite sides of a horizontal line drawn through their intersection point to intersect the F_Z line at D
e) Calculate the beam depth from the equation shown with the illustration Fig. 2.4.

11- Proportion the steel reinforcing from Table 2.2.

Table 2.2. Recommended beam spacing and slab panel reinforcement (After Holland et al. 1980).

Edge Distance ft	Steel bar (rebar) slab		Post-Tensioned slab		Fiber Steel
	Steel $in^2/in.x10^{-3}$	Maximum internal Beam Spacing (ft)	Cable Spacing (ft)	Maximum internal Beam Spacing (ft)	Maximum internal Beam Spacing (ft)
e<1.5	7.4	No Internal Beams	6.6	No Internal Beams	Depends on the mix
1.5<e<3.0	9.7	20	6.0	26	
e>3.0	9.7	15	5.0	20	

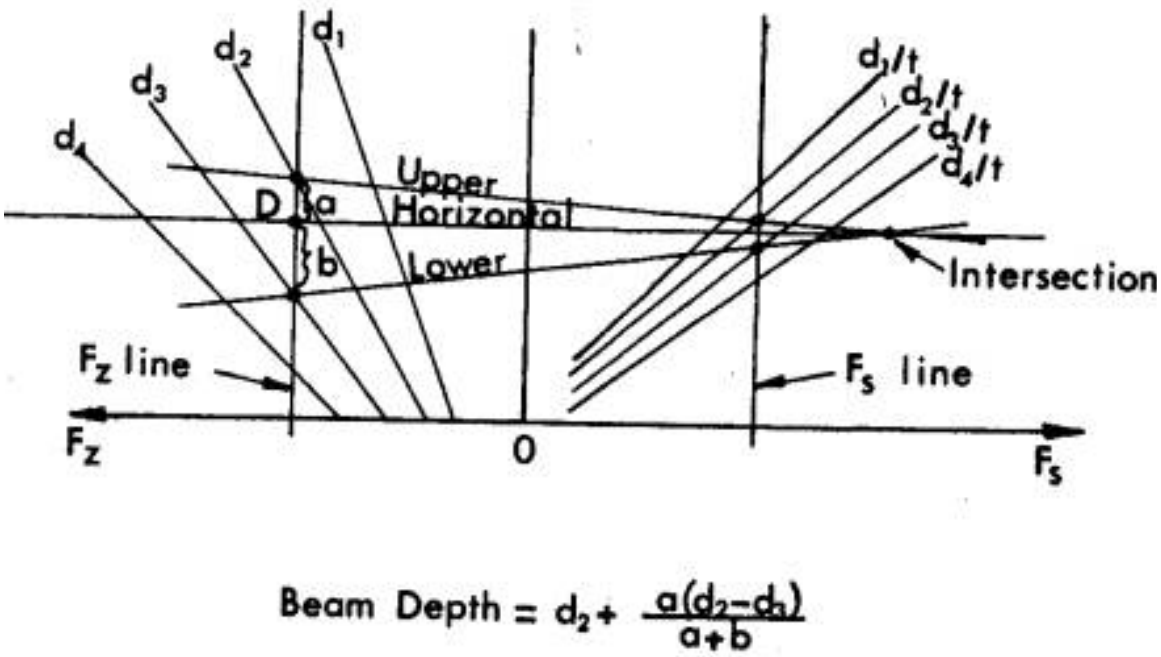

Fig. 2.4. Usage of Swinburne design chart III (After Holland et al. 1980).

12- If required beam depth is greater than about 30 inches, consideration should be given to reduce the edge distance value, e, and to redesign the slab using the new edge distance value.

The Swinburne design method is limited to a maximum slab length 100 feet, a maximum mound differential heave (y_m) of 5 in., 28 Day Laboratory Concrete Compressive Strength ($F_{c'}$) less than 3600 psi, and edge distance e<10 ft.

2.7 PTI (1996, 2004)

2.7.1 Post-tensioning institute -PTI-method (1996)

The Post-Tensioning Institute design method is based on research work by Wray (1978). This approach is based on analysis of a plate resting on a semi-infinite elastic continuum.

The PTI design method can be summarized as follows (PTI design manual 1996):

1- Determine Thornthwaite Moisture index, I_m, from US map Fig. 2.5.

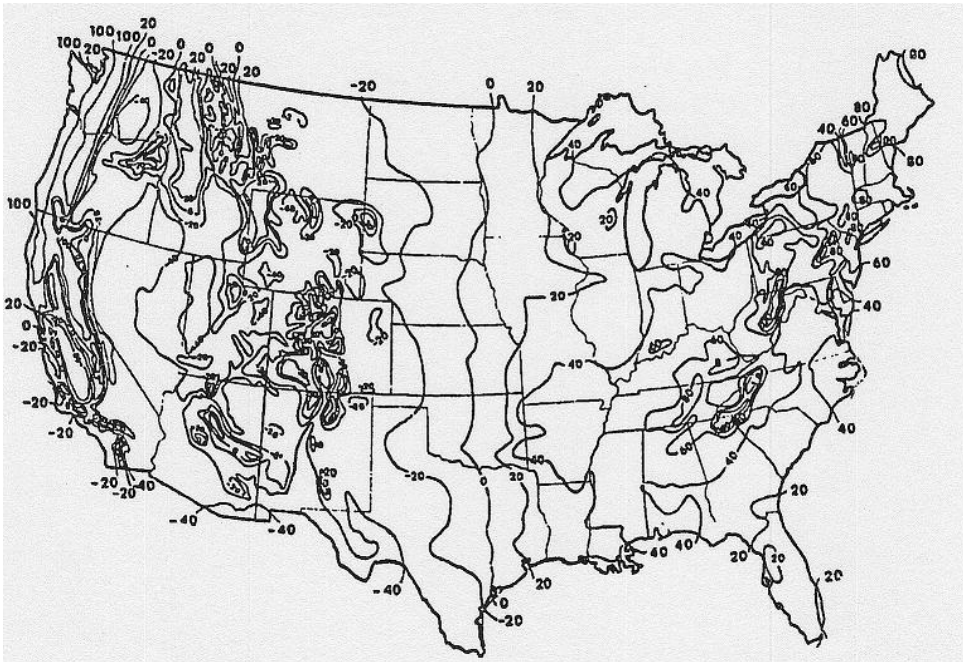

Fig. 2.5. Thornthwaite Moisture Index distribution in the United States (After Thornthwaite, 1948).

2- Consider the depth of active zone as the depth to constant ratio of water content-to-plastic limit (PL)

3-Use the Cation Exchange Activity "CEA_c" and the Activity Ratio, "A_c" to determine the predominant clay mineral using Fig. 2.6.

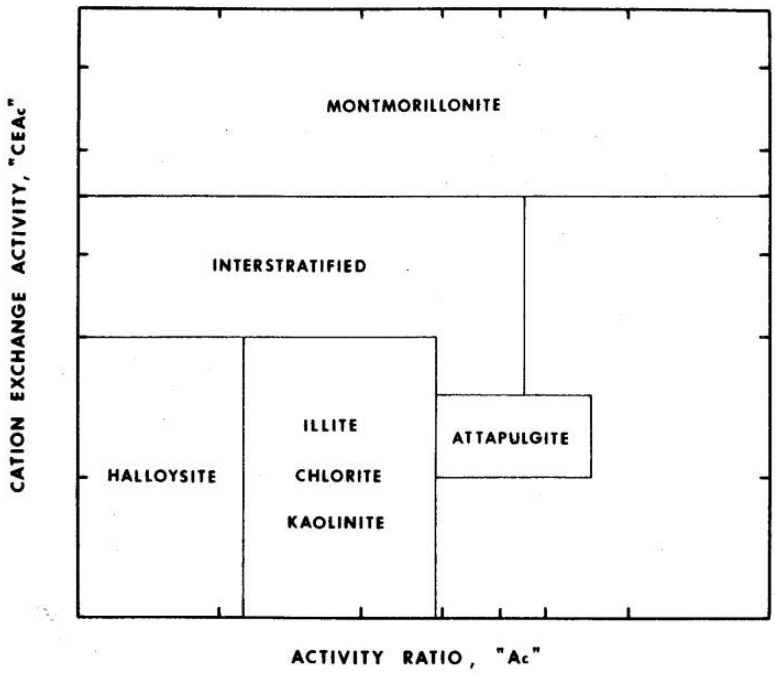

Fig. 2.6. Clay type classification to cation exchange and clay activity ratio (After PTI, 1996).

4- Using the Thornthwaite Moisture Index "I_m", determine the constant suction below depth of active zone using Fig.2.7 and to estimate moisture velocity (v) using the following equation:

v (in/month) = $I_m/24$ where I_m in (in/yr) and $0.5 \leq v \leq 0.7$

5- 4- Use the Thornthwaite Moisture Index "I_m" to determine the edge moisture penetration distance "e_m" using Fig. 2.8.

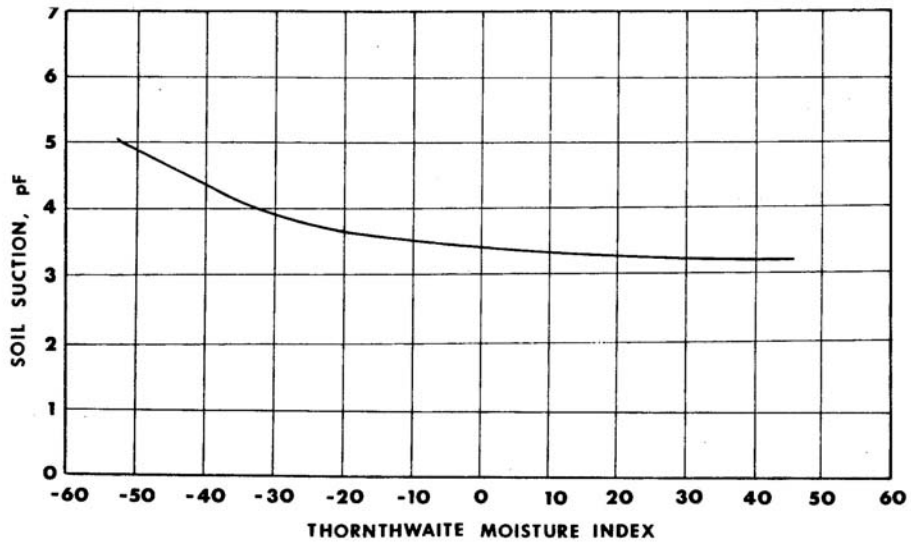

Fig. 2.7. Variation of constant soil suction with Thornthwaite Moisture Index (After PTI, 1996).

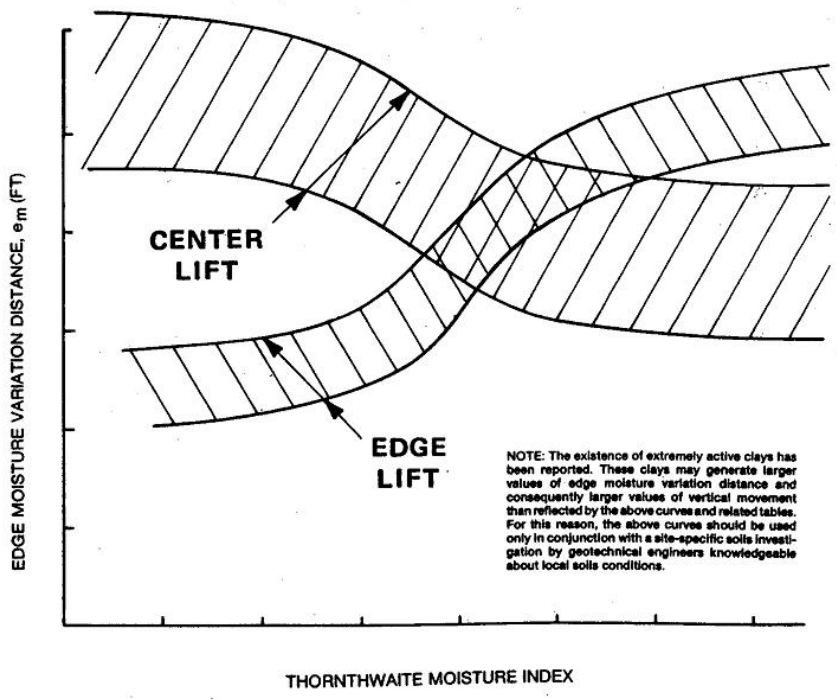

Fig. 2.8. Relationship between Thornthwaite Moisture Index and edge moisture variation distance (After PTI, 1996).

6- PTI manual provides several tables PTI (1996) pp.49-56 to estimate the expected vertical movement "y_m" for both center lift and edge lift cases using clay percent, the predominant clay mineral, depth of constant suction, velocity of moisture flow and the constant suction.

7- Divide the slab into overlapping rectangles.

8- Assume beams breadth and spacing.

9- Use PTI (1996) p.21 equations to estimate a trial beam depth.

10-Determine the trial section properties like the moment of inertia, section modulus, and cross sectional area of the slab and beams.

11-Go through calculating slab maximum applied design parameters such as moments, shears, and differential deflections in both directions utilizing e_m & y_m in design equations shown in PTI (1996) pp 22-24.

12- If the applied stresses and differential deflections is larger the permissible increase beam section and redo steps 8 through 11 until fulfilling the allowable stresses and differential deflections limits.

2.7.2 Post-tensioning institute -PTI-method (2004)

The PTI design method 2004 has significantly modified PTI 1996 procedures for e_m & y_m determination as follows:

1- Calculate the Plasticity Index (PI) = LL - PL

2- Calculate % fine clay (%fc) = (%-2μ / % -#200)*100

; Where (%-2μ) is percentage of soil passing No. 200 sieve expressed as a percentage of the total soil sample & (%-#200) is percentage of soil finer than 2 microns expressed as a percentage of the total soil sample

3- Determine Zone using the Mineral Classification Chart Fig. 2.9.

4- Calculate the Activity Ratio (PI / %fc)

5- Calculate LL / % fc

6- Determine γ_0 using the corresponding Zone Chart Fig. 2.10.

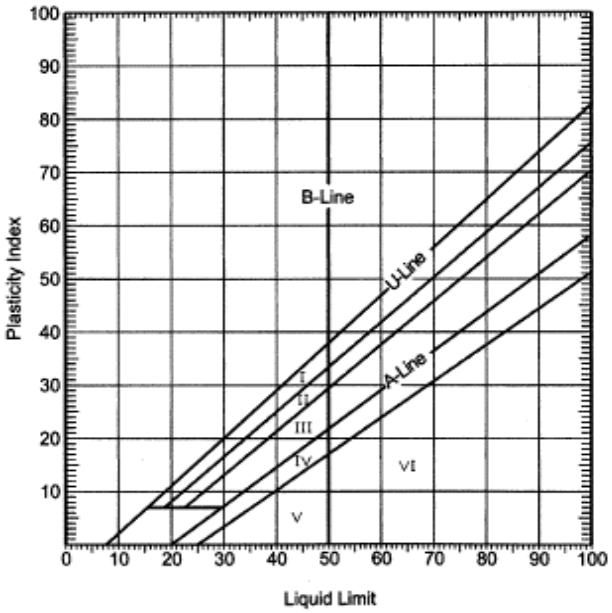

Fig. 2.9. Mineral classification chart (After PTI, 2004).

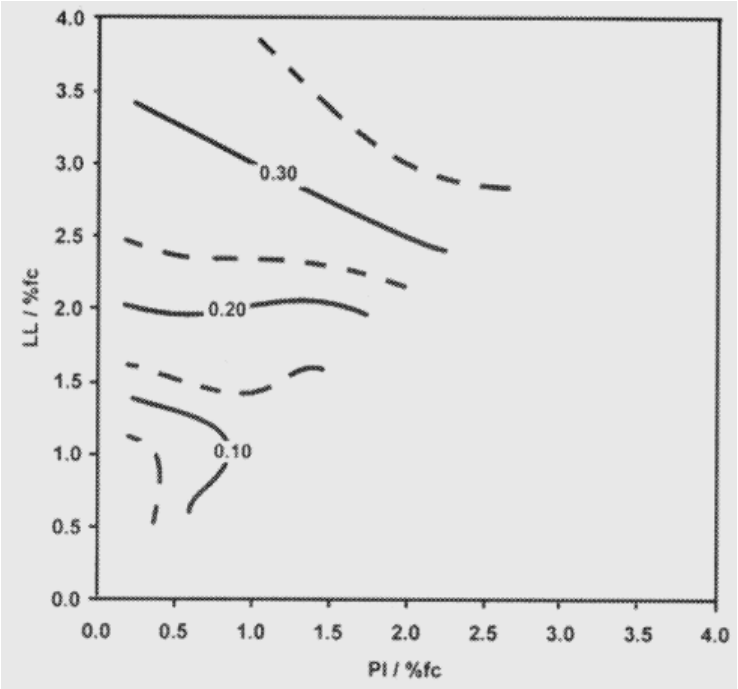

Fig. 2.10. Example γ_0 chart for Zone I (After PTI, 2004).

7- Calculate Suction Compression Index (γ_h)

$$\gamma_{h\ swell} = \gamma_0\, e^{\gamma 0}\ (\%\ fc/\ 100) \qquad (2.17)$$

$$\gamma_{h\ shrink} = \gamma_0\, e^{-\gamma 0}\ (\%\ fc/\ 100) \qquad (2.18)$$

PTI 2004 also suggests three alternative ways to determine ($\gamma_{h\ swell}$) using the expansion index (ASTM D 4829) procedure, consolidation-swell pressure test (ASTM d 4546 Method C) procedure, and overburden pressure swell test procedure. PTI 2004 gives empirical equations correlating the ($\gamma_{h\ swell}$) with indices resulting from these tests. In addition, PTI 2004 affords empirical correction equation of (γ_h) for soils have coarse - grained content.

8- Calculate Unsaturated Diffusion Coefficient (α):

$$\alpha = 0.0029 - 0.000162\ (S) - 0.0122\ (\gamma_h) \qquad (2.19)$$

where:

$$S = -20.29 + 0.1555\ (LL) - 0.117\ (PI) + 0.0684\ (\%\ -\#200) \qquad (2.20)$$

9- Calculate the Modified Unsaturated Diffusion Coefficient (α'):

$$\alpha' = \alpha\ F_f \qquad (2.21)$$

where:

F_f is the soil fabric factor that depends on soil profile content of roots, layers, fractures or joints: $F_f = 1.0$ (no more than 1 per vertical foot),

$F_f = 1.3$ (2 to 4 per vertical foot), and

$F_f = 1.4$ (5 or more per vertical foot).

10- Determine Thornthwaite Moisture index, I_m, from US map Fig. 2.5.

11- Determine e_m based on I_m for center and edge lift using Fig. 2.11.

12- Calculate the weighted (α'):

$$\alpha'_{weighted} = (\Sigma\ F_i\ x\ D_i\ x\ \alpha'_i\ ) / (\Sigma F_i\ x\ D_i\ ) \qquad (2.22)$$

where:

D is the layer thickness, and

F is the layer weight factor (for example, F=3 for the top layer in a three-layer active zone).

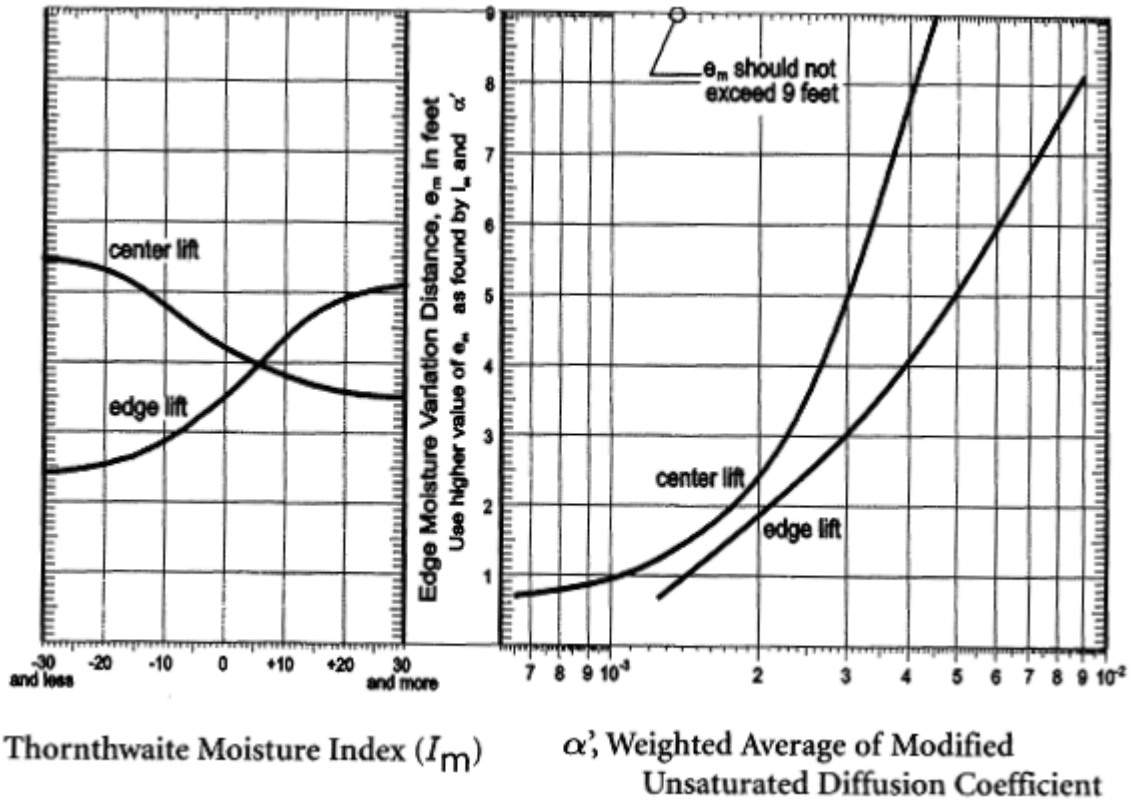

Fig. 2.11. e_m design chart (After PTI, 2004).

13- Determine e_m based on weighted (α') for center and edge lift using Fig. 2.11 and use maximum values of e_m obtained from this step and step 11.

14- Determine the Equilibrium Suction based on I_m using Fig. 2.12.

15- Determine the wet and dry suction profiles at the surface with the guidance of the PTI recommended values (2.5 pF the wettest if measured under soaking conditions, 4.5 pF the driest if the surface suction is controlled by vegetation, or 6.0 pF the driest if the surface suction is controlled by evaporation from bare soil)

16- Determine Stress Change Factors (SCF) for center and edge lift from (Table 3.2. in PTI 2004 manual).

17- Determine weighted Suction Compression Index ($\gamma_{h\ mod}$) in the same weighting manner as mentioned in step 12.

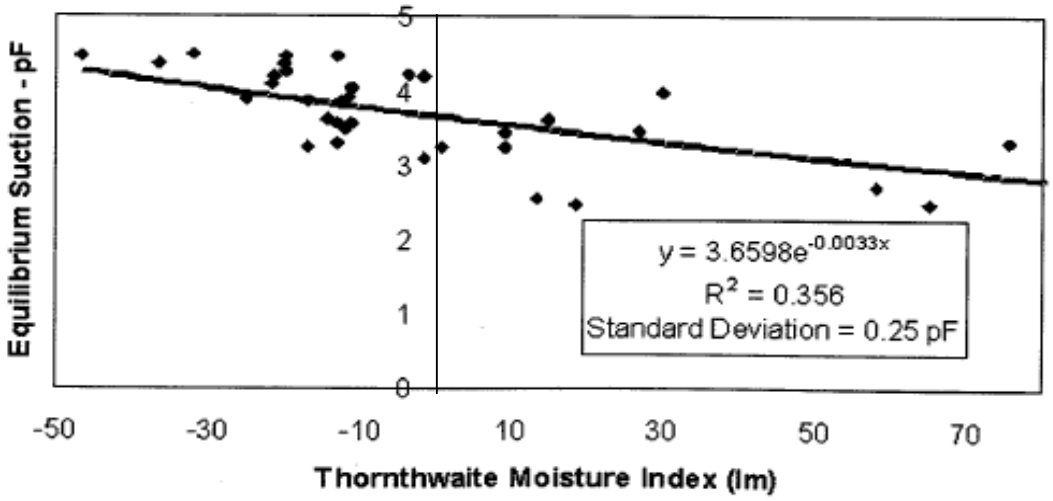

Fig. 2.12. Equilibrium suction design chart (After PTI, 2004).

18- Calculate y_m for center and edge lift as follows;

$$y_{m\ edge} = (SCF_{edge})\ (\gamma_{h\ swell\ mod}) \tag{2.23}$$

$$y_{m\ center} = (SCF_{center})\ (\gamma_{h\ shrink\ mod}) \tag{2.24}$$

Follow the same aforementioned structural design procedure of PTI (1996) (i.e. from step 7 to 12 in the previous section) to complete the design.

2.8 Australian Standard AS 2870 (1996)

The Australian Standards was prepared by Committee BD-025, Residential Slabs and Footings to supersede AS 2870.1-1988 and AS 2870.2-1990. It was approved on behalf of the Council of Standards Australia on April 12th, 1996 and published on June 5th, 1996. The AS 2870 design method can be summarized as follows:

1-Obtain the design movement, which is the characteristic movement (y_s), for site classification obtained by summing the movement for each layer as follows:

$$y_s = \frac{1}{100}\int_0^{H_s} I_{pt}\,\Delta u\,\Delta h \tag{2.25}$$

where:

H_s = depth of design suction change, AS 2870 introduces a map for different climatic zones in Australia and a table for H_s values for each zone Table 2.3.

I_{pt} = effective instability index, which is defined as the percent vertical strain per unit change in suction including allowance for lateral restraint and vertical load = α x I_{ps}

I_{ps} = shrinkage index or instability index without lateral restraint or loading of soil.

$\alpha = 1.0$ in the cracked zone (unrestrained)

$\alpha = 2.0 - z/5$ in the uncracked zone (restrained laterally by soil and vertically by soil weight)

z = the depth from the finished ground level to the point under consideration in the uncracked zone.

The depth of the cracked zone can be taken as 0.33 H_s to H_s.

Δu = suction change at depth (z) from the surface, expressed in pF units.

2- Classify the site by characteristic soil surface movement as follows Table 2.4

3- Knowing the site class and slab dimensions you can get beam depth, reinforcements, beam spacing, and slab mesh from AS 2870-1996 standard raft designs tables and figures pp 24-29

Table 2.3. Depth of design suction change for different climatic zones (After AS2870, 1996).

Climatic zone	Description	H_s
1	Alpine/ wet coastal	1.5 m
2	Wet temperate	1.8 m
3	Temperate	2.3 m
4	Dry temperate	3.0 m
5	Semi-arid	4.0 m

Table 2.4. Site classification by characteristic soil surface movement (After AS2870, 1996).

Surface movement	**Primary classification of site**
0 mm < $y_s \leq$ 20 mm	**S** – Slightly reactive clay sites with only slight ground movement from moisture changes
20 mm < $y_s \leq$ 40 mm	**M** – Moderately reactive clay or silt sites, which can experience moderate ground movement from moisture changes
40 mm < $y_s \leq$ 70 mm	**H** – Highly reactive clay or silt sites, which can experience high ground movement from moisture changes
y_s > 70 mm	**E** – Extremely reactive clay or silt sites, which can experience extreme ground movement from moisture changes

4- We can use also the following procedures using Fig. 2.13 since it is an empirically fitted line to the values of the y_s/Δ and $\log\{\sum\left(\frac{B_w D^3}{12}\right)/W\}$ for the standard designs.

- Choose appropriate value of the permissible differential movement corresponding to the type of construction from this Table 2.5.

- Calculate y_s/Δ, then find out the corresponding $\log\{\sum\left(\frac{B_w D^3}{12}\right)/W\}$ value

from the following Fig. 2.13

where:

$\log\{\sum\left(\frac{B_w D^3}{12}\right)/W\}$ is the stiffness parameter; the summation is determined over all the edge and internal beams

B_w is the beam web width (mm),

d is the overall depth of the beam (mm), and

W is the overall width of the slab in (m) normal to the direction of the beam spacing considered.

Table 2.5. Permissible differential movement values corresponding to the type of construction (After AS2870, 1996).

Type of construction	**Maximum differential footing movement Δ, mm**
Clad frame	40
Articulated masonry veneer	30
Masonry veneer	20
Articulated full masonry	15
Full masonry	10

-

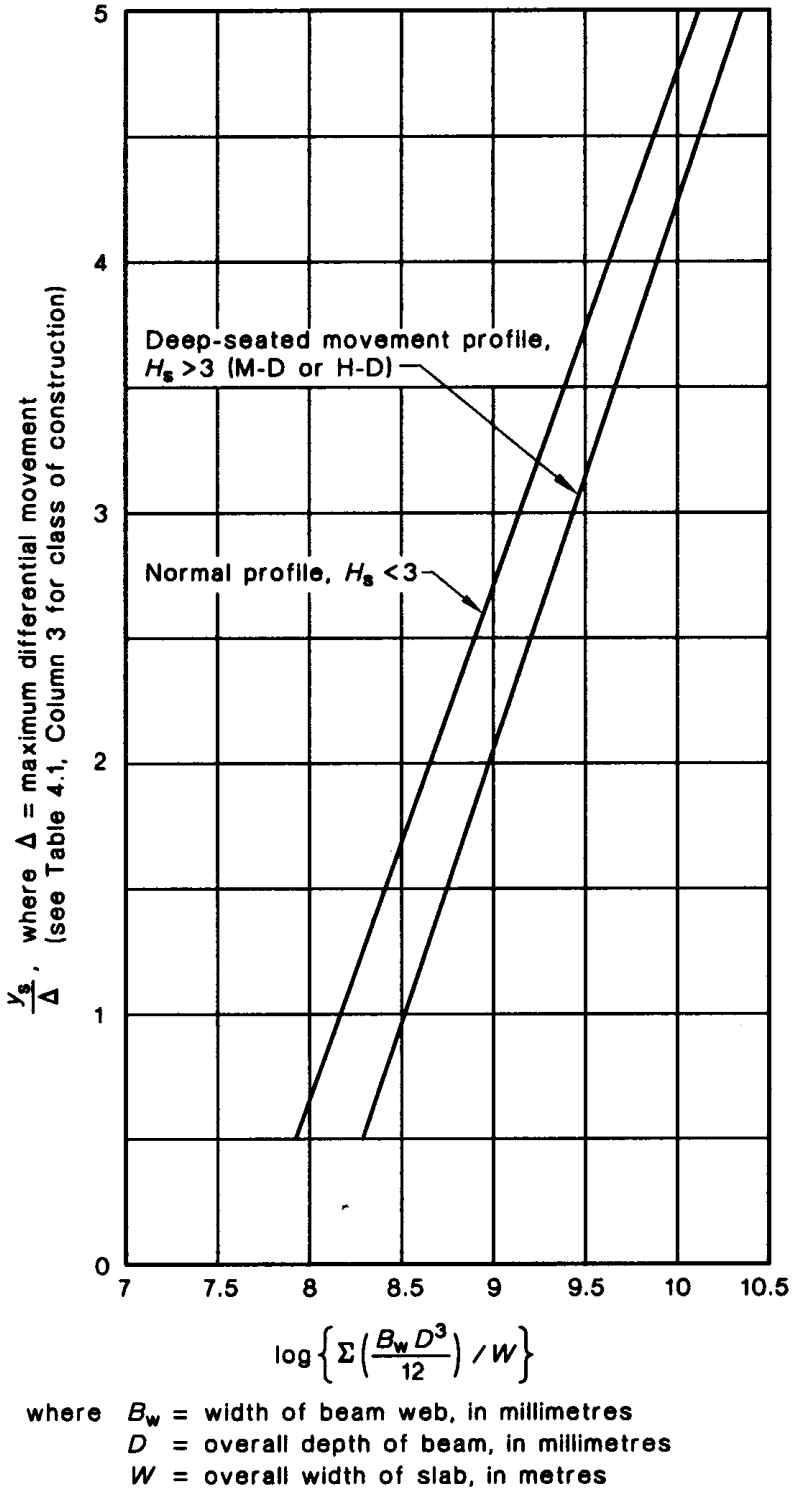

Fig. 2.13. Movement ratio versus unit stiffness.

Knowing $\log\{\sum\left(\frac{B_w D^3}{12}\right)/W\}$, B_w, and W we can get D

Also, AS 2870 – 1996 recommends a procedure, which is a computer analysis for actual loading pattern in accordance with the (Walsh and Walsh, 1986) or (Mitchell, 1984) methods that allow for an interaction of structure with some representation of the stiffness of the foundation and the assumed mound shape for calculating the structural moments.

2.9 WRI (1981, 1996)

WRI Method (1981, 1996) (Wire Reinforcement Institute) was developed by Walter L. Snowden, P.E., of Austin, Texas. It is empirically derived by observing slab performance and modifying equations to give results approximating the foundations that had been found to give satisfactory results. WRI uses the same approach as the BRAB method and can be considered as a modified version of BRAB.

The WRI design procedures can be summarized as follows:

1- Determine the effective plasticity index (Eff. PI) of the underlying 15 feet using weighting factors 3, 2, and 1 for the first, second, and third 5-feet-layer respectively.

2- Modify Eff. PI for natural ground slope and overconsolidation using the correction coefficients obtained from charts.

3- Divide slabs of irregular shape into overlapping rectangles of length (L) and width (L').

4- Choose the climatic rating index, C_W, the same as BRAB Fig.2.1.

5- From Fig.2.14, select the soil-climate support index, indicated as (1-C).

6- Determine beam spacing, S, using Fig.2.15.

7-Determine the cantilever length as soil function, l_c.

8- Determine length modification factors for long and short directions k_L &k_s respectively from Fig.2.16.

9- The modified cantilever lengths (L_c) in both directions will be $k_L\ l_c$ & $k_S\ l_c$

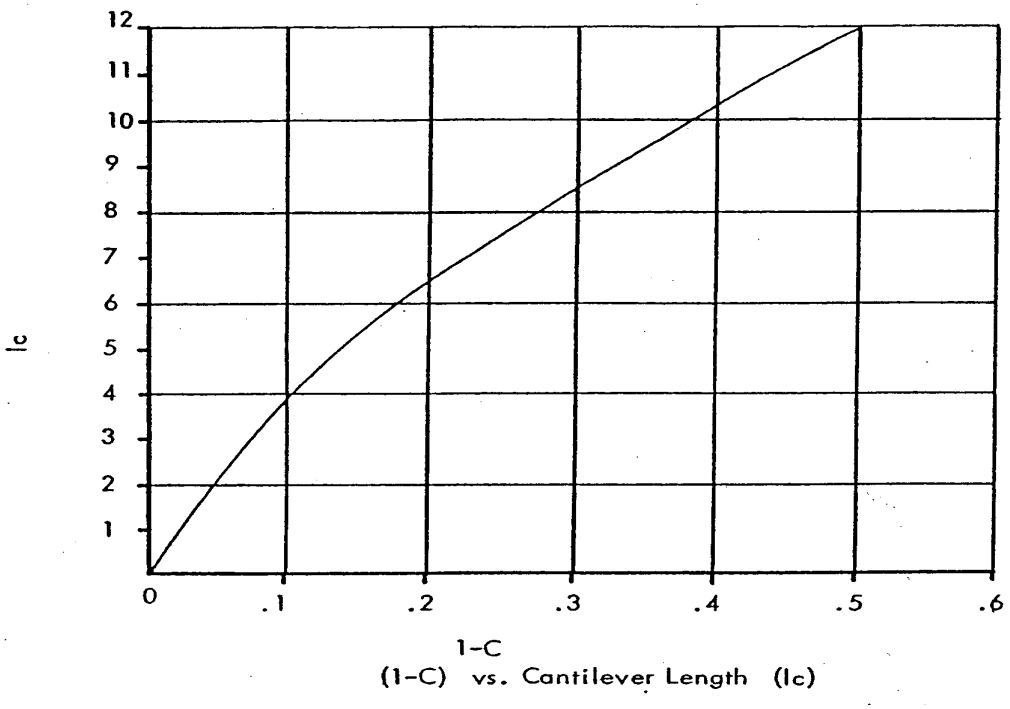

Fig.2.14. Cantilever length.

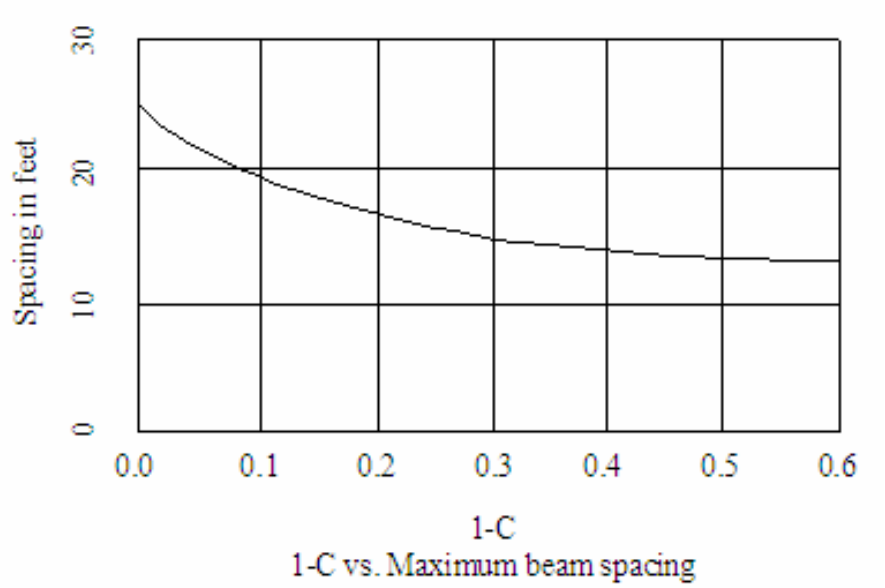

Fig.2.15. Beam spacing.

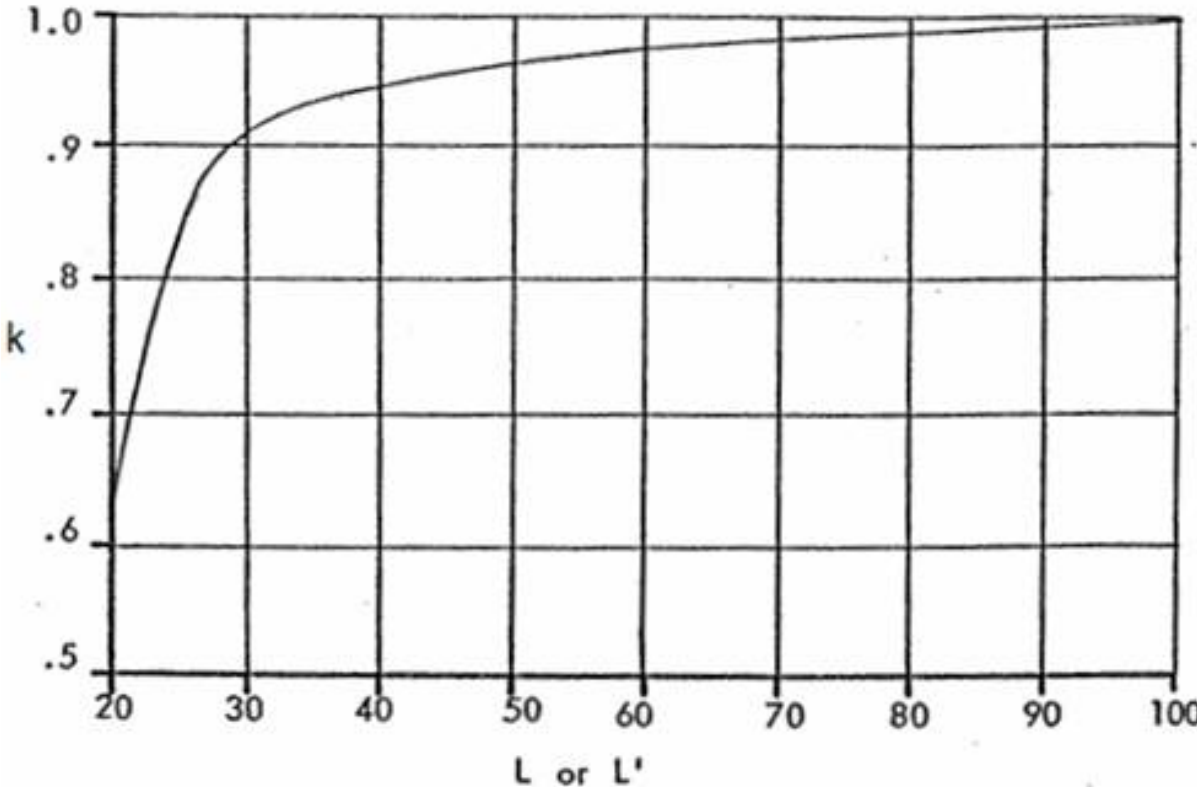

Fig.2.16. Slab length modification factor.

10- Calculate the number of beams in both directions as follows:

$$N_L = L'/S + 1 \ \& \ N_S = L/S + 1$$

11- Maximum bending moment, shearing force and differential deflection can be calculated for each direction from using Eqs. (2.26)

12- Assume beam widths and calculate, B, sum of all beam widths.

13- Calculate beam depth either for reinforced steel or prestressed using the Eqs. (2.27)

$$M = \frac{wL'(L_c)^2}{2}$$
$$V = wL'(L_c) \qquad (2.26)$$
$$\Delta = \frac{w(L_c)^4 L'}{4E_c I}$$

Where: M = Moment, positive or negative
D = Deflection in inches
E_c = Creep modulus of elasticity of concrete
I = Moment of inertia of section

Reinforced Steel $$d = \sqrt[3]{\frac{664ML_c}{B}}$$ (2.27)

Prestresses $$d = \sqrt[3]{\frac{553ML_c}{B}}$$

where:

M = Moment in KF, and

L_c = Cantilever length (k l_c) in ft

2.10 Summary

Many attempts have been made since the early 1950's to develop design procedures for stiffened slabs on grade on shrink-swell soils including methods to predict the vertical movement. This process continues.

The first BRAB (Building Research Advisory Board) study of slabs-on-ground that dealt with structurally related problems dates back to 1955. A final report was published in September 1962. In 1968, a revised version of the 1962 report was published which incorporated further information developed through field studies particularly in shrink-swell soil areas. BRAB 1968 assumes a rectangular mound shape (i.e. the slab stiffness doesn't influence the unsupported distance) and introduces an empirical support index related to climatic rating and soil properties.

Lytton slab design procedures (1970, 1972, and 1973) were developed using closed form solutions except for the 1972 procedure. This procedure used a finite difference analysis of a beam on a curved mound, a coupled spring foundation model for edge heave and a Winkler foundation for center heave analysis.

Walsh procedure (1974 and 1978) is based on analysis of a beam on an elastic coupled Winkler foundation. Walsh concluded that the shear strength of the slab was not an important design consideration. Based on a parametric study of soil and structural variables, Walsh provided equations for design moment and deflection using two support indices.

Fraser and Wardle (1975) developed a three-dimensional finite element model for plates resting on a semi-infinite elastic soil, modeling the soil as a system of elastic layers of finite thickness, based on Boussinesq's solution of the load-deflection relationship. They stopped short of producing a general design procedure. Their model was analyzed using the Commonwealth Scientific and Industrial Research Organization (CSIRO) FOCALS computer program.

Swinburne Method (1980) was developed by Holland et al. (1980) from an exhaustive analysis, as they stated, of a modified version of Fraser and Wardle (1975) method and the observed behavior of research slabs and production house slabs. Holland et al. introduced a design procedure consisting mainly of three design charts to calculate moment, deflection, and beam depth.

WRI Method (1981, 1996) (Wire Reinforcement Institute) was developed by Walter L. Snowden, P.E., of Austin, Texas. It is empirically derived by observing slab performance and modifying equations to give results approximating the foundations that had been found to give satisfactory results. WRI uses the same approach as the BRAB method and can be considered a modified version of BRAB.

The Post-Tensioning Institute (PTI) design method (1996, and 2004) is based on research work conducted at Texas A&M University by Wray and Lytton (Wray, 1978). This approach is based on analysis of a plate resting on a semi-infinite elastic continuum. The design equations included in the PTI manuals derive from nonlinear regression analyses of parametric study results. Using these equations, design moment, shear, and deflection can be found for center heave and edge heave conditions.

Australian Standard AS 2870 method (1996) was prepared by the Standards Australia Committee BD-025, Residential Slabs and Footings. This standard

recommends profiles of soil suction changes for different climatic zones of Australia and classifies the site using an index called the characteristic soil surface movement index. The standard provides a table of recommended stiffened raft designs, based on the "Beam On Mound" Walsh model (BOM) modified to fit with previous experience for several site classes (Walsh and Cameron, 1997).

CHAPTER III

ANALYSIS OF IMPLEMENTED WEATHER-SOIL-STRUCTURE INTERACTIONS MODELS IN THE COMMONLY USED DESIGN METHODS OF FOUNDATIONS ON SHRINK-SWELL SOILS

3.1 Introduction

From another perspective, each of the aforementioned design methods can be examined as a compilation of weather model, weather-soil interaction model, and soil-structure interaction model. The following chapter will discuss the implemented models in BRAB, WRI, PTI, and AS 2870 design methods. Moreover, this chapter presents a parametric study comparing beam depths resulted from different design methods and another parametric study examining the influence of Texas ASCE guidelines on the resulting beam depths using BRAB 1968 and WRI 1996.

3.2 Weather models

3.2.1 Climatic rating index

BRAB 1968 developed a US continental map for a climatic rating index C_W based on US Weather Bureau precipitation data. Unfortunately, BRAB 1968 manual does not explain how the climatic rating index, C_W, was developed in details. Nevertheless, the climatic rating index, C_W, depends on rainfall and the number of rainfall occurrence. Evaporation, evapotranspiration, and the factors influencing them such as solar radiation, temperature, relative humidity and wind speed are not considered. BRAB 1968 claims the unimportance of these factors saying *"While it is recognized that other factors such as temperature and relative humidity also influence loss or gain of soil moisture, the effects exerted are comparatively unimportant"*.

WRI design method, as well as BRAB, uses the same climatic rating index as the key weather parameter.

3.2.2 Thoronthwaite moisture index

The Thornthwaite Moisture Index, I_m (Thornthwaite 1948) was developed as a rational parameter by which different climatic zones may be defined. It describes soil moisture balance in terms of rainfall, potential evapotranspiration and the depth of available moisture stored in the rooting zone of vegetation at a particular site. The PTI (1996, 2004) design methods use the Thornthwaite Moisture Index, I_m as the main weather parameter.

Thornthwaite method estimates potential evapotranspiration (PET) by making use of air temperature solely. PET estimates are based upon a 12-hour day (amount of daylight) and 30-day month. The Thornthwaite method was developed for the east-central U.S. The method requires a constant ratio of reflected radiation to incident radiation (albedo), no advection of wet or dry air, and a constant ratio of the energy used in evaporation to the energy used to heat the air. The formulae are based on the catchment-area data and controlled experiments.

$$PET = 1.6x\frac{\left(10T_{mean}\right)^{a}}{I} \tag{3.1}$$

where:

PET=Potential evapotranspiration, *cm/mon*,

x=Adjustment factor related to hours of daylight and latitude,

T_{mean}=Mean monthly air temperature^{o}C,

I=Heat Index

where $I = \sum_{i=1}^{12} \frac{\left(T_{mean}\right)_i^{1.5}}{5}$, and

a=A function of the Heat Index given by

$$a = 0.49 + 0.0179I - 7.71\times10^{-5}I^2 + 6.75\times10^{-7}I^3 \tag{3.2}$$

The Thornthwaite Moisture Index, I_m moisture balance is based on the average, over a significant period of time, of the rainfall in excess or deficit of average transpiration rates. I_m is calculated on an annual basis but uses a monthly moisture accounting scheme to drive the overall moisture balance for each year. The moisture balance is computed on

monthly basis and requires input of monthly precipitation, monthly potential evapotranspiration, and the depth of available moisture. The monthly potential evapotranspiration is a function of the monthly mean air temperature only.

On completion of the moisture balance computation for each year the Thoronthwaite Moisture index is given by:

$$I_m = \frac{100R - 60DEF}{PET} \tag{3.3}$$

where:

R = runoff moisture depth (m of water),

DEF = deficit moisture depth (m of water), and

PET = the total potential evapotranspiration for the year (m of water).

For any region under consideration, positive I_m indicates that it has an average annual runoff, while negative I_m indicates that there is a water deficiency which is informative for irrigation planning purposes. However, for foundation slabs on shrink-swell problems, the main concern is the amount of moisture infiltration or evapotranspiration not the moisture surplus or deficit within the depth of available moisture zone.

I_m considers only the heat index for assessing the monthly potential evapotranspiration; this creates an underestimation of the evapotransporation in cooler months where the effects of wind and relative humidity may play a more important role in moisture loss than just the temperature as stated by Gay (1994). In addition, I_m gives an average, over a significant period of time, of the water balance (input minus output, assuming for the sake of argument that surplus minus deficit is correlated to infiltration minus evapotranspiration) and does not consider the duration of weather cycles. [For instance, suppose you have two locations with identical soil logs and the same difference between input and output soil surface moisture over a long period of time. Suppose also that the first location has a very short time period of wet-dry cycles and the second one has a very long time period of wet-dry cycles. Both will possess the same I_m but the second location will have a lot larger soil surface suction changes, hence larger movements.]

However, the Thornthwaite Moisture Index, I_m is still a rational parameter by which different climatic zones may be defined, for irrigation planning purposes. Also, the Thornthwaite Moisture Index, I_m may be a good parameter to correlate with the depth of active moisture zone as it is based on the average, over a significant period of time, of the water balance.

3.2.3 Suction profiles

The mobilized volumetric strains of shrink-swell soils are directly related to suction changes and water content changes. Consequently, the usage of design suction profiles that address the influence of the weather on the soil seems to be a very relevant approach to the problem of soil volume changes induced by seasonal weather variation.

The AS 2870 design method provides tables recommending boundary soil suction profiles by giving a change in suction at the surface and a depth of suction change for different climatic zones in Australia. These recommendations are based on field measurements extrapolated using Thornthwaite Moisture index, I_m. The idea of using boundary soil suction profiles as a weather parameter is very appropriate but requires a lot of field measurements made over a long period of time. The Australian field data does not seem to be documented in details but simply summarized in AS 2870 according to Walsh (2005).

3.3 Weather-soil interaction models

3.3.1 Support index

BRAB and WRI design methods provide a relationship among the support index, the climatic rating, and the plasticity index. There does not seem to be any data available to document the choices made for these two methods. It appears that the experience of a number of people dictated the preparation of these methods. Therefore, it is not possible to provide an independent evaluation of the basis of the method except for common sense and logic. More over, the plasticity index plays a role in the prediction process but is not the only parameter influencing movement. The swell index and PVC “Potential

Volume Change" readings have the same shortcoming as the PI; indeed they are very sensitive to initial conditions of the soil specimen, particularly the moisture contents that vary with weather and time.

3.3.2 Edge moisture variation distance

PTI (1996) method estimates the edge moisture variation distance as a function of I_m only using the recommended chart. It is reasonable to think that the edge moisture variation distance depends also on the soil type, the soil permeability, the location and the extent of the vegetation, the foundation stiffness, and the site drainage. In order to obtain the recommended chart, Wray (1978) used back-calculation procedures for three stiffened slab foundation designs, which were known to have worked satisfactorily in San Antonio, Dallas-Fort Worth, and Houston for several years. Wray used the results to develop the relationship between I_m and the maximum edge moisture variation distance that these designs could withstand. This work was theoretically based and Wray stated in his dissertation that actual measurements needed to be obtained: "*...these measurements are a research effort that is badly needed*". The PTI (1996) manual considered Wray's center lift and edge lift curves as lower bound curves and added upper bound curves with a 0.7 ft offset for the edge lift and a 1.6 ft offset for the center lift curves. Wray (1989) in his extensive research project sponsored by the National Science Foundation took measurements at two sites, College Station, Texas (I_m= 0.0) and Amarillo, Texas (I_m= -22.0). Thanks to those precious measurements, he was able to add two scatter measurement bars to the e_m - I_m chart. The PTI procedure to determine the expected vertical movement "y_m" faces some difficulties such as:

I) The insensibility in the determination of the predominant clay mineral using the Cation Exchange Activity "CEA_c" and the Activity Ratio, "A_c".

II) The empirical equation used to estimate the moisture velocity (v) seems to be unconvincing as it relates the moisture velocity to I_m, which represents an overall moisture balance. It is more convincing to relate the inlet moisture velocity to rainfall that will impact the y_m value in edge lift case and to relate the outlet moisture velocity to

the potential evapotranspiration that will impact the y_m value in center lift case. This means, in using this empirical equation, you will have the same moisture velocity for two different sites having the same Thornthwaite Moisture index while they may have very different rainfall and potential evapotranspiration patterns.

PTI (2004) method enhances the PTI (1996) weather-soil interaction model significantly by introducing another design chart to estimate the edge moisture variation distance, e_m based on the weighted average of modified unsaturated diffusion coefficient, (α') besides the original Warren K. Wray (1978) design chart relating e_m to I_m (i.e. without adding the upper bound curves), the designer has to choose the e_m of larger value of the two charts.

The α'- design chart is based on the pioneer research work done by Mitchell (1980), which introduced a closed form analytical solution to the partly saturated diffusion partial differential equation. α'- design chart relies on a solid base, (Mitchell (1980) research work), it is difficult to determine α' experimentally. This forces PTI (2004) to introduce a long procedure to estimate it empirically based on LL and PL. This procedure possesses a high degree of empiricism. Loosely speaking, you have to implement LL and PL through an empirical equation or chart to get a parameter, and use them along with the parameter again in another empirical equation or chart get to another parameter and so on, about four or five times at least. These successive empiricisms along with the modification using the soil fabric factor, F_f , raises questions about the reliability assessment of the modified unsaturated diffusion coefficient, α'. PTI (2004) method also refines y_m determination by replacing using the unique value of the suction compression Index γ_h with two indices, $\gamma_{h\ shrink}$ & $\gamma_{h\ swell}$, which is more realistic. Moreover, PTI (2004) utilizes Naiser (1997) improvements of y_m determination. Naiser (1997) procedures are applicable to several moisture effect cases such as surface bare soils, grass, trees, and flowerbeds, in addition to the effects of vertical and horizontal barriers.

Another main concern regarding e_m estimation is that: the maximum e_m value that you can get using PTI 1996 e_m design chart is about 1.95 m (6.5 ft), and 2.7 m (9 ft) if

you are using the PTI 2004 e_m design chart. However, Dean B. Durkee (2000) concluded in his dissertation that PTI (1980) underestimates e_m . Dean B. Durkee (2000) measured edge moisture variation distance at the Colorado State University research site slabs up to 4.5 m (15 ft).

3.3.3 Characteristic movement

AS 2870 uses the characteristic movement y_s, as the main design parameter that incorporates the recommended soil suction change profiles along with the effective instability index, I_{pt}. The I_{pt} addresses the cracks zone effect in allowance for lateral restraint and vertical load. AS 2870 does not use any edge moisture variation distances, but it assumes a mound shape with a parabolic edge effect P. F. Walsh and S. F. Walsh (1986).

3.4 Soil-structure interaction models

3.4.1 Structurally determined models

In BRAB and WRI design methods, two dimensional slab design is simplified into two one dimensional designs and assumes the load distribution and the reaction force provided by the soil are uniform and does not consider the influence of the superstructure stiffness. These simplifications are conservative. BRAB provides an unreasonable linear relationship between the unsupported distance in each direction and the corresponding slab dimension, that may lead, in slabs of big aspect ratios, to huge beam depths in long directions and small beam depths in short slab directions. WRI tries to mitigate this serious drawback by introducing a chart with a slightly nonlinear relationship between the support index and a cantilever length (with a maximum value of 12 ft); the average slope of this curve is not a function of the slab dimension as in BRAB method.

3.4.2 Winkler foundations models

AS 2870 uses an elementary model consisting of beam-on-mound on a coupled Winkler

model with an initial mound heave to afford standard designs for different site classes and construction types. This model has a particular feature; the swell-stiffness, k_s is related to the sensitivity of the foundation heave to surcharge pressure rather than to elastic properties of the soil. P. F. Walsh and S. F. Walsh (1986) reasoned this stating "Since the contact pressures for house foundations are usually low, the simple linear stiffness was chosen for the analysis". AS 2870 philosophy for choosing the beam on mound model is to compromise between accuracy and simplicity as the development of a sophisticated model is further restricted by lack of reliable material data P. F. Walsh and S. F. Walsh (1986).

P. F. Walsh and D. Cameron (1997) declared that "*The justification of the beam on mound methods is that they have been found to give reasonable range of designs in comparison with experience, with experimental data and failure*". The AS 2870 modification procedure is simply an empirically fitted line to the values of parameters y_s/Δ and $\log\{\sum\left(\frac{B_w D^3}{12}\right)/W\}$ for the standard designs P. F. Walsh and D. Cameron (1997).

Limitations of using the AS 2870 can be inferred from the modification procedure as follows:

a) y_s range was 10 mm to 70 mm if $H_s > 3$ m or 100 mm if $H_s < 3$m
b) Δ range was 5 mm to 50 mm
c) Span range was 5 m to 30 m
d) Beam depth range was 250 mm to 100 mm
e) Beam width range was 110 mm to 400 mm
f) Average load range was up to 15 kPa
g) Edge line load range was up to 15 kN/m

3.4.3 Foundations on elastic half space models

PTI (1996, 2004) methods rely on a well-established theoretical base for their soil-structure interaction model, but the nonlinear regression analysis of the parametric study

results carried out by Wray (1978) limits these design equations to the ranges of design parameters used in this parametric study such:

a) "y_m" values were (0.0, 1.0, and 4.0 inches) in center lift case and (0.0, and 1.12 inches) in edge lift case.
b) "e_m" values were (0.0, 2, 5, and 8 feet)
c) Beam depths were 18 and 30 inches.
d) Beam spacing values were 12 and 20 feet.
e) Perimeter loading were 613 and 1477 pounds per linear foot.
f) Slab length values were (24, 48, 96, and 144 feet).
g) Constant beam widths of 8 inches.
h) Constant uniform loading of 40 psf.

These limits constrain PTI method so that it can not efficiently accommodate interior loads such as load- bearing walls and column loads in addition to heavy uniform loads. Moreover, research efforts are needed to check the applicability of these design equations beyond the parameter ranges that have been used in Wray's parametric study.

3.5 Comparison of beam depths for stiffened slabs on shrink-swell soils using WRI, PTI 2004 and AS 2870

The most common foundation for light structures founded on shrink-swell soils is the stiffened slab on grade. The beam depth is an intrinsic design parameter for this type of foundation, it usually ranges between 0.6 and 1.2 m with common beam spacing of 3 to 6 m placed in both directions. The following methods are among the most common methods used to calculate the beam depth, spacing, and reinforcement needed for a safe and serviceable foundation: 1) BRAB Method (1968); 2) WRI Method (1980, 1996); 3) PTI Method (1996); 4) AS 2870 (1996); 5) PTI Method (2004). WRI and PTI Method (2004) are the most recently developed method in the USA while the AS 2870 is the most recent version of the Australian Standards. For the same input design data, applying these three design methods may result in different beam depths. In order to compare these methods, 27 cases are designed. They include three simple rectangular

stiffened slabs subjected to three different weather patterns, built on three different shrink-swell soils, and loaded with a uniform pressure and perimeter line load. The resulting beam depths using the WRI, PTI 2004 and the AS 2870 methods in different soil and weather conditions are also presented and discussed is this section.

3.5.1 Input design data

Designing stiffened slabs on shrink-swell soils is a weather-soil-structure interaction problem as weather introduces moisture variations to the surface soil zone, the soil reacts with shrink- swell response according to the moisture variation, and the structure deforms as a result of the soil mound shape. These three design methods model this problem in different ways; consequently, the input design data differs from one method to another. For the sake of consistency in the input data the following assumptions were used:

3.5.1.1 Weather parameters

Three locations were chosen in Houston, College Station, and San Antonio, Texas, US representing wet temperate, temperate, and dry temperate climatic zones.

For WRI input weather data, the climatic rating indices (C_W) for these locations were found to be 17, 21, and 25, respectively, according to the Continental United States climatic rating map.

For PTI 2004 input weather data, the Thornthwaite Moisture index, I_m for these locations were found to be -16, 0, and 18, respectively, according to the Continental United States I_m map.

AS 2870 introduces a table for recommended H_s (depth of design suction change) values for each climatic zone. Correlating the average I_m in each climatic zone with the corresponding H_s, the following equation was concluded and used to calculate H_s for the three locations

$$H_s = 1.387 + 0.939e^{\left(\frac{-I_m}{24.843}\right)} \qquad (3.4)$$

where:

H_s in (m)

For AS 2870 input weather data, depths of design suction change H_s were found to be 3.3, 2.4, and 1.8 m, respectively.

The wet and dry suction profiles at the surface were assumed, for all locations, considering the guidance of the PTI recommended values (2.5 pF for the wettest condition as in the case of prolonged heavy rain and no drainage, 4.5 pF for the driest condition if the surface suction is controlled by vegetation).

3.5.1.2 Soil parameters

Three soils were chosen representing very high, high, and moderate shrink-swell potential.

For WRI and PTI 2004 input soil data, the liquid limits were assumed to be 90%, 70%, and 50%, respectively with corresponding plasticity indices of 60%, 45% and 30%.

For PTI 2004 input soil data, the % fine clay was assumed to be 70% and the % passing sieve # 200 was assumed to be 100% for all soils. Applying these input data in PTI procedures, the Suction Compression Indices (γ_h) were found to be 0.133, 0.077, and 0.028 (pF^{-1}).

The Suction Compression Index represents the slope of the volumetric strain versus suction in pF units and the Shrinkage Index or the Instability Index without lateral restraint and without loading of the soil (I_{ps}) represents the slope of the vertical strain versus suction in pF units. The I_{ps} values were assumed to be one third of the corresponding γ_h values considering that the vertical strain is one third of the volumetric strain.

Consequently, for AS 2870 input soil data, the I_{ps} values were found to be 0.0443, 0.0257, and 0.0093.

3.5.1.3 Structural parameters

Three slabs were chosen of dimensions 12X12, 24X24, and 24X12 m representing

different aspect ratios and different slab sizes. The beam spacing was chosen to be 3m in both directions. For all slabs a masonry veneer super structure was chosen.

3.5.2 Results comparison

The resulting beam depths are tabulated in the appendix. To compare these beam depths, the average beam depth for each design case was calculated and considered as the reference parameter in the comparison. Fig. 3.1, Fig. 3.2, and Fig. 3.3 show the resulting beam depths using the three design methods.

The percentage difference between the design depth and the average design depth for all cases was also calculated. Fig. 3.4 shows the percentage difference from the average beam depths for all cases.

Of the 27 design cases, only one case gives identical beam depths using the three design methods, this case was in a wet temperate climatic zone and has a very high shrink-swell potential soil and the smallest slab size (12X12 m).

Among these design methods, WRI beam depths and PTI 2004 beam depths shows the closest correlation, meanwhile PTI 2004 beam depths and AS 2870 beam depths shows the poorest correlation.

3.5.2.1 WRI

Of the 27 cases, 6 cases resulted in beam depths smaller than the average beam depths, 3 cases resulted in the average beam depths, and 18 cases resulted in beam depths larger than the average beam depth. The maximum beam depth was 0.9 m and the minimum was 0.4 m. The maximum percentage difference from the average beam depth was 21.62%, the minimum was -4.0%, and the average of all cases was 5.46%.

3.5.2.2 PTI 2004

Of the 27 cases, 4 cases resulted in beam depths smaller than the average beam depths, one case resulted in the average beam depths, and 22 cases resulted in beam depths larger than the average beam depth. The maximum beam depth was 1.05 m and the

minimum was 0.45 m. The maximum percentage difference from the average beam depth was 44.0%, the minimum was -20.75%, and the average of all cases was 16.597%.

3.5.2.3 AS 2870

Of the 27 cases, 21 cases resulted in beam depths smaller than the average beam depths, one case resulted in the average beam depths, and 5 cases resulted in beam depths larger than the average beam depth. The maximum beam depth was 1.1 m and the minimum was 0.25 m. The maximum percentage difference from the average beam depth was 24.53%, the minimum was -52.63%, and the average of all cases was -22.63%.

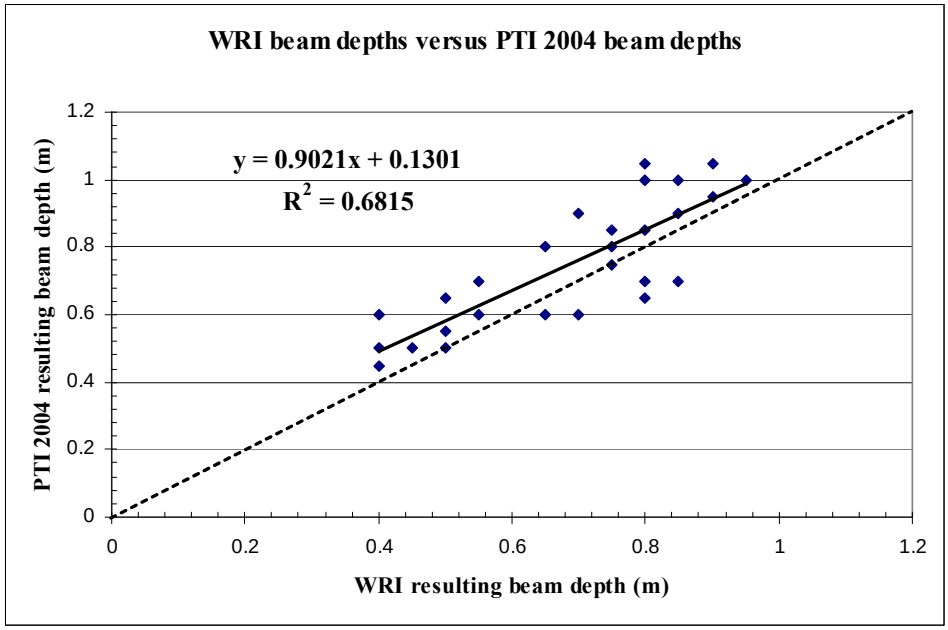

Fig. 3.1. WRI beam depths versus PTI 2004 beam depths.

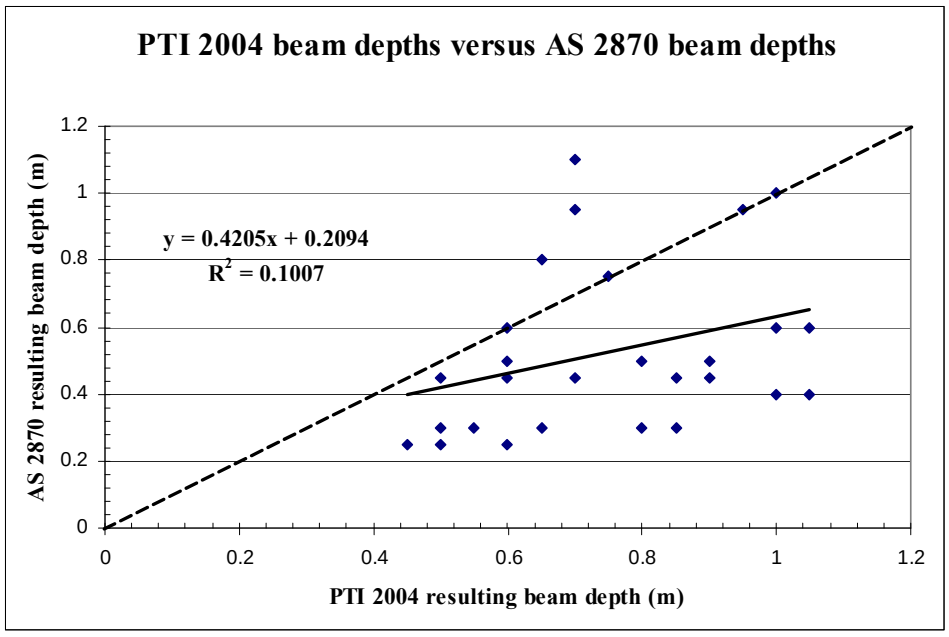

Fig. 3.2. PTI 2004 beam depths versus AS 2870 beam depths.

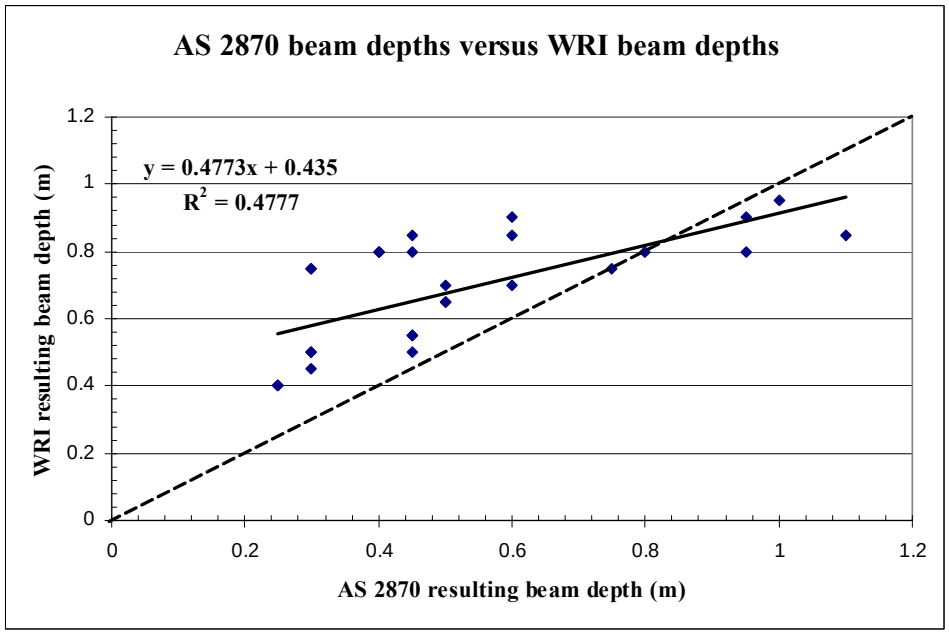

Fig. 3.3. AS 2870 beam depths versus WRI beam depths.

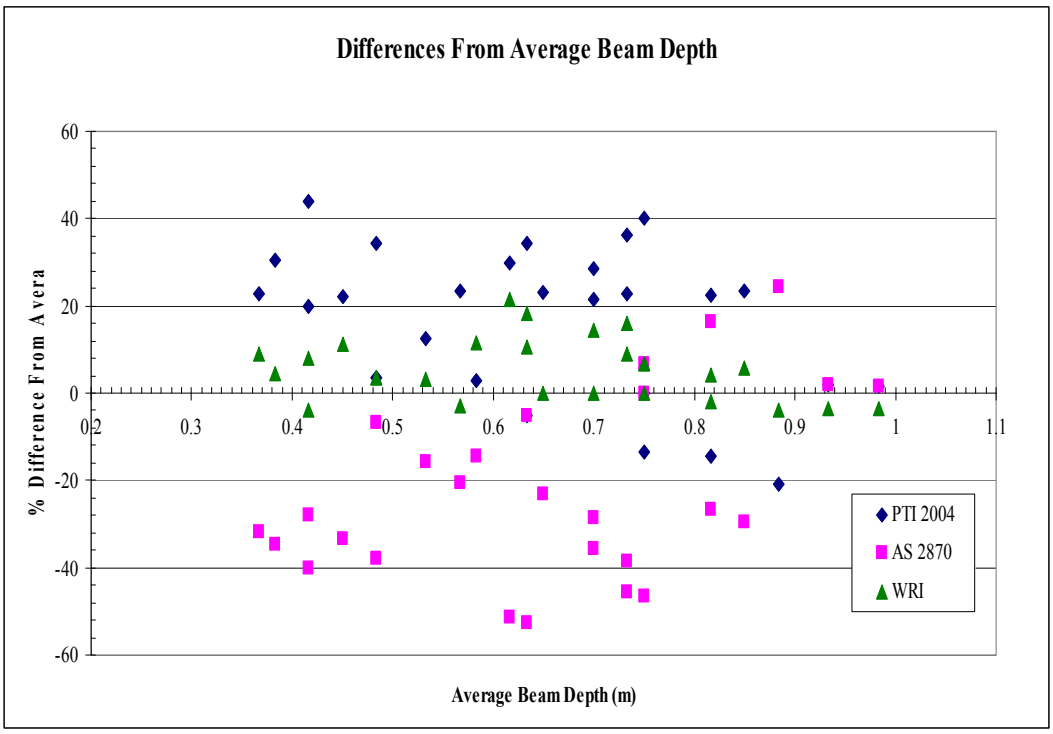

Fig. 3.4. The percentage of the difference from the average beam depths.

3.5.3 Conclusions

This parametric study provides a table of resulting beam depths using three commonly used design methods for 27 cases that cover a range of soils of very high, high, and moderate shrink-swell potential, range of weather patterns of wet temperate, temperate, and dry temperate climatic zones, and range of slab sizes of dimensions 12X12, 24X24, and 24X12 m. The table of results may provide guidance for consultants who deal with similar design situations.

A technique was suggested to apply input design data for the three design methods with reasonable consistency, which enables consultants to use these three design methods despite the variation in the required input data for each method.

For the chosen 27 cases, the beam depth predicted by the WRI design method gives results closest to the average beam depth obtained by all methods with an average percentage difference of 5.46%, PTI 2004 gives beam depths larger than the average

beam depth by 16.597%, and AS 2870 gives beam depths smaller than the average beam depth by 22.63%.

For the chosen 27 cases, applying these three design methods shows discrepancies between recommendations of beam depths that raise the need for comparison with observed field data.

3.6 Influence of the 2002 Texas section of ASCE recommended practice on the beam depths for stiffened slabs on shrink-swell soils using BRAB and WRI

In 2002, the Texas section of ASCE provided recommended practice for the design of residential foundations that impacts the beam depth using WRI and BRAB. To examine the influence of this recommended practice in the resulting beam depths, 27 cases are designed. They include three simple rectangular stiffened slabs subjected to three different weather patterns, built on three different shrink-swell soils, and loaded with a uniform pressure and perimeter line load. The resulting beam depths using the WRI and BRAB methods with and without the recommendations of the Texas section of ASCE are presented and discussed for different soil and weather conditions. The PTI and Australian method are also presented for additional comparison purposes.

3.6.1 Texas Section of the American Society of Civil Engineers guidelines

The Texas Section of the American Society of Civil Engineers (ASCE-Tx) adopted guidelines for residential foundation engineering on October 3, 2002. These guidelines are to reflect engineering opinions and practices of committee members which are representative of most residential foundation design engineers in the state of Texas, USA. The purpose of this document (ASCE-Tx Section Doc. No. 4.6.5.2.1) is to present recommended practice for the design of residential foundations to augment current building codes to help reduce foundation related problems. The Texas ASCE guidelines recommendations are:

- For WRI and BRAB design methods, beam analysis length should be limited to a maximum of 50 feet, regardless of actual beam length.

- For BRAB design method, use long-term creep factor as provided in ACI 318, Section 9.5.2.5.
- For WRI design method, the minimum design length (L_c) shall be increased by a factor of 1.5 with a minimum increased length of 6 feet.

3.6.2 Input design data

Designing stiffened slabs on shrink-swell soils is a weather-soil-structure interaction problem as weather introduces moisture variations to the surface soil zone, the soil reacts with shrink- swell response according to the moisture variation, and the structure deforms as a result of the soil mound shape. To comprise this parametric study, three different soils, three different locations, and three different slabs were chosen, the same way as in (Abdelmalak& Briaud, 2006), to form 27 cases representing typical design situations.

3.6.2.1 Weather parameters

Three locations were chosen in Houston, College Station, and San Antonio, Texas, US representing wet temperate, temperate, and dry temperate climatic zones.

For WRI and BRAB input weather data, the climatic rating indices (C_W) for these locations were found to be 17, 21, and 25, respectively, according to the Continental United States climatic rating map.

3.6.2.2 Soil parameters

Three soils were chosen representing very high, high, and moderate shrink-swell potential.

For WRI and BRAB input soil data, the liquid limits were assumed to be 90%, 70%, and 50%, respectively with corresponding plasticity indices of 60%, 45% and 30%.

3.6.2.3 Structural parameters

Three slabs were chosen of dimensions 12X12, 24X24, and 24X12 m representing

different aspect ratios and different slab sizes. The beam spacing was chosen to be 3m in both directions. For all slabs a masonry veneer super structure was chosen.

The 27 cases were designed with 4 different procedures; using BRAB design method, using WRI design method, using BRAB design method and the Texas ASCE guidelines (BRAB-Tx ASCE), and using WRI design method and the Texas ASCE guidelines (WRI-Tx ASCE),

3.6.3 Results and discussion

The resulting beam depths using the 4 different procedures and another two design methods, PTI 2004 and AS2870 (Abdelmalak& Briaud, 2006) are tabulated in the Appendix B.

To compare these beam depths, the average beam depth for each design case using the 4 different procedures (denoted as $\mathbf{D_{ave\ 4}}$) was calculated and considered as the reference parameter in the comparison. Figs. 3.5 and 3.6 show the resulting beam depths using the BRAB and WRI design methods with and without the (Tx ASCE) recommendations. The percentage difference between the design depth and the average design depth for all cases (denoted as $\mathbf{\%\Delta_{\ design\ method,\ ave\ 4}}$) was also calculated.

Similarly, another average beam depth for each design case using the 6 different procedures (BRAB and WRI design methods with and without the (Tx ASCE) recommendations and PTI 2004 and AS2870) was calculated (denoted as $\mathbf{D_{ave\ 6}}$). The percentage difference between the design depth and this average design depth for all cases (denoted as $\mathbf{\%\Delta_{\ design\ method,\ 6}}$) was also calculated.

3.6.3.1 Influence of Tx ASCE guidelines on BRAB beam depths

Applying the Tx ASCE guidelines for the 27 design cases significantly reduced the BRAB beam depths with a percentage reduction ranging between 0% and 41.4% with an average percentage reduction of 25.4% as shown in Fig. 3.5. The reason for the decrease in beam depth is that for slab lengths larger than 50 ft, it is recommended to use 50ft

rather than the actual slab length. This resulted in this parametric study in a limit on the beam depth of 0.85 m (Fig. 3.5).

3.6.3.2 Influence of Tx ASCE guidelines on WRI beam depths

Applying the Tx ASCE guidelines for the 27 design cases significantly increased the WRI beam depths with a percentage increase ranging between 20% and 55.6% with an average percentage reduction of 41.6% as shown in Fig. 3.6. Despite the Tx ASCE guidelines limitation of 50 ft on the maximum slab dimension, no obvious upper bound emerged from the parametric study for the resulting beam depth. The reason is that the beam depth in the WRI method is nearly equally sensitive to the slab dimension, the soil type, and the weather parameters. However, increasing the minimum design length (L_c) by a factor of 1.5, which is recommended by the TxASCE guidelines, had an important impact and increased the resulting beam depth.

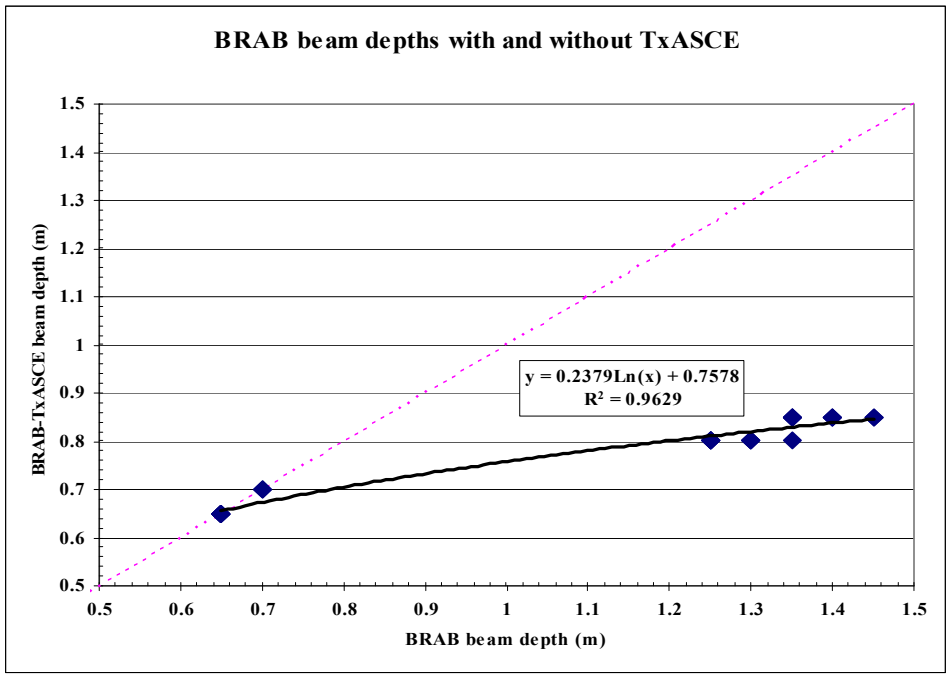

Fig. 3.5. Influence of TxASCE guidelines on BRAB beam depths.

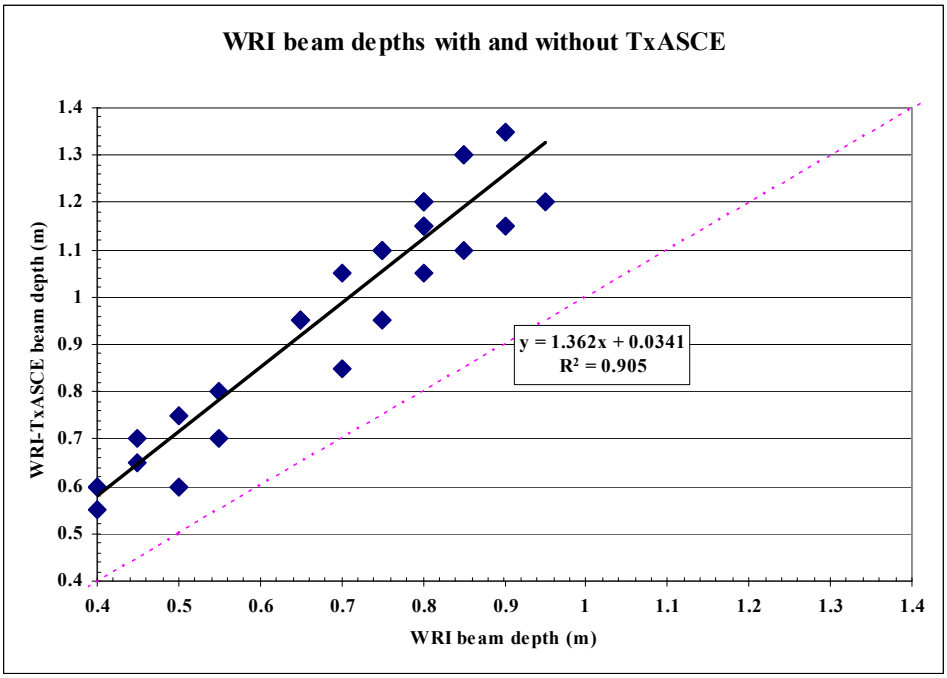

Fig. 3.6. Influence of TxASCE guidelines on WRI beam depths.

3.6.3.3 Comparing the 4 design procedures (BRAB, WRI, BRAB-TxASCE, and WRI-TxASCE) to their average

Applying the Tx ASCE guidelines for the 27 design cases using BRAB design method decreased the average value of the $\%\Delta_{BRAB,\ ave\ 4}$ from 24.7% (the range was from 66.7% to -21.1%) to -11.1% (the range was from 13.0% to -24.4%). On the other hand, applying the Tx ASCE guidelines for the 27 design cases using the WRI design method increased the average value of the $\%\Delta_{WRI,\ ave\ 4}$ from -22.9% (the range was from -47.5% to -1.5%) to 9.3% (the range was from -26.7% to 46.5%) as shown in Fig. 3.7.

3.6.3.4 Comparing the 4 design procedures to an average of 6 methods (BRAB, WRI, BRAB-TxASCE, WRI-TxASCE, PTI 2004, and AS2870)

Applying the Tx ASCE guidelines for the 27 design cases using BRAB design method decreased the average value of the $\%\Delta_{BRAB,\ ave\ 6}$ from 39.1% (the range was from 97.4%

to -21.5%) to -1.3% (the range was from -21.5% to 30.0%). On the other hand, applying the Tx ASCE guidelines for the 27 design cases using WRI design method increased the average value of the $\%\Delta_{WRI,\ ave\ 6}$ from -15.3% (the range was from -37.7% to 2.1%) to 20.0% (the range was from -14.3% to 48.2%) as shown in Fig. 3.8 .

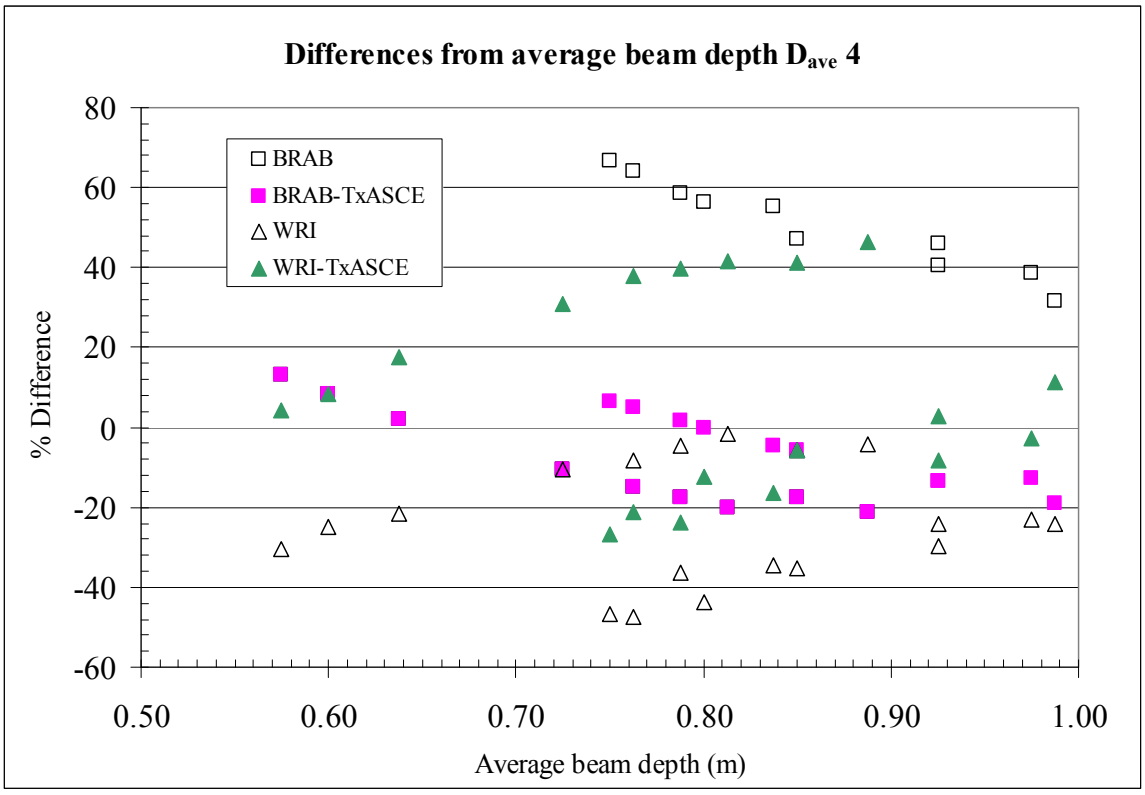

Fig. 3.7. The percentage of the difference from the average beam depths using 4 design procedures (BRAB, WRI, BRAB-TxASCE, and WRI-TxASCE).

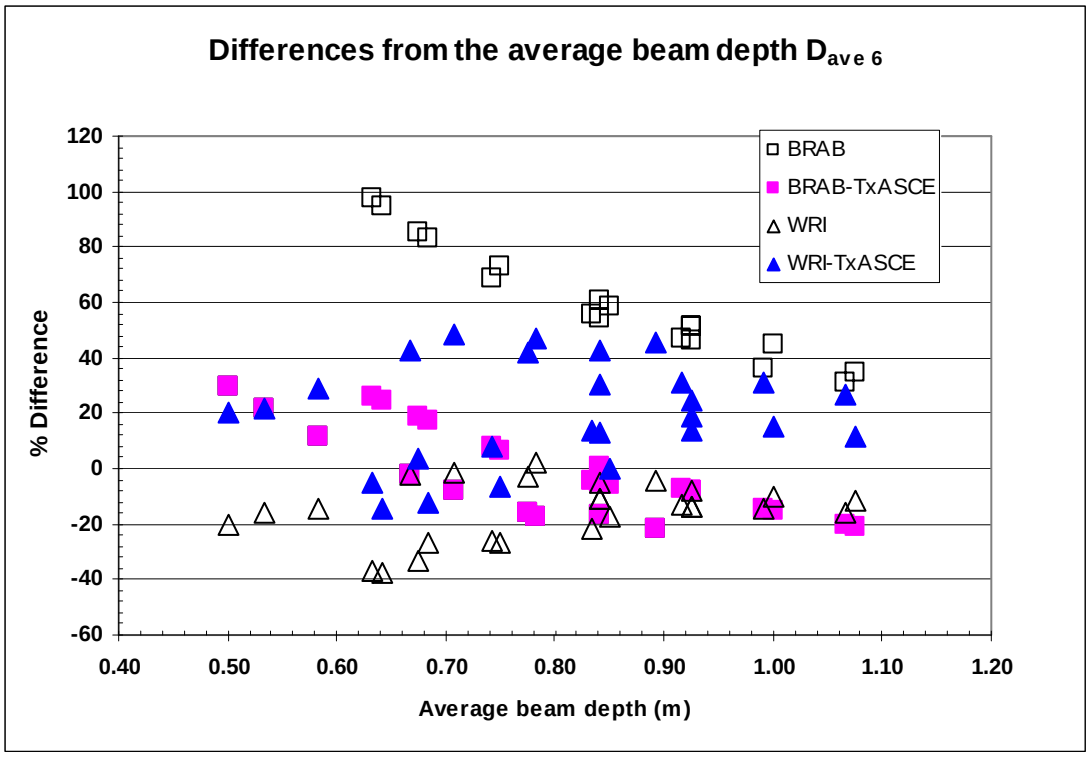

Fig. 3.8. The percentage of the difference from the average beam depths using 6 design procedures (BRAB, WRI, BRAB-TxASCE, WRI-TxASCE, PTI 2004, and AS2870).

3.6.4 Conclusions

This parametric study provides a table of beam depths using two common design methods, BRAB and WRI, with and without applying the TxASCE guidelines. 27 cases are used to cover a range of soils of very high, high, and moderate shrink-swell potential, range of weather patterns of wet temperate, temperate, and dry temperate climatic zones, and range of slab sizes of dimensions 12X12, 24X24, and 24X12 m. The table of results may provide guidance for consultants who deal with similar design situations.

The BRAB (1968) is a design method for reinforced concrete slabs; it is mostly empirical, but it is a simple method which is attractive to foundation designers. It can lead to large beam depths for large slabs as the cantilever length is directly proportional to corresponding slab dimension. WRI (1996) is very similar to BRAB with a significant

modification to the cantilever length as it is proportional to the support index. It is also a method exhibiting empiricism. Unlike BRAB (1968), WRI (1996) can handle both post tensioned and reinforced concrete slabs.

For the chosen 27 cases, applying the TxASCE guidelines significantly reduced the beam depths using the BRAB method and increased the beam depths using the WRI method. The beam depth predicted by the BRAB-TxASCE design method gives results closest to the average beam depth obtained by all aforementioned methods with an average percentage difference of -1.3%. BRAB gives beam depths larger than the average beam depth by 39.1%, WRI gives beam depths smaller than the average beam depth by -15.3%, and WRI-TxASCE gives beam depths larger than the average beam depth by 20.0%.

For the chosen 27 cases, applying these 4 design methods shows discrepancies between recommendations of beam depths that raise the need for comparison with observed field data.

CHAPTER IV

PROPOSED MOISTURE DIFFUSION AND SOIL VOLUME CHANGE MODEL

4.1 Introduction

Two important phenomena influence the soil behavior under foundations on shrink-swell soils besides the soil-structure interaction process; the moisture diffusion through the soil and the soil volume change response to moisture variations. Developments in the soil volume change response models have been taking place since the early 1950's concluding with reasonably accurate and practical soil volume change models. Yet, developments in the soil moisture diffusion models face difficulties with determining the coefficient of unsaturated diffusivity, α; it requires very accurate suction measurements, which are not available in common small size geotechnical laboratories. This chapter will propose a moisture diffusion soil volume change model.

4.2 Soil suction

Soil suction is commonly referred, in soil physics, to as the free energy state of soil water. This free energy can be measured in the terms of partial vapor pressure. The relationship between the soil suction and partial vapor pressure is given in Eq. 4.1 as (Richards, 1965):

$$\psi = -\frac{RT}{\nu_{w0}\omega_v}\ln\left(R_h\right) \tag{4.1}$$

where:

ψ = soil suction

R = universal gas constant

T = absolute temperature

ν_{w0} = specific volume of water

ω_v = molecular mass of water

The soil suction is also known as total suction and comprises of two components namely matric suction and osmotic suction. The total suction is the equivalent suction derived from the measurement of the partial pressure of the water vapor in equilibrium with the soil water, relative to the partial pressure of water vapor in equilibrium with free pure water. It can be expressed mathematically as (Fredlund and Rahardjo, 1993):

$$\psi = (u_a - u_w) + \pi \tag{4.2}$$

where:

$(u_a - u_w)$ = matric suction

u_a = pore-air pressure

u_w = pore-water pressure

π = osmotic suction

The matric suction is related with the capillary phenomena occurring due to surface tension of water. The capillary water has negative pressure with respect to the air pressure thus; matric suction is a negative quantity. It is the equivalent suction derived from the measurement of the partial pressure of the water vapor in equilibrium with the soil water, relative to the partial pressure of the water vapor in equilibrium with a solution identical in composition with the soil water. Matric suction varies with the environmental conditions such as temperature and atmospheric suction. This relationship is studied with the help of soil-moisture characteristic curves (Fredlund and Rahardjo, 1993).

The osmotic suction is due to the dissolved salts in the pore water of the soil sample. It is related to the tendency of water to move from the region of low salt concentration to high concentration. The changes in osmotic suction have effect on the mechanical behavior of the soil i.e. there is change in volume and shear strength (Fredlund and Rahardjo, 1993).

Suction is measured in units of water pressure. Typical suction range is from 1 kPa, for a very wet soil close to 100% degree of saturation, to a 10^6 kPa, for an oven dried soil sample. Since the value of suction can be very high, it is usually expressed on a logarithmic scale. The commonly used pF scale, U (pF) = $\log_{10}| u_w |$ provides another

alternative unit to measure of suction where u_w is the total suction expressed in units of cm of water head.

4.3 Models of moisture movements

4.3.1 Darcy's law

The movement of the water in the saturated soils is described by Darcy's law (Darcy, 1856), which is, the flow of the water in the soil is proportional to the hydraulic gradient. Darcy's law is written as follows:

$$q_i = ki_i = k\frac{dh}{dx_i} \tag{4.3}$$

where q_i= Darcy's flux in i-direction; k = hydraulic conductivity, which is a function of matric suction; h= hydraulic head, and x_i is the i- direction coordinate.

For unsaturated soils, Childs and Collis -George (1950) proposed that water can be visualized as flowing only through the pore space filled with water. The air-filled pores in an unsaturated soil can be considered as behaving similarly to the solid phase, and the soil can be treated as a saturated soil having reduced water content (Childs, 1969). Subsequently, the validity of the Darcy's law can be verified in the unsaturated soil in the similar manner to its verification for a saturated soil. The requirement for the Darcy's law is that the water flow is Newton's flow, for the soil with very low water content, the water in the soils is absorbed water and it is non-Newtonian flow. Therefore, Darcy's law is not applicable. However, the coefficient of permeability used in this dissertation is a function of both the mechanical stress and matric suction of the unsaturated soils. Under this condition, the Darcy's law holds for any small range of pore water pressure change.

4.3.2 Richard's equation

The water continuity equation in an unsaturated soil is actually the equation of soil water mass conversation, which can be written as follows:

Net water flow in+ water source (if any) = rate of change of stored water

By applying the continuity equation to Darcy' law, together with the Bernoulli's equation (relationship between the hydraulic head and pore water pressure), Richard's equation for the water movements in unsaturated soils can be obtained. There are three versions of differential equation for the moisture movements in unsaturated soils, which are listed as follows:

$$\frac{\partial}{\partial z}\left(K\frac{\partial u_w}{\partial z}\right)+\frac{\partial K}{\partial z}=C\frac{\partial u_w}{\partial t} \tag{4.4a}$$

$$-\frac{\partial}{\partial z}\left(K\frac{\partial u_w}{\partial z}\right)-\frac{\partial K}{\partial z}=\frac{\partial \theta}{\partial t} \tag{4.4b}$$

$$\frac{\partial}{\partial z}\left(\frac{K}{C}\frac{\partial \theta}{\partial z}\right)-\frac{\partial K}{\partial z}=\frac{\partial \theta}{\partial t} \tag{4.4c}$$

where,

K = the permeability of unsaturated soils, which is a function of negative pore water pressure (matric suction),

u_w= pore water pressure, (or matric suction),

θ= volumetric water content,

C= slope of the soil water characteristic curve,

z= Coordinate in z direction,

t= time

All these three equations are considered as forms of Richard's equation (Swartzendruber, 1969). As can be seen, Equation 4.4a derived the differential equation for water continuity in terms of pore water pressure (matric suction) only, Equation 4.4c derived the differential equation in terms of volumetric water content only, while Equation 4.4b used a combination of pore water pressure and volumetric water content. The transformations were performed by assuming a single-valued soil water characteristic curve, that is, hystersis is neglected. Both Equation 4.4a and 4.4b have been used in the geotechnical engineering extensively while equation 4.4c was only used in soil physics. Some people also use differential equation for heat transfer to describe

the moisture movements of water in soils because the Richard's equation is the same as heat transfer equation when the influence of gravity is neglected.

4.3.3 Mitchell's moisture diffusion equation

Although moisture flow in unsaturated soils is a viscous flow only through the pore space filled with water, yet it can be also visualized as a diffusion of suction or the negative pore water pressure through a porous media; this visualization introduced the term moisture diffusion in the world of unsaturated soil mechanics. Mitchell (1979) developed a simplified formulation of moisture diffusion by assuming the value of n in the Laliberte and Corey's (1967) permeability equation (Eq. 4.5) to be one. He formulated the diffusion equation using the Laliberte and Corey's (1967) permeability equation and mass balance equation for unsteady fluid flow. These assumptions were supported by experimentation and theoretical approach.

$$k = k_0 \left(\frac{u_{w0}}{u_w} \right)^n , u_w > u_{w0} \tag{4.5}$$

where:

u_{w0} = total suction of approximate 10 kPa (100 cms of water head)

n = positive constant, which for clay is close to 1, for sands is of the order of 4 or more

k_0= coefficient of saturated permeability (corresponding to a total suction is equal to10 kPa.)

Mitchell proposed two diffusion test having different boundary conditions named the drying test and wetting test. Mitchell used the relationship between permeability and matric suction formulated by Laliberte and Corey assuming n = 1, which gives the following permeability function Eq. 4.6.

$$k = k_0 \left(\frac{u_{w0}}{u_w} \right), u_w > u_{w0} \tag{4.6}$$

Also, Mitchell assumed that the water content is linearly related to the suction in terms of pF unit; the soil-water characteristic curve is expressed as,

$$w = C_w \log_{10}\left(u_a - u_w\right) + D \tag{4.7}$$

where:

C_w is slope of the soil water characteristic curve when it is plotted in a semi-log scale. Assuming that $U = \log_{10}\left(u_a - u_w\right)$,

In this way, Mitchell transformed the differential equation into linear equation and gave some analytic solutions for sinusoidal suction change at the soil surface.

$$\frac{\partial^2 U}{\partial x^2} + \frac{\partial^2 U}{\partial y^2} + \frac{\partial^2 U}{\partial z^2} = \frac{1}{\alpha}\frac{\partial U}{\partial x} \tag{4.8}$$

where:

U is the matric suction in pF units, and

α = diffusion coefficient for the soil, and

$\alpha = \dfrac{k_0 u_0}{0.4343 \dfrac{G_s}{1+e} C_w}$,. $\alpha = \dfrac{P\gamma_w}{\gamma_{dry} C_w}$, and $P = \dfrac{k_0 u_0}{0.4343}$ = unsaturated permeability

Mitchell (1979) proposed two different setups for the determination of diffusion coefficient. Two tests were namely wetting test and drying test. In both the tests diffusion coefficient is determined from the suction measurements made at varying distance and time. The experimental procedures have been briefly discussed below.

1) Drying test

The initial suction value of the soil sample was measured (U_0). The cylindrical sample was enclosed at one end and the sides with an impermeable membrane to avoid any loss or gain of moisture. The atmospheric suction (U_a) was also determined and the moisture was allowed to flow out from the open end. The suction was measured at different distances on the soil sample at different time intervals. The experimental setup has been shown in Fig. 4.1.

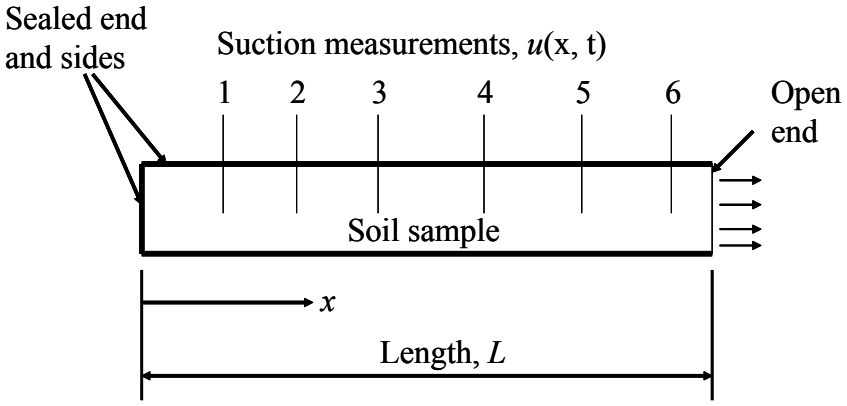

Fig. 4.1. Mitchell's drying test (after Mitchell, 1979).

Mitchell (1979) developed a closed form solution for the drying test using the Eq. 4.8 and the following boundary conditions:

Sealed boundary: $$\frac{\partial U(0,t)}{\partial x} = 0 \qquad (4.9a)$$

Open boundary: $$\frac{\partial U(L,t)}{\partial x} = -h_e\left[U(L,t) - U_a\right] \qquad (4.9b)$$

Initial suction: $U(x,0) = U_0$ (4.9c)

Solution of Eq. 4.8 using the boundary conditions Eq. 4.9 leads to the following equation:

$$U = U_a + \sum_{n=1}^{\infty} A_n \exp\left(-\frac{z_n^2 t\alpha}{L^2}\right)\cos\left(z_n \frac{x}{L}\right) \qquad (4.10)$$

where:

$$A_n = \frac{2(U_0 - U_a)\sin z_n}{z_n + \sin z_n \cos z_n},$$

z_n = solutions of the equation $\cot z_n = \dfrac{z_n}{h_e L}$

U = suction as function of distance and time

t = time

x = distance from closed end

L = total length of the soil sample

U_0 = initial suction of the soil sample

U_a = atmospheric suction

h_e = evaporation coefficient in cm^{-1}

2) Wetting test

For the wetting test, the soil sample of known initial suction was enclosed in a cylindrical container allowing change in moisture only for one end. The open end was exposed to a liquid of known suction (U_1) for 4 days. Then the suction was measured along the length of the sample at different time intervals. The experimental setup is shown in Fig. 4.2.

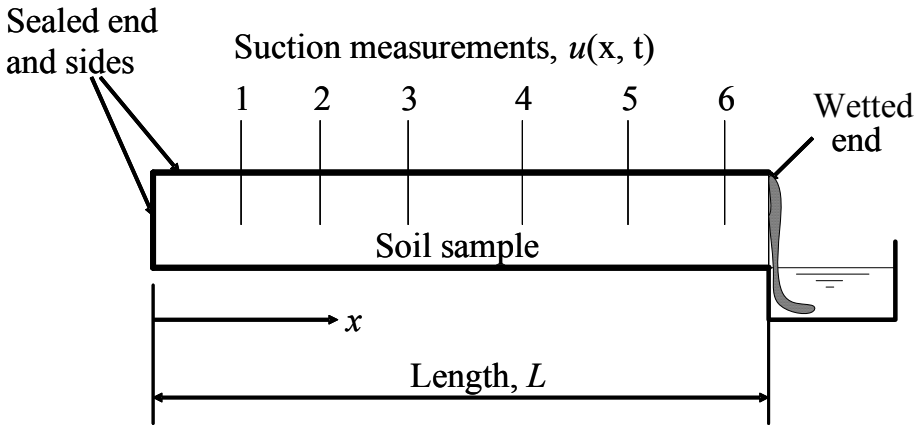

Fig. 4.2. Mitchell's wetting test (after Mitchell, 1979).

Mitchell (1979) developed a closed form solution for the drying test using the Eq. 4.8 and the following boundary conditions:

Sealed boundary: $$\frac{\partial U(0,t)}{\partial x} = 0 \qquad (4.11a)$$

Open boundary: $$U(L,t) = U_1 \qquad (4.11b)$$

Initial suction: $U(x,0) = U_0$ (4.11c)

Solution of Eq. 4.8 using the boundary conditions Eq. 4.11 leads to the following equation:

$$U = U_1 + \frac{4(U_1 - U_0)}{\pi}\sum_{n=1}^{\infty}\frac{(-1)^n}{2n-1}\exp\left(-\frac{(2n-1)^2\pi^2 t\alpha}{4L^2}\right)\cos\frac{(2n-1)-x}{2L} \qquad (4.12)$$

Where:

U = suction as function of distance and time

t = time

x = distance from closed end

L = total length of the soil sample

U_0 = initial suction of the soil sample

U_1 = suction of the liquid

The advantage of Mitchell's equation is that it transforms the nonlinear equation into linear equation, which allows developing closed form solutions for different problems, and also allows using flow net technique to solve many different problems.

4.4 New technique to determine the coefficient of unsaturated diffusivity

4.4.1 Main idea

There is a strong similarity between the partial differential equations that govern both the unsaturated diffusion, (Eq. 4.13a), and the consolidation phenomena, (Eq. 4.13b). This research proposes to take the advantage of this similarity to determine α in the laboratory in a similar way to c_v laboratory determination. The main advantage is that: c_v determination procedure is based on measuring soil sample volume changes with time. Consequently the conventional sophisticated suction measurements will be replaced with simple volume measurements to determine α. Moreover, the geotechnical practitioners are very familiar with the consolidation test, which will promote their acceptance and usage of this new technique.

$$\frac{\partial U}{\partial t} = \alpha \frac{\partial^2 U}{\partial z^2} \qquad U = \log_{10} |u_w| \qquad \text{(4.13a)}$$

$$\frac{\partial u_w}{\partial t} = c_v \frac{\partial^2 u_w}{\partial z^2} \qquad \text{(4.13b)}$$

where:

u_w = the pore water pressure

c_v = the coefficient of consolidation

t = the time.

Also we can see, there are close similarities between the coupled thermal stress problem and the coupled consolidation theory for unsaturated soils. The thermodynamic analogue to process of consolidation was first proposed by K. Terzaghi to facilitate the visualization of the mechanics of consolidation and swelling. The continuity equation for the water phase is similar to that for heat transfer. Terzaghi (1943) stated that "If we assume γ_w =1", the differential equation of Terzaghi's consolidation theory "becomes identical with the differential equation for the non-stationary, one-dimensional flow of heat through isotropic bodies, proved we assign the symbols in the equation the following physical meanings (Table 4.1).

Table 4.1. Thermodynamic analogues to the process of consolidation (after Zhang, 2004).

Theory of consolidation	symbol	Units	Thermodynamics
Excess hydraulic pressure	u	kPa	Temperature
Time	t	Sec.	Time
Coefficient of permeability	k	m/sec	Coefficient of heat conductivity
Coefficient of volume change	$\alpha_v / (1+e_0)$	kPa^{-1}	Heat capacity times unit weight
Coefficient of consolidation or swelling	c_v	m^2/sec	Diffusivity

c_v determination requires applying mechanical stress on the soil sample, which will squeeze the water out of the soil allowing the mobilized pore water pressure to diffuse

by time; the proposed technique will expose the soil sample to the atmospheric suction, which will draw the moisture out of the soil allowing the soil suction to change by time. That means, the consolidation process for c_v determination will be replace by a shrinkage process for α determination (I'll refer to the new technique with the α-shrink test).

Yet, to determine α based on measuring volume change with time in a similar way to c_v determination, we have to over come some difficulties such as: c_v determination takes place during a one dimensional consolidation process, However, we can't avoid the lateral shrinkage consequently will have a two-dimensional axi-symmetric shrinkage test. That means we can not use the same T_v design charts as they were derived based on a closed form solution of the on dimensional consolidation problem. Another difficulty with the α-shrink test is the development of cracks in the soil, which affects the accuracy of volume change measurements.

4.4.2 Mathematical expression for 2D axi-symmetric diffusion problem

Fig. 4.3 sketches the α-shrink test showing dimensions and boundary conditions. The partial differential equation that governs the suction diffusion in the α-shrink test is the cylindrical coordinates form of Eq. 4.8., which is given by Eq. 4.14.

$$\frac{\partial^2 U}{\partial r^2} + \frac{1}{r}\frac{\partial U}{\partial r} + \frac{\partial^2 U}{\partial z^2} = \frac{1}{\alpha}\frac{\partial U}{\partial t} \tag{4.14}$$

where:

U is the matric suction in pF units, and

α = diffusion coefficient for the soil, and

t = time

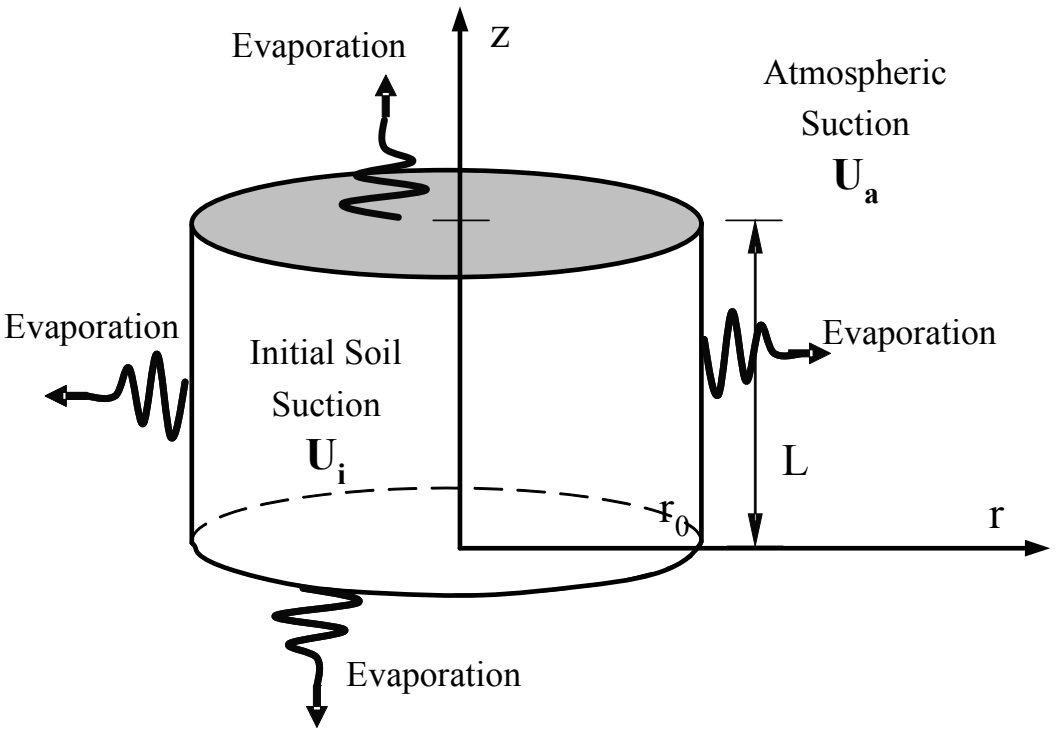

Fig. 4.3. Sketch of the α-shrink test.

The boundary conditions of the α-shrink test are given by Eq. 4.15.

Perimeter boundary surface:	$U(r_0, z, t) = U_a$	(4.15a)
Bottom boundary surface:	$U(r, 0, t) = U_a$	(4.15b)
Top boundary surface:	$U(r, L, t) = U_a$	(4.15c)
Initial conditions:	$U(r, z, 0) = U_i$	(4.15d)

It may be observed that the boundary conditions at the soil sample surface (Eqs. 4.15a, 4.15b, & 4.15c) are not the same as what was used in Mitchell's drying test (Eq. 4.9b); careful investigation of the thermodynamics of soil moisture reveals that Eq. 4.9b violates the soil thermodynamics rule of equilibrium of free energy, as it requires that $U(L,t) \neq U_a$ during evaporation process. Soil thermodynamics refers to the soil suction as the free energy (pressure can be visualize as energy per unit volume and

having the same units). Edlefson and Anderson (1943) is their analysis to the problem of the equilibrium of a vapor with the liquid through a curved vapor-liquid interface; the curved vapor-liquid interface resembles the contractile skin that separates the soil water from the atmospheric vapor. Edlefson and Anderson (1943) stated that "The water in the dish (the meniscus of the contractile skin membrane) is in equilibrium with its vapor; their free energies must be the same". Edlefson and Anderson (1943) analysis justifies the proposed boundary conditions at the soil sample surface given by (Eqs. 4.15a, 4.15b, & 4.15c)

$$\Delta f_L = \Delta f_v \tag{4.16}$$

where:

Δf_L is the free energy of the liquid = the matric suction (u_a-u_w), and

Δf_v is the free energy of the vapor = the atmospheric suction Eq. 4.1.

Taking the advantage of the similarity between Mitchell's diffusion equation and head transfer diffusion equation, the research proposes using a closed form solution of a heat transfer problem similar to the 2D axi-symmetric suction diffusion problem**.** Glen Myers (1971) derived a solution for the transient heat transfer problem of a short cylinder initially at a uniform temperature subjected to a step change in surface temperature. Hence, the solution of the Eq. 4.14 for the boundary conditions 4.15, which assumes a uniform initial suction in the soil sample and constant atmospheric suction, is given by Eq. 4.17.

$$U(r,z,t) = U_a + R(r,t)Z(z,t) \qquad (4.17a)$$

$$R(r,t) = 2(U_i - U_a)\sum_{m=1}^{\infty} \frac{J_0(\lambda_m r)e^{-[\lambda_m r_0]^2 \alpha t / r_0^2}}{(\lambda_m r_0)J_1(\lambda_m r_0)} \qquad (4.17b)$$

$$Z(r,t) = \frac{4}{\pi}\sum_{m=1}^{\infty} \frac{\sin[(2n+1)\pi z/L]}{2n+1} e^{-(2n+1)^2 \pi^2 \alpha t / L^2} \qquad (4.17c)$$

where:

λ_m satisfy $J_0(\lambda_m r_0)$

$J_0(x)$ is the Bessel function of the first kind and order zero

$J_1(x)$ is the Bessel function of the first kind and order one

4.4.3 T_v charts for 2D axi-symmetric diffusion problem

In a similar way to the one dimensional consolidation time factor charts, this section will develop time charts for two dimensional axi-symmetric diffusion problem for α-shrink test. Firstly, the percentage diffusion, similar to percentage consolidation, is defined as given in Eq. 4.18. Then, the time factor, T_v, is defined as given in Eq. 4.19.

$$\%Diffusion(t) = \frac{\sum_{z=0}^{z=L}\sum_{r=0}^{r=r_0}\Delta U(r,z,t)r \Big/ \sum_{r=0}^{r=r_0} r}{\sum_{z=0}^{z=L}\sum_{r=0}^{r=r_0}\Delta U(r,z,\infty)r \Big/ \sum_{r=0}^{r=r_0} r} \qquad (4.18)$$

where:

$\Delta U(r, z, t)$= the change of suction value at time t $= U(r, z, t) - U(r, z, 0)$

$\Delta U(r, z, \infty)$ = the suction value at time $\infty = U(r, z, \infty) - U(r, z, 0t)$

It is known that $U = \varepsilon_v / \gamma$; where ε_v is the volumetric stain and γ is the slope of the middle linear portion of the SWCC expressed as ε_v versus U as shown in Fig. 4.4.

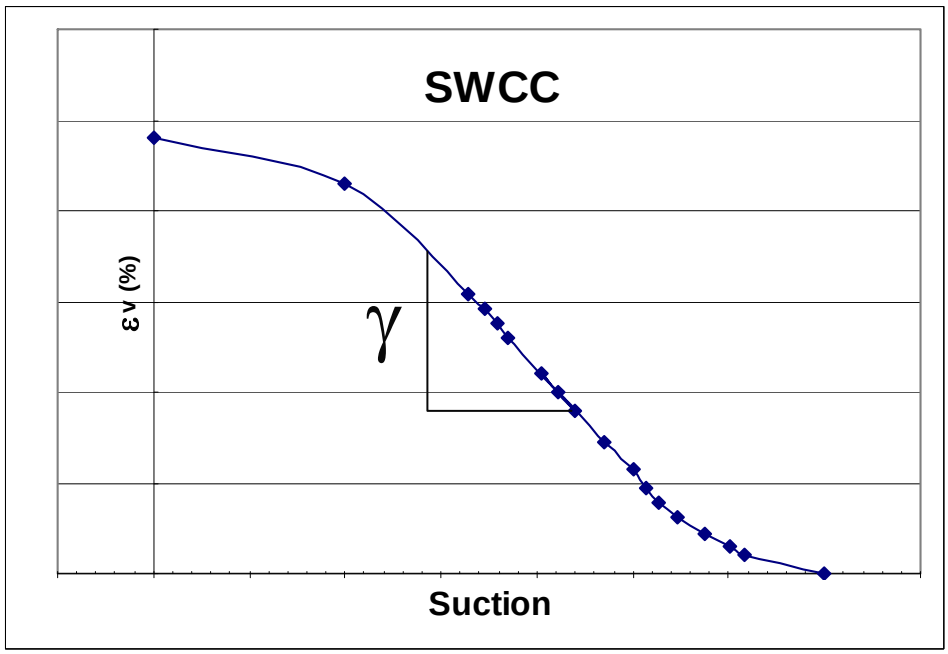

Fig. 4.4. Typical SWCC expressed as ε_v versus U.

It is recommended that the α-shrink test takes place during the the middle linear portion of the SWCC, at which γ is constant. Hence, we can use the relationship:

$$\Delta U = \Delta\varepsilon_v / \gamma \tag{4.19}$$

Substituting Eq. 4.19 in Eq. 4.18 will give Eq. 4.20

$$\%Diffusion(t) = \frac{\Delta V_t}{\Delta V_{final}} \tag{4.20}$$

where:

ΔV_t = change of the total sample volume at time t = $V_t - V_o$

ΔV_{final} = change of the total sample volume at time t = $V_{final} - V_o$

V_0 = initial total sample volume

Eq. 4.21 defines the α-shrink time factor, a dimensionless quantity, in a similar way to the consolidation test time factor.

$$T_{v(\%diffusion)} = \frac{\alpha t_{(\%diffusion)}}{L_D^2} \tag{4.21}$$

where:

α is the coefficient of unsaturated diffusivity (L^2T^{-1})

t is the time (T)

L_D is a characteristic diffusion length (L)

L_D = L (for single diffusion; evaporation takes place only on perimeter and top surfaces)

L_D = L/2 (for double diffusion; evaporation takes place on perimeter, top, and bottom surfaces)

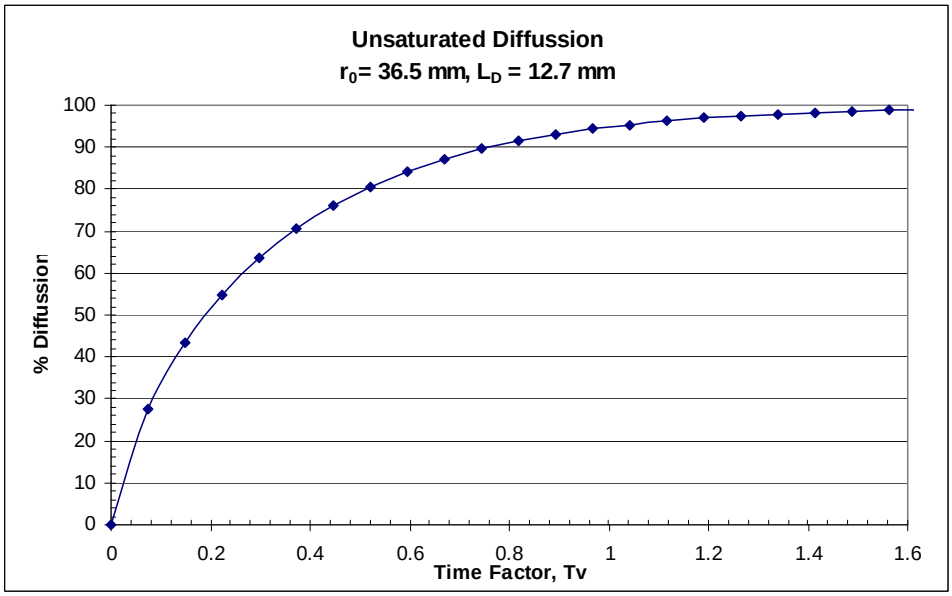

Fig. 4.5. A typical time factor chart.

Fig. 4.5 shows a typical time factor chart for a sample with radius, r_0 of 36.5 mm, L_D = 12.7 mm, α = 0.005 cm^2/min, U_i = 2.5 pF, and U_a = 5.97 pF. To develop a time factor chart, the following steps should be followed:

1) Assume problem parameters: α, L_D, r_0, U_i, and U_a.

2) Discretize the 2D axi-symmetric plane (L_D, r_0) into finite elements.
3) Calculate the suction value at all grid nodes for all time steps using Eq. 4.17.
4) Calculate % diffusion at all time steps using Eq. 4.18.
5) Calculate corresponding time factors at all time steps using Eq. 4.21.
6) Plot % diffusion versus corresponding time factors.

4.4.4 Factors influencing T_v charts

Similarly to consolidation test time factor charts, the α-shrink test time charts are independent of initial and atmospheric suction values and the coefficient of unsaturated diffusivity, α and this is can be imputed to the linearity of the problem. However, having the α-shrink test as a 2D axi-symmetric problem instead of 1D in consolidation test may get the sample size and proportions to influence the time factors charts.

a) influence of sample size:

To examine the influence of sample size on time factor charts, three samples sizes have been chosen; the three samples have the same, α (= 0.005 cm^2/min), U_i (= 2.5 pF), U_a (= 5.97 pF), and aspect ratio (r_o/L_D = 2.874). Yet, the samples radii, r_0 were 73, 36.5, and 18.25 mm, and the characteristic diffusion lengths, L_D were 25.4, 12.7, and 6.35 mm respectively. Fig. 4.6 shows that the T_v charts are independent of the sample size for the same aspect ratio; the three curves are identical in Fig. 4.6

b) influence of sample proportions (aspect ratio r_o/L_D):

To examine the influence of sample proportions on time factor charts, six samples sizes have been chosen; the six samples have the same, α (= 0.005 cm^2/min), U_i (= 2.5 pF), U_a (= 5.97 pF), and radius r_0 = 36.5 mm. Yet, the samples characteristic diffusion lengths, L_D were 12.7, 19.05, 25.4, 38.1, 76.2, and 152.4 mm, and the corresponding aspect ratios r_o/L_D were 2.874, 1.916, 1.437, 0.958, 0.479 and 0.240 respectively. Fig. 4.7 shows the T_v charts for the six samples. It is shown that the smaller the aspect ratio

r_o/L_D the steeper is the slope of the % diffusion versus time factor curve. And since the maximum % diffusion equal = 100% for all aspect ratios, it can be visualized that the larger the aspect ratio r_o/L_D the smother the curvature of the % diffusion versus time factor curve (i.e. the larger the radius of curvature).

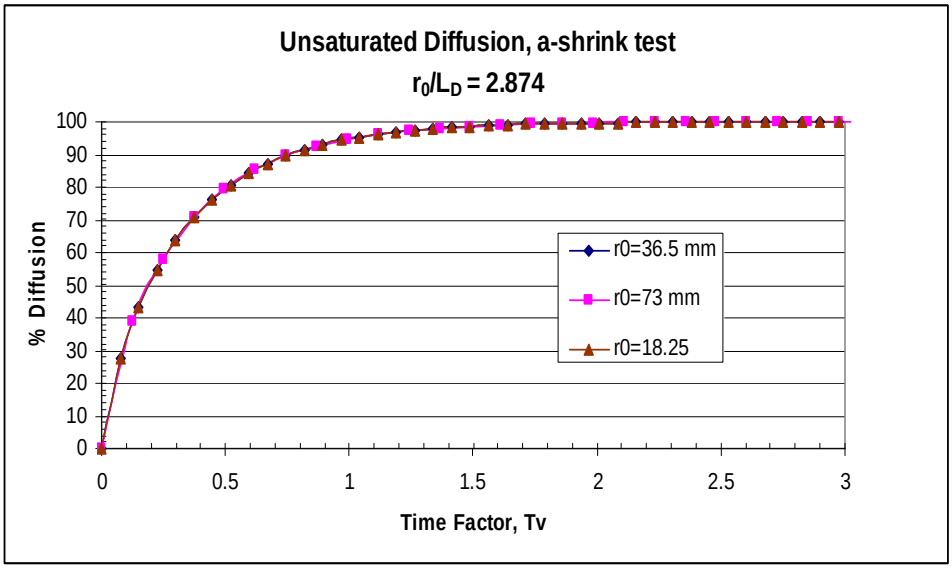

Fig. 4.6. Influence of the sample size on T_v charts.

4.4.5 Procedure and data reduction of α-shrink test

Similarly to consolidation test procedure, the α-shrink test procedure can be summarized as follows:

1) Prepare a perfectly right short cylindrical soil samples; using a metal ring or tube as a trimming guide is preferable to help obtaining the right cylinder. The following section will recommend the sample dimensions to be 63.5 mm (2.5 inches) in diameter and 19.05 mm (0.75 inches) in height, and also recommends using the conventional consolidation metal ring a trimming guide.

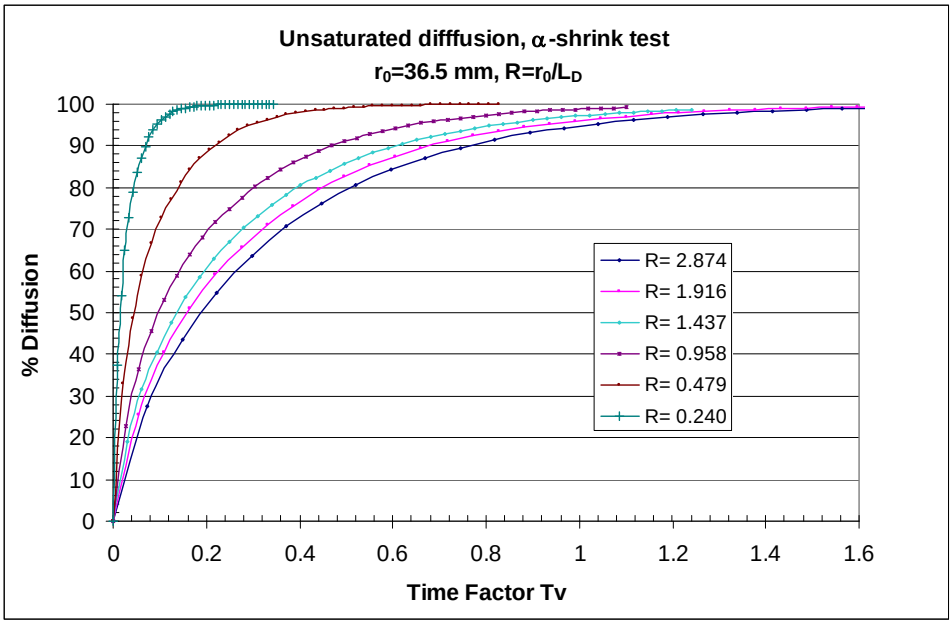

Fig. 4.7. Influence of the sample proportions on T_v charts.

2) Mark the perimeter of the soil samples top surface three marks at equal perimeter length, (i.e. the three radii connecting the center of the top center to each mark divide the circular surface into three identical sectors with apex angle = 120˚ as shown in Fig. 4.8.
3) Using a caliper, measure the initial diameters; D1 = Aa, D2 = Bb, and D3 = Cc, and also measure the initial heights; H1 = AA', H2 = BB', and D3 = CC'.
4) Record the time as the starting time of the test or, in case of using a stop watch, set it to start timing your test. It is very important to minimize the time of all previous steps as soil samples start to lose moisture once get exposed to the ambient suction.
5) Redo step 3 at different time steps with recording the total elapsed time; it is preferable (not a must) to take dimension measurements at a constant time intervals of one to two hours for the first 12 hours, then time intervals of 12 to 24 hours.

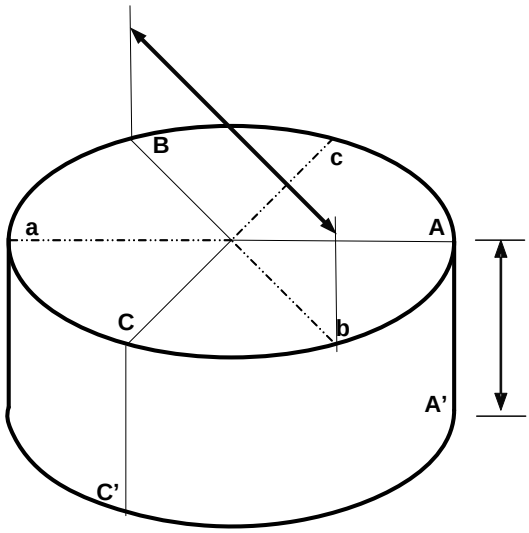

Fig. 4.8. Preparing the soil sample for α-shrink test.

6) Taking dimensions measurements should take place until the soil stops shrinking. The end of shrinkage can easily be figured out by observing the dimension measurements.
7) Carry out data reduction as follows:
    a. Calculate the average sample diameter, D_{ave} = (D1+D2+D3)/3, at each time step.
    b. Calculate the average sample height, H_{ave} = (D1+D2+D3)/3, at each time step.
    c. Calculate the sample volume, $V = H_{ave} (\pi D_{ave}^2)/4$, at each time step.
    d. Calculate the change of volume, $\Delta V = V - V_{initial}$, at each time step.
    e. Calculate the final change of volume, $\Delta V_{final} = V_{final} - V_{initial}$,
    f. Calculate the percentage diffusion, $= \Delta V / \Delta V_{final}$, at each time step.
    g. Using Fig. 4.7., calculate the time factor corresponding to the %diffusion at each time step.
    h. Knowing the time and the time factor at each time step, calculate the coefficient of unsaturated diffusivity, α, from Eq. 4.21.

i. Take the average of α calculated in step (h); the following section recommends discarding αs that correspond to %diffusion less than 20% and greater than 80%.

4.4.6 Optimum sample size dimensions for α-shrink test

Fig. 4.7 solved one of the α-shrink test difficulties by providing time factor charts for different aspect ratios. This means that, theoretically, the α-shrink test can be done for any sample dimensions. Yet practically, the development of cracks in the soil upon shrinkage affects the accuracy of volume change measurements significantly. The a-shrink test monitors changes of the outer dimensions upon shrinkage; cracks development gets the soil sample to shrink internally, which we can not measure. Consequently, cracks development overestimated the sample volume and under estimates its change in volume introducing a noticeable error in calculating α. Moreover, crack existence changes the problem boundary conditions as it introduces many other evaporative surfaces. It was noticed, during many shrink tests, that small samples develop less cracks than large samples. Yet, the error in measured volume increases with the decrease of initial sample size.

The α-shrink test data reduction gives a for each volume measurement, which theoretically should give the same value; a good α-shrink test gives the minimum coefficient of variation or minimum scattering of data point around the average value.

Cracks development is not the only factor that contributes to scattering of α values; sand and sits presence besides nonlinearity in the SWCC at high suction values contribute as well. The linearity in Mitchell's diffusion equation was based on Mitchell's assumption of using n=1 in Eq. 4.5, which is typical for clay, yet the coarser the soil the farther we deviate from this assumption. Also, it was assumed that the slope of the SWCC, γ, is constant during the α-shrink test, yet typical room atmospheric suction ranges from 5.5 to 6.2 pF, which usually falls in the curved portion of the SWCC causing this assumption not to be perfectly valid during the α-shrink test.

To find out the optimum sample size, five samples of the same soil but different sizes were used to determine α. The soil was composed of a 20% bentonite clay and 80% porcelain clay. The identification properties of this soil will be shown in section 4.7, the dimensions (Diameter X Height) of the five samples were 3X3, 3X2, 3X1.5, 2.5X0.75, and 1.5X1.0 inches; note that 2.5X0.75 inches is the size of the conventional consolidation soil sample. The testing procedure was followed as mentioned in section 4.4.5. The sample 2.5X 0.75 inches was trimmed using the conventional consolidation ring as a trimming guide similarly to consolidation test sample preparation, the rest of the samples were trimmed using a trimmer setup usually used to prepare unconfined compression test samples.

Fig. 4.9 shows the results of the five α-shrink tests; it is clear that the scattering of the α values increases when % diffusion is less than 20% and more than 80%. Moreover, sample 2.5X 0.75 inches has the minimum scattering around its average value as its size compromises between cracks development and volume measurements errors.

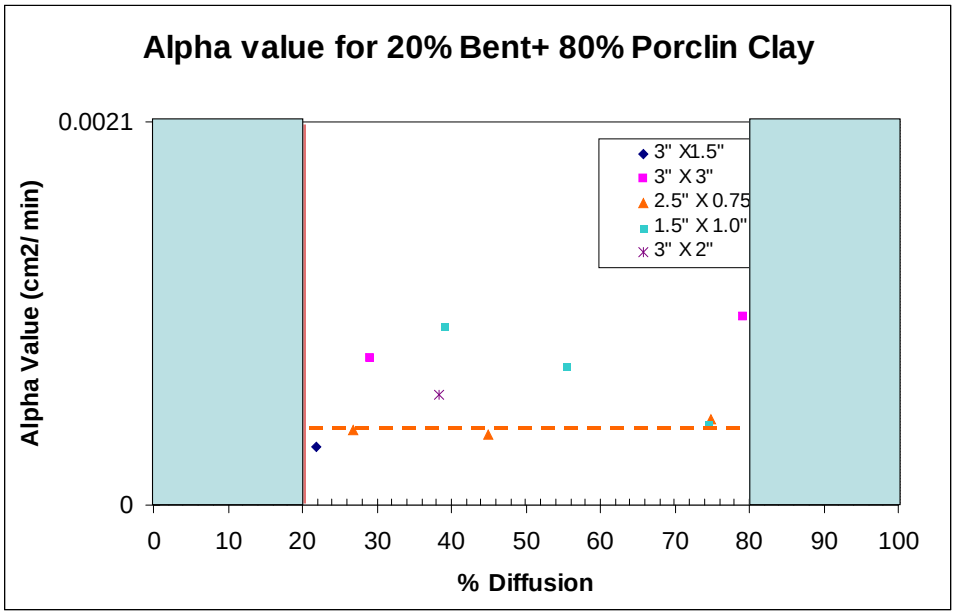

Fig. 4.9. Results of the five α-shrink tests.

4.5 New technique to address cracks network influence on the coefficient of unsaturated diffusivity at field

4.5.1 Cracks networks

Soil cracks networks may be considered as the biggest stumbling block in modeling moisture diffusion through unsaturated shrink-swell soils, macro-scale diffusion takes place through cracks network in addition to the micro-scale diffusion through the intact soil masses. Moreover, it is difficult to either map the cracks networks experimentally or model their development and distribution theoretically. However, ignoring them by assuming that a $\alpha_{field} = \alpha_{lab}$ decreases α_{field} by roughly one to two orders of magnitudes.

Knight (1972) observed that crack depth in soils approximately equals crack spacing. Aubeny & Lytton (2004) used Knight (1972) study findings to assume a staggered pattern of soil cracking with crack depth is equal to crack spacing. Aubeny & Lytton (2004) postulated that the rate of moisture transmission along cracks is much more rapid than through intact soil, consequently they assumed that suction on the surface of the cracks equals the suction at the free surface. Aubeny & Lytton (2004) evaluated their proposed moisture diffusion model in light of 34 documented shallow slide failures in embankments constructed using Texas high plasticity clays.

4.5.2 Proposed technique to estimate α_{field} numerically

This research proposes to extend the usage of Aubeny & Lytton (2004) diffusion model in unsaturated cracked soils for shallow foundations to find the coefficient of unsaturated diffusivity at field as follows:

1) Carrying out 2D finite element plane stain moisture diffusion analyses for a field having a network of cracks as shown in Fig. 4.10 (a) applying a sinusoidal surface suction variation for a one year time period. The sinusoidal surface suction variation resembles the soil surface suction changes due to cyclic weather effects.
2) Calculating the average suction profile (suction values with depth) at each time step.

3) Finding the maximum and minimum suction values with depth for the one year period, which will form the bounding suction envelops.
4) Back-calculating the field coefficient of unsaturated diffusivity using curve fitting techniques of the suction envelope.
5) Carrying out a parametric study with different intact coefficient of unsaturated diffusivities, different ratios of crack depths to active moisture zone depths in order to develop a design chart relating α_{field} to α_{lab}.

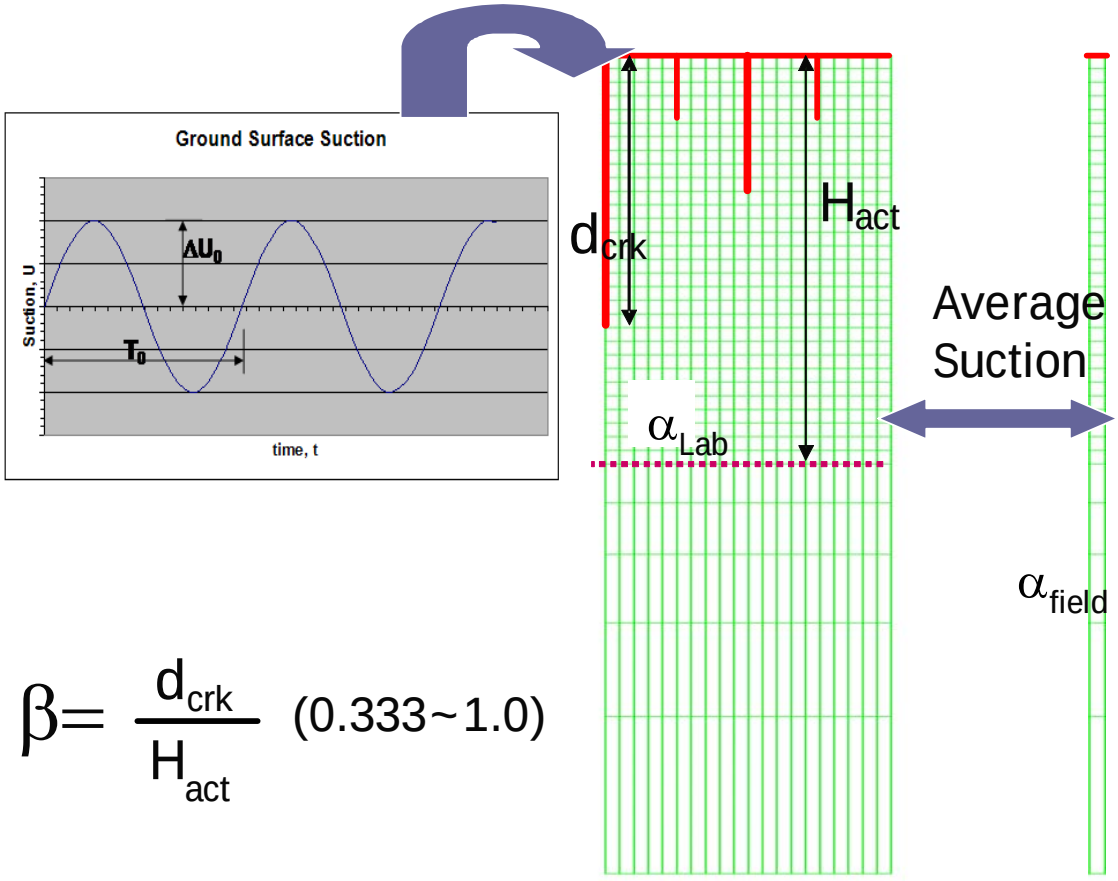

Fig. 4.10a. Finite element plain stain moisture diffusion analyses for cracked soil.

4.5.3 Factors influencing the numerically estimated α_{field}

To address all factors influencing α_{field}, it is important to do a dimensional analysis including all parameters involved in this problem, which are: α_{field}, α_{lab}, d_{crk}, H_{act}, T_0, ΔU_0, and cracks pattern. Simple dimensional analysis of all these parameters gives Eq. 4.22

$$\frac{\alpha_{field}}{\alpha_{lab}} = f\left(\Delta U_0, \beta, \frac{\alpha_{lab} T_0}{H_{act}}\right) \tag{4.22}$$

The ratio $\frac{\alpha_{field}}{\alpha_{lab}}$ will be denoted by the cracked soil diffusion factor, F_{CrkDif} .

Before carrying out a parametric study, the sensitivity of the F_{CrkDif} to crack pattern and ΔU_0 will be examined.

a) Amplitude of surface suction change, ΔU_0

Maximum anticipated ΔU_0 =1 pF (knowing that the wilting point suction is less than 4.5 pF and the field capacity suction is about 2.5 pF). To asses the influence of this factor on cracked soil diffusion factor, F_{CrkDif} , two simulations were carried out using the same parameters $\beta, \frac{\alpha_{lab} T_0}{H_{act}}$ considering secondary cracks ; β = 0.6667, α_{lab} = 14.4 cm^2/day, T_0 = 365 days, and H_{act} = 360 cm. Yet the first simulation has ΔU_0 =1 pF, and the second has ΔU_0 =0.5 pF. Details of these finite element simulations will be mentioned in the following section.

The resulting F_{CrkDif} were 19.59, and 19.25 for ΔU_0 = 1 and 0.5 pF respectively. This means for these two simulations, reducing ΔU_0 by 50% reduced F_{CrkDif} by only 1.74%, which is negligible.

b) Crack pattern:

What level of crack pattern should be considered in the numerical model? This question should be answered before carrying out the parametric study as we can consider only primary, up to secondary, up to tertiary, or may be up to a higher level of cracking. And this choice will affect the resulting F_{CrkDif} . To assess this factor, three simulations

were carried out using the same parameters $\Delta U_0, \beta, \frac{\alpha_{lab} T_0}{H_{act}}$; $\Delta U_0 = 1$, $\beta = 0.6667$, $\alpha_{lab} = 14.4\ cm^2/day$, $T_0 = 365$ days, and $H_{act} = 360$ cm. Yet the first simulation considered only the primary crack, the second one considered up to the secondary cracks, and the third one considered up to the tertiary cracks. Details of these finite element simulations will be mentioned in the following section as well.

The resulting cracked soil diffusion factor, F_{CrkDif} from these three simulations is presented in Fig. 4.10 (b).

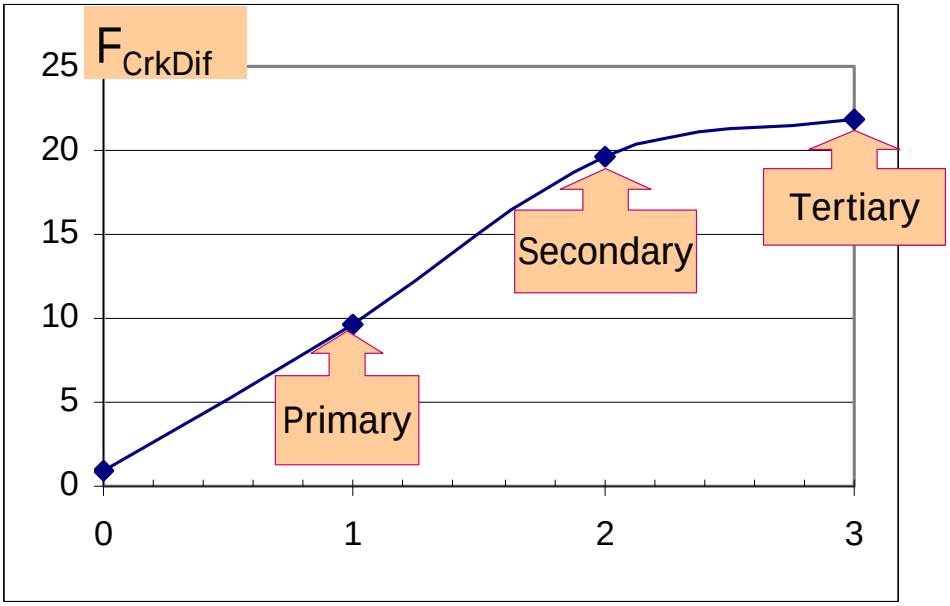

Fig. 4.10b. Cracked soil diffusion factor, F_{CrkDif} for different cracking patterns.

By definition, $F_{CrkDif} = 1$ when there is no cracks at all, the resulting F_{CrkDif} were 9.56, 19.59, and 21.87 for primary, secondary, tertiary simulations respectively. It is obvious that increasing the considered cracking level increases F_{CrkDif} , as we add more cracks to the system, which promote diffusion through the soil mass. Considering secondary cracks approximately doubled F_{CrkDif} obtained by considering only primary

cracks. However, considering tertiary cracks increased F_{CrkDif} obtained by considering secondary cracks by only 11.6%. Increasing the considered crack level beyond this will slightly increase F_{CrkDif} . And since increasing the considered crack level is costly, from the computational time consuming point of view, the research will consider cracks pattern consists of cracks up to the tertiary cracks as shown in Fig. 4.10 (b).

4.5.4 Numerical modeling

The finite elements comprehensive software package, ABAQUS/STANDARD, was used to for suction diffusion simulations, which is analogous to the thermal diffusion phenomena in heat transfer. This strong enabled us to use available thermal diffusion software packages, existed in ABAQUS/STANDARD, to do suction diffusion simulations. Zhang (2004) successfully used this technique to carry out coupled suction diffusion-stress displacement analysis, and he presented symbols comparison table as shown in Table 4.2. The ABAQUS/STANDARD coupled thermal stress displacement analysis can also be used for the uncoupled thermal diffusion problems and also for the uncoupled stress displacement problems.

The material properties were: Density = 1.6315 g/cm^3 (16 kN/m^3), slope of SWCC (expressed as gravimetric water content versus suction), C_w = 0.1 (equivalent to specific heat), coefficient of unsaturated permeability, P = 2.3496 cm^2/day (equivalent to coefficient of thermal conductivity). Recall that, the coefficient of unsaturated diffusivity, $\alpha = \frac{P\gamma_w}{\gamma_{dry} C_w}$, which gives α=14.4 cm^2/day.

Fig. 4.11 shows the geometry of the problem; H_{act} was equal to 360 cm for all the simulations, $d_{Crk} = \beta.H_{act}$, β = 0.667 for primary and secondary cracks simulations and β = 0.5, 0.667, and 0.8 for tertiary cracks simulations. This problem is a 2D plane strain problem; the ABAQUS/STANDARD CPE4T "Continuum Plain Strain 4-nodes Temperature" element was chosen in the simulation.

The initial conditions was a constant suction value of 3.5 pF (equivalent to T= -3.5 C˚). The boundary conditions were: the bottom boundary has a constant suction value of

3.5 pF (equivalent to T= -3.5 C°), the right side boundary and the left side boundary, except the crack portion, has no flux, and the top boundary and cracks (drawn in red color in Fig. 4.11) has a sinusoidal function, $U = -3.5 + \Delta U_0 \sin\left(\frac{2\pi t}{365}\right)$, for the suction values during the one year simulation; where: t is time in days and ΔU_0 =1.0.

Table 4.2. The Comparisons in symbols between the coupled consolidation theory and the coupled thermal stress problem (after Zhang, 2004).

	Coupled Consolidation Theory		**Coupled Thermal Stress Problem**	
	Physical Meaning	Symbol	Physical Meaning	Symbol
Mechanical	Stress	σ–u_a	Stress	σ
	Strain	ε	Strain	ε
	Displacement	*u, v, w*	Displacement	*u, v, w*
	Young's Modulus	E	Young's Modulus	E
	Poisson's Ratio	μ	Poisson's Ratio	μ
	Coefficient of Expansion due to Water Pressure Variation	α	Coefficient of Expansion due to Temperature Variation	α
Thermodynamic (or, Water Phase Continuity)	Coefficient of permeability	k	Coefficient of conductivity	k
	Specific Water Capacity	C_w	Specific Heat Capacity	CT
	Dry Unit Density	ρ_d	Density	ρ
	Volumetric Water Content Variation	$-m_1^w \frac{\partial(\sigma_m - u_a)}{\partial t}$	Heat Generation	S
	Time	t	Time	t

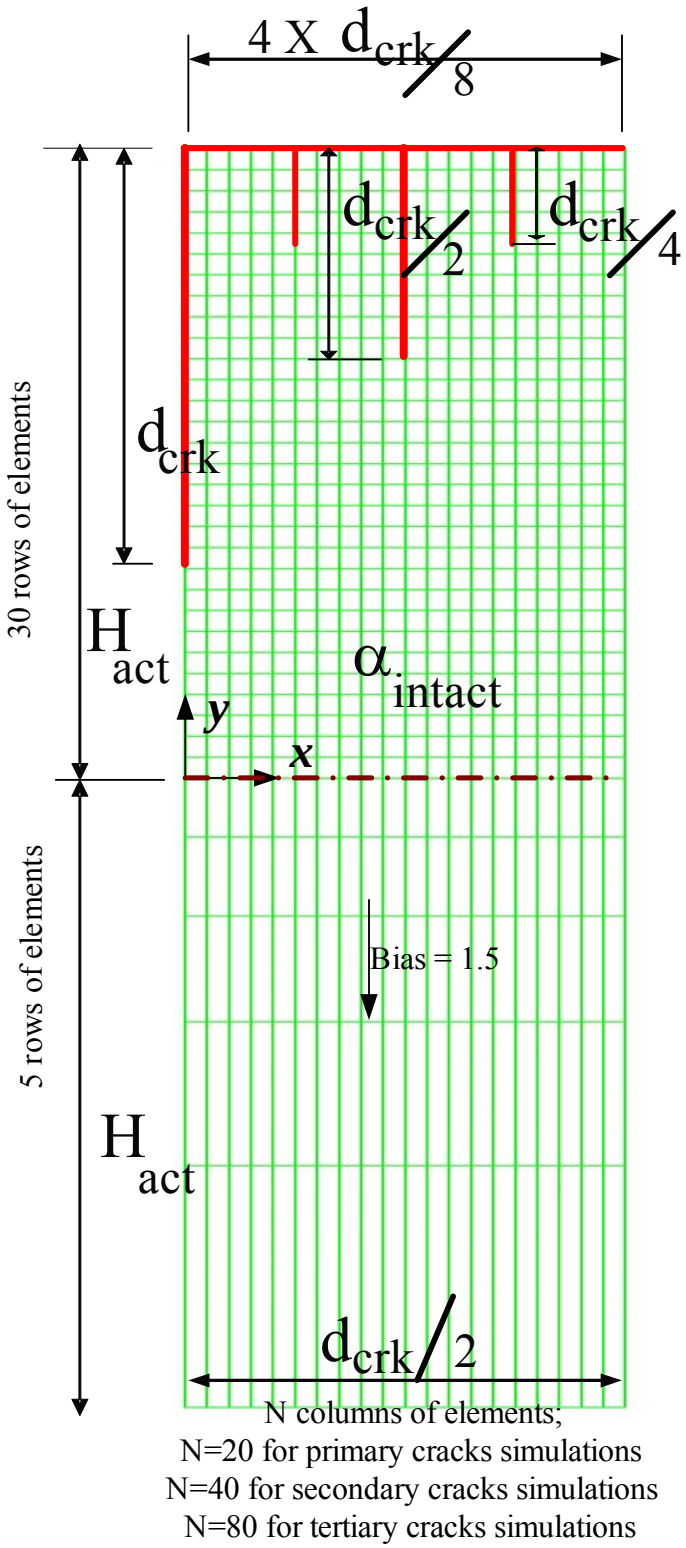

Fig. 4.11. Model used for finite element simulation.

Appendix C presents the ABAQUS/STANDARD input files for these simulations.

At each time step, the average suction values with depth were calculated (i.e., taking the average of all suction value having the same y-coordinate at each depth). Fig. 4.12 shows the resulting suction profiles from a one year simulation of suction diffusion in a soil mass with a primary crack pattern.

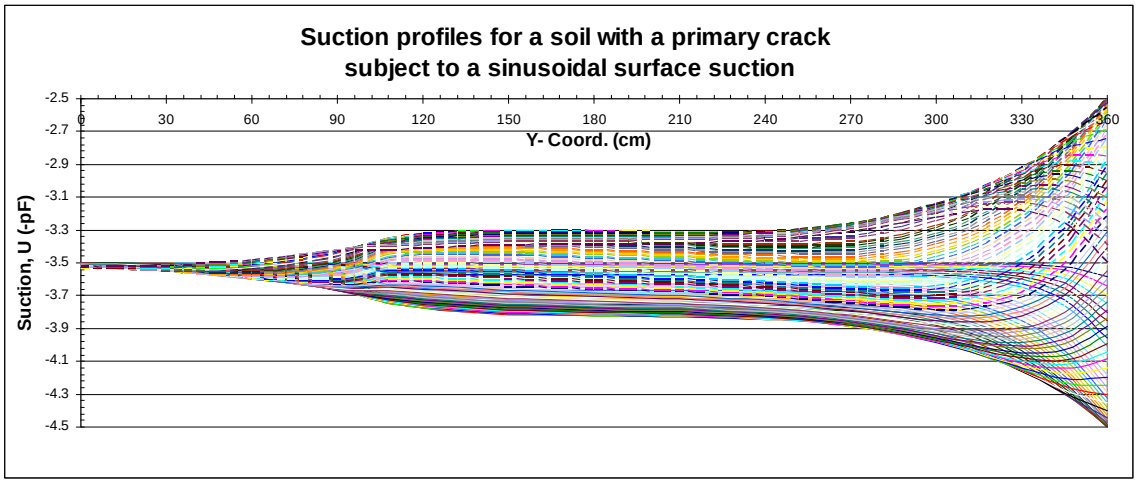

Fig. 4.12. Suction envelopes for a soil with a primary crack pattern.

Mitchell (1979) derived a closed form solution for the intact soil mass, (i.e., without any cracks), subject to sinusoidal surface suction change. Eq. 4.23 gives the transient suction value with depth for this problem derived by Mitchell (1979),

$$U(y,t) = U_i + \Delta U_0 \exp\left(-\sqrt{\frac{\omega}{2\alpha}}\right)\cos\left(\omega t - \sqrt{\frac{\omega}{2\alpha}}y\right) \qquad (4.23)$$

where:

ω is the frequency of surface suction change cycles $=2\pi / T_0$

Since the main objective of this research is to develop a design procedure, the bounding suction envelops are of great importance as they will be bases of the soil mound shape equations, which will be discussed in detail in Chapter VI. The suction envelops for Eq.

4.23 can be derived by finding the minimum and maximum suction values at by depth as follows:

Find the first derivative with respect with time for Eq. 4.23

$$\frac{dU(y,t)}{dt} = \Delta U_0 \exp\left(-\sqrt{\frac{\omega}{2\alpha}}\right)\left[-\omega \sin\left(\omega t - \sqrt{\frac{\omega}{2\alpha}} y\right)\right] \tag{4.24}$$

At maximum and minimum values $\frac{dU(y,t)}{dt} = 0 \Rightarrow \sin\left(\omega t - \sqrt{\frac{\omega}{2\alpha}} y\right) = 0$

$\Rightarrow \cos\left(\omega t - \sqrt{\frac{\omega}{2\alpha}} y\right) = \pm 1$, and substituting in Eq. 4.23

$$U_{envelop}(y) = U_i \pm \Delta U_0 \exp\left(-\sqrt{\frac{\omega}{2\alpha}}\right) \tag{4.25}$$

The absolute of the difference between the minimum suction envelop or the maximum suction envelop and initial suction value will be

$$\Delta U(y) = \Delta U_0 \exp\left(-\sqrt{\frac{\omega}{2\alpha}}\right) \tag{4.26}$$

Using Eq. 4.25 and the suction envelops calculated from the FE simulation, a curve fitting using the least square error technique was implemented to estimate the α_{feild} value, (i.e., varying α in Eq. 4.25 to fit a curve that gives the best matching to the FE simulation envelops), as shown in Fig. 4.13

This technique may be considered as a first order approximation to this complicated problem. The technique simplifies the complicated micro/macro scale diffusion problem through intact soil and cracks network to a simple diffusion problem through a homogenous soil continuum with an equivalent (larger) value for the field coefficient of unsaturated diffusivity. The equivalent field coefficient of unsaturated diffusivity estimation shall be based on the bounding suction envelops, because designing the shallow foundation considers the extreme soil mound shapes, which are related to the bounding suction envelops.

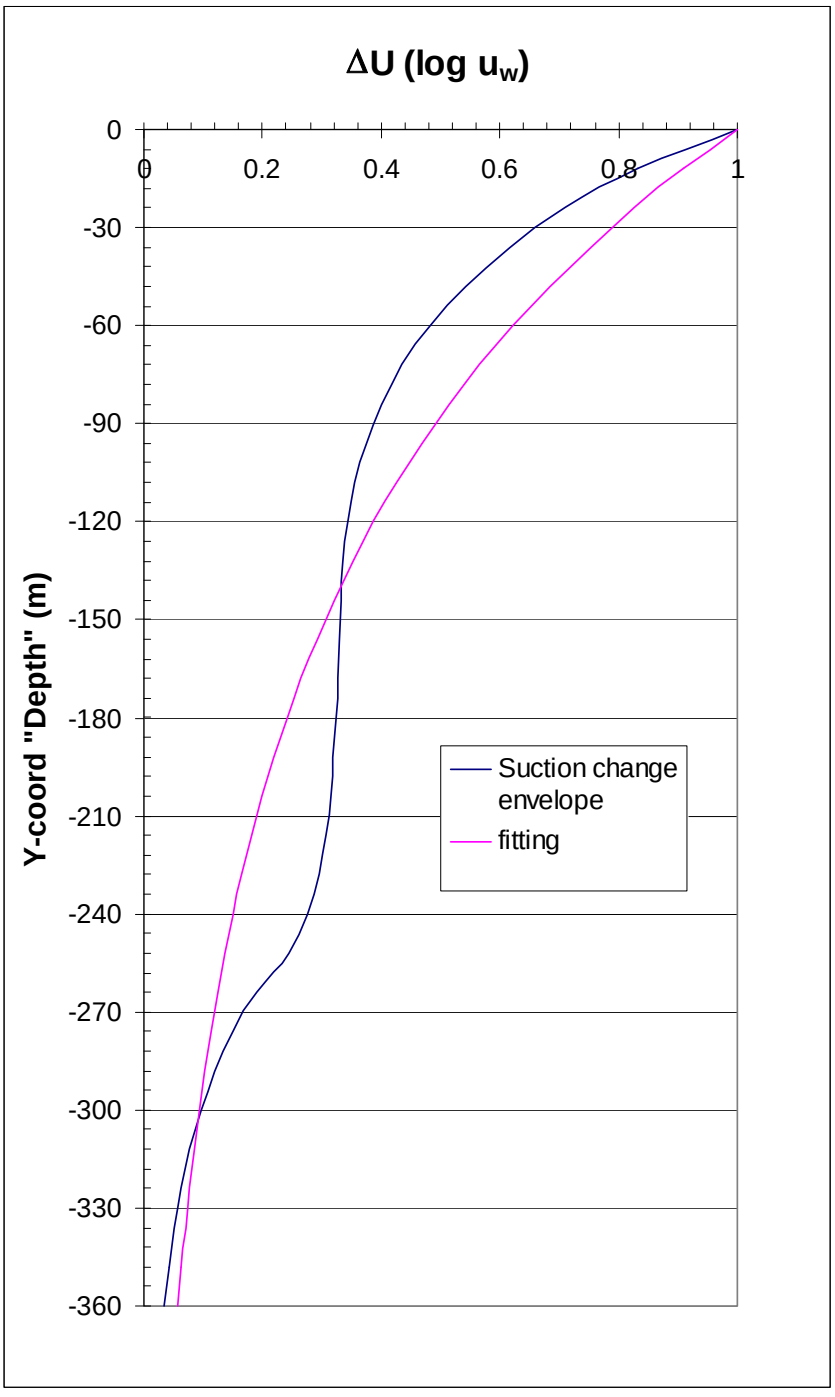

Fig. 4.13. Curve fitting for the suction change envelop.

4.5.5 Parametric study

After discussing all main factors influencing the numerical estimation of the cracked soil diffusion factor, F_{CrkDif} and α_{field}, a parametric study was carried out by choosing three β values and seven $\frac{\alpha_{lab} T_0}{H_{act}}$ values. Reasonable typical values were chosen for T_0 = 365 days, and H_{act} = 360 cm. AS 2870 (1996) mentioned that a typical range of β values is from 0.33 to 1.0, based on field observations. The three chosen values for β were 0.5, 0.667, and 0.8 representing below average, average, and above average suggested values. Seven chosen values were chosen covering a reasonably wide range of possible α_{lab} values as follows: 1.00E-06, 3.00E-06, 1.00E-05, 3.00E-05, 1.00E-04, 3.00E-04, and 1.00E-03 cm^2/sec.

Table 4.3 and Fig. 4.14 show the results of the cracked soil diffusion factor, F_{CrkDif} parametric study. They show that increasing β values increases F_{CrkDif} no matter the $\frac{\alpha_{lab} T_0}{H_{act}}$ value is. At very small and very large ranges of $\frac{\alpha_{lab} T_0}{H_{act}}$ values, the F_{CrkDif} is small than that corresponding to the average range of $\frac{\alpha_{lab} T_0}{H_{act}}$ values. This observation may be reasoned as follows:

In extremely diffusive soils (i.e., α_{lab} value is very high), cracks networks do not significantly increase the overall soil mass diffusivity as the moisture can easily diffuse through the soil almost as easily as it does through cracks network. Consequently, cracked soil diffusion factor, F_{CrkDif} is small for highly diffusive soils. In very poorly diffusive soils (i.e., α_{lab} value is very low), the moisture takes very long time to diffuse either from the top soil surface or from cracks networks. Yet, the applied suction varies with time following a sinusoidal function. When the speed of suction front permeation becomes very slow relatively to the speed of surface suction changes, the suction front penetration becomes very small, which results in a small cracked soil diffusion factor, F_{CrkDif}.

Table 4.3. Cracked soil diffusion factor, F_{CrkDif} parametric study results.

	T_0 (day)	365	365	365	365	365	365	365
	H_{act} (cm)	360	360	360	360	360	360	360
	α (cm²/sec)	1.00E-06	3.00E-06	1.00E-05	3.00E-05	1.00E-04	3.00E-04	1.00E-03
	α (cm²/day)	0.0864	0.2592	0.8640	2.5920	8.6400	25.9200	86.4000
	P (cm²/day)	0.0141	0.0423	0.1410	0.4229	1.4096	4.2288	14.0962
β=0.5	ΔU_0	1	1	1	1	1	1	1
β=0.5	$\alpha T / H^2$	2.43E-04	7.30E-04	2.43E-03	7.30E-03	2.43E-02	7.30E-02	2.43E-01
β=0.5	F_{CrkDif}	**11.529**	**22.353**	**28.905**	**23.789**	**15.738**	**11.092**	**8.540**
β=0.5	RMS	0.0551	0.0641	0.0365	0.0488	0.0969	0.1209	0.1211
β=2/3	ΔU_0	1	1	1	1	1	1	1
β=2/3	$\alpha T / H^2$	2.43E-04	7.30E-04	2.43E-03	7.30E-03	2.43E-02	7.30E-02	2.43E-01
β=2/3	F_{CrkDif}	**12.153**	**30.800**	**43.242**	**36.676**	**25.449**	**19.239**	**17.384**
β=2/3	RMS	0.0656	0.0793	0.0495	0.0514	0.0982	0.1233	0.1226
β=0.8	ΔU_0	1	1	1	1	1	1	1
β=0.8	$\alpha T / H^2$	2.43E-04	7.30E-04	2.43E-03	7.30E-03	2.43E-02	7.30E-02	2.43E-01
β=0.8	F_{CrkDif}	**12.344**	**40.605**	**59.973**	**51.993**	**38.139**	**31.442**	**33.916**
β=0.8	RMS	0.0747	0.0924	0.0603	0.0554	0.0984	0.1169	0.1083

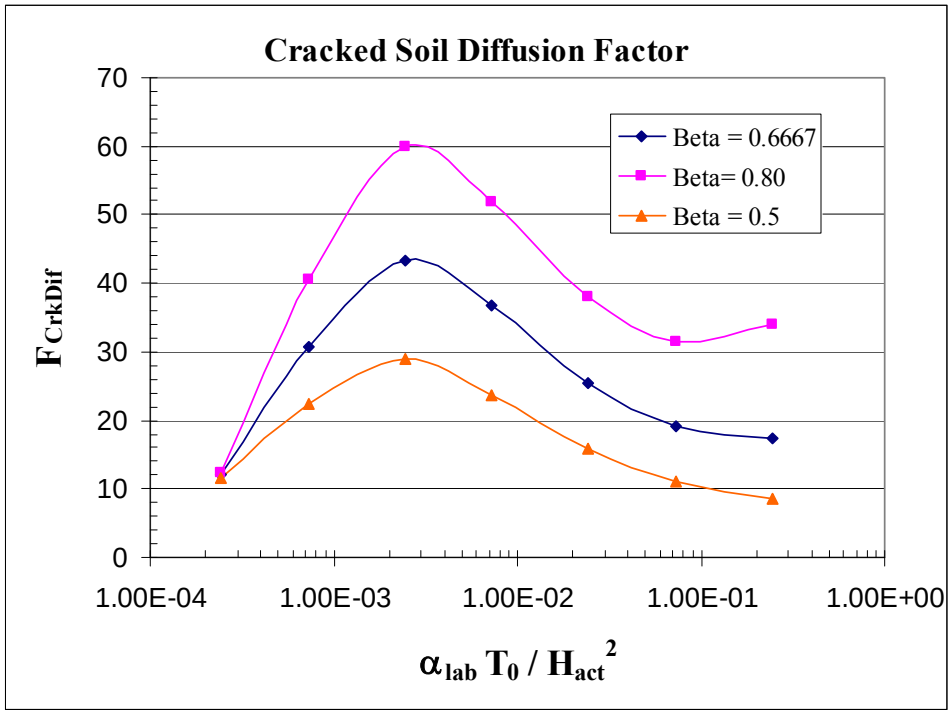

Fig. 4.14. Cracked soil diffusion factor, F_{CrkDif}.

4.6 Model for volume change due to moisture variation

The model is actually the constitutive law for the volume change due to suction variation. Matric suction is sort of hydrostatic pressure, when there is suction variation, the soil volume will change uniformly in all the directions if the soil is homogenous. Two kinds of constitutive laws have been proposed: one is based on matric suction, and the other is based on water content.

4.6.1 Suction based volume change models

The most famous representatives of suction based method are Lytton (1977), Johnson (1977), Fredlund (1979), Mckeen (1981), and Fargher et al (1979) .The basic concept of suction based method is that the volume change of the unsaturated soils due to moisture variation is linearly proportional to the suction variation in log scale, i.e.

$$\gamma_h = \frac{1}{1+e_0}\frac{\Delta e}{\Delta \log(|u_w|)} \tag{4.27}$$

Where the matrix suction compression index γ_h equals to the slope of the void ratio versus the matric suction in log scale.

4.6.2 Water content-based volume change models

Water content-based constitutive law uses water content as a parameter to set up the relationship between volume change and moisture variation. The basic concept is that there is a linear relationship between volume change of unsaturated soil and the water content variation (Briaud et al, 2003), i.e.

$$\frac{\Delta V}{V} = \frac{\Delta w}{E_w} \tag{4.28}$$

where:

E_w is a constant.

The swell test-free shrink test was proposed to get the constitutive law. It is a little bit simpler than the test for obtaining the void ratio versus matric suction curve.

4.6.3 The ratio of vertical to volumetric strain, coefficient *f*

In fact, water content-based and suction-based volume change models may be considered as two sides of the same coin, as water content and suction are related together through the soil water characteristic curve, SWCC. The most difficult thing in any volume change model is to determine the distribution of water content / suction changes through the soil domain under consideration. Finite elements, finite difference, some closed form solutions may be used to estimate the distribution of water content / suction changes through the soil domain under consideration. Yet, to interpret the mobilized volumetric strain, due to moisture movements, to a vertical strain, an important coefficient, *f*, is needed. *f* is defined as the ratio between the mobilized vertical strain to the mobilized volumetric strain (i.e, $f = \varepsilon_{ver} / \varepsilon_{vol}$).

Cracks networks play an important role influencing the coefficient, *f*; Research efforts are badly needed in this area to better understand and accurately estimate *f* for a soil mass with cracks networks. The following discussion will try to find out a reasonable assumption of the *f* value in soil mass with cracks networks:

Fig. 4.15 shows four typical constraining conditions for a homogenous isotropic soil block:

- In Fig. 4.15. (b), the soil block is free to move vertically and horizontally, hence,

$$f = 0.33$$

- In Fig. 4.15. (a), the soil block is free to move only vertically and totally confined horizontally, hence, all the mobilized volumetric stain goes to the vertical direction,

$$f = 1.0$$

- In Fig. 4.15. (c), the soil block is free to move only vertically, and partially confined horizontally, hence, the portion of the mobilized volumetric stain that goes to the vertical direction is more than that to the horizontal direction,

$$0.33 < f < 1.0$$

- In Fig. 4.15. (d), the soil block is partially confined vertically, and partially confined horizontally, hence, the portion of the mobilized volumetric stain that goes to the vertical direction is a function of the relative stiffness, (i.e., the ration between the modulus of subgrade reaction in the vertical direction to that of the horizontal direction, k_v / k_h)

$$k_v / k_h = 0 \rightarrow f = 1.0$$

$$0 < k_v / k_h < 1 \rightarrow 0.33 < f < 1.0$$

$$k_v / k_h = 1 \rightarrow f = 0.33$$

$$k_v / k_h > 1 \rightarrow 0 < f < 0.\ 33$$

$$k_v / k_h = \infty \rightarrow f = 0$$

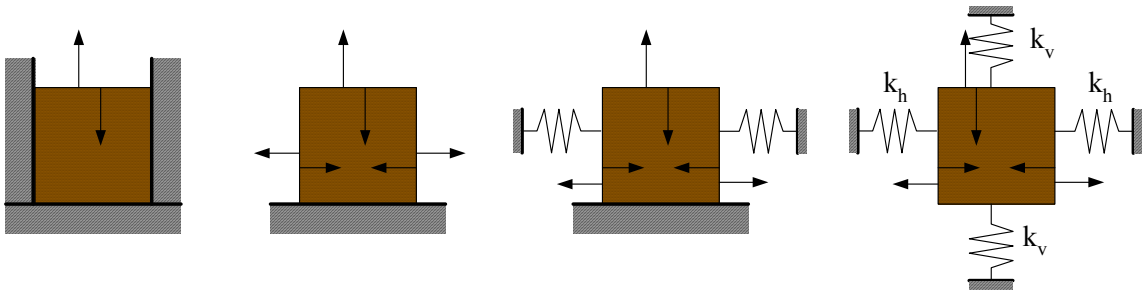

Fig. 4.15. Typical of soil constraining conditions.

Now let us consider a soil mass at the ground surface, as shown in Fig. 4.16, and confined laterally by vertical cracks. The constraining conditions for this soil mass in swelling are different than that when shrinking.

In swell case:

a) The soil outer layer (A) absorbs water and becomes softer, the outer layer expands outwardly closing the cracks' space and heaving up. In this stage the outer layer (A) is free to move vertically and horizontally, similar case to Fig. 4.15 (b), hence, $f = 0.33$.

b) Upon continuous wetting, the wetting front keeps permeating saturating the inner soil block (B), which will expand pushing the outer layer (A) further outwardly. The soil block (B) expands freely, vertically and horizontally, even if the soil cracks get completely closed. Because then, the outer soil layer (A) is very wet and soft behaving like a very compressible caution that can not resist the lateral expansion of the soil block (B). Hence, $f = 0.33$

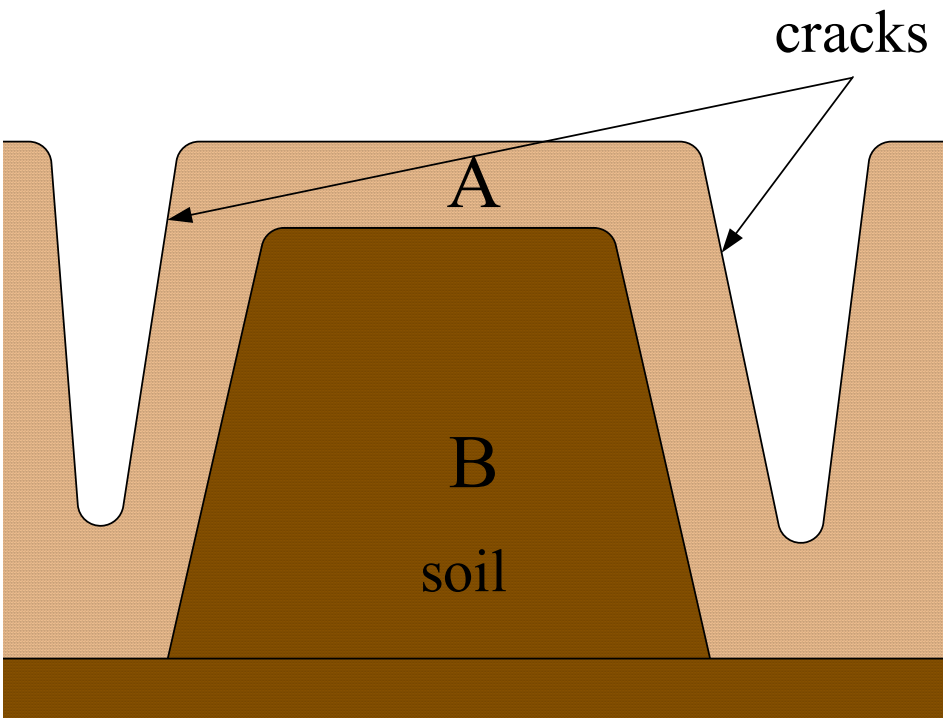

Fig. 4.16. Soil cracks and constraining conditions.

In shrink case:

c) The soil outer layer (A) loses water and becomes stiffer, the outer layer shrinks inwardly opening the cracks' space. In this stage the outer layer (A) is free to move vertically and horizontally, similar case to Fig. 4.15 (b), hence, $f = 0.33$.

d) Upon continuous drying, the he soil outer layer (A) reaches a water content close to the shrinkage limit and becomes very stiff and stops shrinking. The drying front keeps permeating desaturating the inner soil block (B), which will shrinks trying to pull the outer layer (A) inwardly. The soil block (B) freely shrinks in the vertical direction (soil layer (A) is acting like a corrugated stiff sheet put in top of a compressible medium), but not freely in the horizontal direction. Because then, the outer soil layer (A) is very stiff behaving like a rigid frame that can resist the lateral contraction of the soil block (B); Here, the soil block (B) is supported by the rigid frames legs formed by the soil layer (A) , similar case to Fig. 4.15 (c), hence,. Hence, $0.33 < f < 1.0$

Consequently, it may be reasonable to assume the following for the cracks zone:

In swell cases, $f = 0.33$

In short term shrink cases, $f = 0.33$

In long term shrink cases, $f = 0.5$

Yet, below cracks zone, $f = 1.0$ for both shrink and swell cases.

4.7 Soil index, moisture diffusion, and volume change properties

Ten soil samples were tested to determine their index, moisture diffusion, and volume change properties: five natural samples were obtained from Ellison's Office Building (located in College Station, TX denoted as EOB), natural four samples were obtained from Briaud's Tennis Court (located in his house, College Station, TX, denoted as BTC), and one artificial soil (a soil mixture compacted block of 80% Porcelain clay and 20% Bentonite clay, denoted as Bent-Porc), the same soil mixture was used in the large scale laboratory test detailed in the following section but with a lower dry density.

4.7.1 Index properties

Identification tests were performed in order to have a background data base for the soil properties. These tests include Atterberge limits (ASTM D 4318), percentage passing No. 200 sieve (ASTM D 1140), unite dry weight (ASTM D 2166), percentage finer than

2μ (ASTM D 1140), specific gravity of soil solids (ASTM D 854), and swell limit following Briaud et al, (2003) procedure. Table 4.4 presents soil samples index properties.

Table 4.4. Soil samples index properties.

Sample	% LL	% PL	% PI	% I_{sh}	% I_{sw}	% I_{ss}	KN/m^3 γ_{dry}	Gs	% %<# 200	% %<2 μ
Bent-Porc	41.9	16.3	25.6	10.533	31.9	21.367	15.896	2.725	99.7	48
EOB Bench-20	67.4	20.8	46.6	7.86	40.60	32.74	12.244	2.77	98.5	63
EOB B2-7	50.6	17.3	33.3	11.66	40.60	28.94	12.518	2.774	99.3	35.6
EOB B2-11	49.2	13.4	35.8	10.48	35.84	25.36	13.213	2.774	97.4	37
EOB B1-5	58.1	14.1	44	8.38	47.56	39.18	11.556	2.792	99.6	19.4
EOB B1-11	52.3	14.3	38	8.90	35.93	27.04	16.620	2.792	88.9	30.2
BTC B1-3	40.2	8.36	31.84	7.22	25.45	18.23	15.337	2.749	55.7	4
BTC B1-5	32.9	8	24.9	10.87	30.25	19.38	14.212	2.765	41.5	1.5
BTC B2-3	56.4	14	42.4	6.97	29.84	22.86	14.482	2.755	65.5	16.9
BTC B2-7	35	11.6	23.4	9.83	31.38	21.56	14.439	2.797	36.9	12.5

Eight samples were fine grained soil, yet samples BTC B1-5 and BTC B2-7 were coarse grained soils, clayey sand. All the tested samples fall above the A-Line in the plasticity chart, hence the type of soil fines is clay. Fig. 4.17 shows the relationship between the soil plasticity index, PI and the soil shrink-swell index, I_{SS}; the PI is directly proportional to the I_{SS}. A linear curve fitting for the tested samples shows a reasonable correlation between I_{SS} and PI with a coefficient of determination, $R^2 = 0.4965$ as shown in Fig. 4.17. However, relying on the soil shrink-swell index is more representative to the soil shrink-swell potential than the plasticity index as it is based on undisturbed sample meanwhile the plasticity index is for remolded samples (Briaud et al, 2003).

4.7.2 Moisture diffusion and volume change properties

For the ten soil samples, soil coefficients of unsaturated diffusivity were determined using α-shrink test explained earlier in this chapter. The Soil Water Characteristic curves (SWCC), expressed as gravimetric water content versus suction in pF, were determined using chilled mirror dew point psychrometer (Decagon WP4-T Dew Point Potentiameter), slopes of the straight line in the desaturation zone were determined,

which are the specific water capacity indices, $C_w = \frac{\Delta w}{\Delta U}$. Then, suction compressibility indices, γ_h, were calculated using Eq. 4.29.

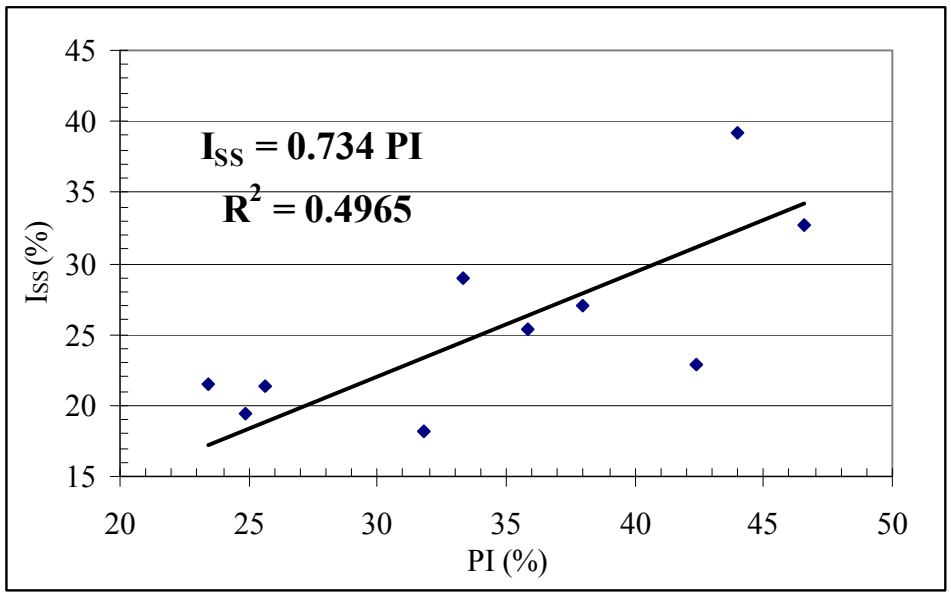

Fig. 4.17. Relationship between shrink-swell index and soil plasticity index.

$$\gamma_h = \frac{\gamma_{dry} C_w}{\gamma_{water}} \tag{4.29}$$

Suction compressibility indices, γ_h, may be also determines using the slope of the Soil Water Characteristic curves (SWCC), expressed as volumetric strain versus suction in pF. However, using specific water capacity indices, C_W to γ_h may be easier and more accurate as it is based on gravimetric water content measurements instead of volumetric strain measurements. Table 4.5 presents soil coefficient of unsaturated diffusivity, α, shrink-swell index, I_{SS}, unite dry weight, γ_{dry}, water specific capacity, C_W, and suction compressibility index, γ_h, for the tested soil.

Fig. 4.18 shows the relationship between the soil water specific capacity, C_W and shrink-swell index, I_{SS}; the C_W is directly proportional to the I_{SS}. A linear curve fitting

for the tested samples shows a strong correlation between I_{SS} and PI with a coefficient of determination, $R^2 = 0.889$ as shown in Fig. 4.18.

Table 4.5. Soil moisture diffusion and volume change properties.

Sample	cm^2/min α	cm^2/sec α	% I_{ss}	% C_w	I_{ss} / C_w	KN/m^3 γ_{dry}	% γ_h
Bent-Porc	0.00025	4.2E-06	21.367	11.37	1.88	15.896	18.44
EOB Bench-20	0.00015	2.4E-06	32.74	16.41	2.00	12.244	20.50
EOB B2-7	0.00027	4.5E-06	28.94	16.69	1.73	12.518	21.32
EOB B2-11	0.00046	7.7E-06	25.36	13.08	1.94	13.213	17.64
EOB B1-5	0.00017	2.8E-06	39.18	22.13	1.77	11.556	26.10
EOB B1-11	0.00045	7.5E-06	27.04	13.41	2.02	16.620	22.74
BTC B1-3	0.00022	3.7E-06	18.23	8.70	2.10	15.337	13.62
BTC B1-5	0.00026	4.4E-06	19.38	8.60	2.25	14.212	12.47
BTC B2-3	0.00015	2.5E-06	22.86	9.47	2.42	14.482	13.99
BTC B2-7	0.00035	5.8E-06	21.56	8.97	2.40	14.439	13.22

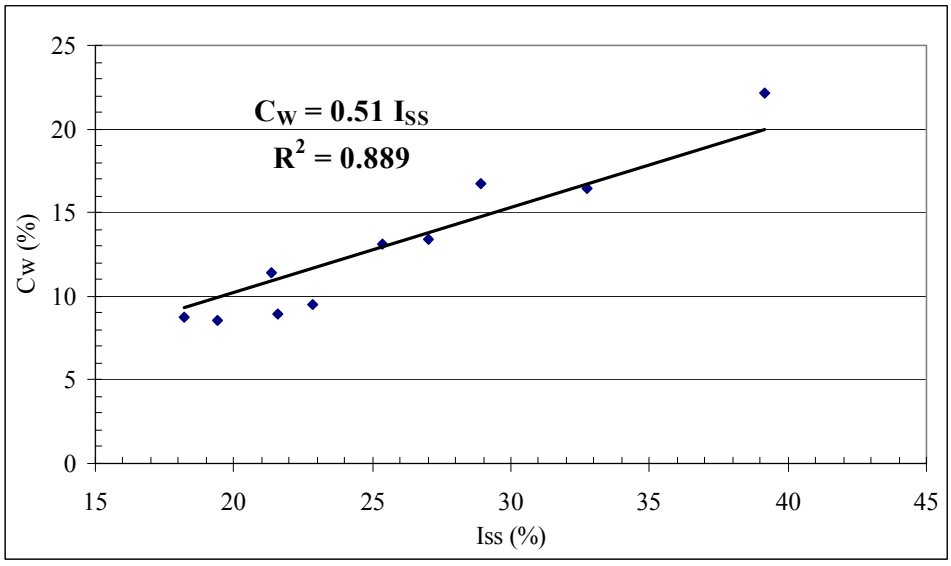

Fig.4.18. Relationship between water specific capacity and shrink-swell index.

4.8 Verification of the proposed soil moisture diffusion and volume change models

4.8.1 Main idea

A large scale laboratory test was carried out to verify the proposed new methods to determine the coefficient of unsaturated diffusivity at laboratory, α_{lab}, and to estimate the coefficient of unsaturated diffusivity at field, α_{field}. The large scale laboratory test was run to model the moisture diffusion in a 1.2 m diameter tank filled with 0.44 m homogeneous soil layer subjected to several wetting and drying cycles as shown in Fig. 4.19. Using the large tank allowed the development of cracks network during the drying cycles. Both the soil movements at different depths and water content logs at the end of each cycle were measured. The experiment had two phases: 1) Uncovered phase-the total surface area is exposed to the ambient suction to allow development of uniformly distributed and steady cracks network. 2) Covered phased-the center of the soil surface is covered with a 0.8 m diameter rubber cover; this phase simulates the 2D axi-symmetric diffusion.

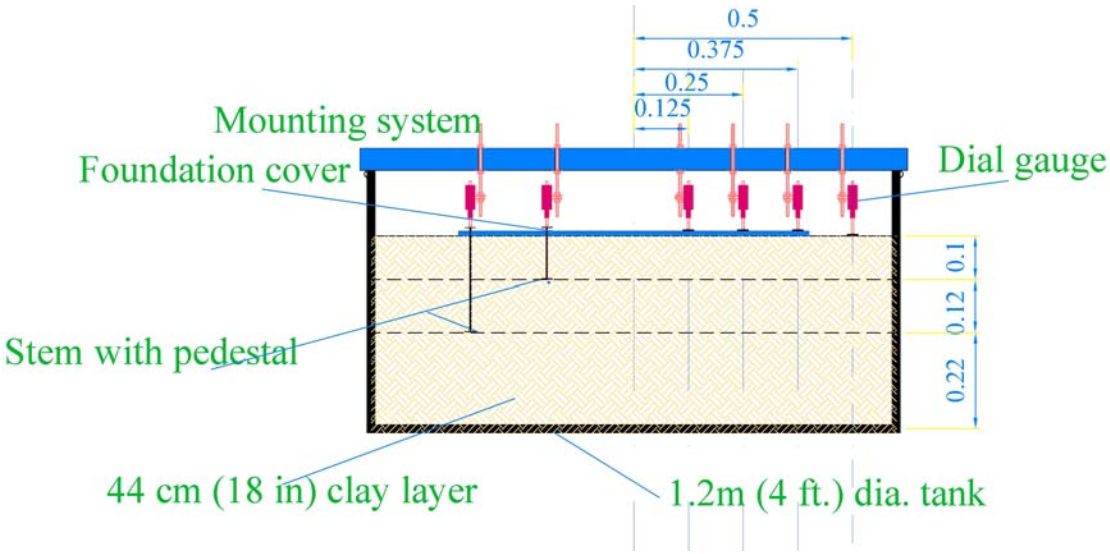

Fig. 4.19. Large scale laboratory test to model moisture diffusion analyses for cracked soil.

Finite element 2D axi-symmetric analyses were carried out using the measured laboratory coefficient of unsaturated diffusivity and the calculated field coefficient of unsaturated diffusivity. Comparing the laboratory measurements with the finite element model results allowed us to validate the proposed new moisture diffusion model.

4.8.2 Experimental setup

a) Soil preparation.

The soil was a mixture composed of 80% porcelain clay and 20% bentonite clay (by weight). Both porcelain clay and bentonite clay were provided by Armadillo Clay& Supplies Inc, Austin, TX, USA in a 50 lb-sacks. First, clays were mixed, dry mixing, according to the weight proportions 4:1 (Porcelain: Bentonite). The total amount of dry-mixed clay was about 800 kg. Then, batches of the dry clay mixture were mixed with a certain amount of pure distilled water. Each clay mixture batch was one kilogram in weight and mixed with 150 gram of pure distilled water. The 150 grams of pure distilled water were sprayed evenly on the 1000 grams of clay mixture with hand mixing to ensure constancy of water content distribution. At the end of hand mixing the moistened clay mixture were lumped forming small balls of clay with a maximum diameter of 5 mm. then, the soil batches were collected and stored in well sealed barrels in a moisture room. This tedious soil mixing procedure were continued for four months to have about 920 kg of homogenous clay soil at certain water content.

b) Soil compaction.

Batches of the prepared soil mixture were put in the 1.2 diameter tank as shown in Fig. 4.20. Each batch was poured in the tank and leveled forming an approximate two inches layer of loose clay soil. Compaction took place using heavy hand compaction hammers. Hammers were dropped from an approximate height two feet; careful efforts were made towards distributing hammer drops evenly on the same layer and consistently on all the compacted layers. This compaction procedure was followed in order to ensure having a compacted soil with homogenous distribution of both water content and dry unite

weight. The process of adding more compacted soil layers continued until reaching an overall soil stratum thickness of 0.44 m and then the top surface was leveled as shown in Fig. 4.21.

c) Instrumentation.

Twenty four dial gauges were installed to monitor the soil movements during the experiment. Eight of them were installed to monitor the soil movements at the soil surface, another eight were for the soil movements monitoring at depth equal to 100 mm, and the last eight were for the soil movements monitoring at depth equal to 220 mm. For each depth, monitoring took place at four radii 125, 250, 375, and 500 mm; two dial gauges were installed at each radius giving a total of eight dial gauges. For each depth, the eight dial gauges were lined to be on the same diameter line as shown in Fig. 4.22. and Fig. 4.23.

Fig. 4.20. Compaction of the clay soil in the tank.

Fig. 4.21. Leveled soil surface after completing compaction.

Fig. 4.22. Instrumentation of the large scale laboratory test tank.

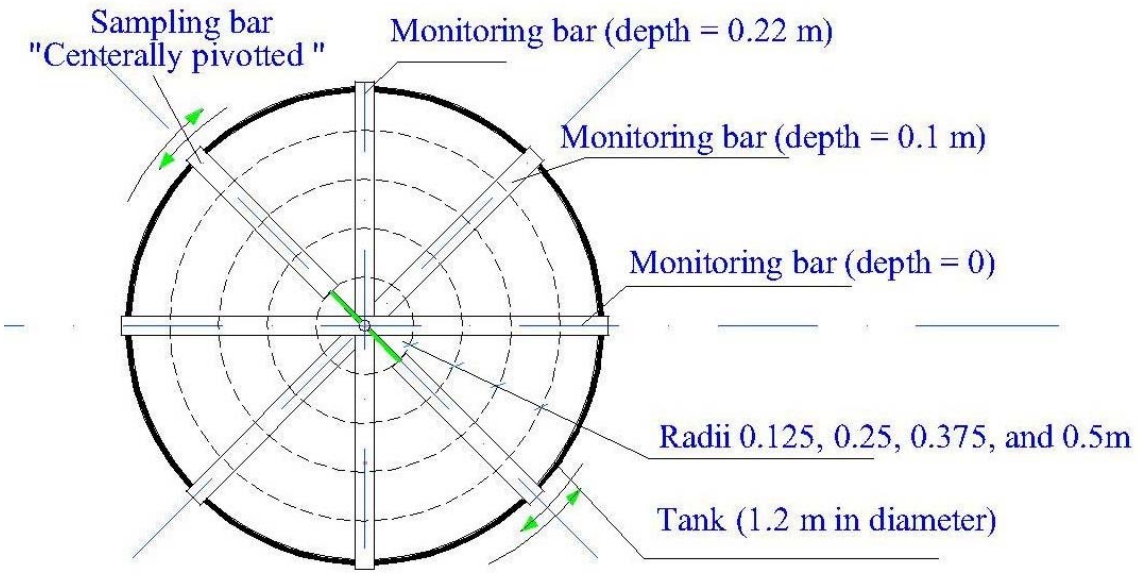

Fig. 4.23. Plan view of the large scale laboratory test tank.

Pedestals (disk with 25mm diameter and 5 mm thickness) were connected to the eight dial gauges monitoring. For points that monitor soil movements at depths 100 mm and 220 mm: a 25.4 mm hole were dug to the proposed monitoring depth, then similar pedestals were embedded at depths 100 mm and 220 mm, the embedded pedestals were connected to 125 mm extension stems as shown in Fig. 4.24, then annuluses around stems were backfilled with the same soil, and finally another similar pedestals were connected to the top of the extension stems. Dial gauges were place in such a way that they touch the top pedestals.

d) Initial soil conditions

To determine the experiment initial conditions, 20 samples were taken for water content and dry unite weight determination. Sample was taken after compaction of each layer by pushing a very thin walled stainless steel tube (10 mm-inner diameter). Then, each extruded sample was tested. The mean value for water content was 20.0 % with a standard deviation of 0.3%. The mean value for dry unite weight was 12.2 kN/m^3 with a

standard deviation of 0.18 kN/m^3. Using the determined SWCC, see the previous section, the initial soil suction corresponding to the mean initial water content value was 4.2163 pF (-1645 kPa).

Fig. 4.24. Installing the extension stems with pedestals.

For the covered phase, which directly followed the uncovered phase, the initial water content distribution was assumed to be the final water content distribution at the uncovered phase. This water content distribution was logged as will be explained in details later.

4.8.3 Procedure and measurements

a) Uncovered phase.

Once the tank has been instrumented, the initial dial gauges readings were taken, and then the soil in the tank was inundated to start the first swell period as shown in Fig.4.25.

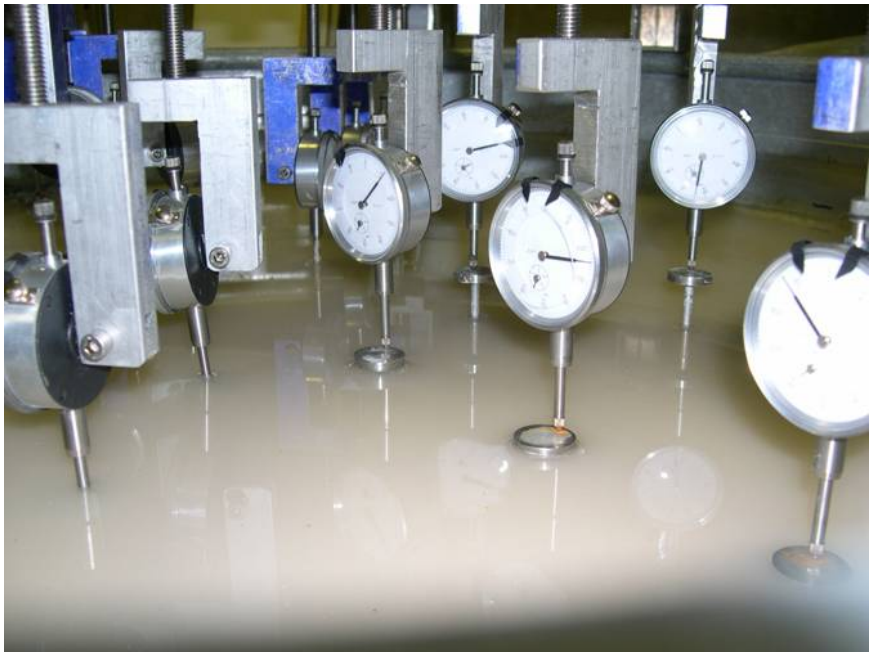

Fig.4.25. Inundation to start the first swell period.

The first inundation period was 7 days, and then the surface water was sucked out and prepared for the first drying period; the surface soil was subjected to the ambient room suction. This process was repeated forming six swell-shrink cycles for a total of 270 days. The cyclic swell-shrink process allowed the crack pattern to develop a steady stat of the shrinkage crack network. Fig. 4.26 shows the developed soil surface cracks after starting the first drying period. Fig. 4.27 shows the inundation to start the second swell cycle.

Daily room relative humidity and temperature were measured to calculate the ambient room suction. For all drying periods the average room suction was calculated using Eq. 4.1 and found to be 5.5 pF (-31622 kPa). The soil surface suction at wetting periods was assumed to be 1 pF (-1 kPa) as shown in Fig. 4.28.

Fig. 4.26. Soil surface cracks after starting the first drying period.

Fig. 4.27. Inundation to start the second swell cycle.

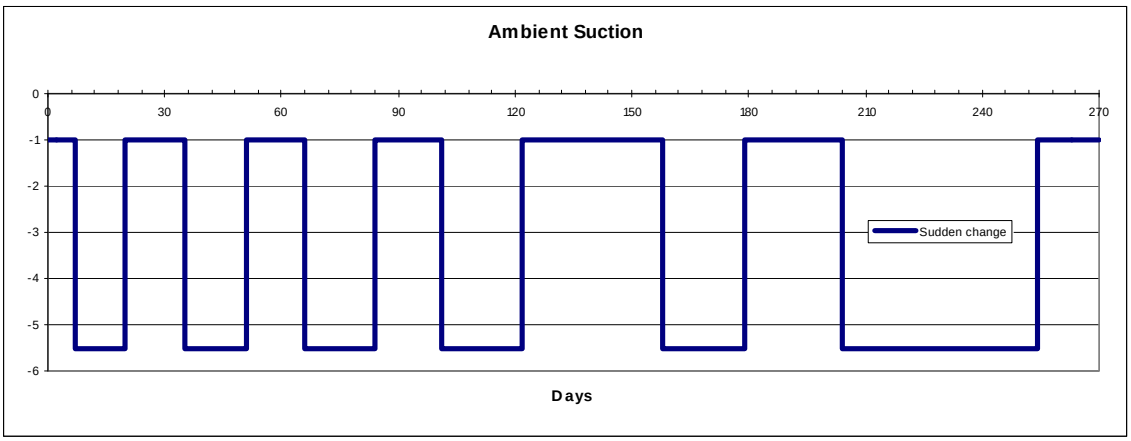

Fig. 4.28. Roam ambient suction.

b) Soil movements monitoring and water content logging

The 24 dial gauges' reading were taken at least twice a week at the first four cycles and once a week for the last two cycles. The average movements for each depth were calculated (8 dial gauges for each depth). At the end of each period, either drying or wetting, the water content was logged. Water content logging was carried out by pushing a vertically guided sampling tube down (for a 100 mm) in the soil mass as shown in Fig. 4.29, then the 100 mm sample was extruded and cut into 5 pieces (20 mm each). Pushing the sampler and extrusion were repeated until sampling the entire depth of the soil mass in the tank. Water content was measured for each piece and assumed to be the water content value at a depth corresponding to the center of the soil piece. The sampling hole was then backfilled by similar soil. The sampling bar was rotated to ensure taking the following water content at a different location.

c) Covered phase.

The purpose of the first phase, the uncovered phase, was to establish a steady state of cracks network distribution and depth of active moisture zone variation. Moreover it allows to validation of the one dimensional moisture unsaturated diffusion and volume change problem. The second phase, the covered phase, was planned to validate the same problem but in two dimension. The cover was a circular rubber sheet (5 mm thick and 800 mm in diameter) with many holes, as shown in Fig. 4.30.

Fig. 4.29. Water content logging.

Fig. 4.30. The rubber cover.

Two sizes of holes were in the rubber cover, 18 holes were with diameters of 33 mm and 12 holes with diameters of 22 mm. At the end of the first phase, dial gauges were removed and the soil surface was cleaned and releveled. Then, the rubber sheet was placed in such a way that the extension stems fits through the cover holes as shown in Fig. 4.31.

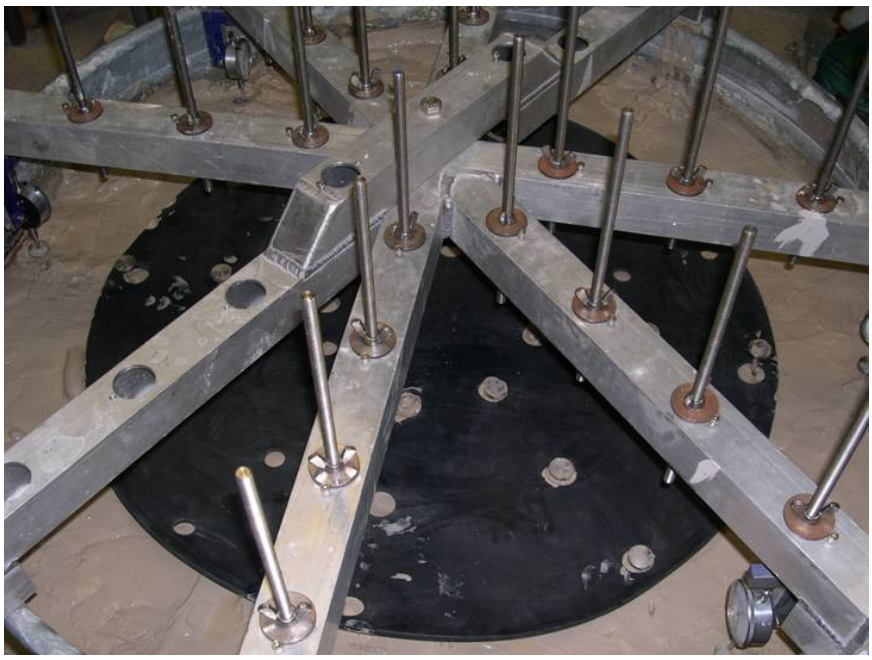

Fig. 4.31. Placing the rubber cover on the soil surface.

Small PVC tubes (15 mm length) were just fitted in rubber cover around the extension stems and the annuluses were filled with Vaseline to allow free stem movements and to prevent water leaks through the annuluses as shown in Fig. 4.32.

The small rubber cover holes were clogged with corks during drying and wetting periods yet opened only to allow soil sampling for water content logging.

After finishing sealing and clogging all holes, the dial gauges were set back in place and their initial readings were taken, Fig. 4.33.

Fig. 4.32. Sealing the rubber cover holes.

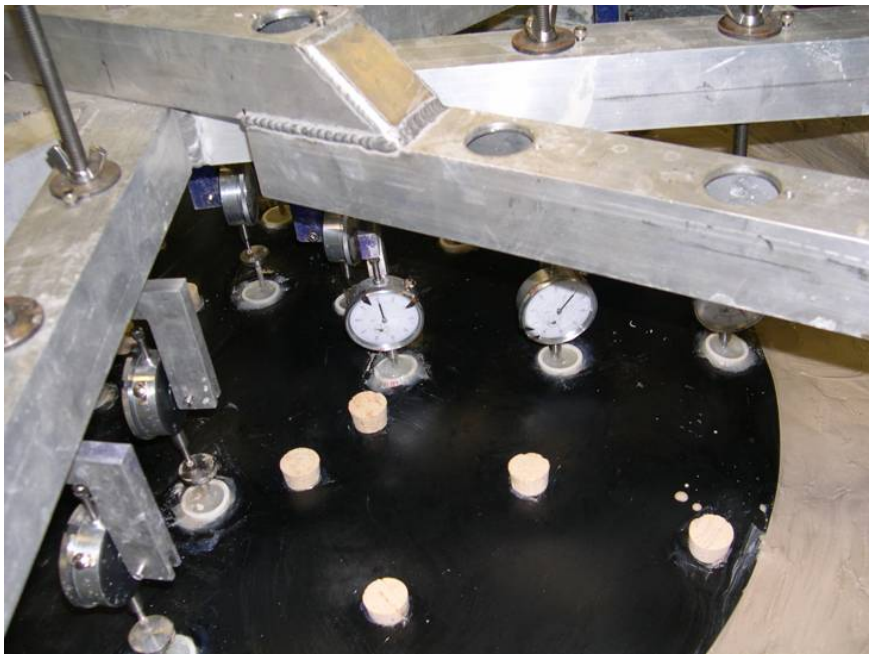

Fig. 4.33. Covered phase after instrumentation.

Once the tank has been instrumented and initial dial gauges readings were taken, the soil in the tank was left to dry under the room ambient suction similarly to the uncovered phase for one month as shown in Fig. 4.34. Then, inundation took place for another month. The covered phase continued for about six months with two shrink-swell cycles, the first cycle lasted about two months and the second cycle lasted about four months.

d) Soil movements monitoring and water content logging.

The water content logging was done in a similar way to the uncovered phase. However, dial gauges reading were not averaged at each depth as what has been done in the uncovered phase. Since, the covered phase is a 2D axi-symmetric problem the average movements were calculated to each two dial gauges having the same radius and depth.

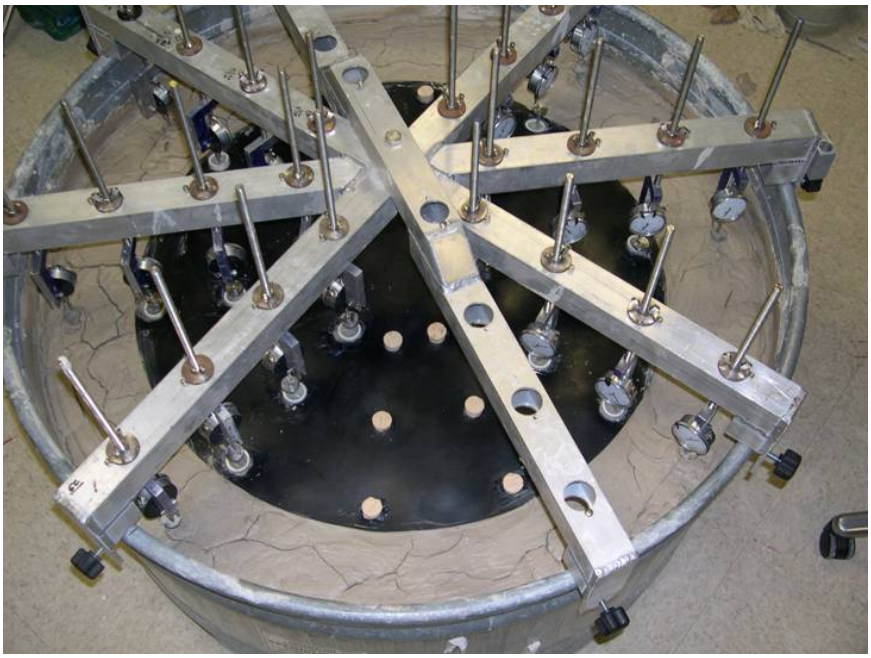

Fig. 4.34. First drying period in the covered phase.

4.8.4 Numerical simulation

The finite elements comprehensive software package, ABAQUS/STANDARD, was used to for suction diffusion simulations, which is analogous to the thermal diffusion phenomena in heat transfer as detailed earlier. Fig. 4.35 shows the geometry of the problem; H_{act} was calculated from the water content log as the depth after which the water content is constant and equal the initial water content, H_{act} was calculated at the beginning and ending of each drying or wetting period and assumed to be linearly varied with time within each period, $d_{Crk} = \beta . H_{act}$, $\beta = 0.667$ and assumed to be constant during simulation. This problem is a 2D axi-symmetric problem; the ABAQUS/STANDARD CAX4T "Continuum Axi-symmetric 4-nodes Temperature" element was chosen in the simulation.

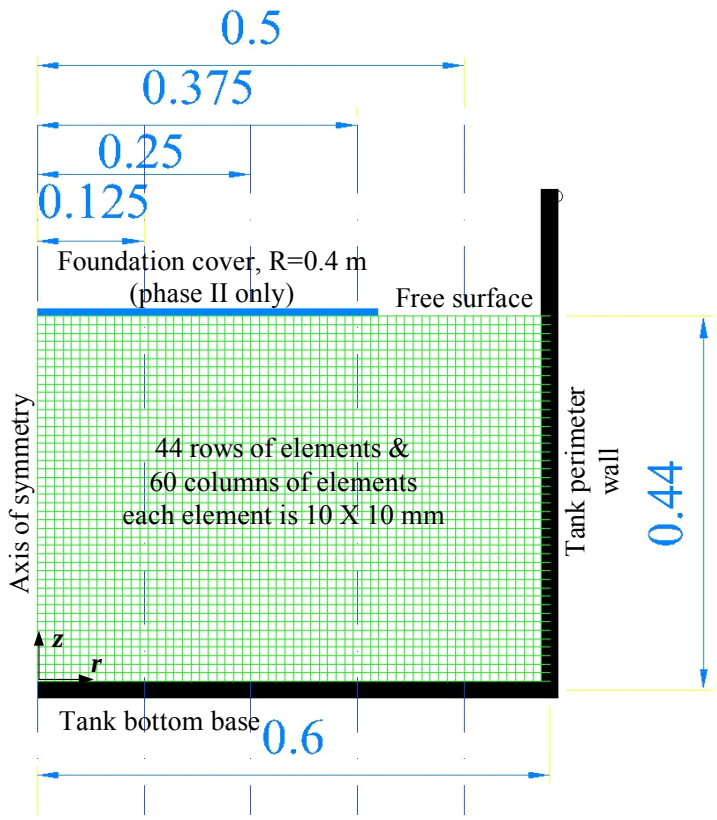

Fig. 4.35. Model used for finite element simulation.

The material properties were: unite dry weight =12.2 kN/m^3, slope of SWCC (expressed as gravimetric water content versus suction), C_w = 0.1 (equivalent to specific heat), initial coefficient of unsaturated permeability, P_{lab} = 0.0437 cm^2/day (equivalent to coefficient of thermal conductivity). Recall that, the coefficient of unsaturated diffusivity, $\alpha = \frac{P\gamma_w}{\gamma_{dry} C_w}$, which gives initial α_{lab}=0.36415 cm^2/day. α & P increased with the increase of d_{Crk}, which was increased linearly with H_{act} . Knowing $\frac{\alpha_{lab} T_0}{H_{act}}$ values, the F_{CrkDif} was calculated using Fig. 4.14, and hence α_{field} = α_{lab} X F_{CrkDif} . & $P_{field} = \frac{\alpha_{field} \gamma_{dry} C_w}{\gamma_w}$. Following this scheme, P_{field} was given as a time dependent variable in the ABAQUS/STANDARD input files

For the uncovered phase, the initial conditions was a constant suction value of 4.2163 pF (-1645 kPa) (equivalent to T= -4.2163 C˚). For the covered phase, the initial soil conditions were the same suction distribution values at the end of the uncovered phase.

For the uncovered phase, the boundary conditions were: the bottom base, the perimeter wall boundary, and axis of symmetry boundary have no flux boundary conditions, and the top boundary. For the covered phase, the boundary conditions were the same as the uncovered phase boundary conditions except for the covered area at which the no flux boundary condition was applied. Appendix D presents the ABAQUS/STANDARD input files for these simulations.

At each time step, suction values were reduced to calculate the soil movements at the dial gauges monitoring points using Eq. 4.27. Eq. 4.27 can be rewritten in the following format:

$$\Delta\varepsilon_{vol} = \gamma_h \Delta U \qquad (4.30a)$$

$$\Delta\varepsilon_{ver} = f\gamma_h \Delta U \qquad (4.30b)$$

where:

γ_h is the suction compression index

$\Delta\varepsilon_{vol}$ is the change in the volumetric strain

$\Delta\varepsilon_{ver}$ is the change in the vertical strain

ΔU is the change in suction in (pF unite)

f is the ratio between the mobilized vertical strain to the mobilized volumetric strain

f value was assumed to be equal to 1.0 for depths greater than the depth of cracked zone, d_{Crk}. For depths smaller than d_{Crk}, *f* value was assumed to be equal to 0.33 for swell cases and 0.5 for shrink cases as has been recommended in the previous section.

Water content profiles at the end of each swell/shrink period were calculated, knowing the suction profile, by using the SWCC curve for the tank soil.

4.8.5 Results

a) Uncovered phase.

Predicted and measured water content results for first swell-shrink cycle are shown in Fig. 4.36. Fig. 4.36 shows a very reasonable matching between the measured water content profiles and the predicted profiles. Fig. D.1, Fig. D.2, Fig. D.3, Fig. D.4, & Fig. D.5 show predicted and measured water content results for second, third, forth, fifth, and sixth swell-shrink cycles respectively. Fig. D.1, Fig. D.2, Fig. D.3, Fig. D.4, & Fig. D.5 show that the very reasonable matching between predicted and measured water content results continued until the end of the uncovered phase. Tables D.1 and D.2 present the tabulated results for the predicted water contents and measured water contents respectively. To assess the resulting matching between the predicted and measured water content profiles, the rout mean square error, between predicted and measured, value (RMS) was calculated for each water content profile and tabulated in Table D.2. The average RMS for all predicted and measured water content profiles was 0.974 %, which is a very reasonable value, especially when you compare it with the average initial water content value 20 %.

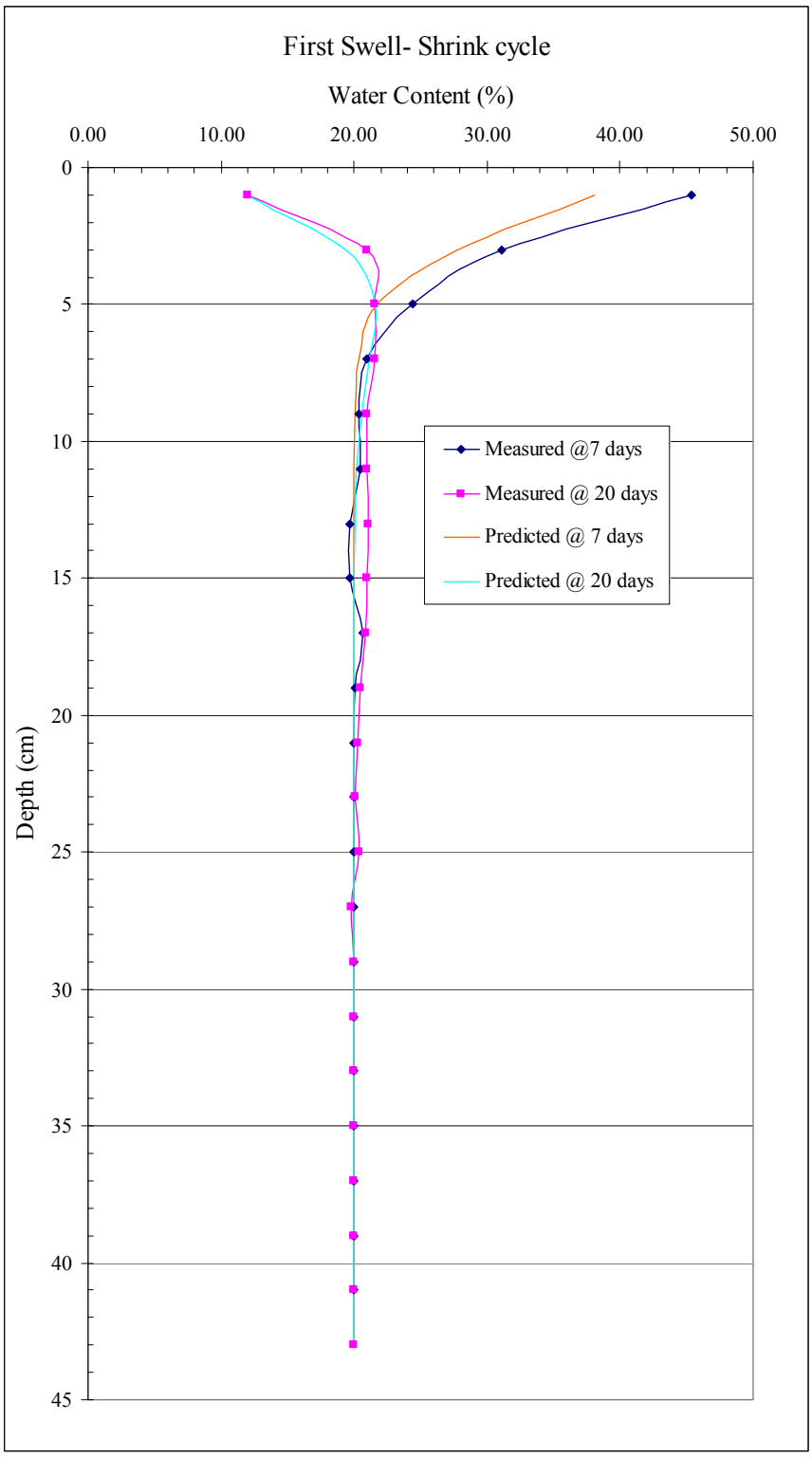

Fig. 4.36. Water content results for first swell-shrink cycle (Uncovered phase).

It was also noticed that, the depth of active moisture variation zone, H_{act} is increasing from cycle to cycle until it reached a constant value, 320 mm, in the last two cycles, which gave an indication of an steady established cracks network was achieved.

Predicted and measured surface soil average movements for the uncovered phase is presented in Fig. 4.37. Again, a strong matching between measured and predicted surface soil average movements is manifested in Fig. 4.37. The RMS error value, between measured and predicted average movements, was 0.511 mm.

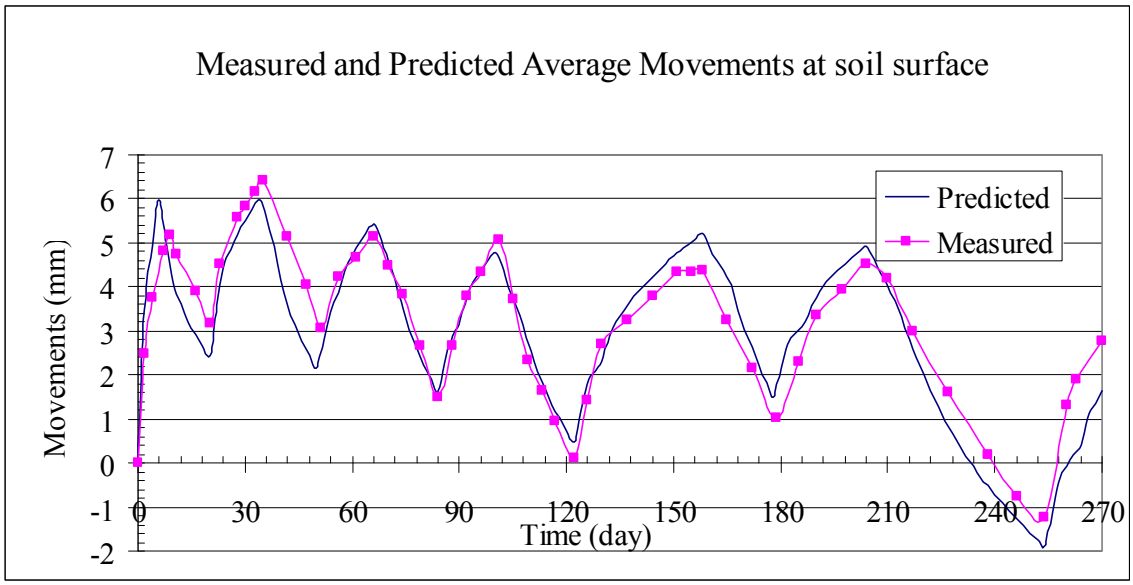

Fig. 4.37. Average soil surface movements (Uncovered phase).

However, obvious discrepancy between predicted and measured soil average movements at depths 100 and 220 mm for the uncovered phase is shown in Fig. 4.38. The reason behind this discrepancy can be referred to the installation method of the embedded pedestals and extension stems. Backfilling the annulus gape between the hole and the extension stem, Fig. 4.24, was very difficult because, the small annulus gape didn't allow good compaction of the soil fillings. Consequently, voids and small pockets

were formed around extension stems, which provided preferential flow passes for moisture diffusion. These preferential flow passes made the deep soil around the embedded pedestals more responsive to surface suction change than it should be, and this is manifested in the cyclic movement pattern of the soil at depths 100 and 220 mm shown in Fig. 4.38.

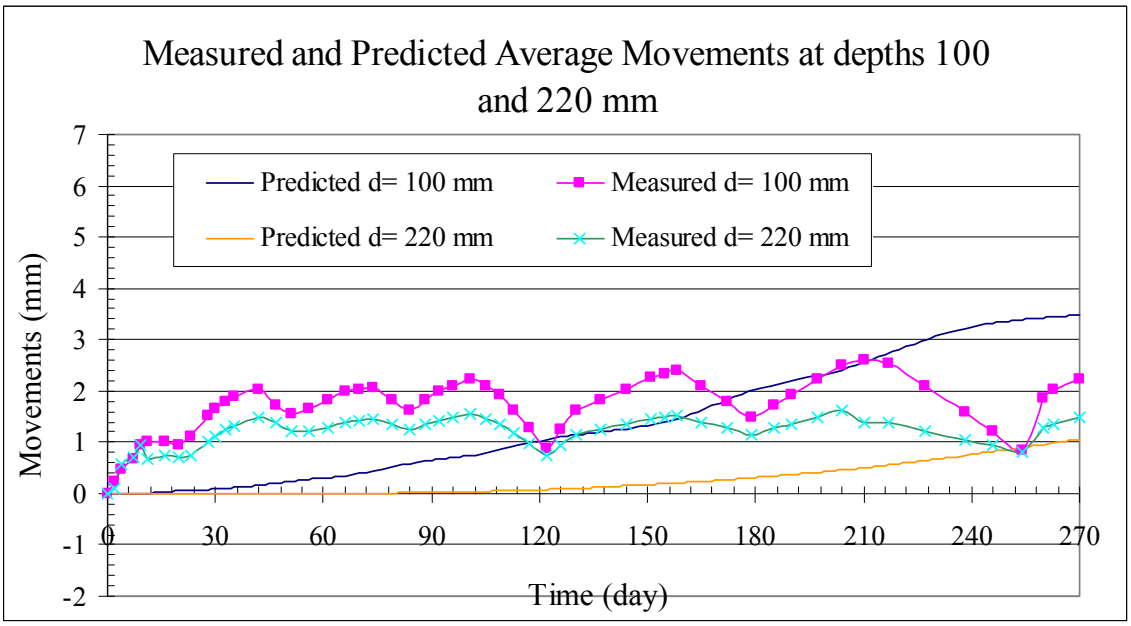

Fig. 4.38. Average soil movements at depths 100 and 220 mm (Uncovered phase).

b) Covered phase.

Predicted and measured surface soil average movements for the covered phase is presented in Fig. 4.39.

A reasonable matching between measured and predicted surface soil average movements, only at radius 500 mm is manifested in Fig. 4.39. However, the rest of the radii measurements follow an oscillating pattern with obvious discrepancy from the predicted values. Roughly speaking, at any radius, the measured value at a depth is close to the average between the surface measurement at that radius and the predicted value at

that depth. This phenomenon was due to surface leaks under the rubber cover; despite all precautions that have been taken, the lateral (radially from the perimeter to the center) soil shrinkage buckled the rubber cover up at many locations inducing horizontal leak passages under the rubber cover. Soil at radius 500 mm did not get influenced with this phenomenon as it was away from the cover.

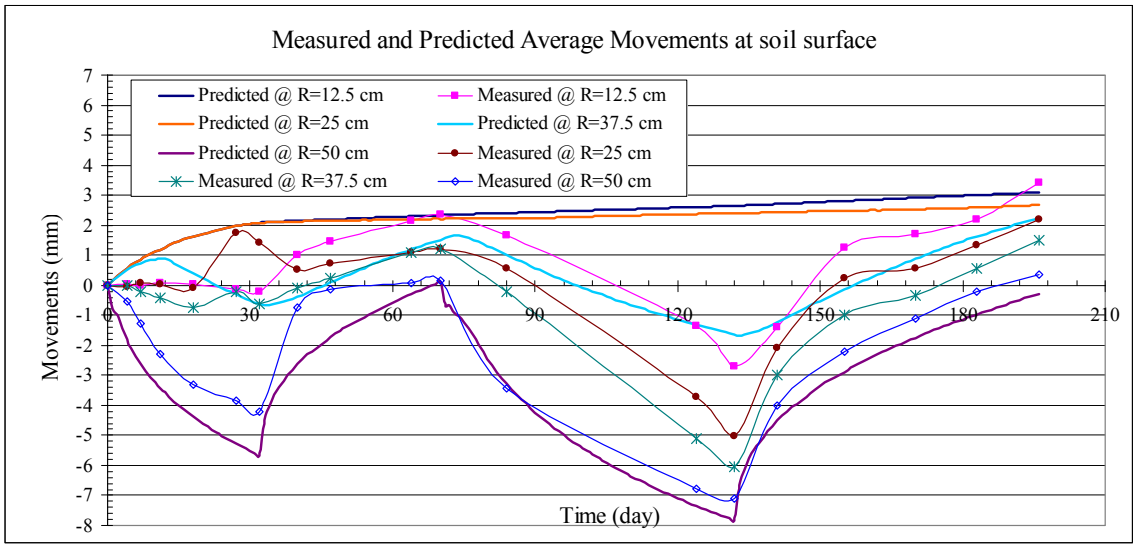

Fig. 4.39. Average soil surface movements (Covered phase).

Predicted and measured water content results after 32 days are shown in Fig. 4.40. Fig. 4.40 shows a reasonable matching between the measured water content profiles and the predicted profiles. Fig. D.6, Fig. D.7 & Fig. D.8 show predicted and measured water content results after 70, 132 and 196 days respectively. Fig. D.6, Fig. D.7 & Fig. D.8 show that the reasonable matching between predicted and measured water content results continued until the end of the covered phase.

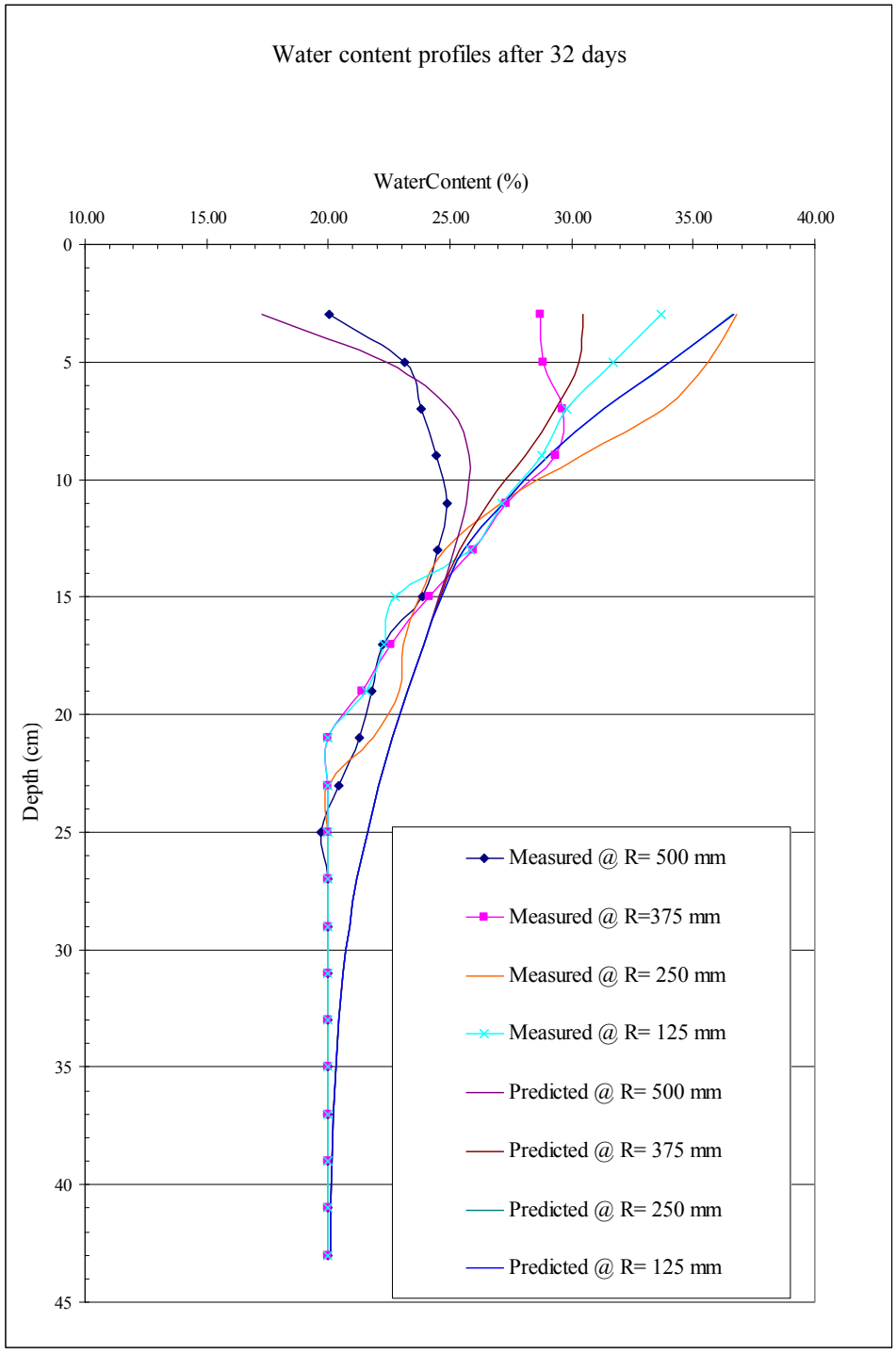

Fig. 4.40. Water content results after 32 days (Covered phase).

Tables D.3 and D.4 present the tabulated results for the predicted water contents and measured water contents respectively. To assess the resulting matching between the predicted and measured water content profiles, the rout mean square error, between predicted and measured, value (RMS) was calculated for each water content profile and tabulated in Table D.4. The average RMS for all predicted and measured water content profiles was 1.183 %, which is a reasonable error value, especially when you compare it with the average initial water content value 20 %.

4.8.6 Conclusions

A large scale laboratory test was carried out to verify the proposed new methods to determine the coefficient of unsaturated diffusivity at laboratory, α_{lab}, and to estimate the coefficient of unsaturated diffusivity at field, α_{field}. The large scale laboratory test was run to model the moisture diffusion in a 1.2 m diameter tank filled with 0.44 m homogeneous soil layer subjected to several wetting and drying cycles with two phases: uncovered phase-and covered phased. The uncovered phase consisted of six shrink-swell cycles that took 270 days, and the covered phase consisted of two shrink-swell cycles tha took 196 days. Cyclic wetting and drying cycles developed a steady crack network with a depth of active moisture changes of 0.32 m. The experiment was numerically simulated using ABAQUS / STANDARD; input parameters were measured in laboratory including the coefficient of unsaturated diffusivity at laboratory, α_{lab}, and the coefficient of unsaturated diffusivity at field, α_{field}. was estimated using the proposed chart Fig. 4.14. the ratio of the vertical strain to the volumetric strain was assumed as has been discussed in section 4.6.

Very reasonable matching between the measured and predicted water content results was observed during the entire experiment. The average RMS values for all predicted and measured water content profiles were 0.974 % for the uncovered phase and 1.183 % for the covered phase.

Strong matching between the measured and predicted average soil surface movements was observed during the uncovered phase, the RMS value was 0.511 mm.

Local preferential moisture diffusion passes around the extension stems influenced the measured average movements at depths 100 and 220 mm inducing discrepancy between the measured and the predicted average movements at those depths.

During the covered phase, reasonable matching between measured and predicted surface soil average movements was manifested only at radius 500 mm yet the rest of the radii measurements follow an oscillating pattern with obvious discrepancy from the predicted values. This phenomenon was due to surface leaks under the rubber cover as the lateral soil shrinkage buckled the rubber cover up at many locations inducing horizontal leak passages under the rubber cover.

The proposed technique consists of measuring the coefficient of unsaturated diffusivity at laboratory, α_{lab}, estimating the coefficient of unsaturated diffusivity at field, α_{field}, and assuming the coefficient f. Generally, the proposed technique succeeded to closely predict water contents measurements and average soil surface movement measurements of this large scale long term laboratory experiment.

CHAPTER V

PROPOSED WEATHER-SOIL INTERACTION MODEL

5.1 Introduction

Zhang, X (2004) was the first researcher who used FAO 56-PM in the geotechnical engineering field to simulate the foundation slab performance on shrink-swell soils. Zhang, X (2004) successfully implemented the FAO 56-PM method to simulate some real shallow foundations performance on shrink-swell soils; the FAO 56-PM provided his simulations with the weather boundary conditions as a daily input/output moisture flux. The usage of FAO 56-PM enabled him to closely match his field measurements.

This chapter explains using the FAO 56-PM method to simulate a weightless cover performance for six cities in US that suffer significantly from shallow foundation problems on shrink-swell soils due to seasonal weather variations. These simulations provide us with more accurate weather site-specific parameters of such as the range of surface suction variations. The proposed weather-site specific parameters will be input parameters to the soil structure models.

5.2 FAO 56-PM method

5.2.1 General

To compute the volume change of saturated and unsaturated soils, the boundary conditions at the ground surface must be known. The prescribed water flux boundary condition specifies the rate of water loss or gain at the soil surface can be estimated using the FAO 56-PM method. Although there is no theoretic method to evaluate the evaporation accurately, empirical methods for estimating the evaporation have been well established in the agriculture engineering field. In May 1990, FAO organized a consultation of experts and researchers in collaboration with the International Commission for Irrigation and Drainage and with the World Meteorological Organization, to review the FAO methodologies on crop water requirements and to

advise on the revision and update of procedures. The panel of experts recommended the adoption of the Penman-Monteith combination method as a new standard for reference evapotranspiration and advised on procedures for calculating the various parameters.

The FAO 56-PM method is an hourly or daily grass reference ET "EvapoTranspiration" equation derived from the ASCE PM-90 by assigning certain parameter values based on a specific reference surface. This surface has an assumed height of 0.12 m, a fixed surface resistance of 70 s/ m, and an albedo of 0.23. The zero plane displacement height and roughness lengths are estimated as a function of the assumed crop height, so that e_a becomes a function of only the measured wind speed. The height for the temperature, humidity, and wind measurements is assumed to be 2 m. The latent heat of vaporization (λ) is assigned a constant value of 2.45 MJ/kg. The FAO 56 Penman-Monteith form of the combination equation is:

$$ET_0 = \frac{0.408\Delta\left(R_n - G\right) + \gamma \frac{900}{T+273} u_2 \left(e_s - e_a\right)}{\Delta + \gamma\left(1 + 0.34 u_2\right)} \quad (5.1)$$

Where:

ET_0 = reference evapotranspiration (mm day^{-1}),

R_n = net radiation at the crop surface (MJ m^{-2} day^{-1}),

G = soil heat flux density (MJ m^{-2} day^{-1}),

T = air temperature at 2 m height (°C),

u_2 = wind speed at 2 m height (m s^{-1}),

e_s = saturation vapor pressure (kPa),

e_a = actual vapor pressure (kPa),

e_s - e_a = saturation vapor pressure deficit (kPa),

Δ = slope vapor pressure curve (kPa $°C^{-1}$), and

γ = psychrometric constant (kPa $°C^{-1}$).

5.2.2 An example: reference ET for a site at College Station , Texas, USA

A site at College Station, Texas is used as an example to calculate the reference ET. The calculation will be also used for five more cities with different soils to estimate the soil surface suction changes. The Southern Regional Climate Center at Louisiana State University provided hourly or daily weather data such as temperature, relative humidity, wind speed, and rainfall, which was used in all soil-weather simulations in this chapter.

a). Extraterrestrial radiation (Ra)

The principle source of heat energy for ET is solar radiation for the sun. The solar radiation received at the top of the earth's atmosphere on a horizontal surface is called the extraterrestrial (solar) radiation, R_a. If the sun is directly overhead, the surface is perpendicular to the sun's rays at the top of the earth's atmosphere and the radiation is constant (about 0.082 MJ m-2 min-1). It is also called the solar constant. The actual intensity of radiation is determined by the angle between the direction of the sun's rays and the normal to the surface of the atmosphere. This angle will change during the day and will be different at different latitudes and in different seasons. However, for the same place and the same day in the year, it is the same. The extraterrestrial radiation, R_a, for each day of the year and for different latitudes can be estimated from the solar constant, the solar declination and the time of the year by:

$$R_a = \frac{24(60)}{\pi} G_{sc} d_r \left[\omega_s \sin\varphi \sin\delta + \cos\varphi \cos\delta \sin\omega_s \right] \tag{5.2}$$

where

R_a extraterrestrial radiation [MJ m^{-2} day^{-1}],

G_{sc} solar constant = 0.0820 MJ m^{-2} min^{-1},

d_r inverse relative distance Earth-Sun, $d_r = 1 + 0.0033\cos\left(2\pi J / 365\right)$,

ω_s sunset hour angle [rad], $\omega_s = \arccos[-\tan(\varphi)\tan(\delta)]$,

φ latitude [rad],

δ solar decimation, $\delta = 0.409\sin\left(2\pi J / 365 - 1.39\right)$,[rad],

J is the number of the day in the year.

All the data needed for Equation 5.2 are the latitude of the site and the day number for each day. College Station has latitude of 30.616 N, and average elevation of 103m (338ft).

R_a is expressed in the above equation in MJ m^{-2} day^{-1}. The corresponding equivalent evaporation in mm/day is obtained by multiplying R_a by 0.408.

b) Solar or shortwave radiation (R_s)

When there are clouds, some of the radiation is scattered, reflected or absorbed by the atmospheric gases, clouds and dust. The amount of radiation reaching a horizontal plane is known as the solar radiation, R_s. For a cloudless day, R_s is roughly 75% of extraterrestrial radiation. On a cloudy day, the radiation is scattered in the atmosphere, but even with extremely dense cloud cover, about 25% of the extraterrestrial radiation may still reach the earth's surface mainly as diffuse sky radiation. Solar radiation is also known as global radiation, meaning that it is the sum of direct shortwave radiation from the sun and diffuse sky radiation from all upward angles.

R_s can be calculated with the Angstrom formula which relates solar radiation to extraterrestrial radiation and relative sunshine duration:

$$R_s = \left(a_s + b_s \frac{n}{N} \right) R_a \tag{5.3}$$

where

R_s= solar or shortwave radiation [MJ m^{-2} day^{-1}],

n =actual duration of sunshine [hour],

N =maximum possible duration of sunshine or daylight hours [hour],

n/N =relative sunshine duration [-],

R_a =extraterrestrial radiation [MJ m^{-2} day^{-1}],

α_s =regression constant, expressing the fraction of extraterrestrial radiation reaching the earth on overcast days (n = 0), a_s+b_s fraction of extraterrestrial radiation reaching the earth on clear days (n = N).

Because the actual duration of sunshine n is not available for the site, the Hargreaves' radiation formula was used to calculate the R_s,

$$R_s = k_{Rs}\sqrt{(T_{\max} - T_{\min})}R_a \quad (5.4)$$

Where

Ra extraterrestrial radiation [MJ m^{-2} d^{-1}],

T_{max} maximum air temperature [°C],

T_{min} minimum air temperature [°C],

k_{Rs} adjustment coefficient (0.16~0.19), k_{Rs} is taken as 0.18 [$°C^{-0.5}$].

c) Clear-sky solar radiation (R_{so})

The clear-sky radiation, R_{so}, when n = N for R_s, is calculated by the following equation:

$$R_{so} = (0.75 + 2 \times 10^{-5} z)R_a \quad (5.5)$$

where:

z station elevation above sea leveling meter, which is 103m (338ft) for the site.

d) Net solar radiation (R_{ns})

A considerable amount of solar radiation reaching the earth's surface is reflected. The fraction of the solar radiation R_s that is not reflected from the surface is called the net solar radiation, R_{ns}. The net solar radiation, R_{ns}, is the fraction of the solar radiation R_s that is not reflected from the surface. It is calculated by the following equation,

$$R_{ns}=(1-\alpha)R_s \quad (5.6)$$

For the green grass reference crop, α is assumed to have a value of 0.23.

e) Net long wave radiation (R_{nl})

The rate of long wave energy emission is proportional to the absolute temperature of the surface raised to the fourth power. This relation is expressed quantitatively by the Stefan-Boltzmann law. The net energy flux leaving the earth's surface is, however, less than that emitted and given by the Stefan-Boltzmann law due to the absorption and downward radiation from the sky. Water vapor, clouds, carbon dioxide and dust are

absorbers and emitters of long wave radiation. Their concentrations should be known when assessing the net outgoing flux. As humidity and cloudiness play an important role, the Stefan-Boltzmann law is corrected by these two factors when estimating - the net outgoing flux of long wave radiation. It is thereby assumed that the concentrations of the other absorbers are constant:

$$R_{nl} = \sigma \left[\frac{T_{\max,K}^{\ 4} + T_{\min,K}^{\ 4}}{2} \right] \left(0.34 - 0.14\sqrt{e_a}\right) \left(1.35 \frac{R_s}{R_{s0}} - 0.35\right) \qquad (5.7)$$

Where

R_{nl} net outgoing longwave radiation [MJ m^{-2} day^{-1}],

σ Stefan-Boltzmann constant [4.903 X 10^{-9} MJ K^{-4} m^{-2} day^{-1}],

T_{max}, K maximum absolute temperature during the 24-hour period [K = °C + 273.16],

T_{min}, K minimum absolute temperature during the 24-hour period [K = °C + 273.16],

e_a actual vapour pressure [kPa],

R_s/R_{so} relative shortwave radiation (limited to £ 1.0),

R_s measured or calculated (Equation 5.4) solar radiation [MJ m^{-2} day^{-1}],

R_{so} calculated (Equation 5.5) clear-sky radiation [MJ m^{-2} day^{-1}].

An average of the maximum air temperature to the fourth power and the minimum air temperature to the fourth power is commonly used in the Stefan-Boltzmann equation for 24-hour time steps. The term $\left(0.34 - 0.14\sqrt{e_a}\right)$ expresses the correction for air humidity, and will be smaller if the humidity increases. The effect of cloudiness is expressed by $\left(1.35 \frac{R_s}{R_{s0}} - 0.35\right)$. The term becomes smaller if the cloudiness increases and hence Rs decreases. The smaller the correction terms, the smaller the net outgoing flux of longwave radiation. Note that the R_s/R_{so} term in Equation 5.7 must be limited so that $R_s/R_{so} \leq 1.0$.

f) Net radiation (R_n)

The net radiation (R_n) is the difference between the incoming net shortwave radiation (R_{ns}) and the outgoing net long wave radiation (R_{nl}):

$$R_n = R_{ns} - R_{nl} \quad (5.8)$$

g) Soil heat flux (G)

Complex models are available to describe soil heat flux. Because soil heat flux is small compared to R_n, particularly when the surface is covered by vegetation and calculation time steps are 24 hours or longer, a simple calculation procedure is presented here for long time steps, based on the idea that the soil temperature follows air temperature:

$$G = C_s \frac{T_i - T_{i-1}}{\Delta t} \Delta z \quad (5.9)$$

Where

G soil heat flux [MJ m^{-2} day^{-1}],

C_s soil heat capacity [MJ m^{-3} $°C^{-1}$],

T_i air temperature at time i [°C],

T_{i-1} air temperature at time i-1 [°C],

Δt length of time interval [day],

Δz effective soil depth [m].

As the soil temperature lags air temperature, the average temperature for a period should be considered when assessing the daily soil heat flux, i.e., Δt should exceed one day. The depth of penetration of the temperature wave is determined by the length of the time interval. The effective soil depth, Δz, is only 0.10-0.20 m for a time interval of one or a few days but might be 2 m or more for monthly periods. The soil heat capacity is related to its mineral composition and water content.

As the magnitude of the day, soil heat flux beneath the grass reference surface is relatively small, it may be ignored and thus:

$$G_{day} \cong 0 \quad (5.10)$$

h) Saturation vapor pressure

Saturation vapor pressure is related to air temperature. It can be calculated from the air temperature by:

$$e^{o}\left(T\right)=0.6108\exp\left[\frac{17.27T}{T+237.4}\right] \tag{5.11}$$

Where

e°(T) saturation vapor pressure at the air temperature T [kPa],

T air temperature [°C]

i). Actual vapor pressure (e_a) can be derived from dew point temperature,

$$e_a=e^{o}\left(T_{dew}\right)=0.6108\exp\left[\frac{17.27T_{dew}}{T_{dew}+237.4}\right] \tag{5.12}$$

j). Slope of saturation vapor pressure curve (Δ)

$$\Delta=\frac{4098\left[0.6108\exp\left(\frac{17.27T}{T+237.4}\right)\right]}{\left(T+237.4\right)^{2}} \tag{5.13}$$

k). Atmospheric pressure (P)

$$P=101.3\left(\frac{293-0.0065z}{293}\right)^{5.26} \tag{5.14}$$

Where

P atmospheric pressure [kPa],

z elevation above sea level [m],

l) Latent heat of vaporization (λ)

λ = 2.45 MJ kg^{-1} is taken in the simplification of the FAO 45 Penman-Monteith equation. This is the latent heat for an air temperature of about 20°C.

m) Psychrometric constant (γ)

The psychrometric constant, γ, is given by:

$$\gamma=\frac{C_p P}{\varepsilon\lambda}=0.665\times10^{-3}P \tag{5.15}$$

Where

γ psychrometric constant [kPa $°C^{-1}$],

P atmospheric pressure [kPa],

λ latent heat of vaporization, 2.45 [MJ kg^{-1}],

C_p specific heat at constant pressure, 1.013 $X10^{-3}$ [MJ kg^{-1} $°C^{-1}$],

ε ratio molecular weight of water vapor/dry air = 0.622.

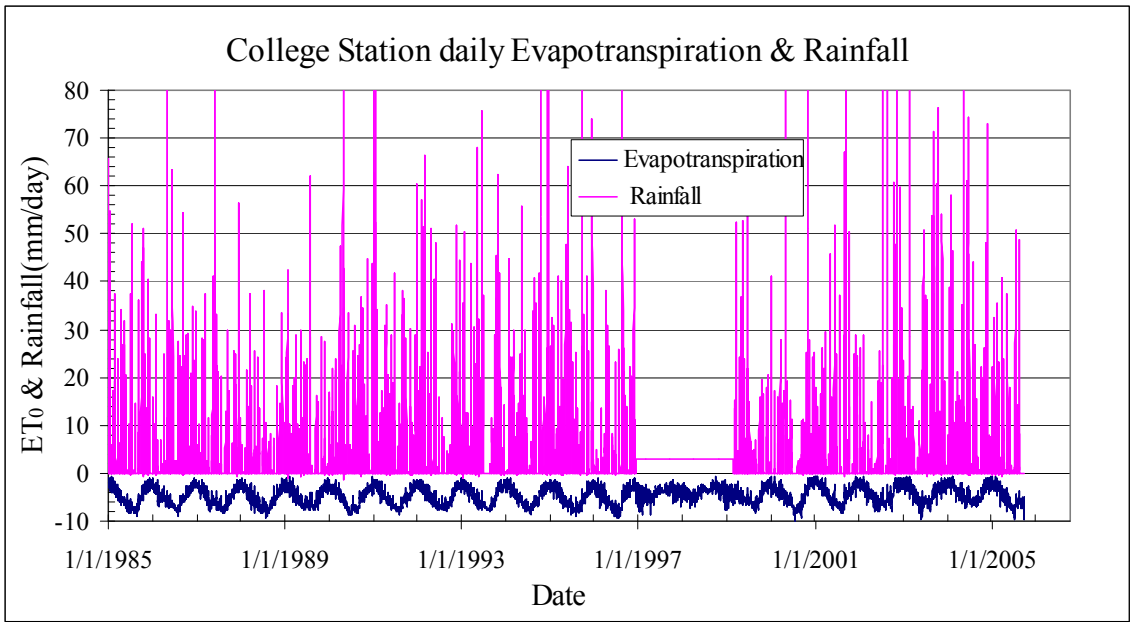

Fig. 5.1. Daily evapotranspiration and rainfall of College Station, Texas from 01/01/1985 to 03/30/2005.

The potential evaporation from 01/01/1985 to 03/30/2005 was calculated and the result is shown in Fig. 5.1. Fig. 5.1. also shows the daily rainfall data for this period. It was assumed that the average value of the rainfall is applied for periods without available rainfall data as can be seen from 1997 to 1999.

5.2.3 Crop evapotranspiration

The above calculation is the reference crop evapotranspiration by assuming that the reference crop has an assumed height of 0.12 m, with a surface resistance of 70 s/m and an albedo of 0.23, which closely resembles the evaporation from an extensive surface of green grass of uniform height, actively growing and adequately watered. The calculation expresses the evaporating ability of the atmosphere at a specific location and time of the year and does not consider the crop characteristics and soil factors.

The crop evapotranspiration differs distinctly from the reference grass evapotranspiration (ET_o) as the ground cover, canopy properties and aerodynamic resistance of the crop are different from grass. In the FAO 56 PM Method, the effects of characteristics that distinguish the cropped surface from the reference surface are integrated into the crop coefficient. Two calculation approaches are used to change the reference grass evapotranspiration in to cropped evapotranspiration (the potential evapotranspiration for actual crop (vegetation)): the single and the dual crop coefficient approach. The single crop coefficient approach was used in this dissertation to show the procedure of the simulation. By multiplying ET_o by the crop coefficient, ET_c, which is called crop evapotranspiration under standard conditions, is determined.

$$ET_c = K_c\, ET_o \tag{5.16}$$

Where

ET_c crop evapotranspiration [mm/ddy],

K_c crop coefficient [dimensionless],

ET_o reference crop evapotranspiration [mm/day].

ET_c represents the evapotranspiration from disease-free, well-fertilized crops, grown in large fields, under optimum soil water conditions and achieving full production under the given climatic conditions. Factors influencing the crop coefficient include the crop type, climate, soil evaporation and crop growth stages. Texas ET Network (http://texaset.tamu.edu/) recommends that the crop coefficient, K_c, for this kind of grass is 0.6 through much of the year. For the dual crop coefficient approach, the principle is

similar. Texas ET Network also recommends that the average water stress coefficient, K_s, for low stress is 0.8 through much of the year.

The evapotranspiration under non-standard conditions ($ET_{c\ adj}$) is the evapotranspiration from crops or vegetations grown under management and environmental conditions that differ from the standard conditions. The actual evapotranspiration in the field may deviate from ET_c due to non-optimal conditions such as the presence of pests and diseases, soil salinity, low soil fertility, water shortage or water logging. This may result in scanty plant growth, low plant density and may reduce the evapotranspiration rate below ET_c. The effects of soil water stress are described by multiplying the basal crop coefficient by the water stress coefficient, Ks

$$ET_{c\ adjusted} = K_s \times K_c \times ET_0 \quad (5.17)$$

5.2.4 Water balance and net water loss

The total available water in the root zone is defined as the difference between the water content at field capacity and wilting point:

$$TAW = 1000(\theta_{FC} - \theta_{WP})\ H \quad (5.18)$$

Where

TAW the total available soil water in the root zone [mm],

θ_{FC} the water content at field capacity [m^3/m^3],

θ_{WP} the water content at permanent wilting point [m^3/m^3],

H the rooting depth [m].

Before further discussion of the application of the actual evapotranspiration to the boundary conditions, the water balance at the root zone is discussed. To determine the actual evapotranspiration at the grass root zone, a daily water balance computation for the grass root zone is required. The daily water content can be expressed in terms of depletion at the end of the day as followings:

$$D_{r,\,i} = D_{r,\,i-1} - (P - RO)_i - I_i - CR_i + ET_{c,\,i} + DP_i \quad (5.19)$$

where

$D_{r,\,i}$ root zone depletion at the end of day i [mm],

$D_{r,\,i-1}$ water content in the root zone at the end of the previous day, i-1 [mm],

P_i precipitation on day i [mm],

RO_i runoff from the soil surface on day i [mm],

I_i net irrigation depth on day i that infiltrates the soil [mm],

CR_i capillary rise from the groundwater table on day i [mm],

$ET_{c,\,i}$ actual evapotranspiration on day i [mm],

DP_i water loss out of the root zone by deep percolation on day i [mm].

Equation 5.19 represents that rainfall, irrigation and capillary rise of groundwater towards the root zone add water to the root zone and decrease the root zone depletion. Soil evaporation, crop transpiration and percolation losses remove water from the root zone and increase the depletion.

The initial depletion of the root zone can be calculated from the constitutive surfaces. The initial depletion is defined as:

$$D_{r,\,i-1} = 1000(\theta_{FC} - \theta_{i-1})\,H \qquad (5.20)$$

where:

θ_{i-1} is the soil volumetric water content for the effective root zone at the end of day i.

The FAO 56 PM method considers that CR can normally be assumed to be zero when the water table is more than about 1 m below the bottom of the root zone. More information on CR is presented in FAO Irrigation and Drainage Paper No. 24. Consequently, Equation 5.19 is converted into,

$$D_{r,\,i} = D_{r,\,i-1} - (P - RO - DP)_i + ET_{c,\,i} \qquad (5.21)$$

The FAO 56 PM Method proposes that, although following heavy rain or irrigation the water content might temporally exceed field capacity, the total amount of water above field capacity is assumed to be lost the same day by deep percolation, following any evapotranspiration for that day. By assuming that the root zone is at field capacity following heavy rain or irrigation, the minimum value for the depletion $D_{r,\,i}$ is zero. As a result of percolation and evapotranspiration, the water content in the root zone will gradually decrease and the root zone depletion will increase. In the absence of any

wetting event, the water content will steadily reach its minimum value θ_{WP}. At that moment no water is left for evapotranspiration in the root zone, K_s becomes zero, and the root zone depletion has reached its maximum value. TAW. The limits imposed on $D_{r,\,i-1}$ and $D_{r,\,i}$ are consequently:

$$0 < D_{r,\,i} < TAW \tag{5.22}$$

If there is no rain during the day, that is, P=0, there will not be runoff, RO=0. The FAO 56 PM method consider that as long as the soil water content in the grass root zone is below field capacity (i.e., $D_{r,\,i} > 0$), the soil will not drain and $DP_i = 0$. Consequently, $\left(P-\left(RO+DP\right)\right)_i$=0. The net water loss therefore is,

$$D_{r,\,i} = D_{r,\,i-1} + ET_{c,\,i} \tag{5.23}$$

Equation 5.33 must be satisfied, hence,

$$0 < D_{r,i} = D_{r,i-1} + ET_{c,i} < TAW \tag{5.24}$$

Substituting Equation 5.20 into 5.24 gives,

$$ET_{c,i} < 1000\left(\left(\theta_{FC}-\theta_{wp}\right)-\left(\theta_{FC}-\theta_{i-1}\right)\right)H \tag{5.25}$$

that is

$$ET_{c,i} < 1000\left(\left(\theta_{i-1}-\theta_{wp}\right)\right)H \tag{5.26}$$

$1000\left(\left(\theta_{i-1}-\theta_{wp}\right)\right)H$ is the water available for evapotranspiration. If the calculated $ET_{c,i}$ is greater than $1000\left(\left(\theta_{i-1}-\theta_{wp}\right)\right)H$, $ET_{c,i}$=$1000\left(\left(\theta_{i-1}-\theta_{wp}\right)\right)H$. In summary, for a day with no rainfall, we have

$$\begin{aligned} &NWL = ET_{c,i}, \ \text{ if } \ ET_{c,i} < 1000\left(\left(\theta_{i-1}-\theta_{wp}\right)\right)H \\ &NWL = 1000\left(\left(\theta_{i-1}-\theta_{wp}\right)\right), \ \text{ if } \ ET_{c,i} \geq 1000\left(\left(\theta_{i-1}-\theta_{wp}\right)\right)H \end{aligned} \tag{5.27}$$

Where:

NWL is the final net water loss or gain.

If there is rainfall during the i^{th} day, the precipitation is equivalent to daily rainfall. It is noted that in only very rare cases, it will rain 24 hours incessantly. Therefore, there is

evapotranspiration even during a raining day and the evapotranspiration is expected to be significant because the water is freely available. The FAO56 PM Method proposes that daily precipitation in amounts less than about 0.2 ET_0 is normally entirely evaporated and can usually be ignored in the water balance calculation, especially when the single crop coefficient approach is being used. Consequently, the effective precipitation is the difference between the daily precipitation and the actual evapotranspiration. It is the actual amount of water available to the soil. The FAO 56 PM method consider that as long as the soil water content in the grass root zone is below field capacity (i.e., $D_{r,\,i} > 0$), the soil will not drain and $DP_i = 0$. Similarly, it is reasonable to assume that if the soil water content in the grass root zone is below field capacity (i.e., $D_{r,\,i} > 0$), there is no runoff.

Therefore, when there is rainfall during a day, two categories of condition needed to be considered. One is when the rainfall is less than the evapotranspiration during the day. The other is when the rainfall is greater than the evapotranspiration during the day.

For the first condition, the daily total evapotranspiration is greater than the rainfall $ET_{c,i} - P_i > 0$, there is net evapotranspiration and no runoff or deep percolation.. The net evapotranspiration will cause the soil to lose water until the soil reaches wilt point. The water needed to make the soil reach the wilt point depends on the current water content, the wilt point water content and the depth of the root zone, which is $1000(\theta_{i-1}-\theta_{wp})H$. $1000(\theta_{i-1}-\theta_{wp})H$ is the maximum water the soil can lose. Equation 5.21 is then written as,

$$D_{r,\,i} = D_{r,\,i-1} + (ET_{c,\,i} - P_i) \tag{5.28}$$

Equation 5.22 must be satisfied, hence, we have,

$$NWL = ET_{c,i} - P_i, \text{ if } 0 < ET_{c,i} - P_i < 1000\left(\left(\theta_{i-1} - \theta_{wp}\right)\right)H \tag{5.29}$$

$$NWL = 1000\left(\left(\theta_{i-1} - \theta_{wp}\right)\right)H, \text{ if } ET_{c,i} - P_i > 1000\left(\left(\theta_{i-1} - \theta_{wp}\right)\right)H \tag{5.30}$$

Equation 5.29 represents that if there is evapotranspiration $ET_{c,i} - P_i > 0$, and the net evapotranspiration ($ET_{c,i} - P_i$) is less than the water available in the soil to lose $1000(\theta_{i-}$

$_1$-θ_{wp})H, then the net water loss (NWL) equals to the net evapotranspiration $ET_{c,i} - P_i$. Equation 5.30 represents that if there is evapotranspiration $ET_{c,i} - P_i > 0$, and the net evapotranspiration ($ET_{c,i} - P_i$) is lager than the water available in the soil, then the actual water loss will be the water available to lose, i.e. $1000(\theta_{i-1}-\theta_{wp})H$ in the soil.

For the second case, if the rainfall is greater than the evapotranspiration $P_i - ET_{c,i} > 0$, there is net infiltration. The infiltration will increase the water content in the soil until the soil arrives at the field capacity. The water needed to make the soil reach the field capacity depends on the current water content, the field capacity and the depth of the root zone, which is $1000(\theta_{FC}-\theta_{i-1})H$. $1000(\theta_{FC}-\theta_{i-1})H$ is the maximum water the soil can absorb. In other words, if it is a really heavy rain, after subtracting the actual evapotranspiration and the amount of water needed for the root zone to reach field capacity, there is still some surplus, then the surplus will be either runoff or deep percolation. Considering Equation 5.21 and 5.22, gives,

$$NWL = ET_{c,i} - P, \text{ if } 0 < P_i - ET_{c,i} < 1000\left(\left(\theta_{CF} - \theta_{i-1}\right)\right)H \tag{5.31}$$

$$NWL = 1000\left(\left(\theta_{CF} - \theta_{i-1}\right)\right), \text{ if } P_i - ET_{c,i} > 1000\left(\left(\theta_{CF} - \theta_{i-1}\right)\right)H \tag{5.32}$$

Equation 5.31 represents that if there is net infiltration P_i-$ET_{c,i}>0$, and the net infiltration (P_i-$ET_{c,i}$) is less than the space available in the soil to store water until it reach the filed capacity, $1000(\theta_{FC}-\theta_{i-1})H$, then the net water gain equals to the net infiltration (P_i-$ET_{c,i}$). Equation 5.32 represents that if the net infiltration (P_i-$ET_{c,i}$) is more than the maximum amount of water the soil can absorb, i.e. $1000(\theta_{FC}-\theta_{i-1})H$, the surplus will be runoff. Fig. 5.2. shows an example of daily NWL from 01/01/1985 to 03/30/2005 for a site with H= 150 mm, θ_{wp} =0.154, and θ_{FC}= 0.979, the site is located at College Station, TX, USA.

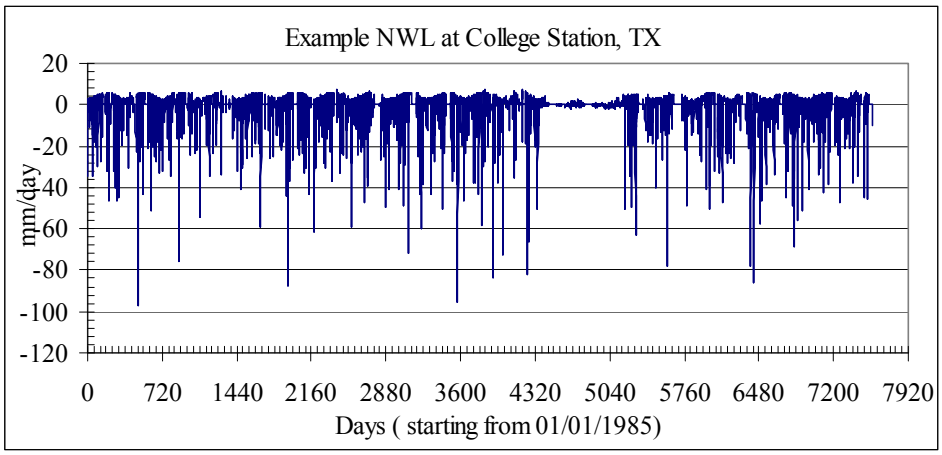

Fig. 5.2. Daily NWL for a site at College Station, Texas from 01/01/1985 to 03/30/2005.

5.3 Numerical model

The finite elements comprehensive software package, ABAQUS/STANDARD, was used to for suction diffusion simulations for a perfectly plastic weightless cover placed on grade, and the free soil surface was subject to weather. Fig. 5.3 shows the geometry of the problem; This problem is a 2D plane strain problem; the ABAQUS/STANDARD CPE4T "Continuum plane strain 4-nodes Temperature" element was chosen in the simulation.

The simulation has 7584 time step (one day each). Table 5.1 shows soil properties used in the soil-weather finite element simulations

Three soils were chosen with field coefficients of unsaturated diffusivity, α_{field}, 0.00724, 0.02042, and 0.26544 m^2/day were derived from three shrink-swell indices, I_{ss} 75, 45, 15% respectively as shown in Table 5.1. The coefficients of saturated permeability and dry densities were assumed to be inversely proportional to the soil plasticity. The range of chosen coefficients of saturated permeability matches the suggested values in Casagrande chart (Holtz & Kovacs, 1981).

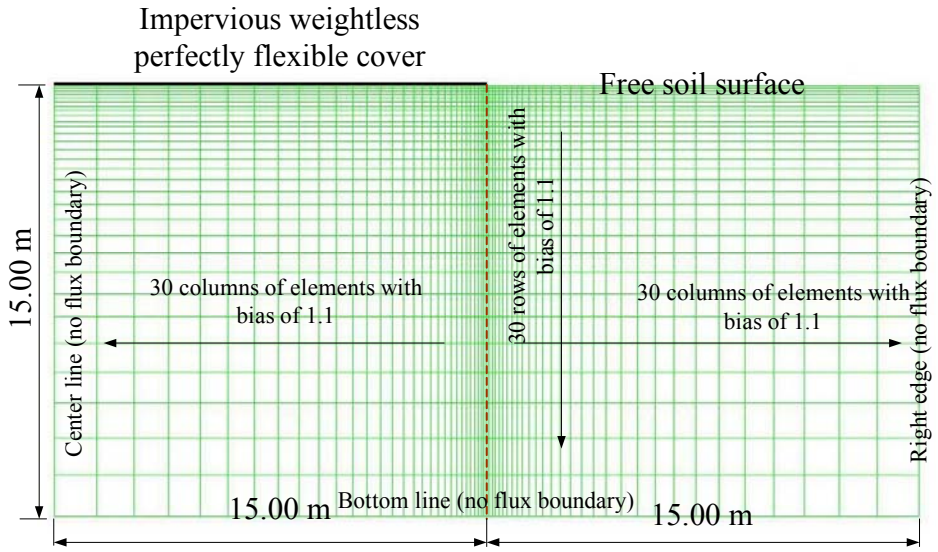

Fig. 5.3. Model used for soil-weather finite element simulation.

Slope of SWCC (expressed as gravimetric water content versus suction), C_w was calculated using I_{ss} using Fig. 4.18 (C_w = 0.5 I_{ss}), and the coefficient of unsaturated diffusivity at laboratory, α_{Lab} was calculated from Eq. 5.33. α_{Lab} was calculated from Eq. 5.34 assuming that cracked soil diffusion factor, F_{CrkDif} = 30 as an average value of F_{CrkDif} values presented in Fig. 4.14.

$$\alpha_{Lab} = \frac{k_{sat} u_{sat}}{0.4343 \frac{\gamma_{dry}}{\gamma_{water}} C_w} \tag{5.33}$$

$$\alpha_{field} = F_{CrkDif} \alpha_{Lab} \tag{5.34}$$

Volumetric water content at wilting point, θ_{wilt} was assumed to be at the soil shrinkage limit, at a suction value of 4.2 pF and calculated from Eq. 5.35. Volumetric water content at field capacity, θ_{FC} was assumed to be at the soil swell limit, at a suction value of 2 pF and calculated from Eq. 5.36. Initial volumetric water content, $\theta_{initial}$ was assumed to be the average of θ_{wilt} and θ_{FC}, at a suction value of 3.1 pF and calculated from Eq. 5.35.

$$\theta_{wilt} = \frac{W_{shrink}\gamma_{dry}}{\gamma_w} \tag{5.36}$$

$$\theta_{FC} = \frac{W_{swell}\gamma_{dry}}{\gamma_w} \tag{5.36}$$

Table 5.1 Soil properties used in the soil-weather finite element simulations.

	(%)		kN/m^3		m^2/sec	m^2/sec	m^2/day
Soil#	I_{ss}	c_w	γ_{dry}	γ_h	α_{Lab}	α_{Field}	α_{Field}
1	75	0.375	11	0.4125	2.793E-09	8.379E-08	0.00724
2	45	0.225	13	0.1730769	7.877E-09	2.363E-07	0.02042
3	15	0.075	15	0.05	1.024E-07	3.072E-06	0.26544

						kN/m.sec	kN/m.day
Soil#	w_{shrink}	θ_{wilt}	w_{swell}	θ_{FC}	$\theta_{initial}$	K_{Cond}	K_{Cond}
1	0.14	0.154	0.89	0.979	0.5665	1.50E-07	0.01296
2	0.12	0.156	0.57	0.741	0.4485	3.00E-07	0.02592
3	0.1	0.15	0.25	0.375	0.2625	1.50E-06	0.12960

The initial conditions was a constant suction value of 3.1 pF (-125.9 kPa) (equivalent to T= -3.1 C°). The boundary conditions were: the bottom base, the right side boundary, the center line boundary, and the covered surface have no flux boundary conditions. The top free surface boundary was subject to a flux (varies daily) equal to the NWL, which was calculated as explained in the previous section. Appendix E presents an example ABAQUS/STANDARD input files for these simulations.

5.4 Six cities weather-soil simulations

The numerical soil-weather interaction simulation was used to predict suction envelopes at six cities in US. The maximum and minimum suction values at each depth were determined from the data reduction of the suction values over the 7584 time steps. The difference between the maximum and minimum suctions versus depth gives the suction

change profile (suction envelope). Two suction envelopes were determined; free field suction envelope, and suction envelope under the slab cover. Carrying out these kinds of numerical simulations is very time consuming, so that only six cities were chosen. However, for future work, it is strongly recommended to carry out these simulations allover the US to develop a map with recommended suction change values and depths of active moisture zone.

Choosing the six cites was guided with by the surveying study provided by (Mr. Gary Osborne, P.E. with Osborne Engineering, 2006). The number of foundation contractors in each US city per population, as shown in Fig. 5.4 and Fig. 5.5 may be used as a rough indicator of the size of the foundation problems due to shrink-swell soils. San Antonio, Austin, Dallas, Houston, and Denver are the top five cities with respect to the number of foundation contractors per population. Out of the research responsibility to serve the community, College Station, TX was also chosen, as it is the home of Texas A&M University and has a considerable amount of foundation problems due to shrink-swell soils.

Fig. 5.6. presents College Station, TX, free field suction envelops. The suction change values at soil surface, ΔU_0, can be estimated from Fig. 5.6 for different soil with different coefficients of unsaturated diffusivity at field. Fig. E.1, Fig. E.2, Fig. E.3, Fig. E.4, & Fig. E.5. present San Antonio-TX, Austin-TX, Dallas-TX, Houston-TX, and Denver-CO free field suction envelops.

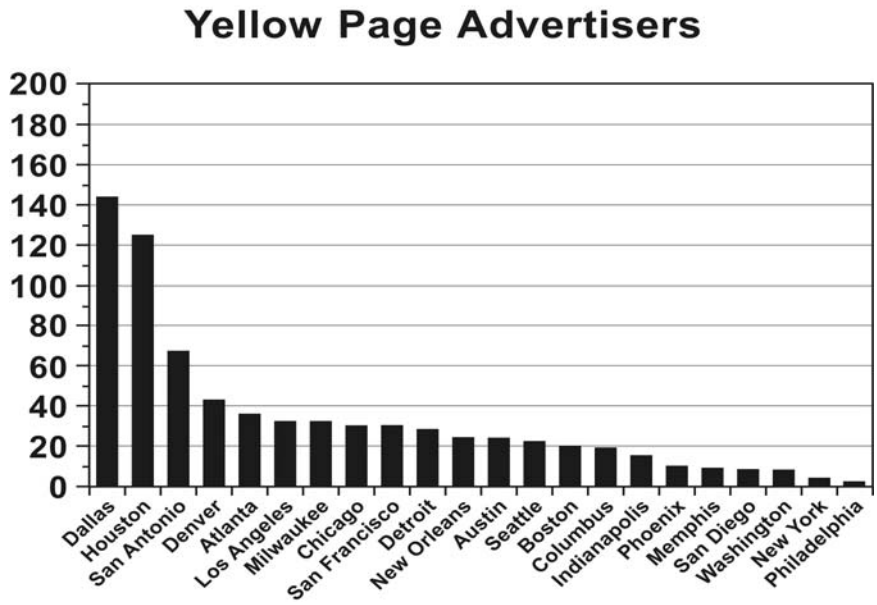

Fig. 5.4. Number of foundation contractors (yellow pages advertisers) versus US cities, (after Osborne, 2006).

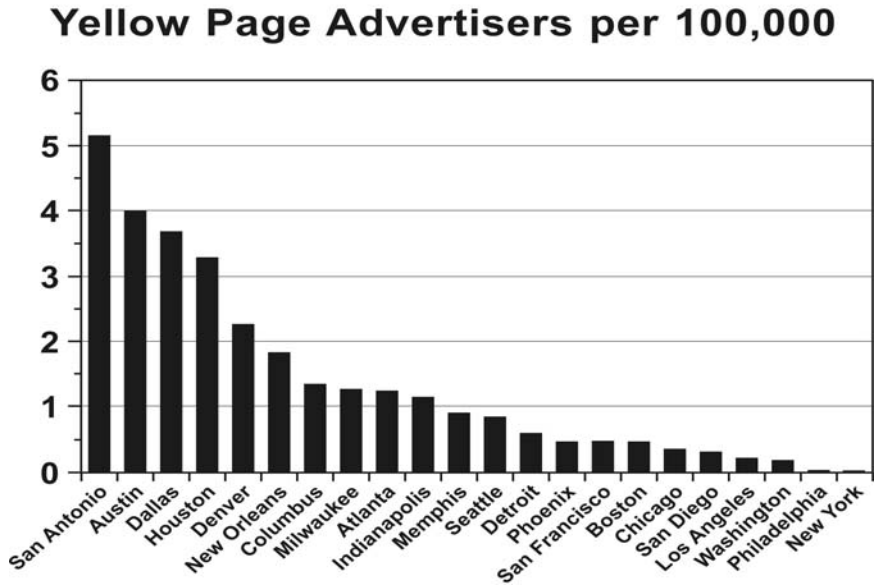

Fig. 5.5. Number of foundation contractors per 100,000 (yellow pages advertisers) versus US cities, (after Osborne, 2006).

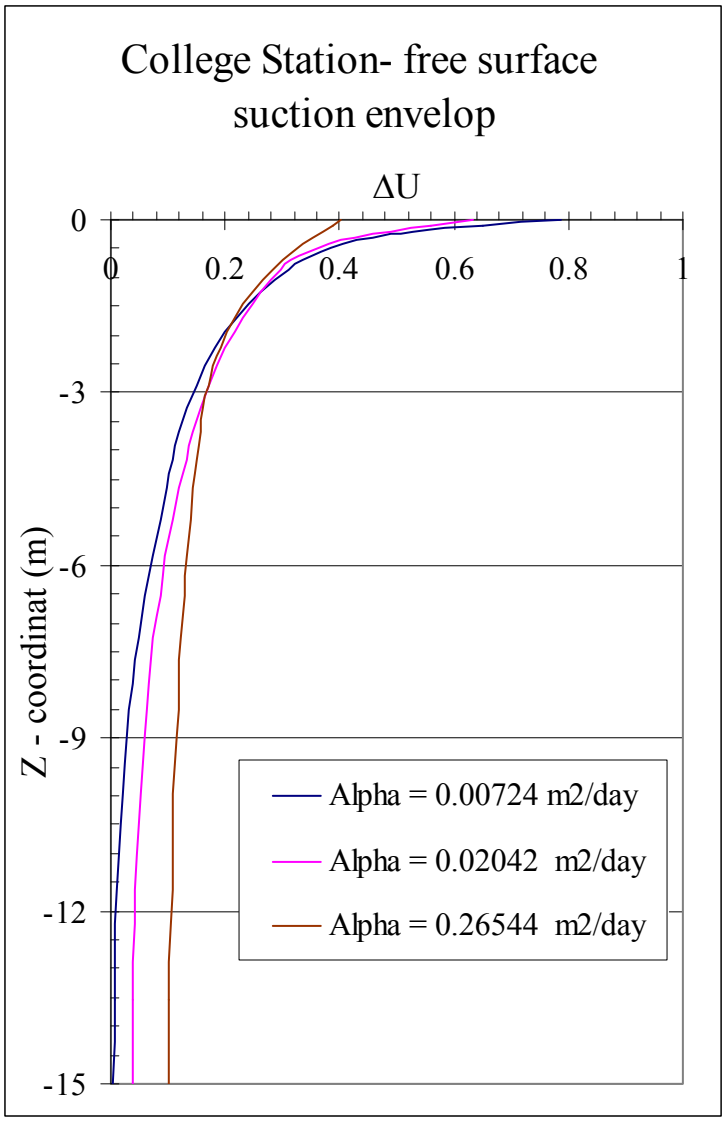

Fig. 5.6. College Station, TX, free field suction envelops.

Fig. 5.7. presents College Station, TX, suction envelops under the weightless impervious perfectly flexible cover. The suction change values directly under the cover edge, ΔU_{edge}, can be estimated from Fig. 5.7 for different soil with different coefficients of unsaturated diffusivity at field. Fig. E.6, Fig. E.7, Fig. E.8, Fig. E.9, & Fig. E.10. present San Antonio-TX, Austin-TX, Dallas-TX, Houston-TX, and Denver-CO suction envelops under the weightless impervious perfectly flexible cover.

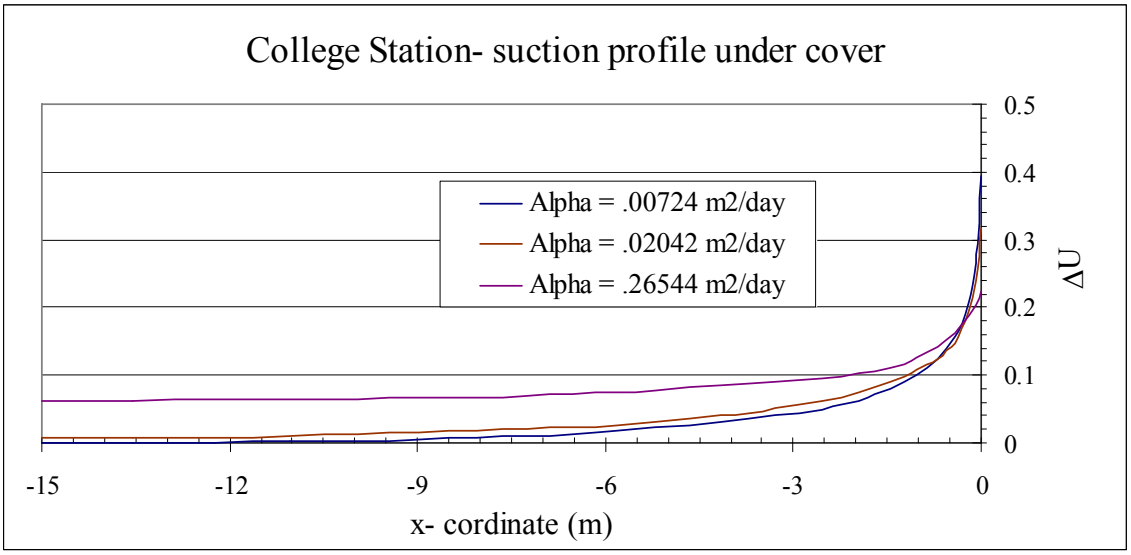

Fig. 5.7. College Station, TX, suction envelops under the weightless impervious perfectly flexible cover.

5.5 Recommended soil surface suction change values

The soil surface suction change values at a free field and under the edge of a covered area are very important parameters for design purposes. Now, these parameters can be easily estimated from suction envelops resulting from the aforementioned soil-weather interaction simulations. Fig. 5.8 shows suction change values at the soil surface of a free field for the chosen six cities. And Fig. 5.9 shows suction change values under the edge of a covered soil surface for the chosen six cities. Fig. 5.8 and Fig. 5.9 suction change values are based on the usage of three soils in the sophisticated and time consuming soil-weather interaction simulations; the three soils were chosen to represent typical very high, average very low shrink-swell potential.

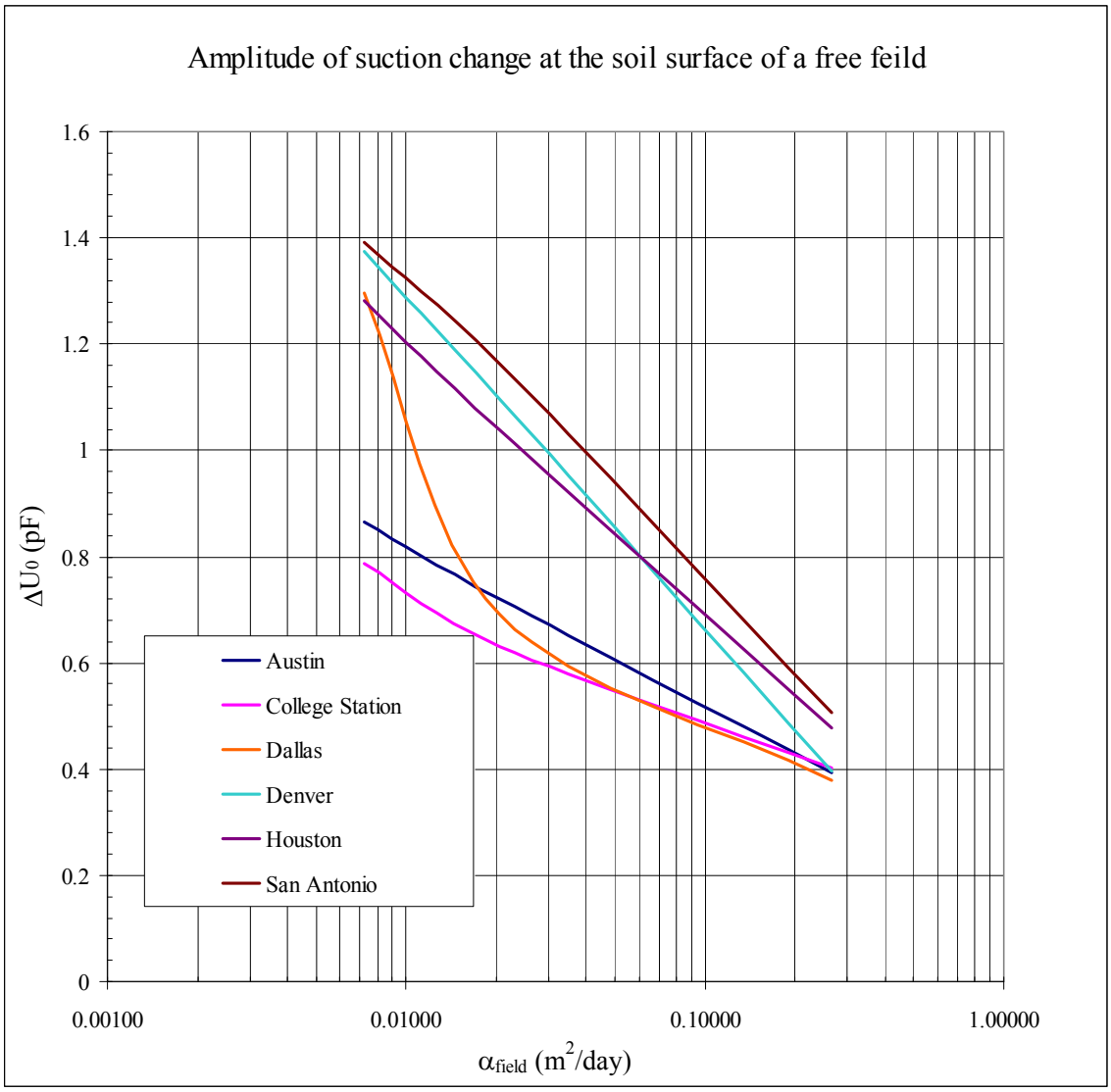

Fig. 5.8. Six cities suction change values at the soil surface of a free field.

It is strongly recommended, for future work, to use actual representative soils at those cities, and the rest of US cities, to get more accurate suction change values. For the time being, it is recommended to use the maximum suction change values for design purposes as shown in Table 5.2

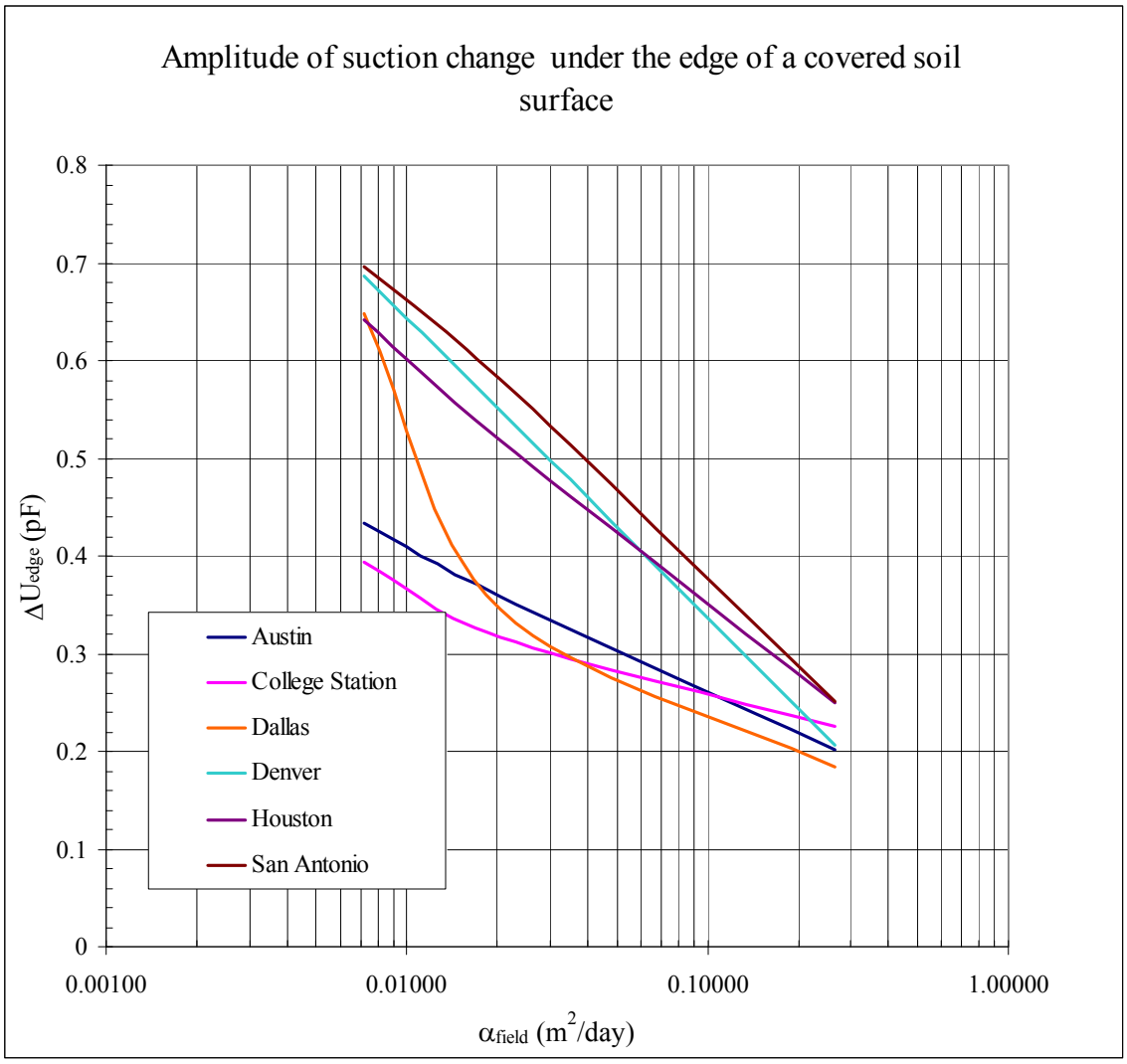

Fig. 5.9. Six cities suction change values under the edge of a covered soil surface.

Table 5.2. Recommended suction change values for design purposes.

	College Station, TX	San Antonio, TX	Austin, TX	Dallas, TX	Houston, TX	Denver, CO
ΔU_0 (pF)	0.788	1.392	0.866	1.295	1.283	1.374
ΔU_{edge} (pF)	0.394	0.696	0.433	0.648	0.642	0.687

CHAPTER VI

PROPOSED SOIL-STRUCTURE INTERACTION MODEL

6.1 Introduction

The effectiveness of implemented soil-structure interaction models in solving the problem of foundation slabs on shrink-swell soils is highly influenced by the soil mound shape. This chapter presents the development of the implemented soil-structure interaction model by using Mitchell (1979) equations for moisture diffusion under covered soil to develop a new closed form solution for the soil mound shape under the foundation slab. Then, it presents a parametric study by carrying out several 2D finite elements plane strain simulations for plates resting on a semi-infinite elastic continuum, and resting on different soil mounds. The parametric study outcomes are then presented in design charts that end with a new design procedure for foundation slabs on shrink-swell soils.

6.2 Soil-structure interaction models

Slabs on Winkler foundation: The Winkler foundation is the simplest and the most widely used soil-structure interaction model in geotechnical engineering. Most of the finite element computer programs in use today are based on the Winkler foundation models, sometimes denoted by the spring foundation model. The simplest simulation of a continuous elastic foundation is assumed to be composed of the number of closely spaced vertical independent linear springs providing vertical reaction only, where the reaction is assumed proportional to the deflection. Winkler foundation system assumes that the vertical force at any point under the foundation slab depends only on the vertical deflection at the same point and is independent of the deflections at all other points. Winkler foundation system indicates that the soil has no shear strength that transfers the load to the adjacent points; the deformation occurs only immediately under the applied

load and the displacements are zero outside the loaded area. Similar methods include Pasternak foundation model, Hetenyi foundation model, Filionenko-Borodich Foundation model and Vlasov Foundation model.

Foundation slabs on elastic half space: Boussinesq formulation gives the solution of a concentrated load applied on an elastic, isotropic, and homogenous semi-infinite continuum with E_s (modulus of elasticity) and μ_s (Poisson's ratio), respectively. In the formulation, the deflection at any point depends not only on the force at the applied point, but also on the force applied on all the other points because of the influence of the shear stress. A comparison between Winkler foundation and elastic continuum foundation indicates that the elastic continuum foundation has a much larger deflection basin (Poulos, 2000). It is closer to reality; however, for slab on expansive soils, the slab is not supported completely on the soil. So, an iteration scheme is needed when this method is used (Rifat Bulut, 2001). Another disadvantage for this method is that the Boussinesq's equation assumed that the load is applied on a semi-infinite continuum. In practice, it is not uncommon that the ground on which the foundation is built has a variety of soil layers with greatly different properties. It will be very difficult to find an equivalent half space Young's Modulus for a real condition.

The effectiveness of a foundation model on simulating foundation slabs on shrink-swell soils depends on: 1) How close is the mathematical model to reality? 2) The accuracy of the soil properties determination. 3) How close is the assumption of mound shape to reality? 4) Model experimental verifications. Research advancements in the first and second factors is reasonable satisfactory. However, the third and fourth factors need significant developments.

Nelson and Miller (1992) summarized the assumption of mound shape in five different design methods as shown in Table 6.1. Many different assumptions have been taken for the mound shape equation since early 1950's; rectangular mound, parabolic mound, flat at center slab portion and parabolic at edges, and flat at center slab portion and cubic at edges. The assumption of the mound shape is very critical for the soil-structure analysis purposes.

Table 6.1 Summary of five stiffened slab-on-grade foundation design methods (Nelson and Miller, 1992).

Design Method	1 BRAB (1968)	2 Lytton (1972)	3 Walsh (1978)	4 Swinburne (Holland et al., 1980)	5 PTI (1980)
Slab load and soil–structure interpretation assumptions	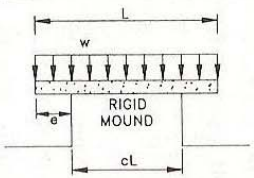	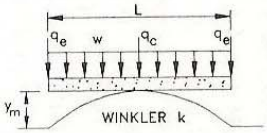	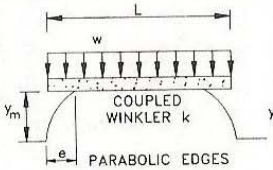	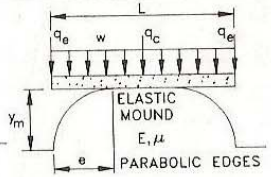	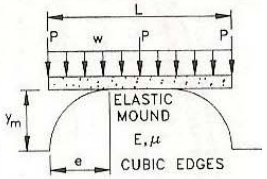
Mound shape assumptions	Rectangular mound. Empirical support index (c) related to climatic rating and soil properties	Parabolic mound $y = ax^m$	Flat under center to a distance of E from edges. Parabolic at edges	Flat under center. Parabolic at edges	Flat under center. Cubic at edges
Design parameters					
1. Climate	1. C_w	1. (N/A)	1. (N/A)	1. (N/A) E_s, ν	1. TMI (Figure 2.5)
2. Soil parameters	2. C	2. y_m	2. y_m, e, k	2. y_m, e	2. y_m, e, q_a, f
3. Loading conditions	3. w	3. w, q_c, q_e	3. w	3. w, l_c, q_c, q_e	3. w, q_e, q_c
4. Slab parameters	4. L, E	4. L, S, E	4. L, E	4. L, b, S, E	4. L, b, d, S, E

[a]Legend: a = mound equation constant; b = beam width; C = support index (Figure 5.18); C_w = climatic rating factor (Figure 2.6); d = beam depth; e = edge distance; E_s = soil modulus of elasticity; k = subgrade modulus; L = slab length; m = mound exponent; ν = Poisson's ratio of soil; w = average foundation pressure; q_a = allowable soil bearing pressure; q_c = center load; q_e = edge load; S = beam spacing; f = slab-subgrade friction coefficient; E = edge distance.

The mound exponent (*m*) defines the curvature of the mound; it has been related to the ratio of the slab length to the depth of the active moisture zone (Mitchell, 1980). By assuming that the mound is flat beneath the interior of the slab, the mound exponent will seldom exceed 7 or 8 (Walsh, 1978). A mound exponent of 2 provides the least support and is the most conservative condition for the analysis purposes (Nelson and Miller, 1992). Mound exponents of 3 or 4 are commonly used for slab design in Australia (Woodburn, 1974).

6.3 Mound shape equation

6.3.1 Derivation of a new mound shape equation

In his pioneer work, Mitchell (1979), derived closed form solutions, Eq. 6.1, for suction distribution on soil; the soil surface was partially covered by a weightless impervious flexible cover as shown in Fig. 6.1.

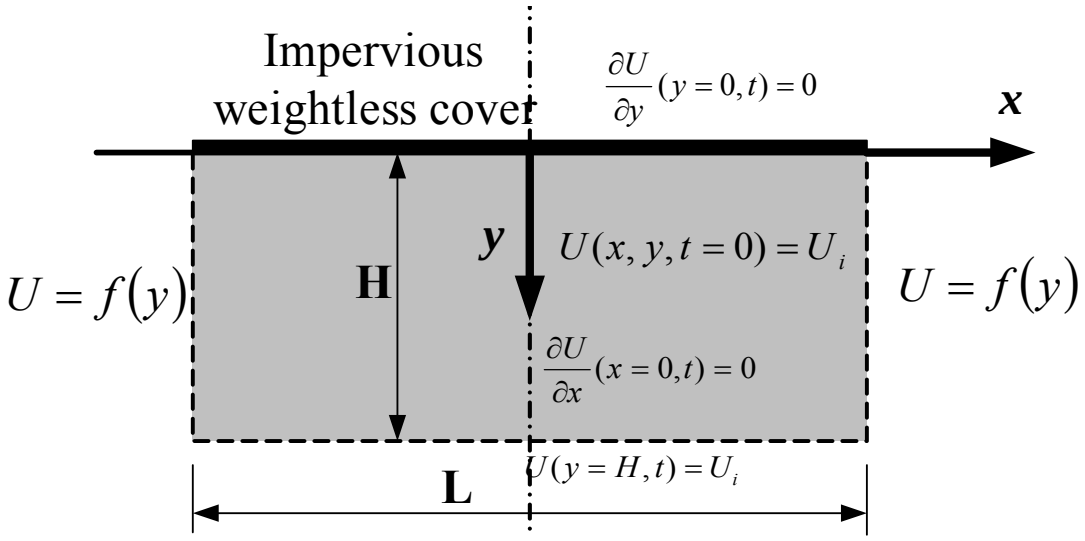

Fig. 6.1. Boundary conditions for the impervious weightless cover problem.

$$U(x,y) = U_i + \sum_{n=1}^{\infty} A_n \frac{\cosh\frac{(2n-1)\pi x}{2H}}{\cosh\frac{(2n-1)\pi L}{4H}} \cos\frac{(2n-1)\pi y}{2H} \tag{6.1.a}$$

where, $$A_n = \frac{2}{H}\int_0^H [f(y) - U_i]\cos\frac{(2n-1)\pi y}{2H}\,dy \tag{6.1.b}$$

Mitchell (1979) derived two closed form solutions for two cases; he assumed that the vertical suction distribution under the cover edge was constant for the first case, Eq. 6.2, and linearly decreasing with depth for the second case, Eq. 6.3. In reality, the suction profile under the cover edge varies with time as the weather input boundary conditions vary with time, yet the suction envelops under the cover edge, subject to a sinusoidal surface suction variation with time, are following an exponential decay trend as has been shown in Eq.4.26.

For $f(y) = U_0$, $$A_n = \frac{-4(-1)^n (U_0 - U_i)}{\pi(2n-1)} \tag{6.2}$$

For $f(y) = U_i + U_0 \frac{H-y}{H}$, $$A_n = \frac{8U_0}{\pi^2(2n-1)} \tag{6.3}$$

Assuming an exponential decay suction distribution under the cover edge, this research will derive a new solution for suction distribution under a partially covered soil using Mitchell's Eq. 6.1 as follows:

$$f(y) = U_i + \Delta U_{edge} \exp\left(-\sqrt{\frac{\omega}{2\alpha_{field}}}\, y\right) \tag{6.4}$$

where $\omega = \frac{2\pi}{T}$ and T is the weather periodic time.

Substituting Eq. 6.4 into Eq. 6.1.b:

$$A_n = \frac{2\Delta U_{edge}}{H}\int_0^H \exp\left(-\sqrt{\frac{\omega}{2\alpha_{field}}}\, y\right)\cos\frac{(2n-1)\pi y}{2H}\,dy$$

$$A_n = \frac{2\Delta U_{edge}}{H}\left|\frac{\exp\left(-\sqrt{\frac{\omega}{2\alpha_{field}}}y\right)}{\frac{\omega}{2\alpha_{field}}+\frac{\pi^2}{H^2}\left(n-\frac{1}{2}\right)^2}\left\{\begin{array}{l}\sqrt{\frac{\omega}{2\alpha_{field}}}\cos\frac{\pi}{2}(2n-1)\left(\frac{y}{H}\right)+\\ \left(\frac{\pi}{2}\frac{(2n-1)}{H}\right)\sin\frac{\pi}{2}(2n-1)\left(\frac{y}{H}\right)\end{array}\right\}\right|_0^H$$

$$A_n = \frac{2\Delta U_{edge}}{H}\left\{\left(\frac{\exp\left(-\sqrt{\frac{\omega H^2}{2\alpha_{field}}}\right)}{\frac{\omega}{2\alpha_{field}}+\frac{\pi^2}{H^2}\left(n-\frac{1}{2}\right)^2}\right)\left(\frac{\pi}{H}\left(n-\frac{1}{2}\right)(-1)^{n-1}\right)+\frac{\sqrt{\frac{\omega}{2\alpha_{field}}}}{\frac{\omega}{2\alpha_{field}}+\frac{\pi^2}{H^2}\left(n-\frac{1}{2}\right)^2}\right\}$$

hence,

$$A_n = \frac{2\Delta U_{edge}\pi\left(n-\frac{1}{2}\right)(-1)^{n-1}\exp\left(-\sqrt{\frac{\omega H^2}{2\alpha_{field}}}\right)+2\Delta U_{edge}\sqrt{\frac{\omega H^2}{2\alpha_{field}}}}{\frac{\omega H^2}{2\alpha_{field}}+\pi^2\left(n-\frac{1}{2}\right)^2} \qquad (6.5)$$

Using Eq. 6.5 along with Eq. 6.1 will give a more realistic suction distribution under a covered area for a soil surface subjected to a cyclic weather pattern. Moreover, Eq. 6.5 along with Eq. 6.1 can be used to develop the mound shape equation. The distribution of change in suction will be integrated with depth to derive the mound shape equation.

$$\rho(x) = \int_0^H f\gamma_h \Delta U(x,y).dy \qquad (6.6)$$

where;

ρ is the surface soil movement under the impervious cover.

f is ratio of the vertical strain to the volumetric strain.

γ_h is slope of the volumetric stain versus suction in pF units.

$\Delta U(x,y)$ is the change in suction, which = $U(x,y)$-U_i

Assuming that f and γ_h are constant values through out the domain under consideration and substituting Eq. 6.1 into Eq. 6.6 gives:

$$\rho(x) = f\gamma_h \int_0^H \sum_{n=1}^{\infty} A_n \frac{\cosh\dfrac{(2n-1)\pi x}{2H}}{\cosh\dfrac{(2n-1)\pi L}{4H}} \cos\frac{(2n-1)\pi y}{2H}.dy \tag{6.7}$$

Noticing that A_n is independent of y, Eq. 6.7 can be rearranged as follows:

$$\rho(x) = \sum_{n=1}^{\infty} f\gamma_h A_n \frac{\cosh\left((n-½)\pi\dfrac{x}{H}\right)}{\cosh\left((n-½)\pi\dfrac{L}{2H}\right)} \int_0^H \cos\left((n-½)\pi\frac{y}{H}\right).dy \tag{6.8}$$

$$\rho(x) = \sum_{n=1}^{\infty} f\gamma_h A_n \frac{\cosh\left((n-½)\pi\dfrac{x}{H}\right)}{\cosh\left((n-½)\pi\dfrac{L}{2H}\right)} \left.\frac{\sin\left((n-½)\pi\dfrac{y}{H}\right)}{(n-½)\dfrac{\pi}{H}}\right|_0^H \tag{6.9}$$

$$\rho(x) = \sum_{n=1}^{\infty} f\gamma_h A_n \frac{\cosh\left((n-½)\pi\dfrac{x}{H}\right)}{\cosh\left((n-½)\pi\dfrac{L}{2H}\right)} \frac{(-1)^{n-1}}{(n-½)\dfrac{\pi}{H}} \tag{6.10}$$

Substituting from Eq. 6.5 into Eq. 6.10 givers the mound shape equation Eq. 6.11:

$$\rho(x) = f\gamma_h H\Delta U_{edge} \sum_{n=1}^{\infty} \left\{ \left[\frac{2\pi(n-½)(-1)^{n-1} \exp\left(-\sqrt{\dfrac{\omega H^2}{2\alpha_{field}}}\right) + 2\sqrt{\dfrac{\omega H^2}{2\alpha_{field}}}}{\dfrac{\omega H^2}{2\alpha_{field}} + \pi^2(n-½)^2} \right] \left[\frac{\cosh\left((n-½)\pi\dfrac{x}{H}\right)}{\cosh\left((n-½)\pi\dfrac{L}{2H}\right)} \frac{(-1)^{n-1}}{\pi(n-½)} \right] \right\} \tag{6.11}$$

6.3.2 Comparing the proposed new mound shape equation to the formerly used equations

To check the discrepancy between the proposed new mound shape equation and the assumed mound shapes in Table 6.1, four soils have been chosen with α_{field} equal to

7.14E-04, 3.85E-03, 1.10E-02, and 3.12E-02 cm^2/sec, three sites have been chosen with H equals to 1, 2.5, and 4 meters, L equals to 12 m, weather cycles periodic time, T_0 = 365 days, and e_m equals to 3 m. The four soils and the three sites give twelve different mound parameters as tabulated in Table 6.2. For the twelve cases, the mound shapes were calculated using Eq. 6.11. And the normalized parameters were calculated according to Eq. 6.12 and plotted as shown in Fig. 6.2.

Table 6.2. Mound parameters.

Mound#	1	2	3	4	5	6	7	8	9	10	11	12
$\alpha_{field}(m^2/day)$	0.0062	0.0062	0.0062	0.0333	0.0333	0.0333	0.0950	0.0950	0.0950	0.2696	0.2696	0.2696
H (m)	1	2.5	4	1	2.5	4	1	2.5	4	1	2.5	4

$$X_N = \frac{x}{L/2} \tag{6.12.a}$$

$$\rho_N = \frac{\rho(x) - \rho_{center}}{\rho_{edge} - \rho_{center}} \tag{6.12.b}$$

where;

$\rho_{edge} = \rho(x = L/2)$, and $\rho_{center} = \rho(x=0)$

y_m is the differential mound elevation = $\rho_{edge} - \rho_{center}$

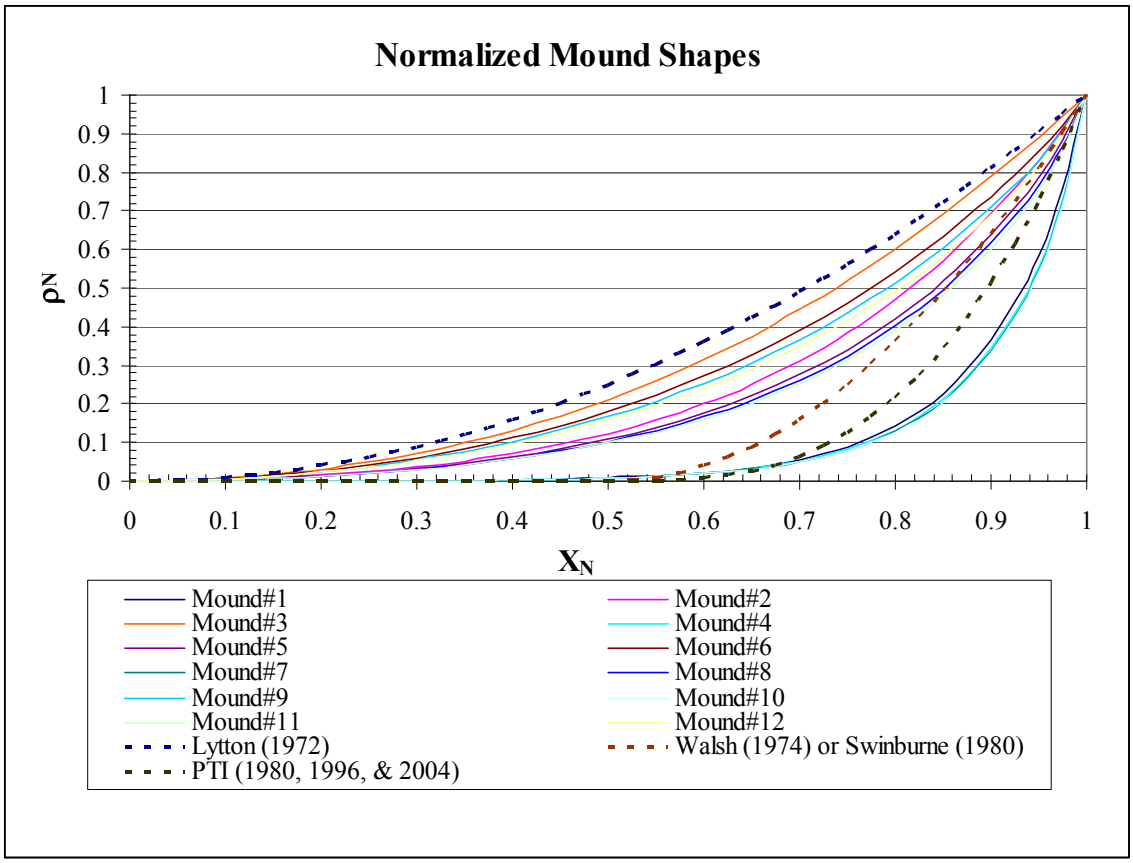

Fig. 6.2. Proposed new mound shapes and formerly assumed mound shapes**.**

Eq. 6.11 shows that the normalized mound shape is dependent on two main parameters: A dimensionless soil diffusion parameter, $\frac{\omega H^2}{2\alpha_{field}}$ and the diffusion domain aspect ratio, $\frac{L/2}{H}$. Fig. 6.3 shows that the curvature of the mound shape is dependent on both soil diffusion parameter and diffusion domain aspect ratio. Increasing any or both of those parameters increases the resistance to the moisture front diffusion, and increases the curvature of the mound shape. For the formally assumed mound equations, the mound exponent was an assumed constant value independent of both soil diffusion parameter and diffusion domain aspect ratio; For the twelve cases, Lytton (1972) gives

the same mound, seminally does Walsh (1974), Swinburne (1980), or PTI (1980, 1996, and 2004).

6.4 Numerical modeling

Finite element simulations for plates resting on a semi-infinite elastic continuum has been carried out many times by different researchers in many different ways, the starting point for all of these trials was to assume a certain soil mound shape. This research proposed the usage of the derived mound shape equation Eq. 6.11 to calculate the initial mound. Then, an iterative finite element simulation was carried out for a flat foundation slab on grade on the calculated mound shape, which resulted in the final slab deflected shape and mobilized bending moments and shear forces.

The finite elements comprehensive software package, ABAQUS/STANDARD, was used to for stress/displacement finite element simulations for plates resting on a semi-infinite elastic continuum. Fig. 6.3 and Fig. 6.4 show geometry and boundary conditions of the problem for edge lift case and edge drop case respectively. This problem is a 2D plane strain problem; the ABAQUS/STANDARD CPE4T "Continuum Plane strain 4-nodes Temperature" element was chosen in the simulation. The CPE4T element can also be used for plane strain stress/ displacement coupled with head transfer, yet this head transfer coupling option was not used in this simulation. Appendices F.1 and F.2 present the ABAQUS/STANDARD input files for edge lift and edge drop simulations respectively.

As a simulation example, consider a plane strain problem for a foundation slab on an edge drop mound: The foundation slab has L=16 m, total load of 7.5 kN/m, concrete young's modulus of, E_{conc} = 20000 MPa, and foundation slab thickness 0f 0.38 m. The foundation rests on an edge drop mound, the soil has α_{field} = 0.02042 m^2/day, young's modulus of, E_{soil} = 60 MPa, H= 3.5 m, and ΔU_{edge}= 0.91 pF

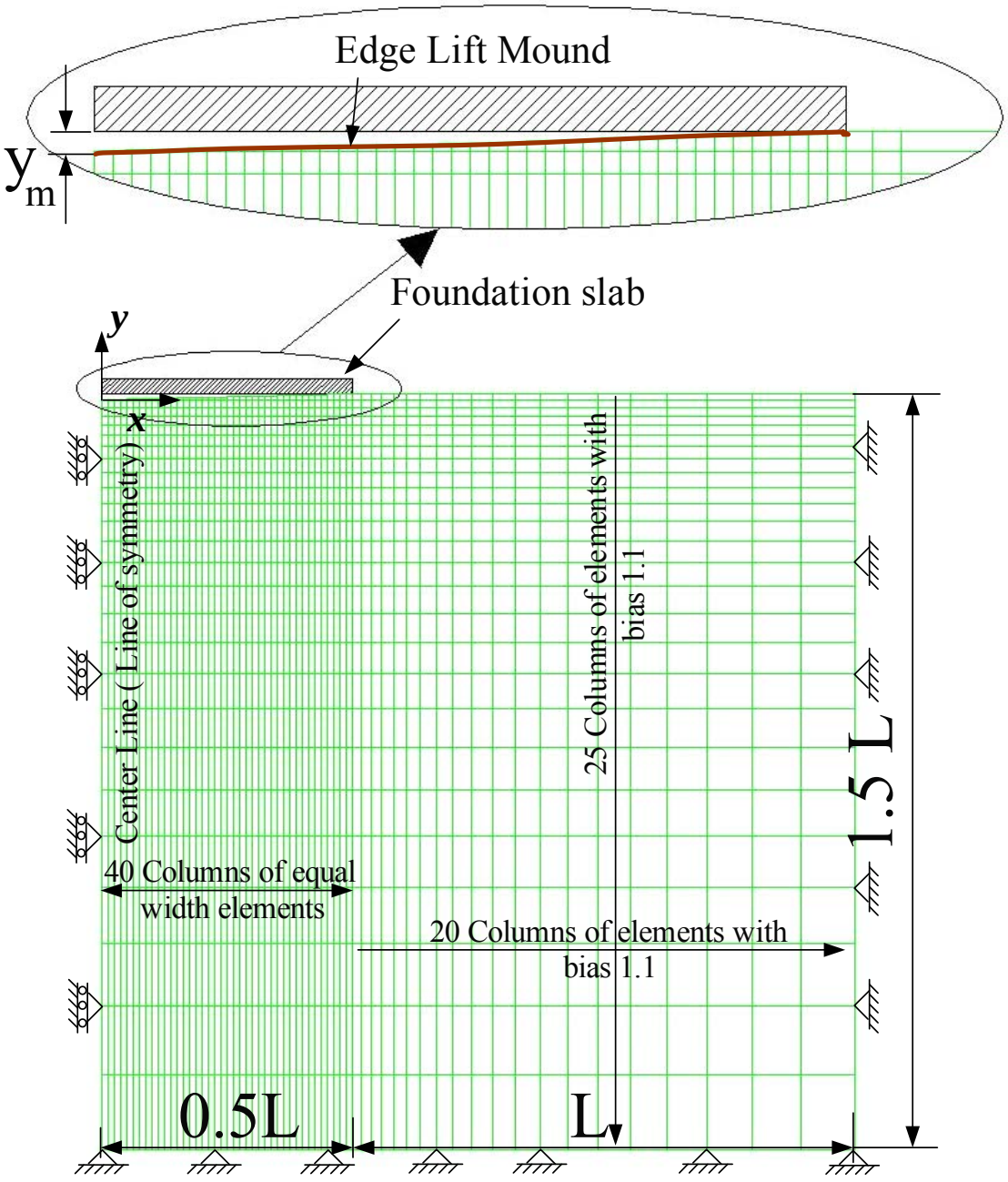

Fig. 6.3. Geometry and boundary conditions for an edge lift case.

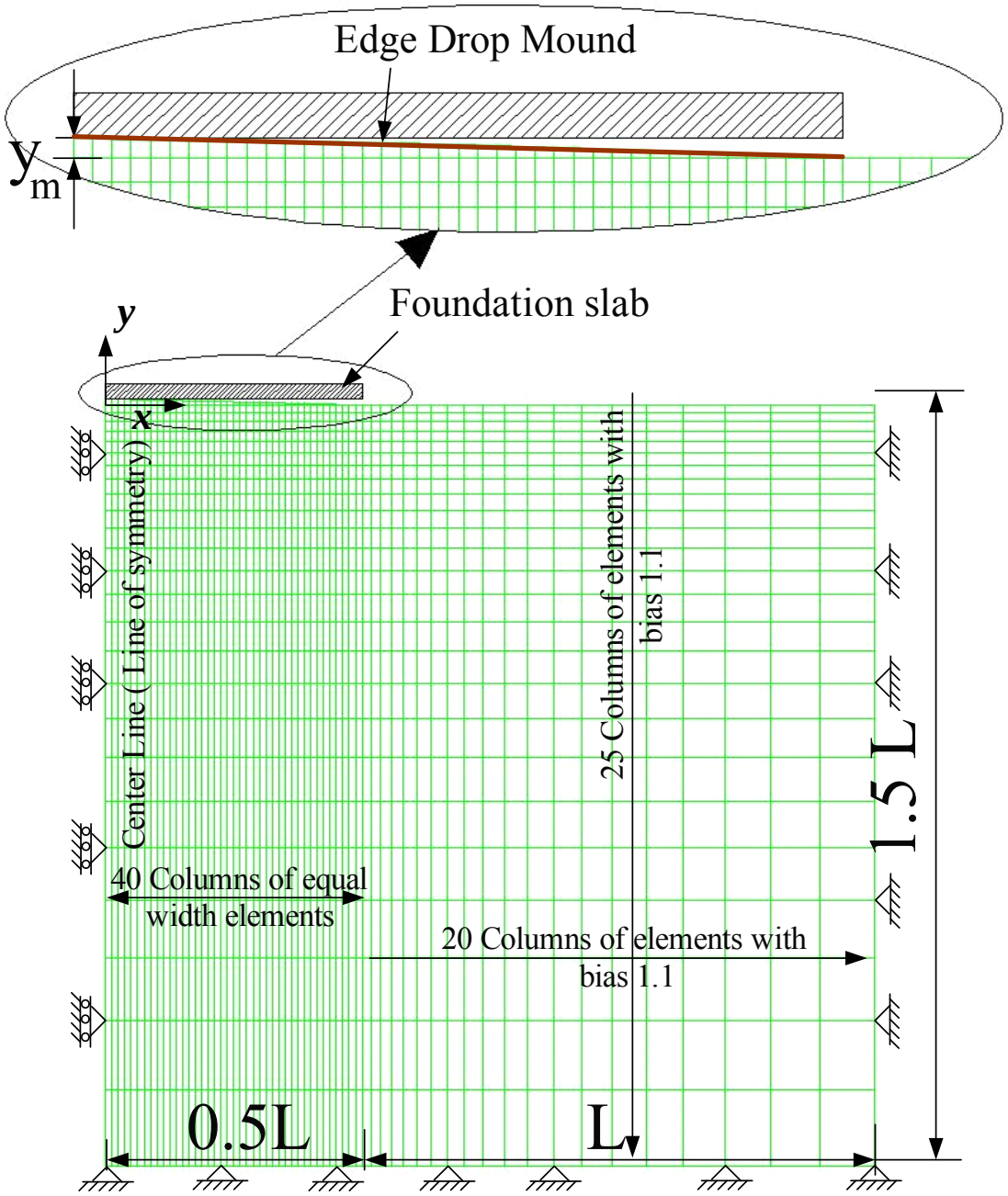

Fig. 6.4. Geometry and boundary conditions for an edge drop case.

Using Eq. 6.11, the soil mound shape was developed as shown in Fig. 6.5 . The numerical simulation was carried out using ABAQUS/STANDARD as has been

detailed. The initial and final soil mound profiles and final foundation slab profile were presented in Fig. 6.5, bending moments and shearing forces results were presented in Fig. 6.6, and final settlements of soil mounds and foundation slab were presented in Fig. 6.7. From Fig. 6.5, Fig. 6.6, and Fig. 6.7, it is observed that: The maximum bending moment coincides with the point of zero-shear as commonly known for any conventional structure analysis problem. The distance from the edge of the slab to the point of separation between soil and slab is smaller that the distance between the edge of the slab and the point of the maximum bending moment. There are soil mound settlements even in the zone of separation between the soil and the slab, which is fore anticipated for elastic half-space continuum simulations. The bending moment at the point of soil and slab separation is smaller than the maximum bending moment, about one third of it. The zone between the minimum and maximum shear has the largest soil mound settlement values, also has the highest contact pressure as can be inferred from the slope of the shearing force curve.

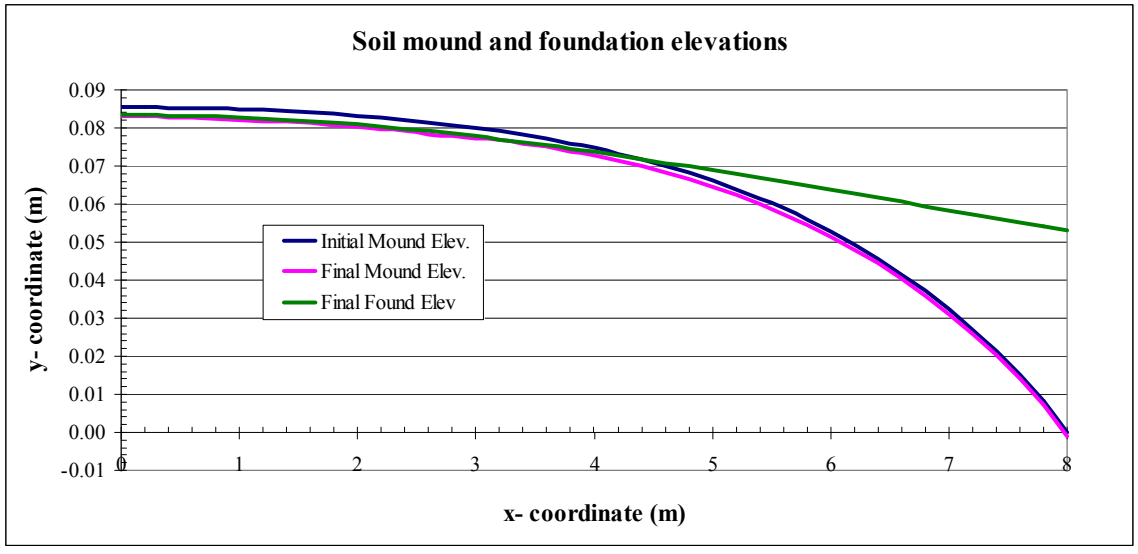

Fig. 6.5. Initial and final soil mound profiles and final foundation slab profile.

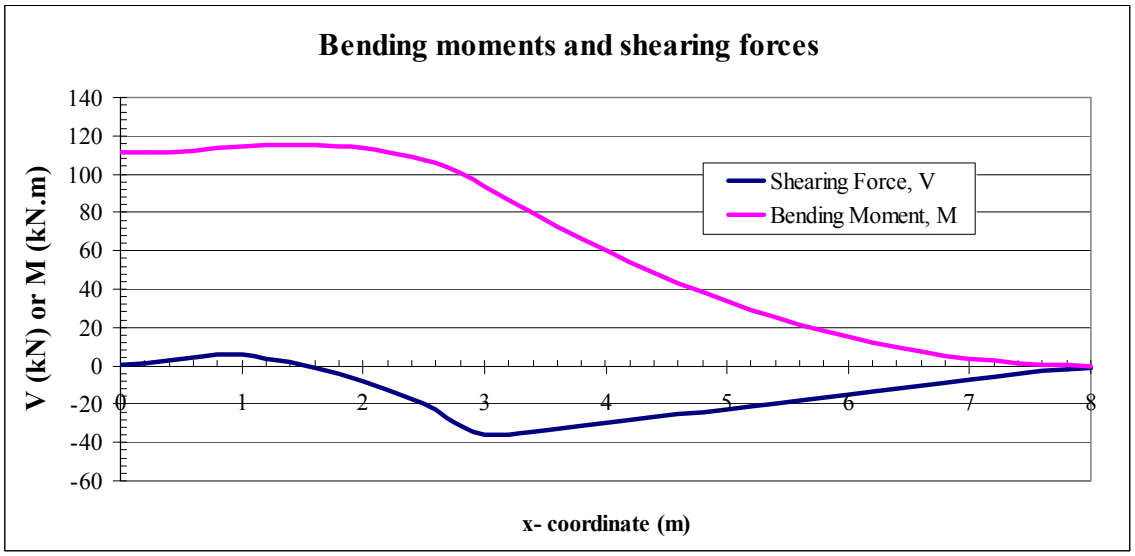

Fig. 6.6. Bending moments and shearing forces results.

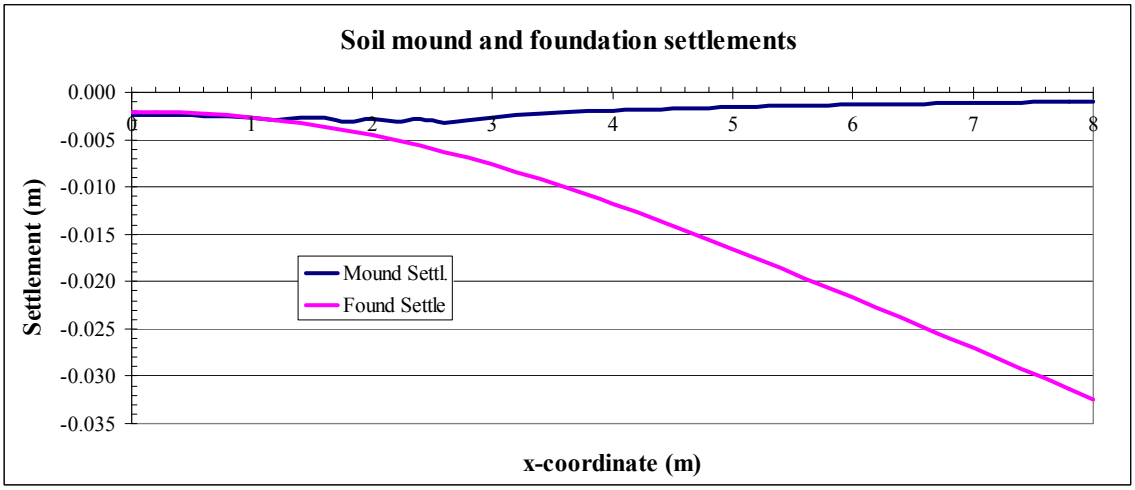

Fig. 6.7. Final settlements of soil mounds and foundation slab.

6.5 Factors influencing the design of stiffened slabs on grade on shrink-swell soils

6.5.1 General

Many factors are involved in the design of foundation slab on a grade of shrink-swell soil; weather factors such as the change of soil surface suction at a free surface, ΔU_0, the

change of soil surface suction at the edge of the foundation cover, ΔU_{edge} soil factors such as soil modulus, E_{soil}, the shrink-swell index, I_{ss} and field coefficient of unsaturated diffusivity, α_{field}, and foundation slab factors such as slab length, L, stiffness, and loading. A huge number of numerical simulations with different parameters' combinations would be required to develop a new design method that includes all these parameters effects. However, carrying out a preliminary sensitivity study that examines how each parameters contributes to design of the foundation slab would be very insightful in addition to significantly decrease the required number of the numerical simulations.

6.5.2 Involved parameters

The parameter ranges in this sensitivity study were chosen to cover anticipated parameters' variations realistically. The change of soil surface suction at a free surface, ΔU_0 recommended by AS 2870 was from 1.2 to 1.5 pF, this recommendation were based on field measurements data bases in Australia. Since we don't have available similar data bases in US, the chosen range of ΔU_0 was expanded to be from 1 to 1.6 pF, five values were examined within that range 1, 1.15, 1.3, 1.45, 1.6 pF. The change of soil surface suction at the edge of the foundation cover, ΔU_{edge} is chosen to be equal to be 0.7 times ΔU_0 as has been shown in Chapter V. Five depths of active moisture zones, H, were examined, 1.5, 2.5, 3.5, 4.5, and 5.5 m. The periodic time for cyclic surface suction change due to weather variations was assumed to be 365 days.

Three soil moduli, E_{soil} were examined for edge drop case (mounds resulting from soil shrinkage); 20, 60, and 100 MPa. Yet, for edge lift case (mounds resulting from soil swelling); 6, 10, 15, 20 MPa with the mound shape elevations, referenced from the soil surface, were scaled down by one half as will be explained later. Five soils were chosen with field coefficients of unsaturated diffusivity, α_{field}, 0.00724, 0.01244, 0.02042, 0.07110, and 0.26544 m^2/day were derived from five shrink-swell indices, I_{ss} 75, 60, 45, 30, 15% respectively as shown in Table 6.3. The coefficients of saturated permeability and dry densities were assumed to be inversely proportional to the soil plasticity. The

range of chosen coefficients of saturated permeability matches the suggested values in Casagrande chart shown in Fig. 6.8.

Table 6.3. Soil parameters used in the sensitivity study.

%	m/sec	kPa		kN/m^3		m^2/sec	m^2/sec	m^2/day
I_{ss}	**K_{sat}**	**u_{sat}**	**c_w**	**γ_{dry}**	**γ_{SWCC}**	**α_{Lab}**	**α_{Field}**	**α_{Field}**
75	5.00E-10	10	0.375	11	0.4125	2.793E-09	8.379E-08	0.00724
60	7.50E-10	10	0.3	12	0.25	4.800E-09	1.440E-07	0.01244
45	1.00E-09	10	0.225	13	0.17307692	7.877E-09	2.363E-07	0.02042
30	2.50E-09	10	0.15	14	0.10714286	2.743E-08	8.229E-07	0.07110
15	5.00E-09	10	0.075	15	0.05	1.024E-07	3.072E-06	0.26544

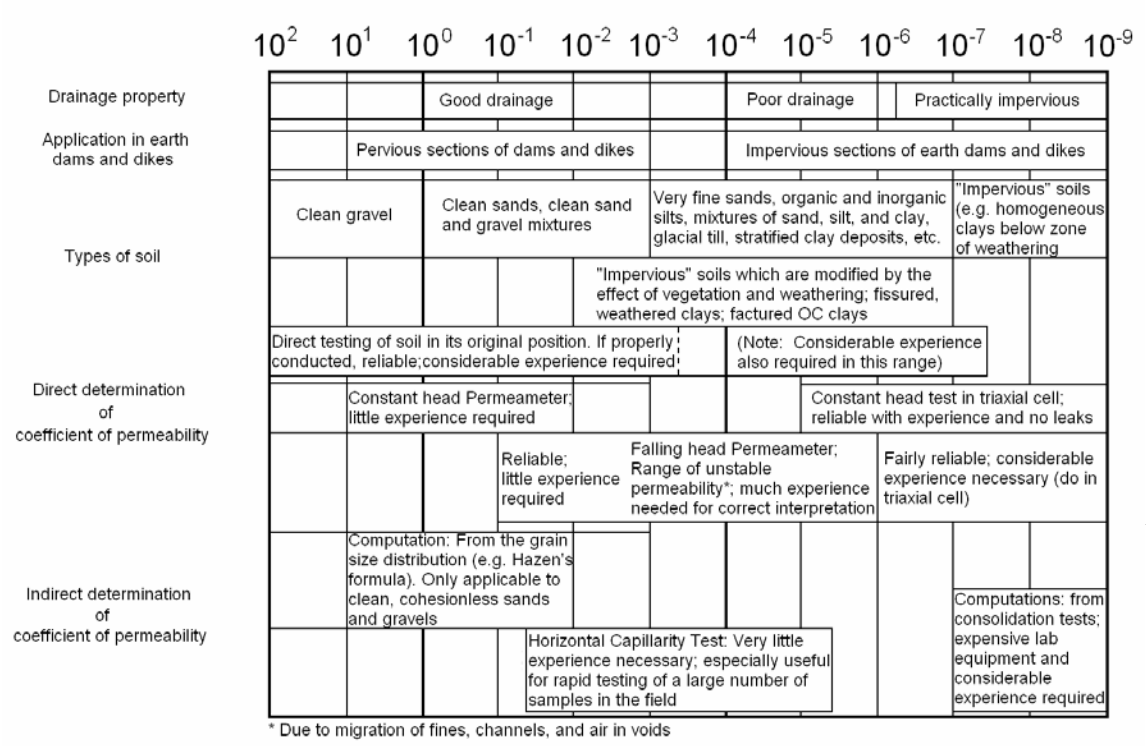

Fig. 6.8. Casagrande chart for coefficient of permeability (k_{sat}- cm/sec) (Holtz & Kovacs, 1981 - After Casagrande, 1938).

C_w was calculated using I_{ss} using Fig. 4.18 (C_w = 0.5 I_{ss}), and the coefficient of unsaturated diffusivity at laboratory, α_{Lab} was calculated from Eq. 6.13. α_{Lab} was calculated from Eq. 6.14 assuming that cracked soil diffusion factor, F_{CrkDif} = 30 as an average value of F_{CrkDif} values presented in Fig. 4.14.

$$\alpha_{Lab} = \frac{k_{sat} u_{sat}}{0.4343 \frac{\gamma_{dry}}{\gamma_{water}} C_w} \tag{6.13}$$

$$\alpha_{field} = F_{CrkDif} \alpha_{Lab} \tag{6.14}$$

The following foundation slab parameters that were examined: slab lengths, L, 4, 6, 8, 10, 12 m. Slab beam depths of 0.3, 0.6, 0.9, 1.2, and 1.5 m with beam width of o.3 m and beam spacing of 4 m, which give stiffness equivalent flat slab thicknesses of 0.127, 0.253, 0.3795, 0.506, and 0.633 m respectively. Slab total imposed area loads of 2, 2.75, 3.5, 4.25, and 5 kPa. The slab concrete modulus of elasticity was chosen to be 20000 MPa.

6.5.3 Notations and definitions

Fig. 6.9 sketches a foundation slab on grade on a curved mound. The following are definitions of terms used in this problem:

H depth of active zone. (Depth to which the variation of water content or suction will create movement of the soil).

Δw_0 change in water content. (Change in water content in the free field at the ground surface)

ΔU_0 change in suction. (Change in suction in log units (pF) in the free field at the ground surface).

I_{ss} shrink-swell index. (Range of water content between the shrinkage limit and the swell limit. Very good indicator of shrink-swell potential).

e_m edge moisture distance. (Distance from the edge of the slab to the point where the water will penetrate horizontally below a weightless perfectly flexible cover).

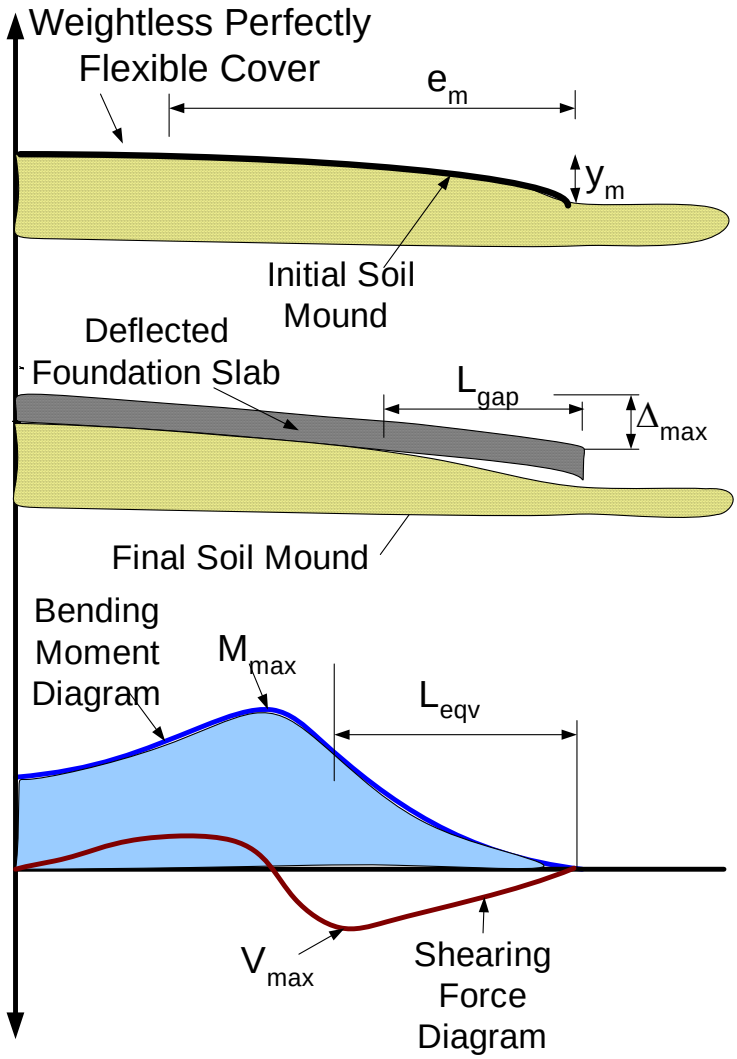

Fig. 6.9. A sketch of a foundation slab on grade on a curved mound.

y_m vertical movement. (Difference in elevation due to swelling or shrinking between the two extremities of the e_m distance).

q Total foundation slab loads (including own weight and imposed loads)

L_{eqv} equivalent cantilever length. (Length of slab which gives the maximum bending moment in the slab when used with the formula $M_{max} = qL_{eqv}^2/2$)

L_{gap} unsupported length. (Length of slab without soil support underneath it).

Δ_{max} difference in elevation between the center of the slab and the edge of the slab.

M_{max} Maximum bending moment in the slab.

V_{max} Maximum shear force in the slab.

$F_{\Delta max}$ maximum deflection factor. $F_{\Delta \max} = \dfrac{qL_{eqv}^4}{\Delta_{\max} EI}$

F_V maximum shear factor. $F_v = \dfrac{V_{\max}}{qL_{eqv}}$

6.5.4 Sensitivity study

Out of each parameter the closest value to the average was chosen to form the reference case; influence of each parameter variations will be compared to the reference case, which is shown in Table 6.4. The equivalent cantilever length, L_{eqv} , was chosen out of resulting parameters to be the comparison parameter; it represents both the resulting bending moment and maximum deflection, consequently controls the design.

Table 6.4. Parameters of used in the reference case.

Parameter	$\mathbf{I_{ss}}$ (%)	**H** (m)	$\mathbf{\Delta U_0}$ (pF)	**D** (m)	**L** (m)	$\mathbf{w_{imposed}}$ (KPa)
Reference case	45	3.5	1.3	0.9	8	3.5

a) Influence of soil shrink-swell potential.

Fig. 6.10 shows the relationship between the soil shrink-swell potential, represented with the shrink-swell index, and the resulting equivalent cantilever length. The increase in the shrink-swell index induces non-linear monotonic increase in the equivalent cantilever length. Because, increasing the shrink-swell index increases the y_m values, increases the soil mound distortion, and consequently increases the foundation slab distortion. The average slopes of the normalized equivalent cantilever length and normalized shrink-swell index curve were about 0.342 and 0.369 for edge drop case and

edge lift case respectively. This slope is an indicator of how the equivalent cantilever length is sensitive to the change of soil shrink-swell potential; this slope is directly proportional to the equivalent cantilever length sensitivity.

b) Influence of depth of active moisture zone

Fig. 6.11 shows the relationship between the depth of active moisture zone and the resulting equivalent cantilever length. The increase in the depth of active moisture zone induces non-linear monotonic increase in the equivalent cantilever length. The slope of the normalized equivalent cantilever length and normalized depth of active moisture zone decreases at depth of active moisture zone values above the average. Increasing the depth of active moisture zone increases the y_m values, increases the soil mound distortion, and consequently increases the foundation slab distortion.

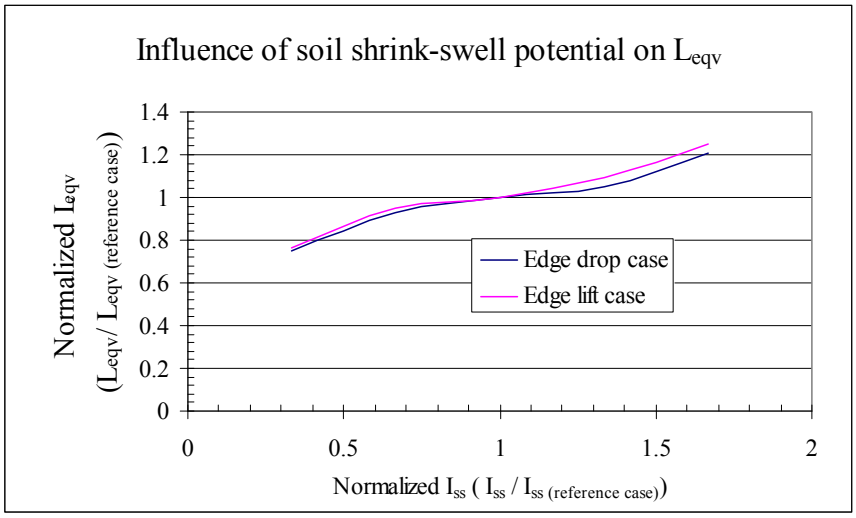

Fig. 6.10. Influence of soil shrink-swell potential on the equivalent cantilever length.

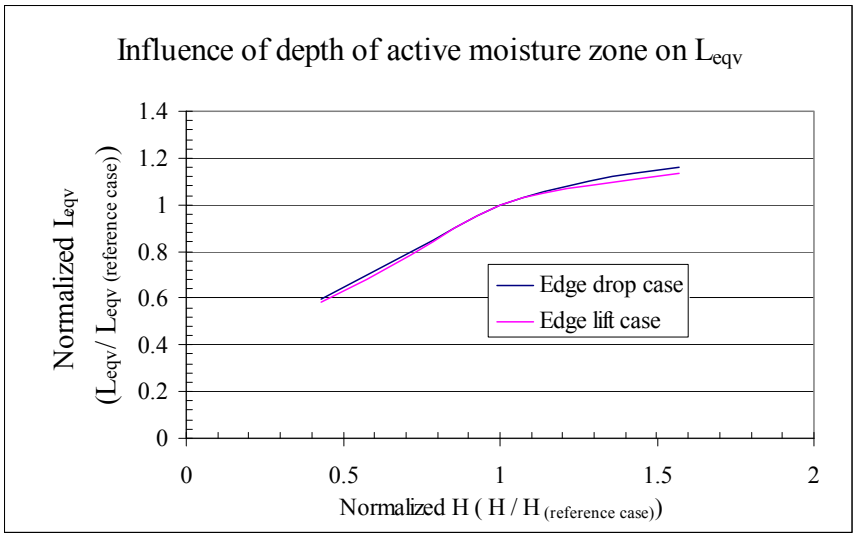

Fig. 6.11. Influence of depth of active moisture zone on the equivalent cantilever length.

The average slopes of the normalized equivalent cantilever length and normalized depth of active moisture zone curve were about 0.493 and 0.483 for edge drop case and edge lift case respectively. This may indicate that the equivalent cantilever length is more sensitive to depth of active moisture zone changes than to the soil shrink-swell potential; however the depth of active moisture zone is also a function of soil shrink-swell potential.

c) Influence of soil surface suction change.

Fig. 6.12 shows the relationship between the soil surface suction change and the resulting equivalent cantilever length. The increase in the soil surface suction change increase, almost linearly, the equivalent cantilever length. The average slopes of the normalized equivalent cantilever length and normalized soil surface suction change curve were about 0.372 and 0.481 for edge drop case and edge lift case respectively. However, the range of the soil surface suction change is smaller than that of either normalized shrink-swell index or normalized of depth of active moisture zone.

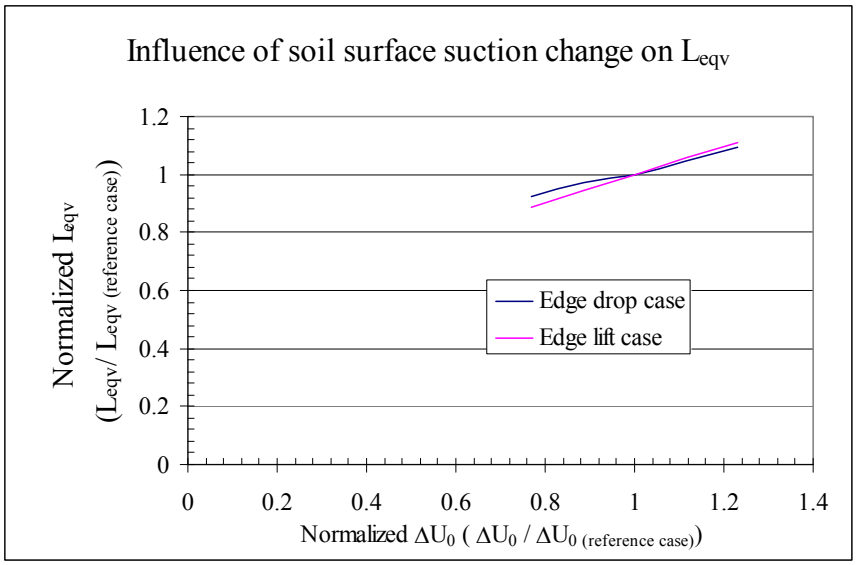

Fig. 6.12. Influence of soil surface suction change on the equivalent cantilever length.

d) Influence of slab stiffness.

Fig. 6.13 shows the relationship between the slab stiffness, represented with the slab beam depth, and the resulting equivalent cantilever length. The increase in slab beam depth significantly increases equivalent cantilever length, this relationship has an almost linear trend up to the average beam depth in this sensitivity study then the curve slope tends to flatten out. Increasing the slab stiffness increases the resulting maximum bending moments as well known in any indeterminate structure problem similar to this soil-structure interaction problem. The significant increase in equivalent cantilever length, due to increasing slab stiffness, reached values close to the half slab length, which added an upper bound to the curve. The average slopes of the normalized equivalent cantilever length and normalized slab beam depth curve were about 0.628 and 0.792 for edge drop case and edge lift case respectively. Yet considering the linear portion only, the average slopes were about 0.904 and 0.98 for edge drop case and edge lift case respectively.

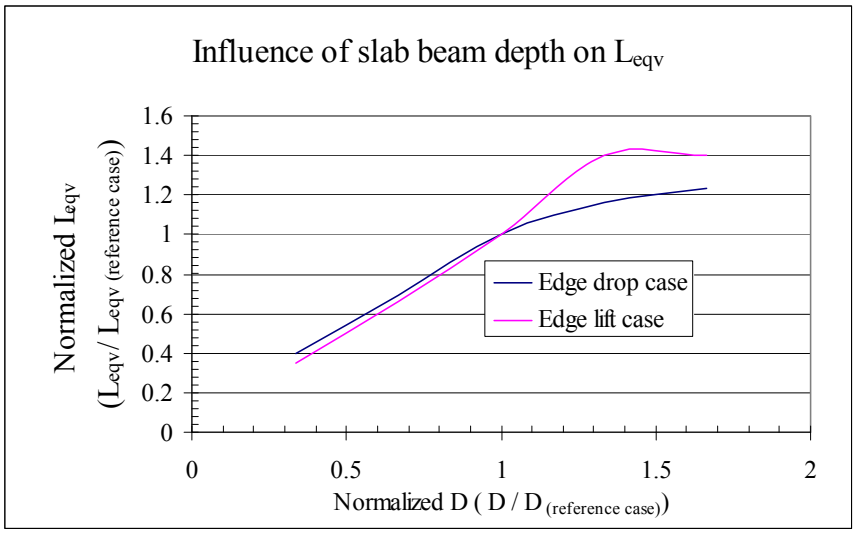

Fig. 6.13. Influence of slab stiffness on the equivalent cantilever length.

e) Influence of slab length.

Fig. 6.14.a shows the relationship between the slab length and the resulting equivalent cantilever length. The increase in slab length almost linearly increases the equivalent cantilever length until reaching a maximum value; then, the increase in slab length decreases the equivalent cantilever length until reaching a constant value. Slab length affects two phenomena, moisture diffusion and slab curvature. Small 0.5 L/ H ratios allows easier moisture passages underneath the area covered by the foundation slab, which decrease the mound shape curvature (the value of suction change under the slab center gets closer to the value of suction change under the slab edge). Consequently, the foundation slab curvature decreases, which decreases the equivalent cantilever length. Meanwhile, increasing slab length decreases the Δ_{max}/L ratio; hence decreases slab curvature and the equivalent cantilever length. These two counteracting effects reaches a balancing point at which the maximum equivalent cantilever length will be.

The equivalent cantilever is sensitive to 0.5 L/ H smaller than that corresponding to the maximum equivalent cantilever length (note that, theoretically, this part of the curve can be extended to the origin point).

Hence, the influence of slab length on the equivalent cantilever length can be addressed by introducing a reduction factor to the equivalent cantilever length. Fig. 6.15 presents the slab length factor, F_{sl} , which can be viewed as an idealized form of chart 6.14. the equivalent length will be estimated based on the rest of the influencing factors and then reduced by multiplying with the slab length factor, F_{sl} as shown in Fig. 6.15

f) Influence of slab imposed area load

Fig. 6.16 shows the relationship between slab imposed area load and the resulting equivalent cantilever length. The increase in slab imposed area load slightly decreases equivalent cantilever length; this relationship has an almost linear trend. Increasing the slab imposed area load compresses the soil mound reducing its curvature, which decreases the resulting equivalent cantilever length. The average slopes of the normalized equivalent cantilever length and normalized slab beam depth curve were about -0.141 and -0.232 for edge drop case and edge lift case respectively.

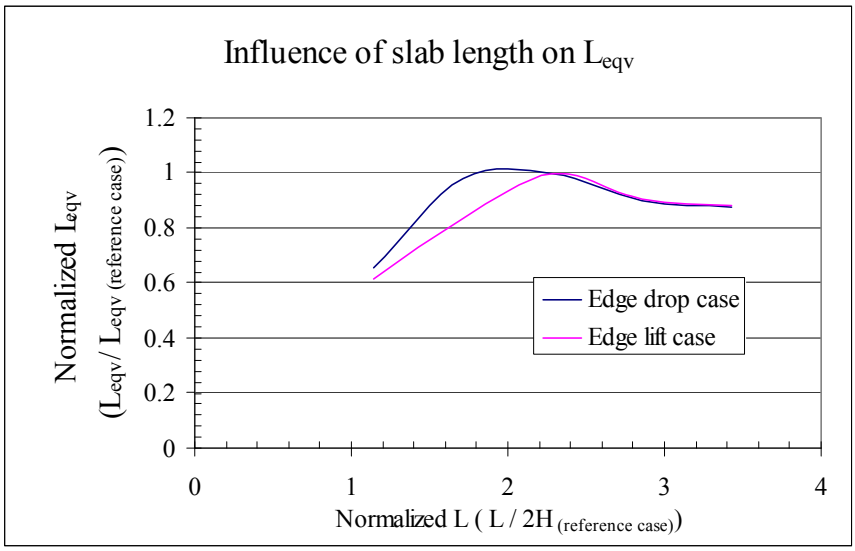

Fig. 6.14. Influence of slab length on the equivalent cantilever length.

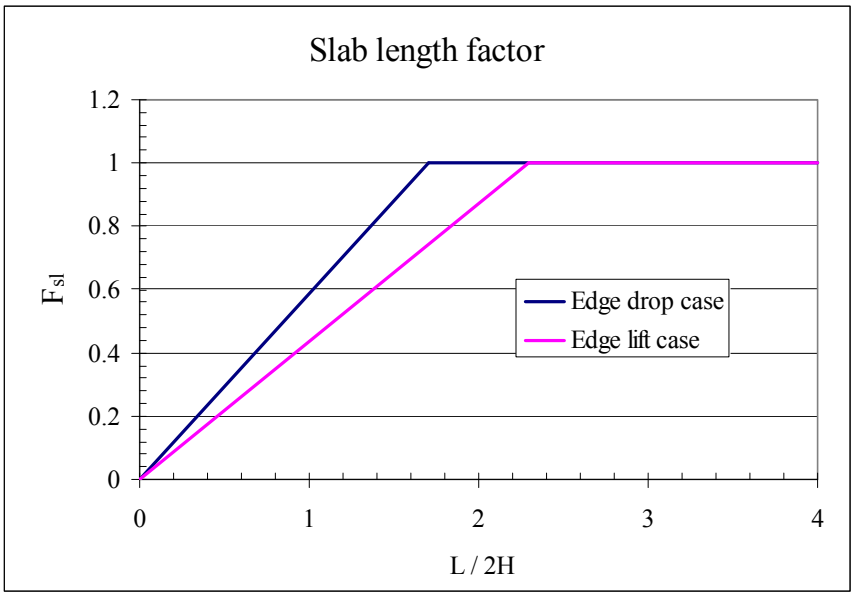

Fig. 6.15. Slab length factor for (a reduction factor to the equivalent cantilever length).

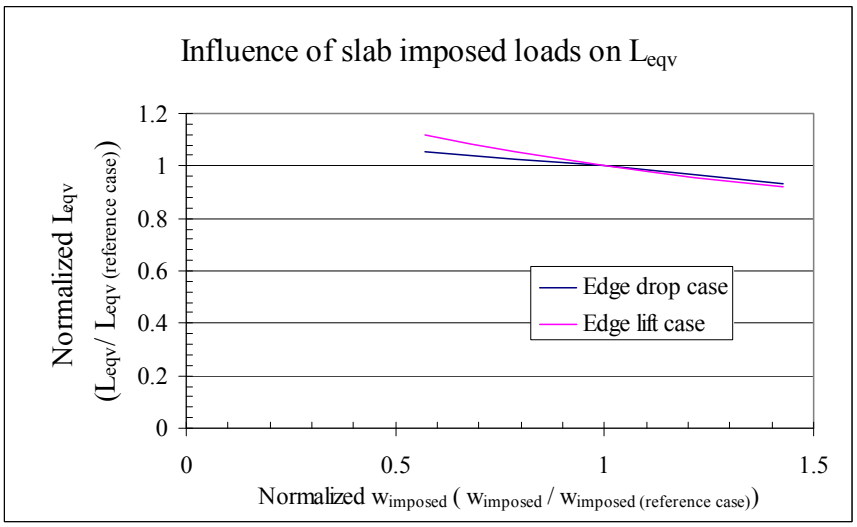

Fig. 6.16. Influence of slab imposed area load on the equivalent cantilever length.

g) Influence of soil modulus of elasticity.

Soil modulus of elasticity, E_s, was assumed to be a constant value throughout the numerical simulations (i.e. the soil modulus was assumed not to be a function of soil suction) as commonly assumed in all the aforementioned design methods. However, the soil modulus for edge drop case was assumed to be different from that of the edge lift case. For edge drop case, the soil is shrinking due to loss of moisture, which considerably increases the soil stiffness; the soil consistency becomes medium to hard. For edge lift case, the soil is swelling due to gain of moisture, which considerably decreases the soil stiffness; the soil consistency becomes very soft to soft. Bowles (1996) recommended typical ranges for soil modulus of elasticity, E_s for different soil consistencies; Table 6.5 presents soil modulus of elasticity, E_s ranges extracted from (Bowles, 1996) for clays only. For edge drop case, the soil is stiff and this makes the assumption of using the mound resulting from unsaturated diffusion under a weightless flexible cover as the initial mound shape under the foundation slab to be reasonably conservative. However, the presence of soft compressible soil, especially close to the slab edge, in edge lift case makes that assumption extremely conservative. Fig. 6.17 shows typical Pressure-Swelling Characteristic of clay (Mitchell, 1979), which disclose that: Although it may take very large pressures to completely restrain clay from swelling, it takes a little pressure to significantly reduce the amount of swell. For example, in Fig. 6.17, a 15 kPa pressure reduces the soil free swell (about 12% by extrapolation) to soil swell % of 6% (i.e., 50% reduction). In fact, the presence of cracks in field may enable a pressure, much smaller than that usually used in laboratory for a fully confined sample, to achieve the same % reduction in soil swell. These facts lead to the assumption of using the half mound in edge lift case simulations (the mound shape elevations, referenced from the soil surface, were multiplied by one half).

Fig. 6.18 shows the relationship of the soil modulus of elasticity and the resulting maximum bending moment, a monotonic increase in M_{max} takes place upon the increase in soil modulus of elasticity.

Table 6.5. Value range for static stress-strain soil modulus, E_s (after Bowles, 1996).

Clay consistency	E_s, MPa
Very soft	2 – 15
Soft	5 – 25
Medium	15 – 50
Hard	50 - 100

Based on Fig. 6.17, Table 6.5, and the previous discussion, the soil modulus was recommended to be: 60 MPa for edge drop case as a reasonable value for design purposes, and 15 MPa with using the half mound assumption for edge lift case as a reasonable value for design purposes. Note that, according to Table 6.5: 60 MPa corresponds to a hard clay consistency, and 15 MPa corresponds to average soft clay consistency and lower bound of medium clay consistency.

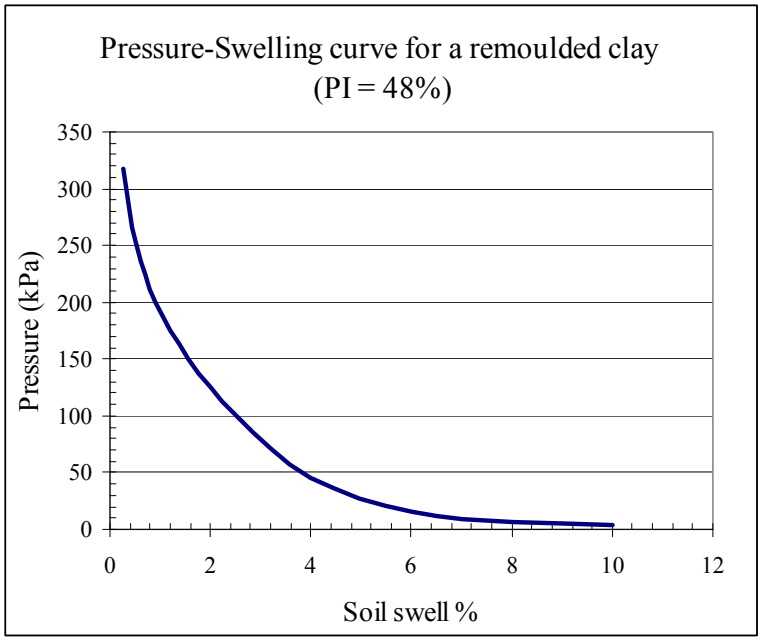

Fig. 6.17. Typical pressure-swelling characteristic of clay (after Mitchell, 1979).

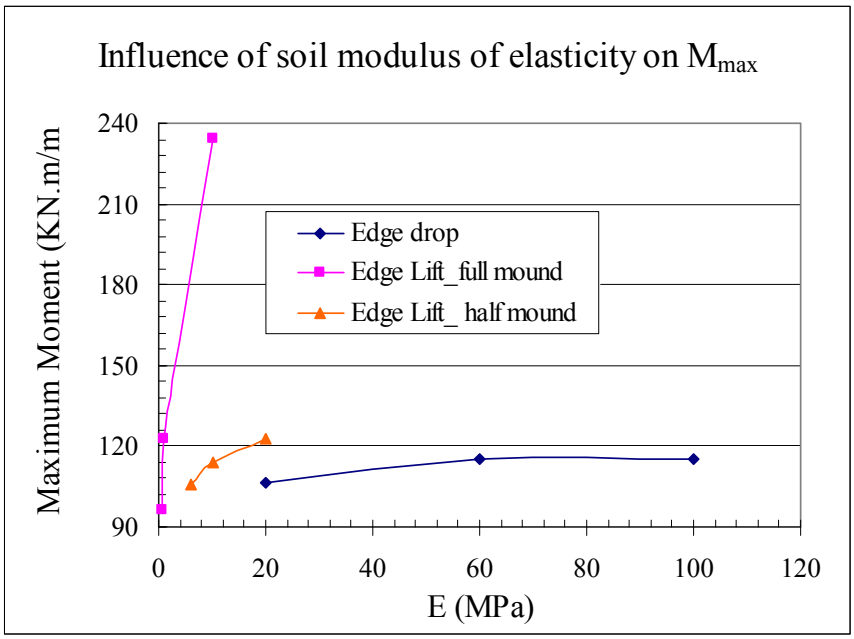

Fig. 6.18. Influence of soil modulus of elasticity on M_{max}.

6.5.5 Conclusions

The sensitivity study showed that the following factors influence the design of foundation slabs on grade on shrink-swell soils (factors are cited according their order of significancy starting from the most significant factor): slab stiffness, depth of active moisture zone, shrink-swell potential, slab length, soil surface suction change, imposed loads, soil stiffness, and many other minor factors. The sensitivity study recommended also reasonable values for parameters of minor significancy.

6.6 New design charts

Expanding the outcomes of the new mound shape equation, a parametric study was carried out in pursuing new design charts that relates the required parameters for design purposes, such as bending moments and deflections, to soil and weather input parameters. This parametric study was designed taking into consideration the sensitivity study recommendations. Both soil parameters and weather parameters influence the

mound shape; hence influence the foundation slab design, note that some parameters are considered soil-weather parameters such as depth of active moisture zone. The parametric study ignored factors of minor effects to minimize the number of simulations and reduce the level of sophistication, in the resulting charts, to a reasonable limit, which doesn't influence the design.

6.6.1 Soil-weather index parameter

In order to develop new simple design charts, soil and weather parameters were combined in a single soil-weather index representing the main problem input parameter. The main theme of the proposed design charts was aimed to be; soil-weather index was represented in the x- axis and the output design parameter was represented in the y- axis, different design curves for different corresponding slab stiffnesses. The influence of slab length was address by using an equivalent cantilever length reduction factor, since slab length influence the equivalent cantilever length only for small L/2H ratios. The increase in shrink-swell index, depth of active moisture zone, and change of soil surface suction, the main soil and weather problem input parameters, almost linearly and monotonically increases the equivalent cantilever length. Hence, the soil-weather index was defined to be equal to the multiplication of the three parameters, Eq. (6.15). Table 6.6 shows the input parameters of some simulations that were carried out in the aforementioned sensitivity study, the simulations that varied slab length and slab stiffness were excluded.

$$I_{S\text{-}W} = I_{SS}.\ H.\ \Delta U_0 \qquad (6.15)$$

Fig. 6.19 shows the relationship between the soil-weather index and the equivalent cantilever length resulting from the tabulated simulations, Table 6.6. A hyperbolic function, in the format shown in Eq. 6.16, gave the best curve fitting with a coefficient of determination equals = 0.944; where, L_0, a, and b are constants.

$$L_{eqv} = L_0 + \frac{aI_{S-W}}{1+bI_{S-W}}, R^2 = 0.944 \qquad 6.16$$

Table 6.6. Simulations input parameters and their corresponding soil-weather index.

I_{S-W}	Comment	I_{ss} (%)	H (m)	ΔU_0 (pF)	D (m)	L (m)	$w_{imposed}$ (kPa)
0	No mound	45	3.5	0	0.9	16	3.5
2.0475	reference	45	3.5	1.3	0.9	16	3.5
3.4125	I_{ss}- Very High	**75**	3.5	1.3	0.9	16	3.5
2.73	I_{ss}- High	**60**	3.5	1.3	0.9	16	3.5
1.365	I_{ss}- Moderate	**30**	3.5	1.3	0.9	16	3.5
0.6825	I_{ss}- Low	**15**	3.5	1.3	0.9	16	3.5
3.2175	H- Very High	45	**5.5**	1.3	0.9	16	3.5
2.6325	H- High	45	**4.5**	1.3	0.9	16	3.5
1.4625	H- Moderate	45	**2.5**	1.3	0.9	16	3.5
0.8775	H- Low	45	**1.5**	1.3	0.9	16	3.5
2.52	ΔU-Very High	45	3.5	**1.6**	0.9	16	3.5
2.28375	ΔU-High	45	3.5	**1.45**	0.9	16	3.5
1.81125	ΔU-Moderate	45	3.5	**1.15**	0.9	16	3.5
1.575	ΔU-Low	45	3.5	**1**	0.9	16	3.5
2.0475	$w_{imposed}$-Very High	45	3.5	1.3	0.9	16	**5**
2.0475	$w_{imposed}$ -High	45	3.5	1.3	0.9	16	**4.25**
2.0475	$w_{imposed}$-Moderate	45	3.5	1.3	0.9	16	**2.75**
2.0475	$w_{imposed}$-Low	45	3.5	1.3	0.9	16	**2**
6.6	All maximums	75	5.5	1.6	0.9	16	**3.5**
0.225	All minimums	15	1.5	1	0.9	16	**3.5**

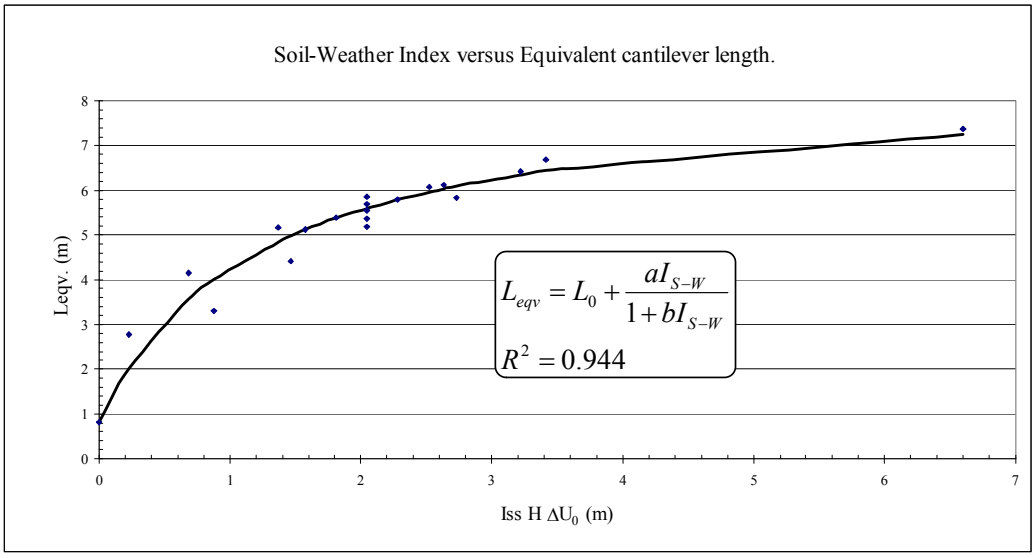

Fig. 6.19. Relationship between soil-weather index and the equivalent cantilever length.

6.6.2 Parametric study

Based on Fig. 6.19, seven mounds were chosen to develop design charts. The seven mounds included mounds with the minimum and maximum soil-weather indices to cover the whole possible range, and five intermediate mounds, which conservatively fell on or above the fitting curve. For each mound, five slab stifnesses were varied and numerically simulated in two cases; edge lift and edge drop as has been explained earlier. Table 6.7 summarizes the input parameters for numerical simulations that have been carried out to construct the proposed design charts. Slab stiffness was represented with the beam depth, D for a constant slab thickness of 0.1 m and a constant beam spacing of 4 m. However, for design purposes, another parameter was introduced to represent the slab stiffness which is the slab equivalent depth, d_{eq}. The slab equivalent depth can be calculated from Eq.6.17, which also represents a slab thickness of a mat foundation with moment of inertia equal to the moment of inertia of a stiffned slab with a beam spacing, S and beam width, b.

$$S.\ d_{eq}^{3} = b.\ D^{3} \qquad (6.17)$$

6.6.3 Suction based design charts

The aforementioned cases were numerically simulated using ABAQUS / STANDARD, as has been explained in detail earlier and the output design parameter were plotted, for both edge drop and edge lift cases, versus the soil-weather parameter. Fig. 6.20, Fig. 6.21, Fig. 6.22, & Fig. 6.23 shows edge drop suction based design charts for L_{eqv} , L_{gap} , $F_{\Delta max}$, and F_V respectively, and Fig. 6.24, Fig. 6.25, & Fig. 6.26 shows edge lift suction based design charts for L_{eqv} , $F_{\Delta max}$, and F_V respectively.

Table 6.7. Design charts simulations input parameters.

Design Curve	I_{ss} (%)	H (m)	ΔU_0 (pF)	D (m)	L (m)	$w_{imposed}$ (kPa)
Curve#1	75	3.5	0	1.5	16	3.5
Curve#1	15	1.5	1	1.5	16	3.5
Curve#1	15	3.5	1.3	1.5	16	3.5
Curve#1	30	3.5	1.3	1.5	16	3.5
Curve#1	45	3.5	1.45	1.5	16	3.5
Curve#1	75	3.5	1.3	1.5	16	3.5
Curve#1	75	5.5	1.6	1.5	16	3.5
Curve#2	75	3.5	0	1.2	16	3.5
Curve#2	15	1.5	1	1.2	16	3.5
Curve#2	15	3.5	1.3	1.2	16	3.5
Curve#2	30	3.5	1.3	1.2	16	3.5
Curve#2	45	3.5	1.45	1.2	16	3.5
Curve#2	75	3.5	1.3	1.2	16	3.5
Curve#2	75	5.5	1.6	1.2	16	3.5
Curve#3	75	3.5	0	0.9	16	3.5
Curve#3	15	1.5	1	0.9	16	3.5
Curve#3	15	3.5	1.3	0.9	16	3.5
Curve#3	30	3.5	1.3	0.9	16	3.5
Curve#3	45	3.5	1.45	0.9	16	3.5
Curve#3	75	3.5	1.3	0.9	16	3.5
Curve#3	75	5.5	1.6	0.9	16	3.5
Curve#4	75	3.5	0	0.6	16	3.5
Curve#4	15	1.5	1	0.6	16	3.5
Curve#4	15	3.5	1.3	0.6	16	3.5
Curve#4	30	3.5	1.3	0.6	16	3.5
Curve#4	45	3.5	1.45	0.6	16	3.5
Curve#4	75	3.5	1.3	0.6	16	3.5
Curve#4	75	5.5	1.6	0.6	16	3.5
Curve#5	75	3.5	0	0.3	16	3.5
Curve#5	15	1.5	1	0.3	16	3.5
Curve#5	15	3.5	1.3	0.3	16	3.5
Curve#5	30	3.5	1.3	0.3	16	3.5
Curve#5	45	3.5	1.45	0.3	16	3.5
Curve#5	75	3.5	1.3	0.3	16	3.5
Curve#5	75	5.5	1.6	0.3	16	3.5

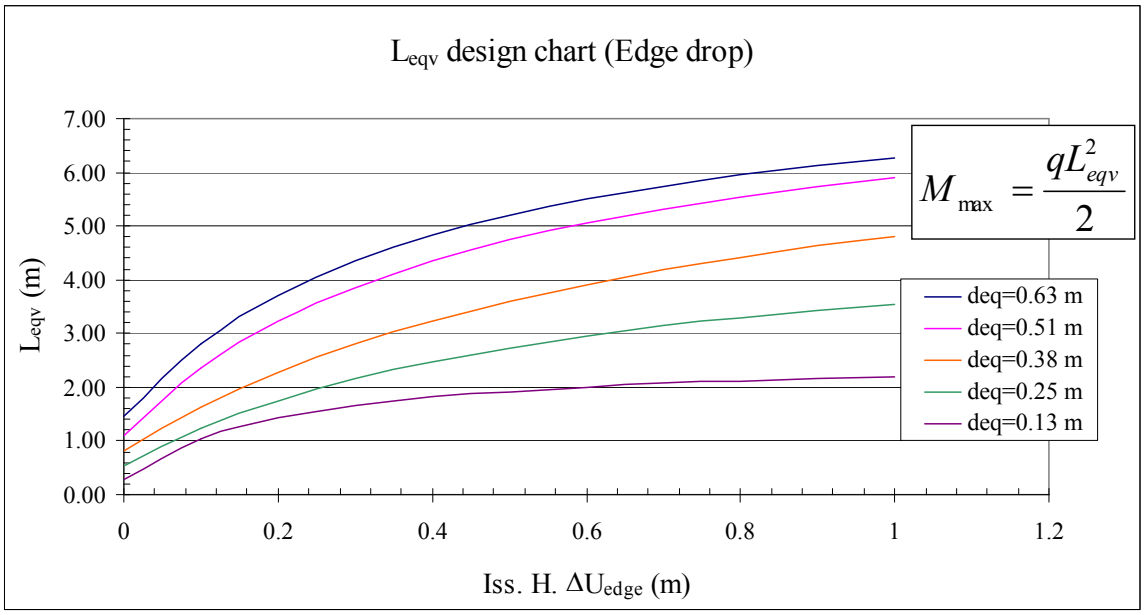

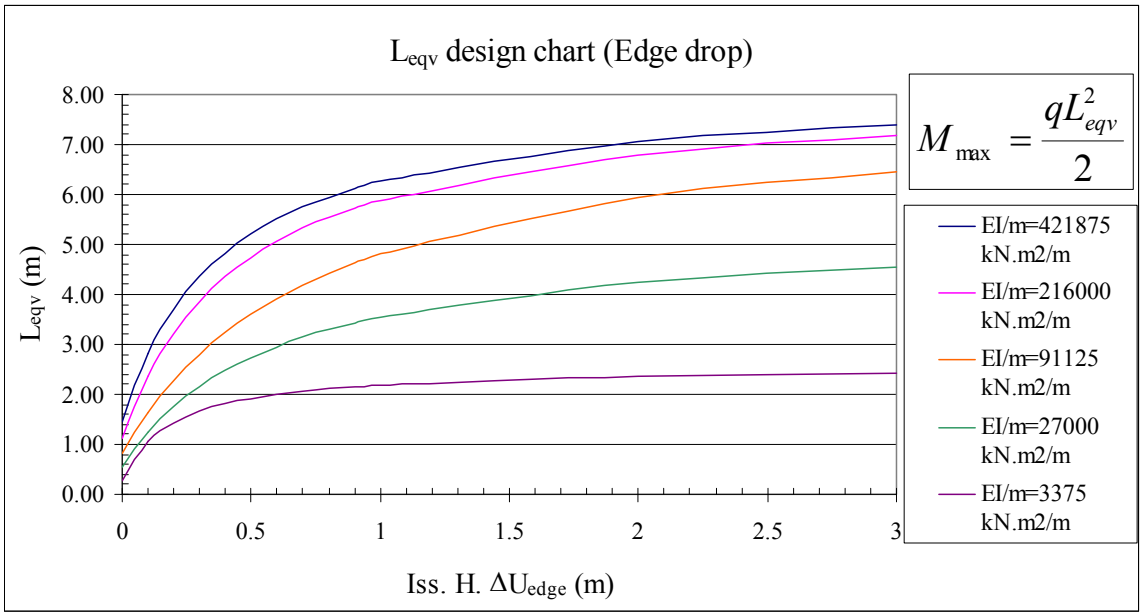

Fig. 6.20. Equivalent cantilever length suction based design chart for edge drop case.

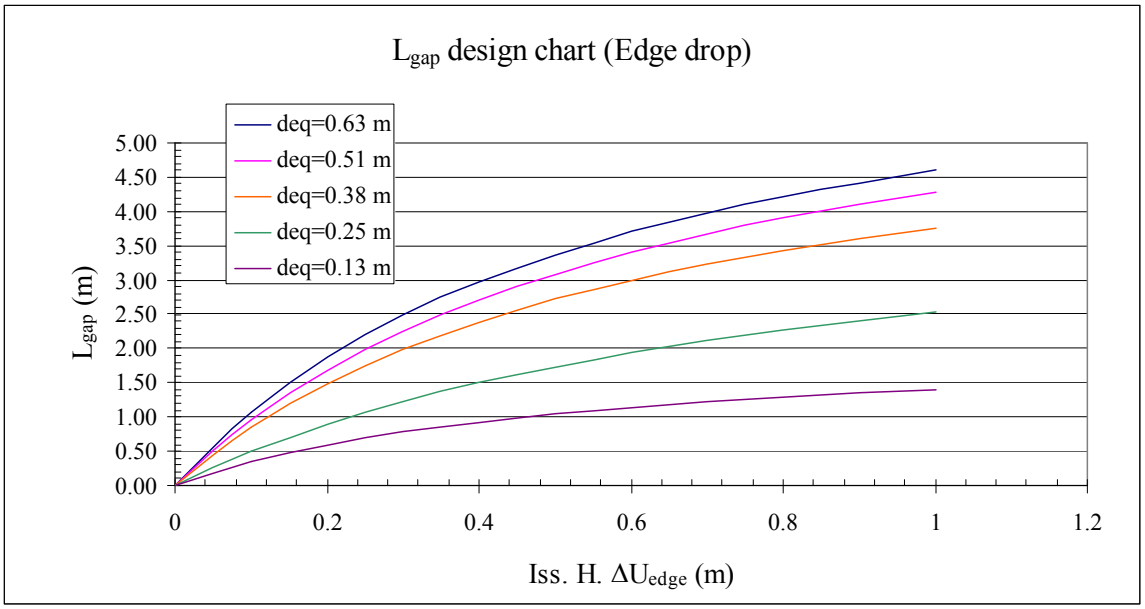

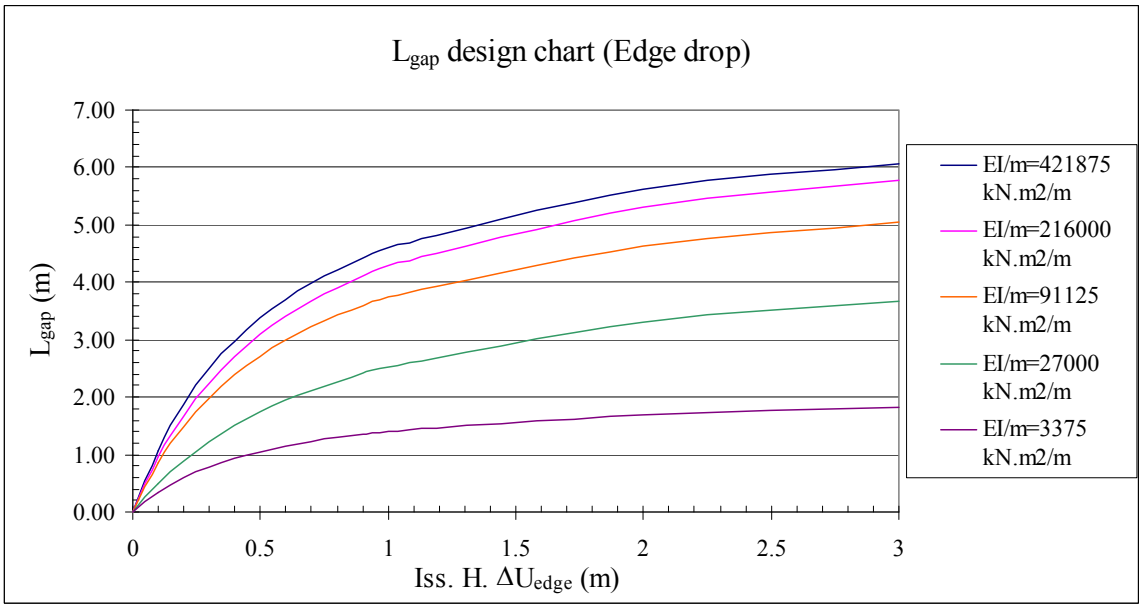

Fig. 6.21. Unsupported length suction based design chart for edge drop case.

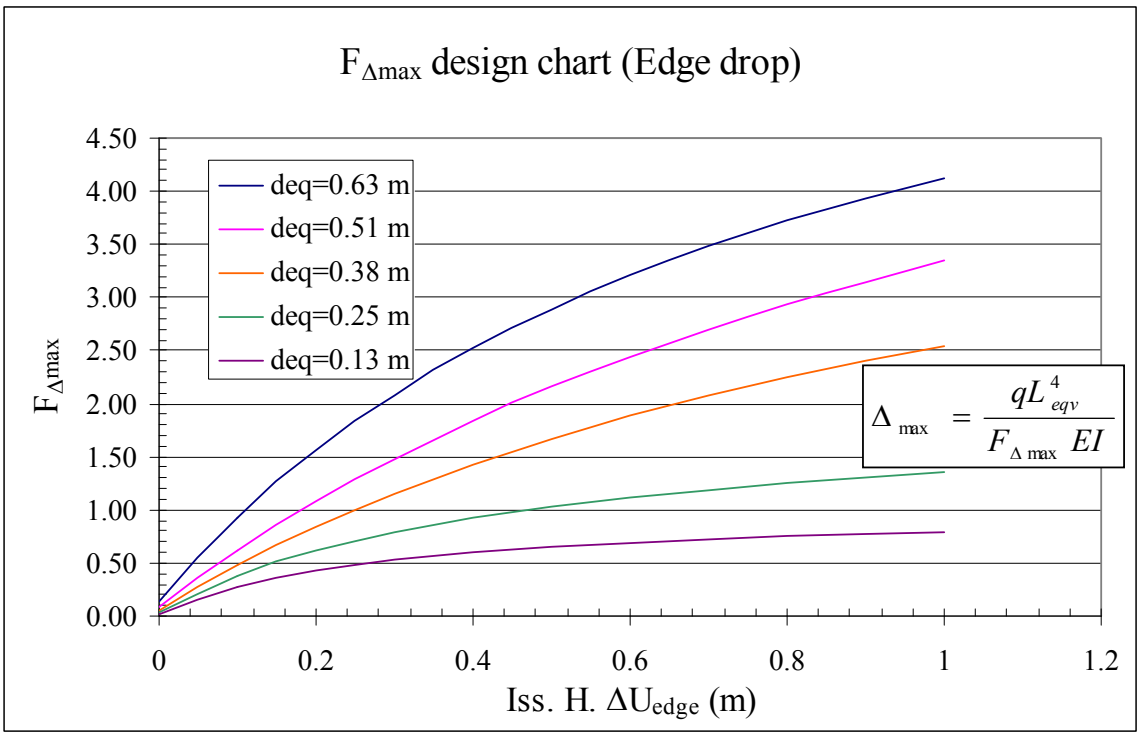

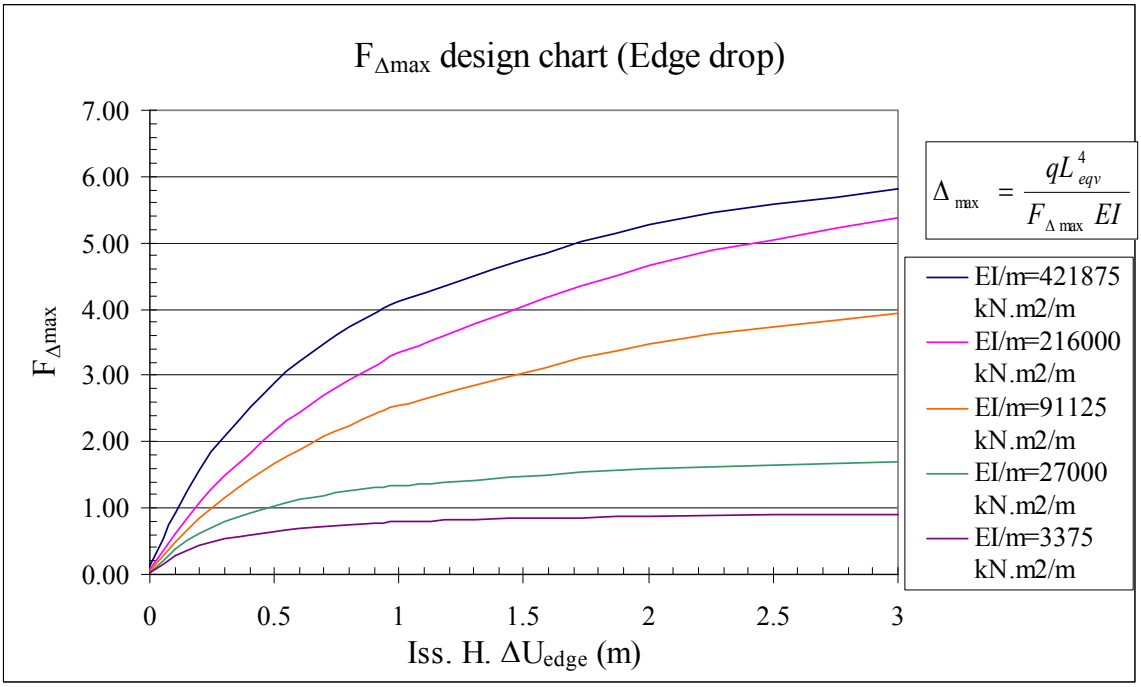

Fig. 6.22. Maximum deflection factor suction based design chart for edge drop case.

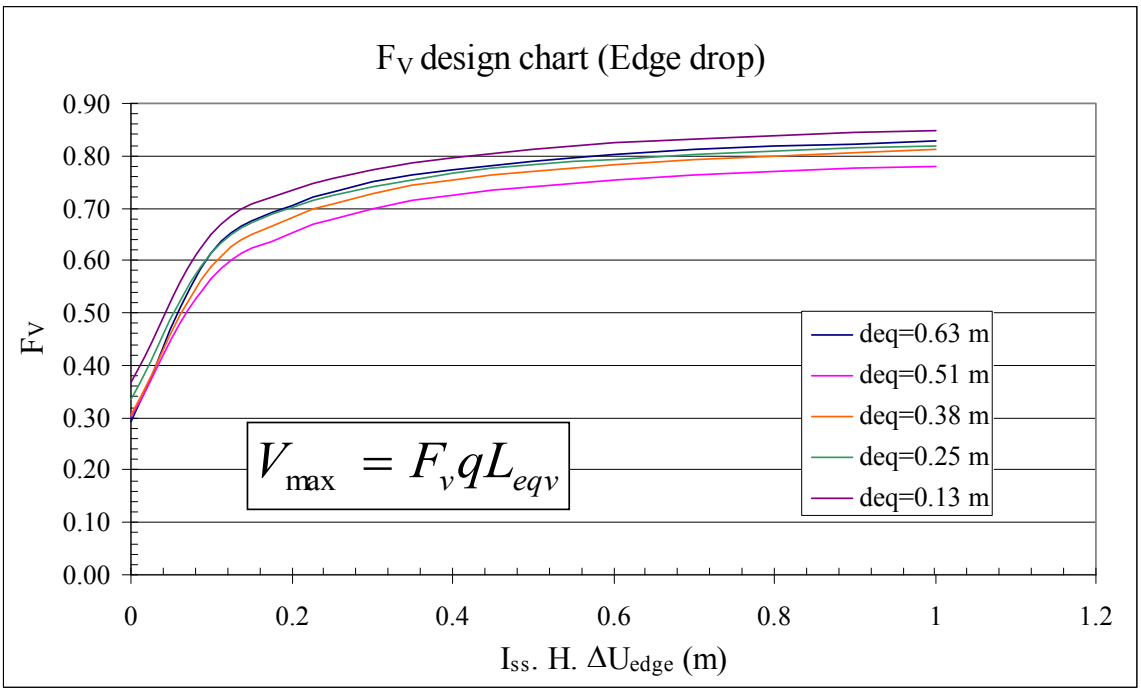

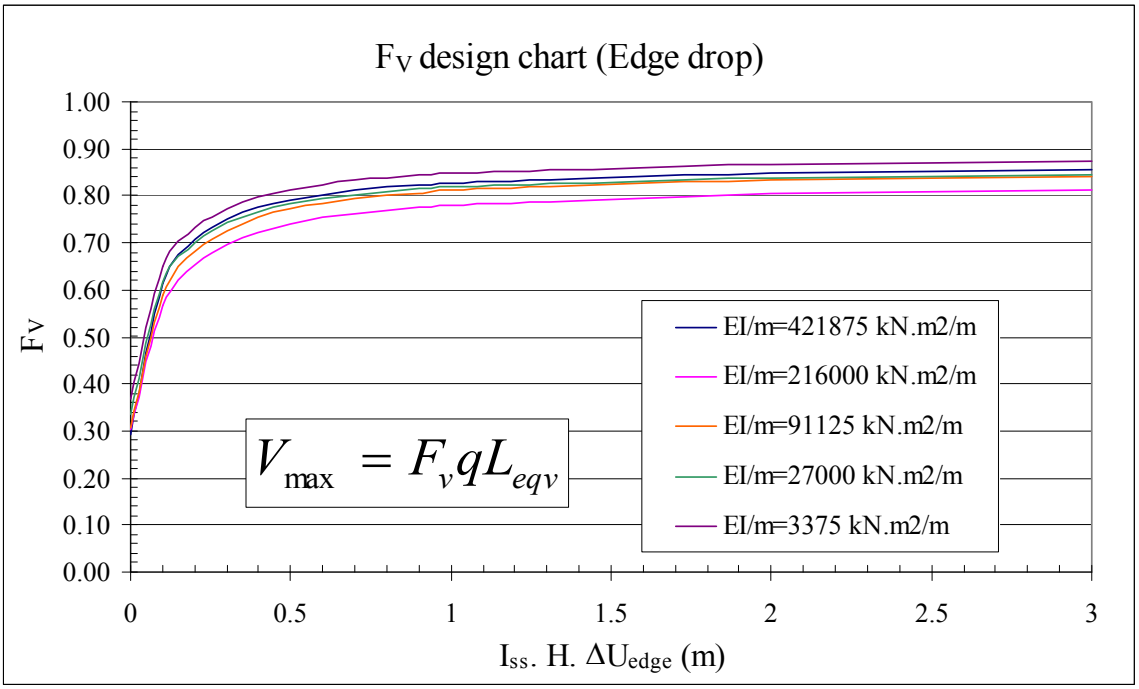

Fig. 6.23. Maximum shear factor suction based design chart for edge drop case.

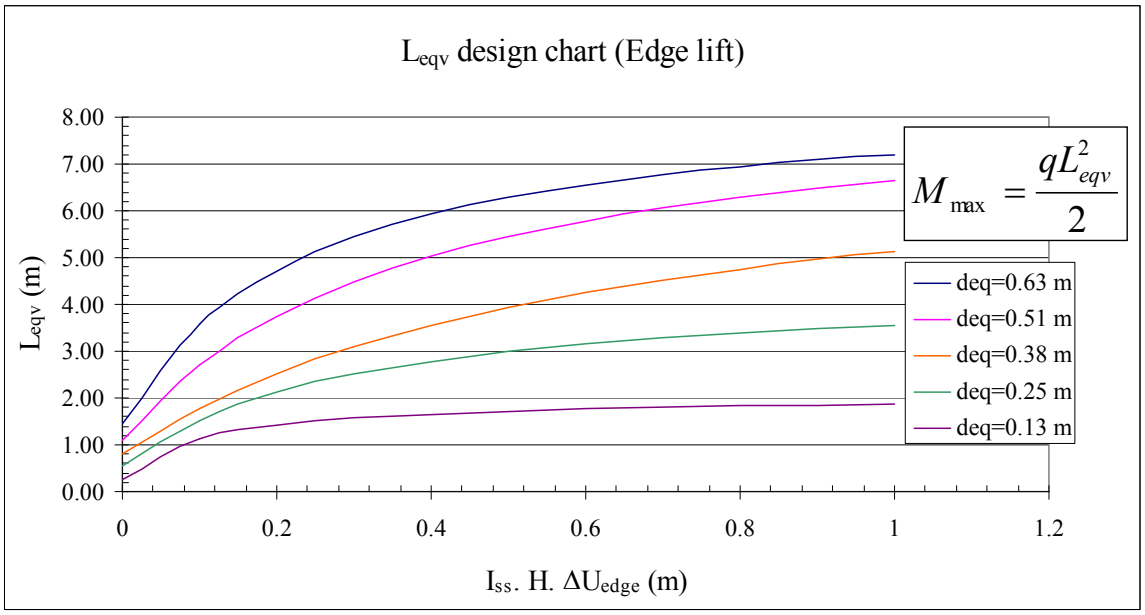

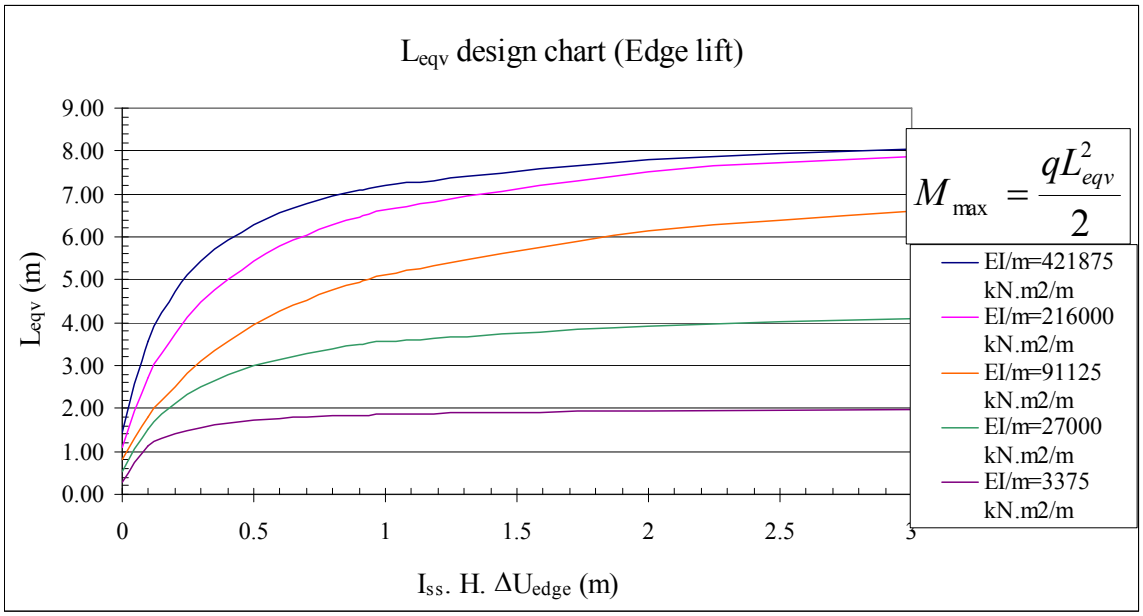

Fig. 6.24. Equivalent cantilever length suction based design chart for edge lift case.

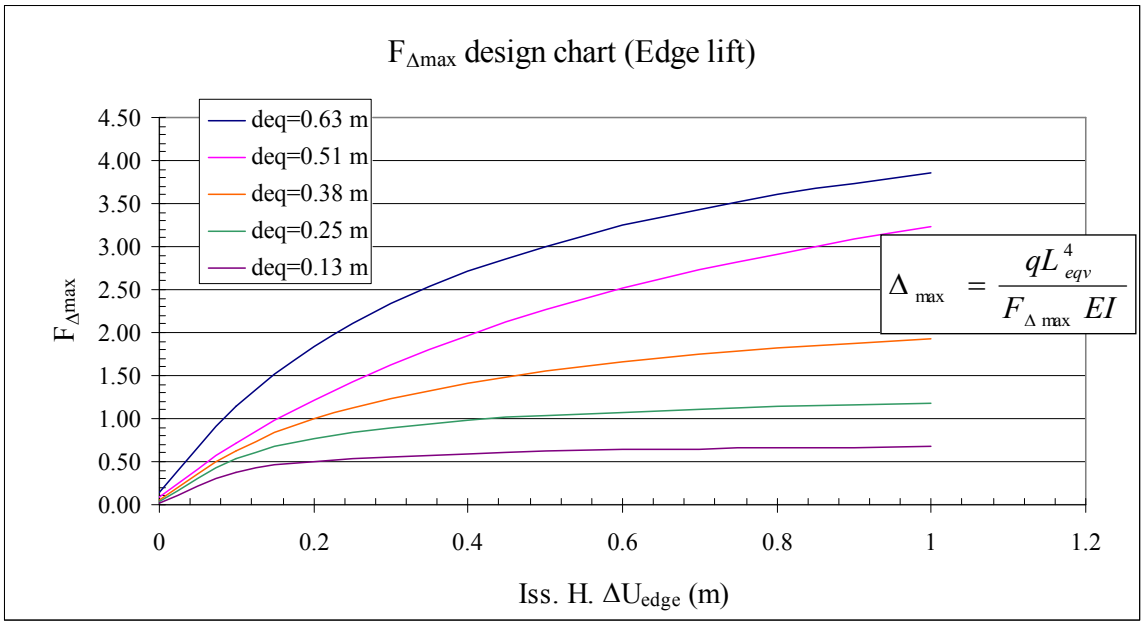

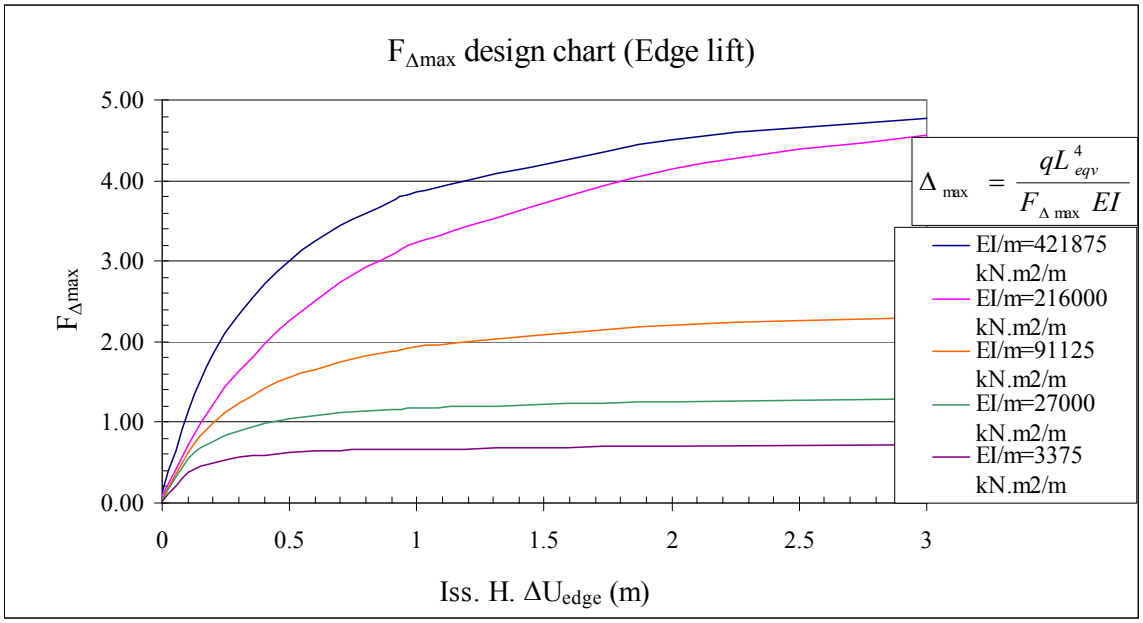

Fig. 6.25. Maximum deflection factor suction based design chart for edge lift case.

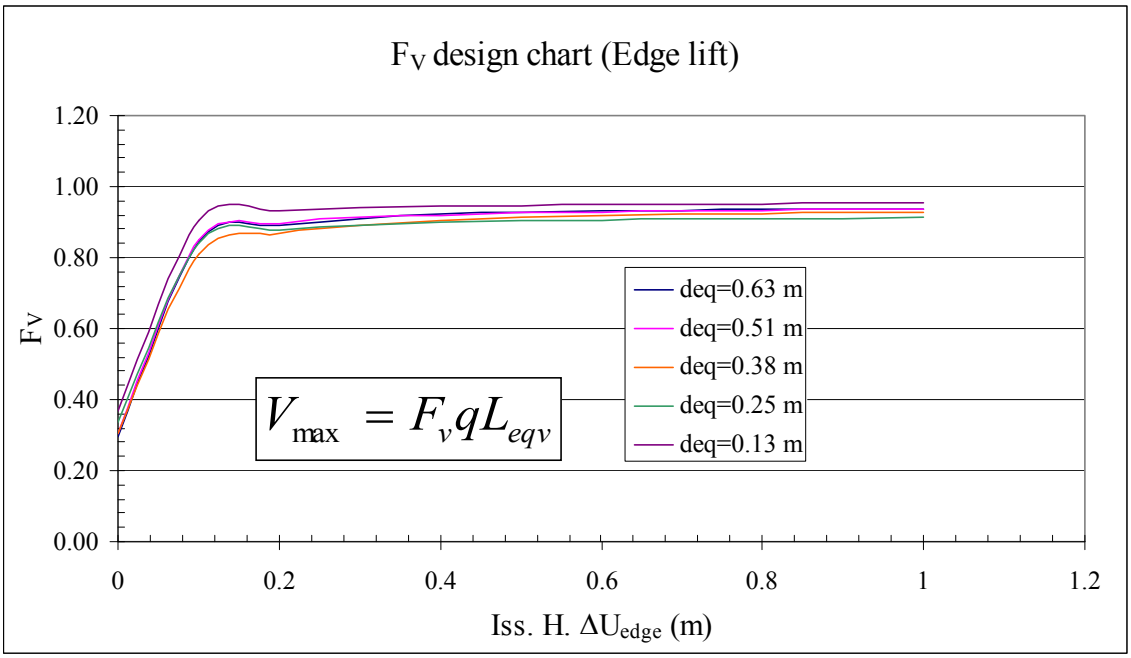

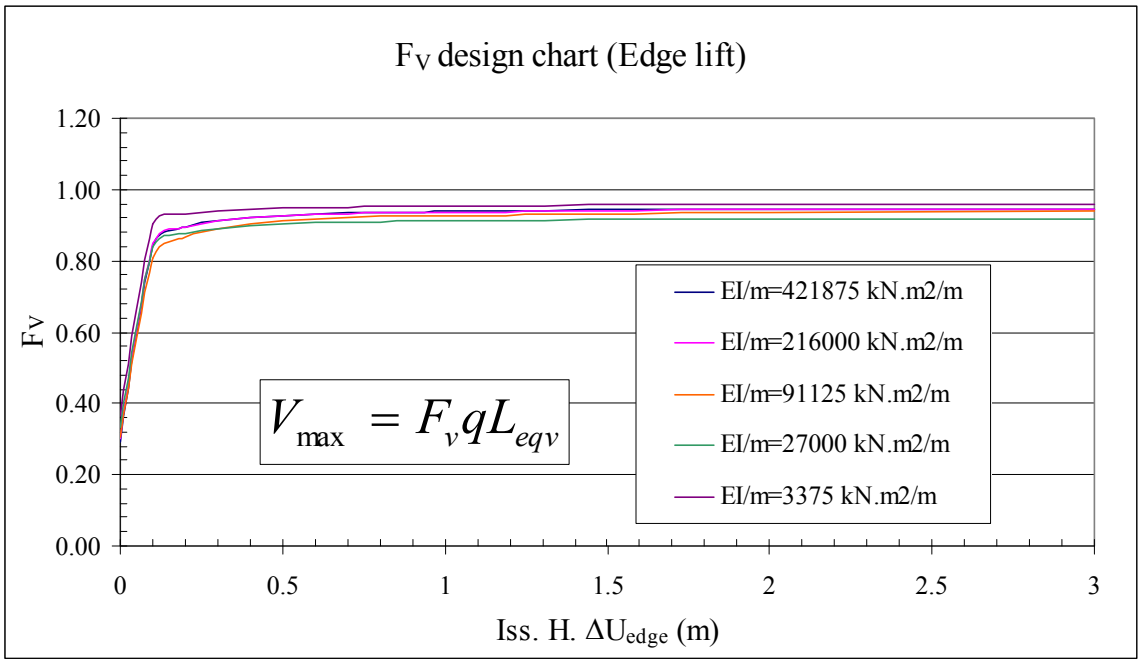

Fig. 6.26. Maximum shear factor suction based design chart for edge lift case.

6.6.4 Water content based design charts

Surface suction change plays an important role in the mound shape; consequently it appears as an intrinsic component in the soil-weather index. However, unfortunately, there is a lack of data bases that afford this important parameter in USA, and many practitioners are not familiar with it. Surface suction change is related to the surface water content change through Eq. 6.18.

$$\Delta w_0 = C_w . \Delta U_0 \qquad 6.18$$

, and $C_w = I_{ss}/2$ as shown in Fig. 4.18, hence, Eq. 6.15 can be rewritten in a format based on surface water content change, Eq. 6.19.

$$I_{S\text{-}W} = 2 . H . \Delta w_0 \qquad 6.19$$

Also, design charts can be reproduced in a similar format based on surface water content change. The water content based design charts will allow the usage of consulting firms local data bases to estimate the surface water content change, since water content measurements are routinely taken, almost in all geotechnical field investigation programs. Fig. 6.27, Fig. 6.28, Fig. 6.29, & Fig. 6.30 shows edge drop water content based design charts for L_{eqv} , L_{gap} , $F_{\Delta max}$, and F_V respectively, and Fig. 6.31, Fig. 6.32, & Fig. 6.33 shows edge lift water content based design charts for L_{eqv} , $F_{\Delta max}$, and F_V respectively.

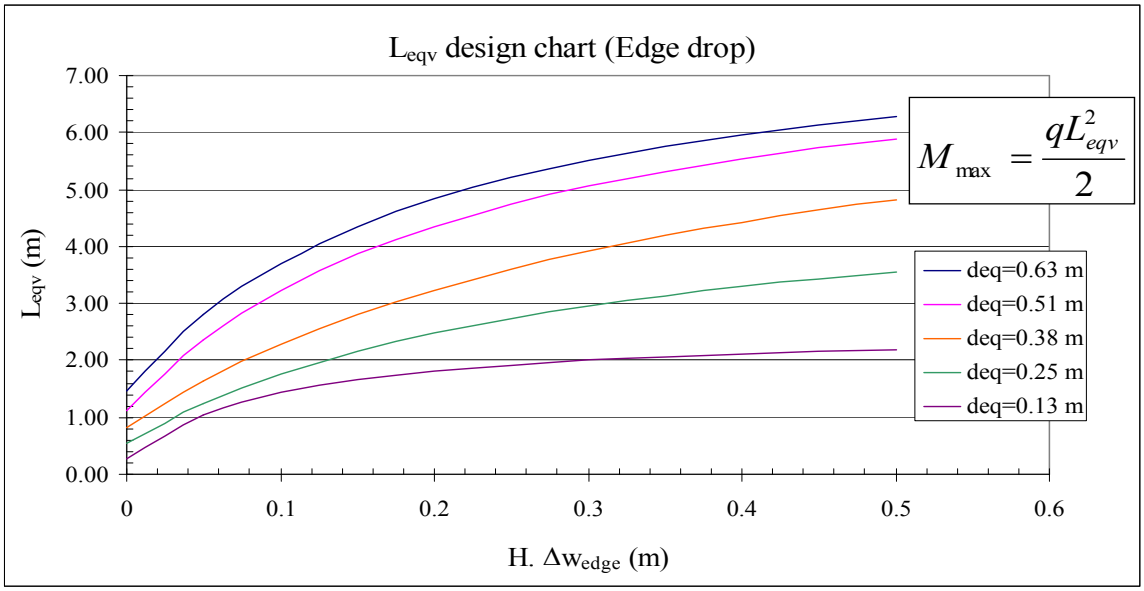

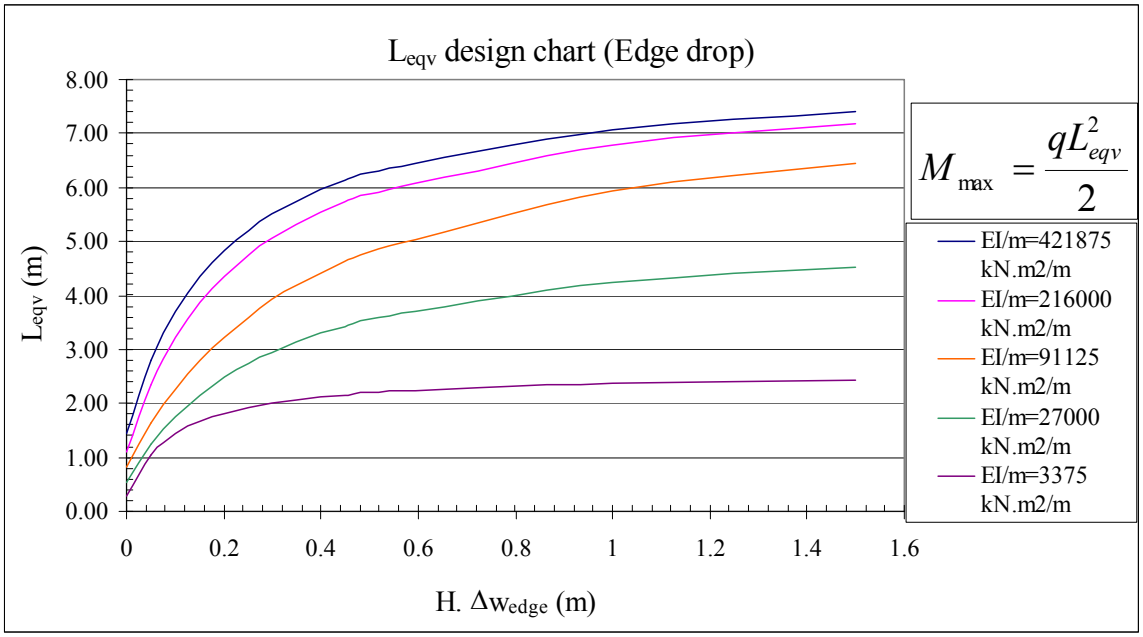

Fig. 6.27. Equivalent cantilever length water content based design chart for edge drop case.

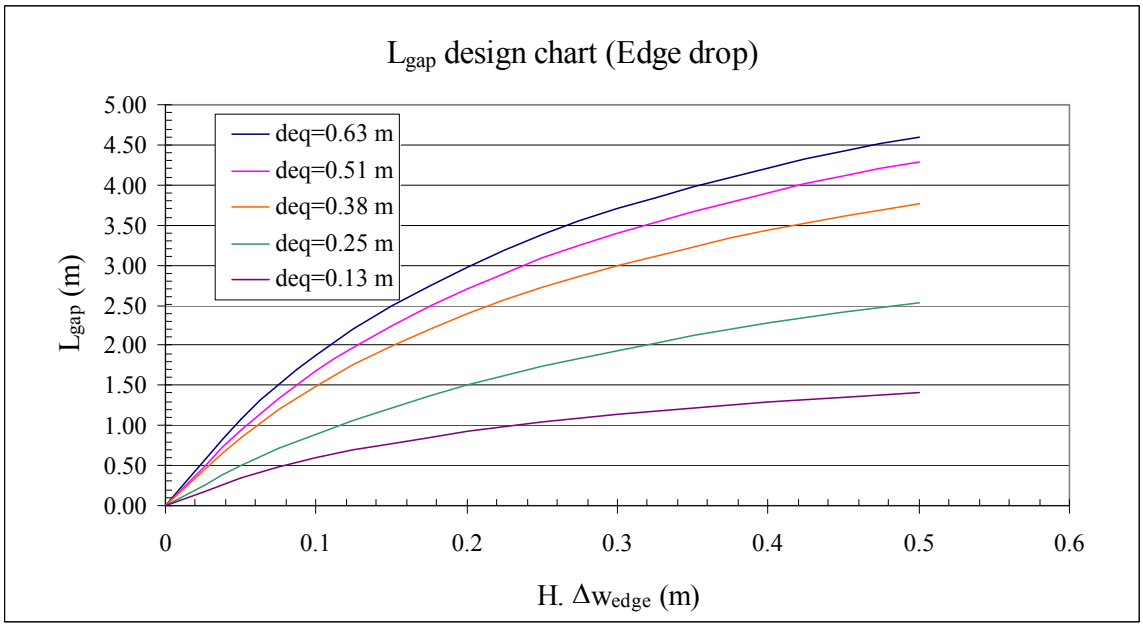

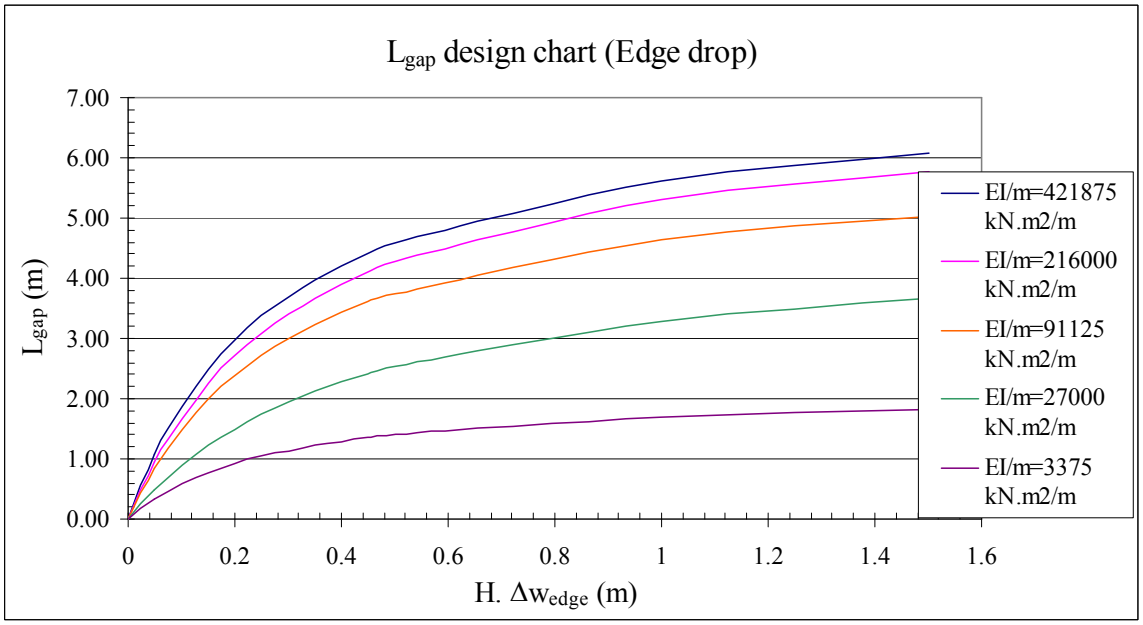

Fig. 6.28. Unsupported length water content based design chart for edge drop case.

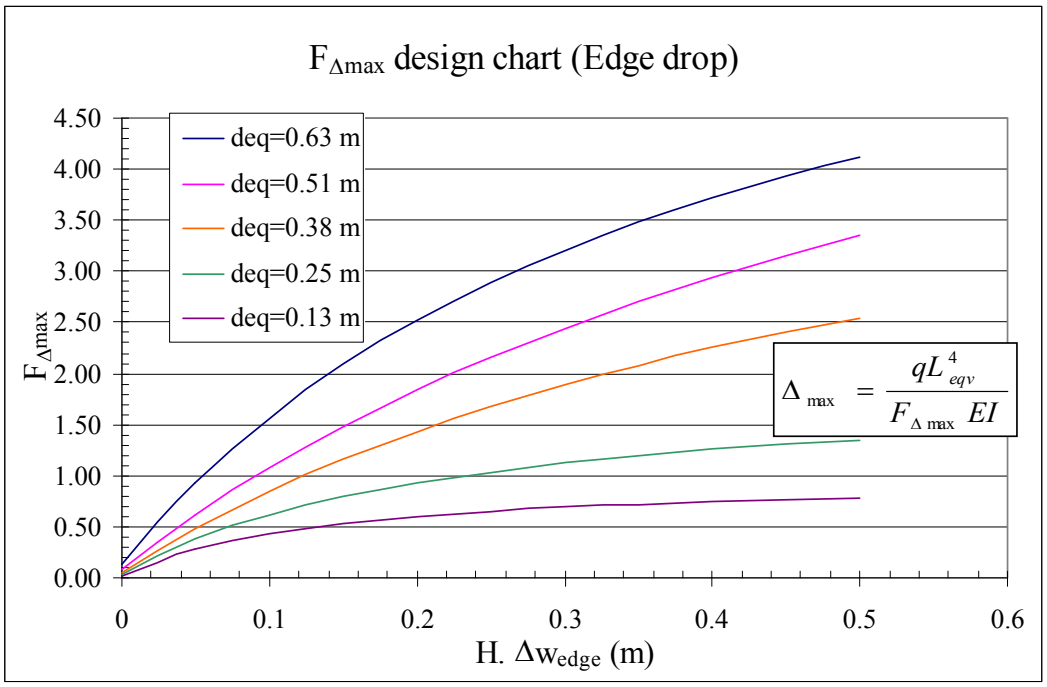

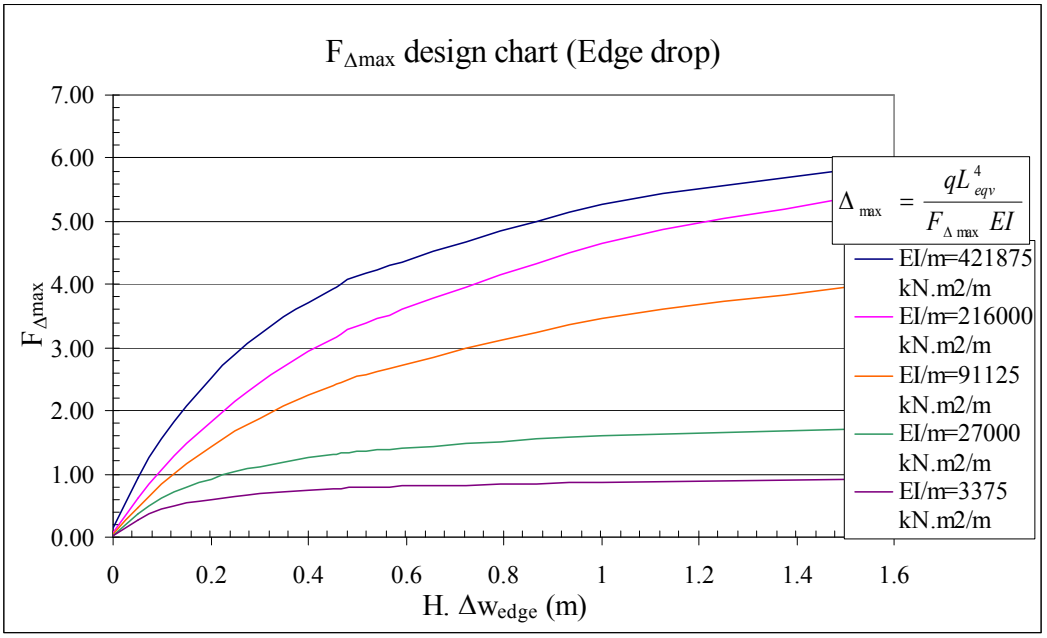

Fig. 6.29. Maximum deflection factor water content based design chart for edge drop case.

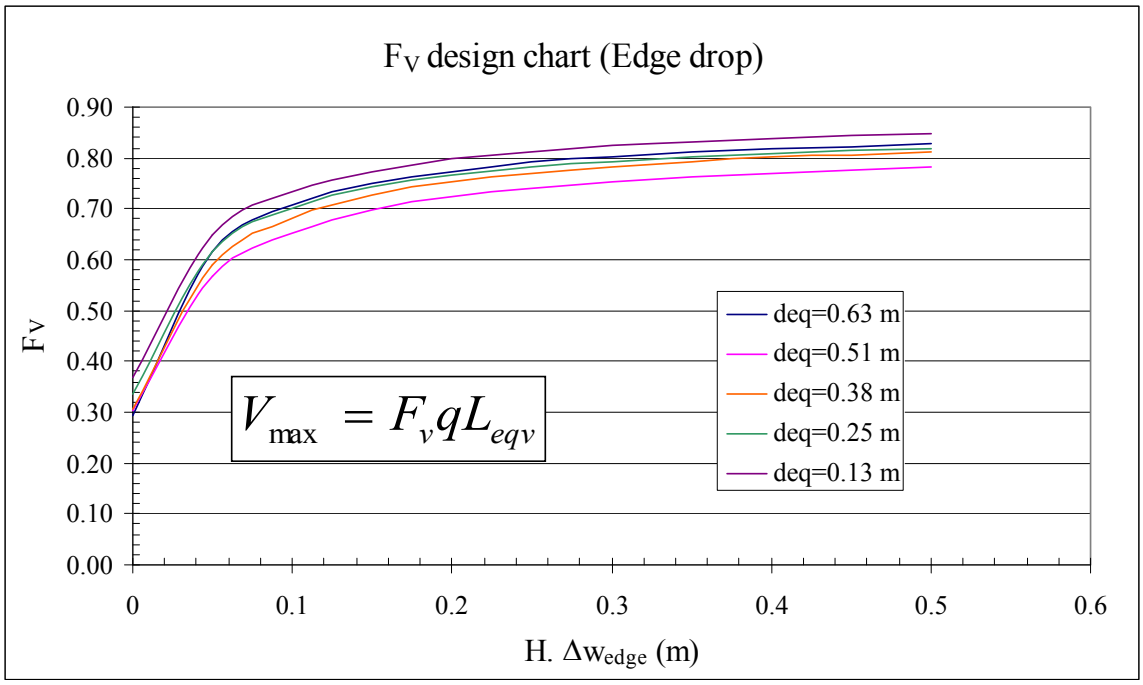

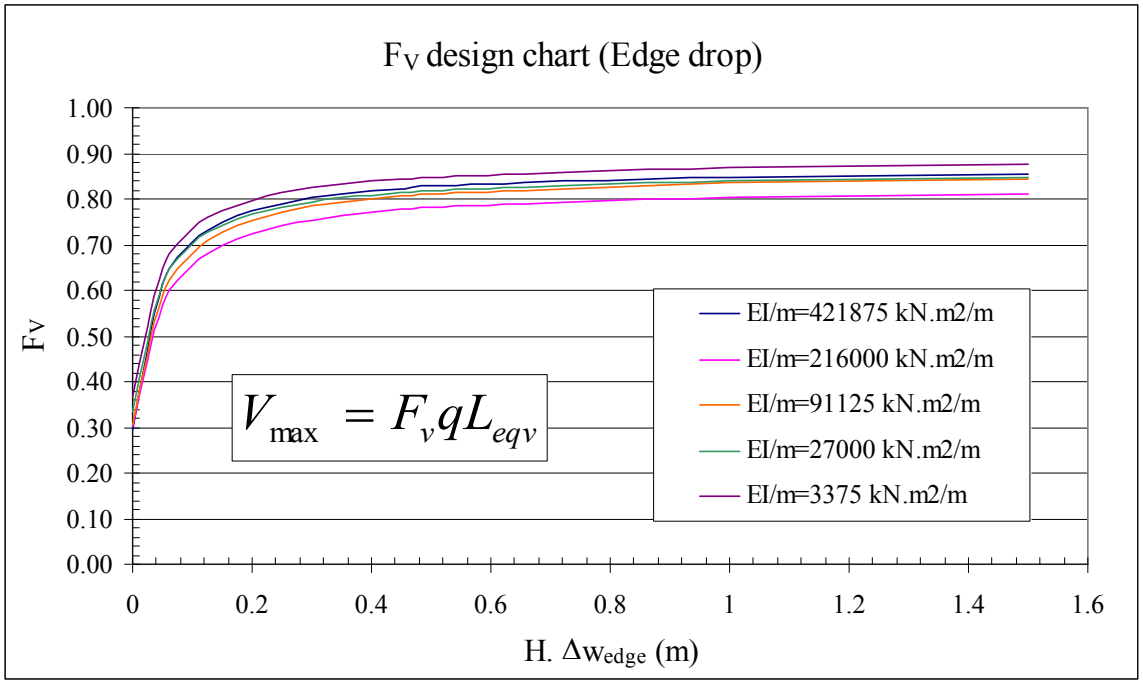

Fig. 6.30. Maximum shear factor water content based design chart for edge drop case.

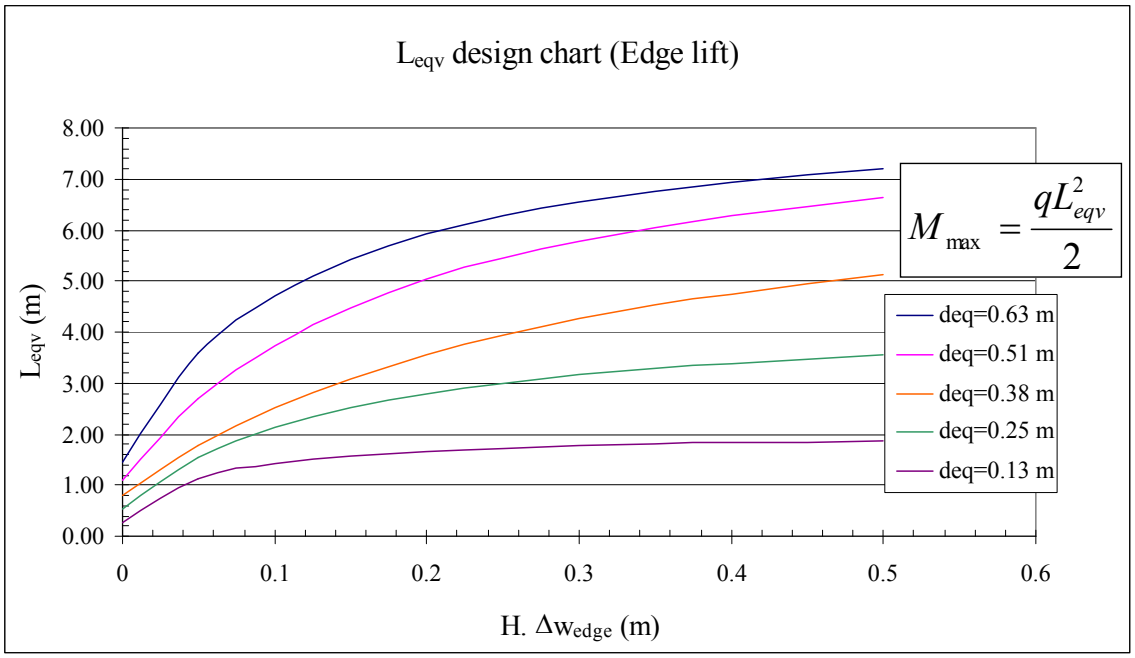

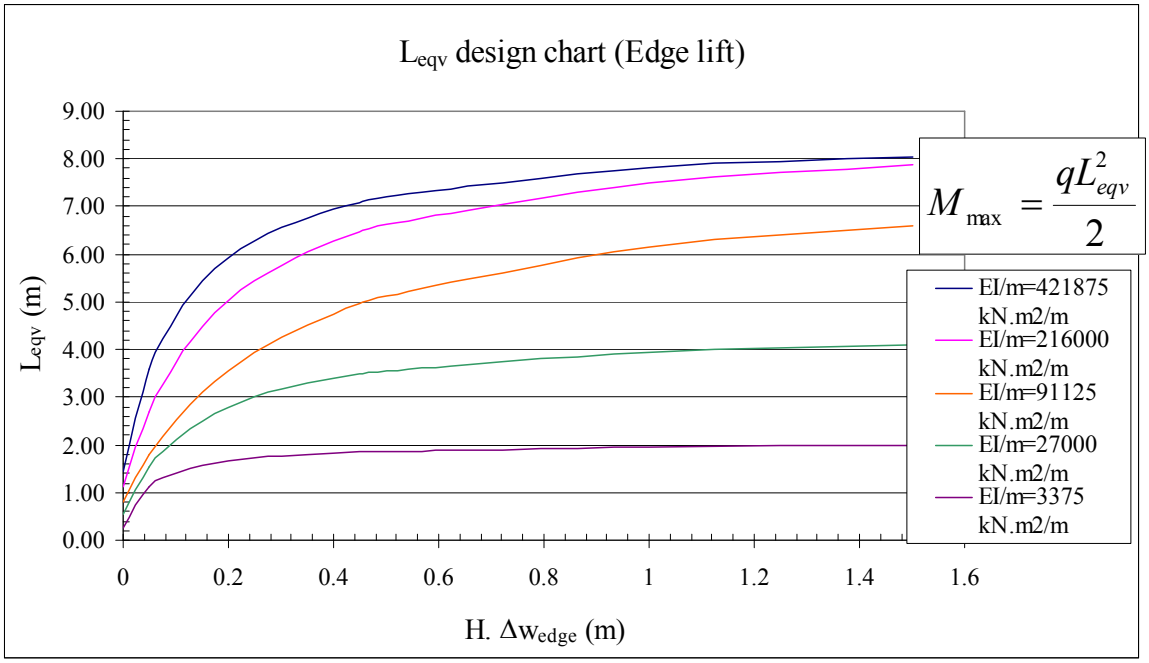

Fig. 6.31. Equivalent cantilever length water content based design chart for edge lift case.

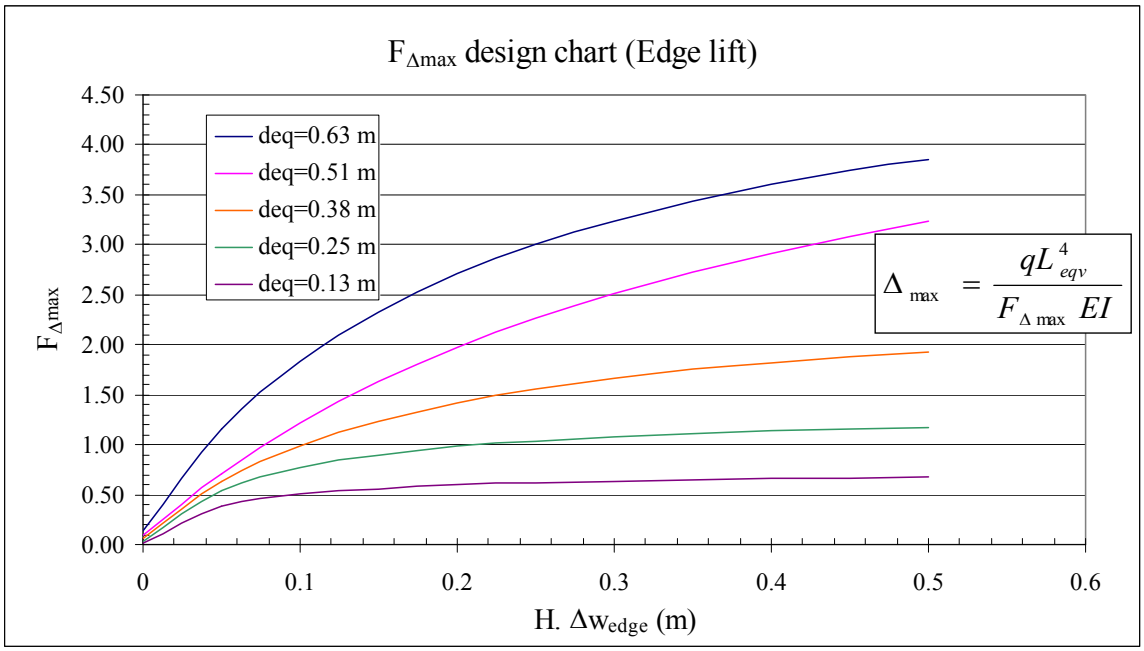

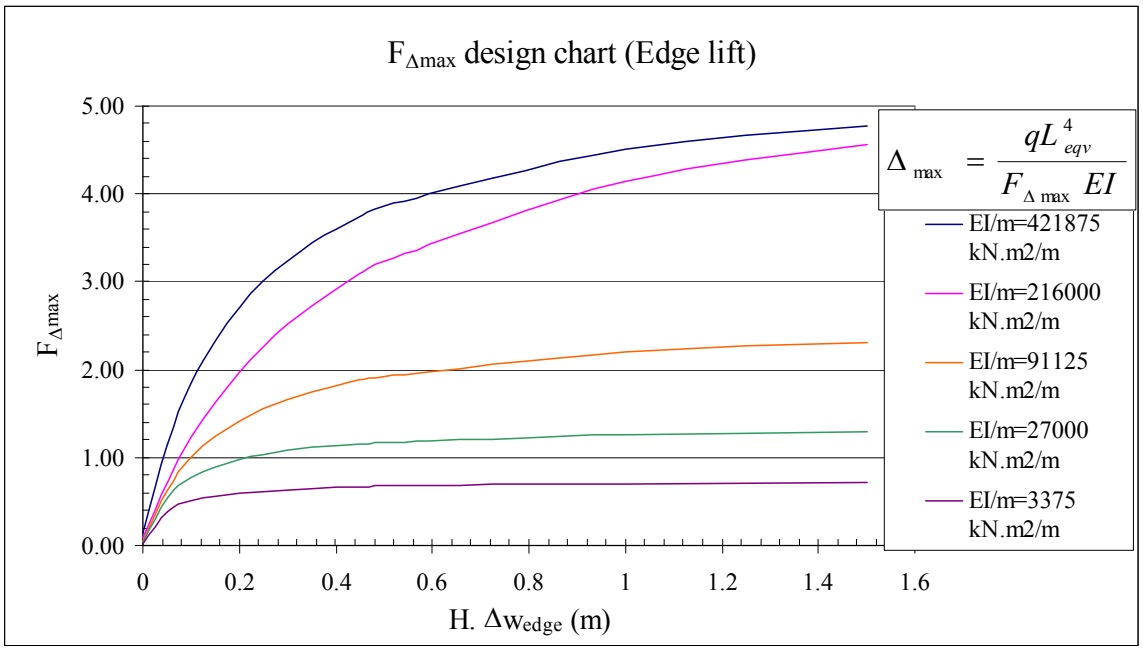

Fig. 6.32. Maximum deflection factor water content based design chart for edge lift case.

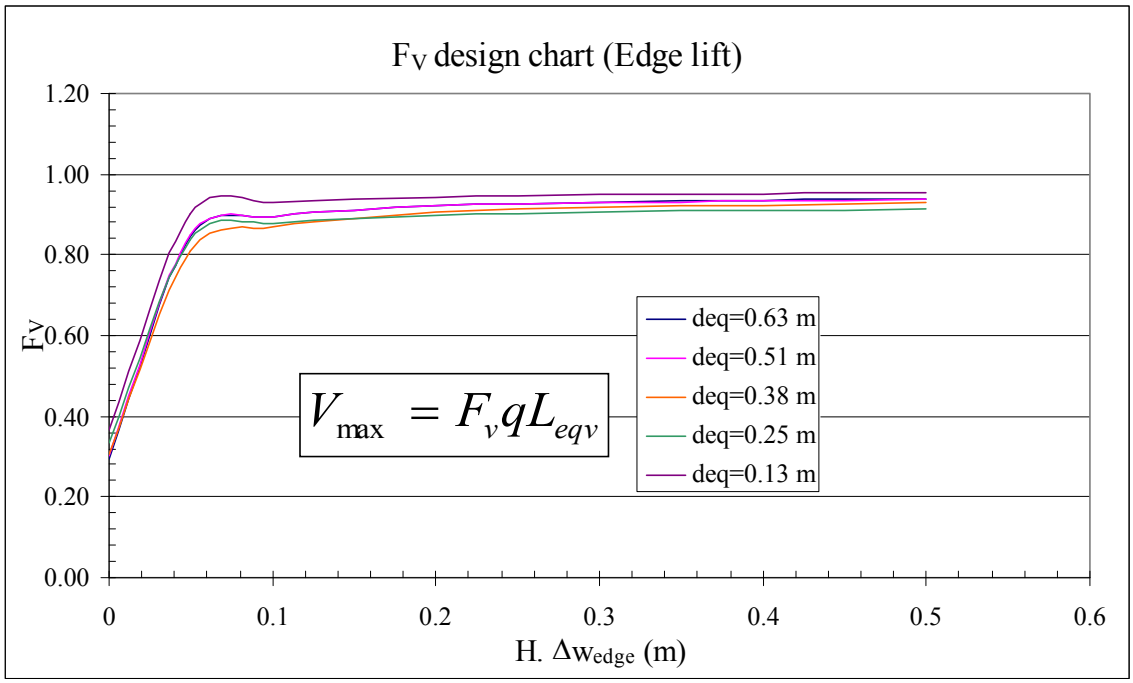

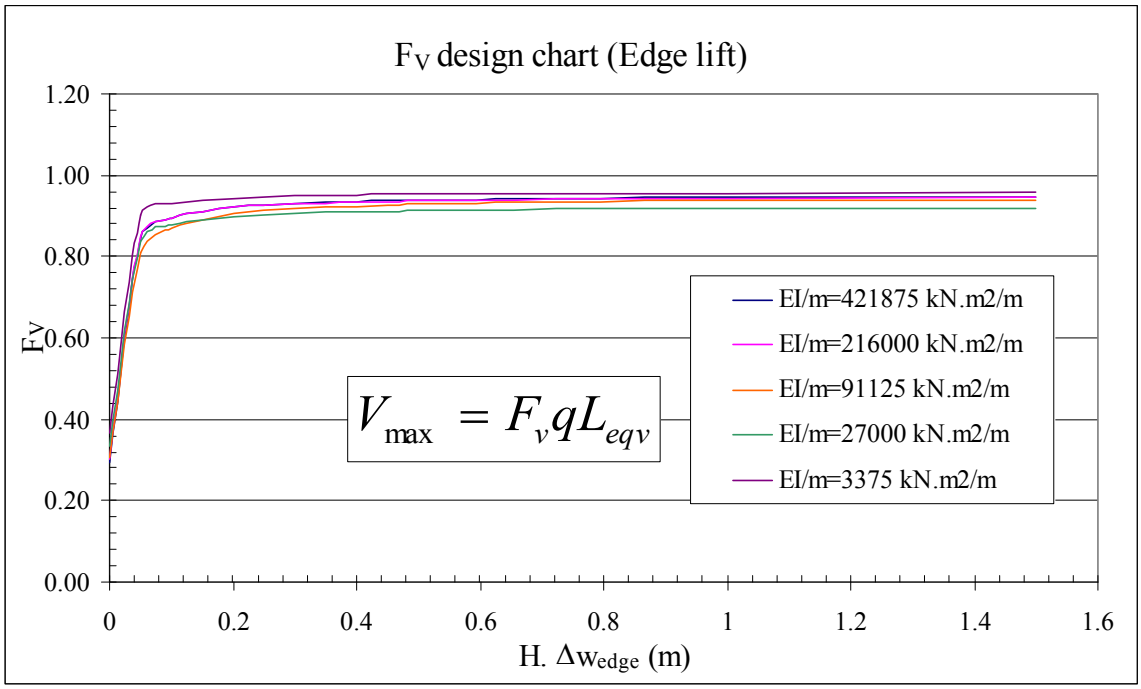

Fig. 6.33. Maximum shear factor water content based design chart for edge lift case.

6.7 A design example

This section details a design example that shows how to use the proposed design charts to design a stiffened slab on grade on shrink-swell soil.

6.7.1 Data

Soil and weather data:

Shrink-swell index, I_{SS} = 0.4

Depth of active moisture zone, H=3.0 m

Soil surface suction change, ΔU_0 = 1.0 pF

Slab data:

Slab dimensions = 12 X 12 m

Beam spacing = 3.0 m (for both directions)

Slab thickness, t_s = 0.1 m

Beam width, b = 0.3 m

Slab live load, w_{LL} = 2 kPa

Slab imposed loads, w_{IL} = 1.5 kPa

Concrete modulus of elasticity, E_{conc} = 20000 MPa

Compressive strength of concrete at 28 days, f'_c = 20.7 MPa

Yield stress of reinforcement in tension, f_y =426.2 MPa

6.7.2 Calculation procedures

1) Calculate soil suction change at the edge of the foundation slab:

$$\Delta U_{edge} = 0.5\Delta U_0$$

$$\Delta U_{edge} = 0.5X1.0 = 0.5pF$$

2) Assume beam depth, D:

D= 0.7 m

3) Calculate the equivalent mat thickness, d_{eq}:

$$Sd_{eq}^3 = bD^3$$
$$3.0Xd_{eq}^3 = 0.3X0.7^3$$
$$d_{eq} = 0.325m$$

4) Calculate the soil-weather index at the slab edge:

$$I_{S-W(edge)} = I_{SS} H\Delta U_{edge}$$
$$I_{S-W(edge)} = 0.4X3.0X0.5$$
$$I_{S-W(edge)} = 0.6m$$

5) Get design parameters from charts corresponding to $I_{S\text{-}W\ (edge)}$:

Fig. 6.20, Fig. 6.21, Fig. 6.22, & Fig. 6.23, give (for edge drop case):

L_{eqv} = 3.5 m, L_{gap} = 2.6 m, $F_{\Delta max}$ = 1.56, and F_V = 0.78 respectively,

Fig. 6.24, Fig. 6.25, & Fig. 6.26 give (for edge lift case):

L_{eqv} =3.78 m, $F_{\Delta max}$ = 1.39, and F_V = 0.91 respectively.

6) Apply equivalent cantilever length and unsupported length corrections:

Fig. 6.15 gives slab length correction factor, F_{SL} = 1.0 (for edge drop case) and F_{SL} = 0.91 (for edge lift case)

$$L'_{eqv} = F_{SL} L_{eqv}$$
$$L'_{eqv} = 1.0X3.5 = 3.5m \quad \text{(For edge drop case)}$$

$$L'_{gap} = F_{SL} L_{gap}$$
$$L'_{gap} = 1.0X2.6 = 2.6m \quad \text{(For edge drop case)}$$

$$L'_{eqv} = F_{SL} L_{eqv}$$
$$L'_{eqv} = 0.91X3.78 = 3.44m \quad \text{(For edge lift case)}$$

7) Beam Loads

Dead Loads:

$$W_{DL} = W_{own} + W_{imposed}$$
$$W_{DL} = \gamma_{conc}\left(St_s + b\left(D - t_s\right)\right) + Sw_{IL}$$
$$W_{DL} = 16.5kN/m'$$

Live Loads:

$$W_{LL} = Sw_{LL}$$
$$W_{LL} = 6kN/m'$$

Total Loads:

$$q_{ult} = 1.2W_{DL} + 1.6W_{LL}$$
$$q_{ult} = 29.40kN/m'$$

$$q_{service} = W_{DL} + W_{LL}$$
$$q_{service} = 22.50kN/m'$$

8) Check for localized bearing capacity failure:

The idealized equivalent cantilever length should not exceed a certain value after which, the contact pressure would induce a localized bearing capacity failure.

$$L'_{eqv\max} = \frac{L}{2}\left(1 - \frac{\frac{S}{S_L+S_s}\frac{q}{b}}{5.14S_u}\right)$$

For edge drop case, S_u is assumed to = 200 kPa, and for edge lift case, , S_u is assumed to = 50 kPa

Hence,

$L'_{eqv\ max}$ = 5.68 m > L'_{eqv} (for edge drop case) → O.K.

$L'_{eqv\ max}$ = 4.7 m > L'_{eqv} (for edge drop case) → O.K.

9) Check for maximum deflection

$$\Delta_{\max allowable} = \frac{L}{480} = \frac{12}{480} = 0.025m$$

$$\Delta_{\max} = \frac{q_{service}L'^4_{eqv}}{F_{\Delta\max}EI_{cr}}$$

Assuming that $I_{cr} = 0.5\ I_g$

(for edge drop case) Δ_{max} = 0.025 m < $\Delta_{max\ allowable}$ → O.K.

(for edge lift case) Δ_{max} = 0.026 m > $\Delta_{max\ allowable}$

Increase the depth to be 0.75 m

(for edge lift case) Δ_{max} = 0.022 m < $\Delta_{max\ allowable}$ → O.K.

10) Check for unsupported length deflection

$$\Delta_{gap\ allowable} = \frac{L'_{gap}}{200} = \frac{2.6}{200} = 0.013m$$

$$\Delta_{gap} = \frac{q_{service} L'^{4}_{gap}}{8EI_{cr}} = 0.012\text{m} < \Delta_{\text{gap allowable}} \qquad \rightarrow \text{O.K.}$$

11) Choose reinforcement

4 bars of #6 give A_S = 1140.6 mm^2, ϕM_u = 282.7 kN.m, and ϕV_u= 147.1 kN

12) Calculate maximum bending moment:

$$M_{\max} = \frac{q_{ult} L'^{2}_{eqv}}{2}$$

(for edge drop case) M_{max} = 182.8 kN.m < ϕM_u $\rightarrow$ O.K.

(for edge lift case) M_{max} = 176.2 kN.m < ϕ M_u $\rightarrow$ O.K.

13) Calculate maximum shearing force

$$V_{\max} = F_v q L'_{eqv}$$

(for edge drop case) V_{max} = 82.5 kN < ϕV_u $\rightarrow$ O.K.

(for edge lift case) V_{max} = 92.0 kN < ϕV_u $\rightarrow$ O.K.

6.8 Comparing the proposed new design procedure to the existing methods

It is important to compare the proposed new design procedure to the existing methods to assess the how the proposed method will influence the practice of designing foundation slabs on grade on shrink-swell soils. This section details a parametric study that compares beam depths resulting from seven design methods; the proposed method and six existing methods.

To comprise this parametric study, three different soils, three different locations, and three different slabs were chosen, the same way as in (Abdelmalak& Briaud, 2007), to form 27 cases representing typical design situations.

6.8.1 Weather parameters

Three locations were chosen in Houston, College Station, and San Antonio, Texas, US representing wet temperate, temperate, and dry temperate climatic zones.

The soil surface suction change, ΔU_0 were 1.283, 0.788, and 1.392, respectively as shown in Chapter V. Depths of active moisture zone were 1.8, 2.4, and 3.3 m, respectively.

6.8.2 Soil parameters

Three soils were chosen representing very high, high, and moderate shrink-swell potential. The soil shrink-swell indices were assumed to be 0.36, 0.27, and 0.18, respectively.

6.8.3 Structural parameters

Three slabs were chosen of dimensions 12X12, 24X24, and 24X12 m representing different aspect ratios and different slab sizes. The beam spacing was chosen to be 3m in both directions. For all slabs a masonry veneer super structure was chosen.

The 27 cases were designed using the proposed method following the same procedure that was detailed in the previous section.

6.8.4 Results and discussion

The resulting beam depths using the proposed design procedure and another six design methods;

WRI, WRI-TxASCE, BRAB, BRAB-ASCE, PTI 2004 and AS2870 (Abdelmalak& Briaud, 2007) are tabulated in the Appendix F.3.

To compare these beam depths, the average beam depth for each design case using the 7 different procedures (Proposed method, BRAB and WRI design methods with and without the (Tx ASCE) recommendations and PTI 2004 and AS2870) was calculated (denoted as $\mathbf{D_{ave\ 7}}$). The percentage difference between the design depth and this average design depth for all cases (denoted as $\mathbf{\%\Delta_{design\ method,\ 7}}$) was also calculated and presented in Fig. 6.34.a.

Fig. 34.b. presents the resulting beam depth using the aforementioned seven design methods versus the average resulting beam depth of all the seven methods.

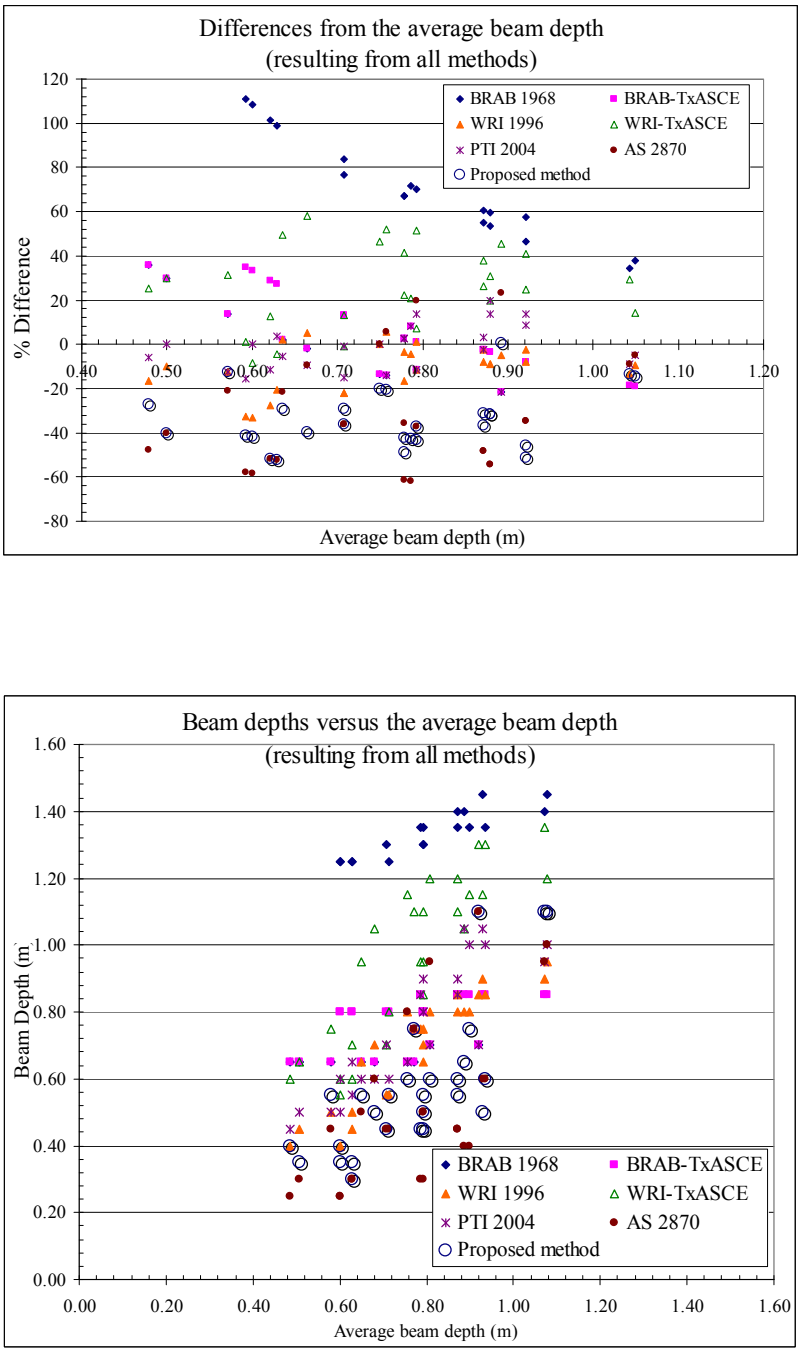

Fig. 6.34. (a) The percentage of the difference from the average beam depths using 7 design procedures (Proposed method, BRAB, WRI, BRAB-TxASCE, WRI-TxASCE, PTI 2004, and AS2870). **(b)** The resulting beam depths from the seven design methods versus the average beam depth The resulting beam depths from the seven design methods versus the average beam depth.

Table 6.8 summarizes the minimum, average, and maximum percentage of the differences from the average beam depths using the 7 design methods. Statistics shown n Table 6.8 indicates that the proposed design method gives beam depths below the average of the seven design methods, in average sense.

Table 6.8. Percentage of the differences from the average beam depths using the 7 design methods.

	BRAB	BRAB-TxASCE	WRI	WRI-TxASCE	PTI 2004	AS 2870	Proposed Method
Average	45.75	3.19	-11.75	24.92	-3.09	-33.17	-25.86
Maximum	108.33	33.82	5.66	54.74	18.55	19.38	19.38
Minimum	-24.03	-24.03	-33.33	-8.33	-24.03	-62.16	-52.27

Fig. 6.35, 6.36, and 6.37 show beam depths resulting from proposed method versus those from the AS 2870, WRI, and PTI 2004 respectively. AS 2870 gives the highest coefficient of determination (R^2=0.66) with the proposed method, meanwhile PTI 2004 gives the lowest coefficient of determination (R^2=0.27) with the proposed method. Compared with WRI and PTI 2004 resulting beam depths, the proposed method gives smaller beam depths, except for very few cases. Only for small beam depth range (less than 0.6 m), the proposed method gave larger beam depths than those resulting from AS 2870.

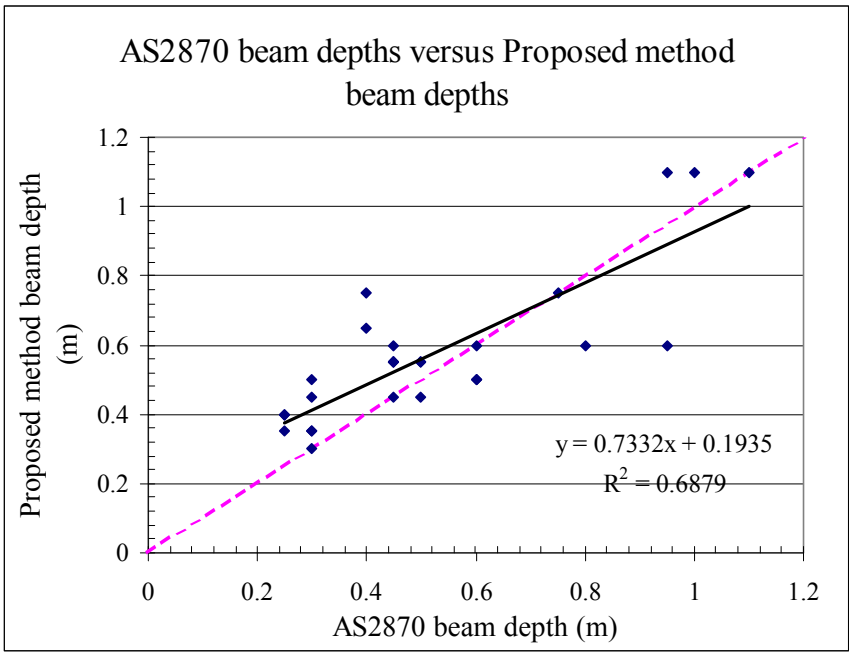

Fig. 6.35. Comparing the proposed method beam depths to AS 2870 beam depths.

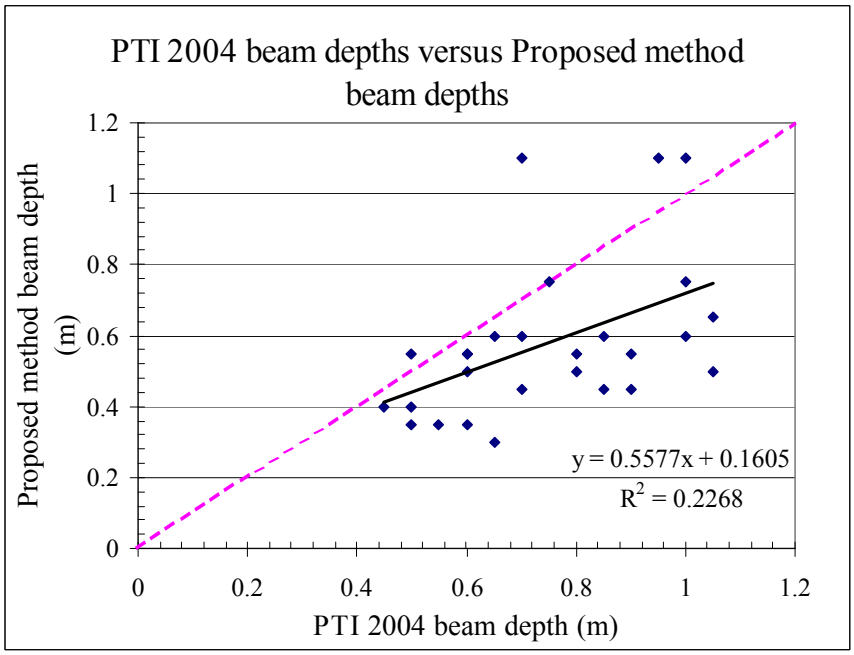

Fig. 6.36. Comparing the proposed method beam depths to PTI 2004 beam depths.

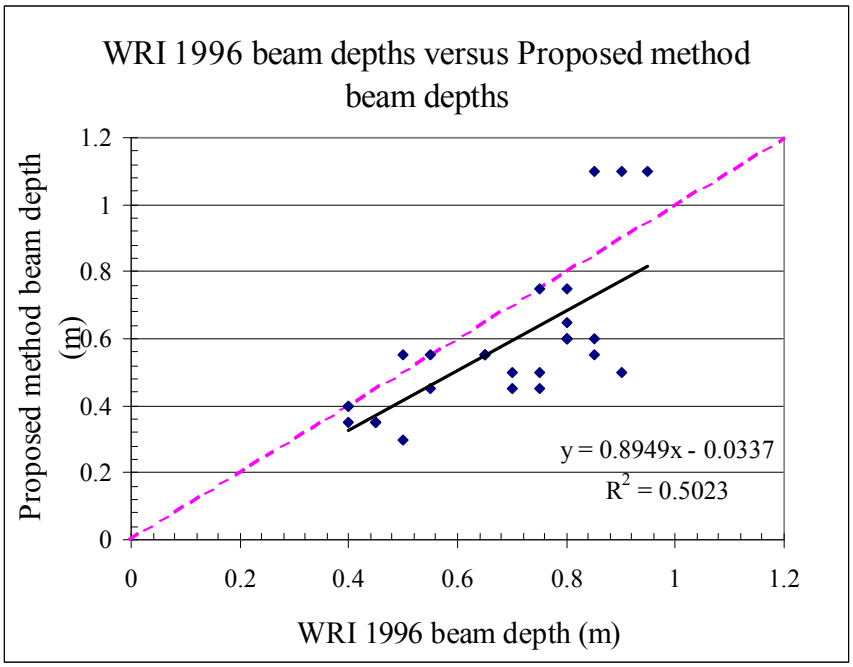

Fig. 6.37. Comparing the proposed method beam depths to WRI beam depths.

CHAPTER VII

CONCLUSIONS

In this dissertation, a new procedure was proposed for designing foundation slabs on grade on shrink-swell soils. The new design procedure begins by considering the weather in the city where the foundation is to be built, the soil parameter will be obtained from a simple shrink-swell test, and then design charts are used to obtain the slab equivalent cantilever length from which the maximum bending moment is calculated and the needed slab stiffness is obtained.

To propose this new design procedure, developments of implemented weather, weather-soil, and soil-structure interaction models were achieved. These developments considered the practitioners' concerns in solving this problem by:

- Taking advantage of the similarity between consolidation and unsaturated diffusion phenomena to determine α in the laboratory in a similar way to c_v laboratory determination.
- Carrying out 2D finite element analyses, addressing the cracks network effects, to develop a design chart relating α_{field} to α_{Lab}.
- Carrying out a large scale laboratory test to model the moisture diffusion in unsaturated soil that will enable the verification of proposed moisture diffusion model.
- Using the FAO 56-PM method to simulate a weightless cover performance for six cities in the United States to provide more accurate weather site-specific parameters of: range of surface suction variations and depth of active moisture zone.
- The proposed weather-site specific parameters will be input parameters to the soil structure models.
- Using Mitchell (1979) equations for moisture diffusion under covered soil to develop a closed form solution for the soil mound shape under the foundation slab.

- Carrying out several 2D finite elements plane strain simulations for plates resting on a semi-infinite elastic continuum, and resting on different soil mounds.

The following conclusions are drawn from the previous chapters:

(1) Comparative studies of commonly used design methods provides tables of resulting beam depths using these design methods for 27 cases that cover a range of soils of very high, high, and moderate shrink-swell potential, range of weather patterns of wet temperate, temperate, and dry temperate climatic zones, and range of slab sizes of dimensions 12X12, 24X24, and 24X12 m. The table of results may provide guidance for consultants who deal with similar design situations.

(2) For the chosen 27 cases in comparative studies, the beam depth predicted by the WRI design method gives results closest to the average beam depth obtained by all methods, PTI 2004 gives beam depths larger than the average beam depth, and AS 2870 gives beam depths smaller than the average beam depth.

(3) The BRAB (1968) is a design method for reinforced concrete slabs; it is mostly empirical, but it is a simple method which is attractive to foundation designers. It can lead to large beam depths for large slabs as the cantilever length is directly proportional to corresponding slab dimension. WRI (1996) is very similar to BRAB with a significant modification to the cantilever length as it is proportional to the support index. It is also a method exhibiting empiricism. Unlike BRAB (1968), WRI (1996) can handle both post tensioned and reinforced concrete slabs.

(4) Comparative studies show that: For the chosen 27 cases, applying the TxASCE guidelines significantly reduced the beam depths using the BRAB method and increased the beam depths using the WRI method. The beam depth predicted by the BRAB-TxASCE design method gives results closest to the average beam depth obtained by all aforementioned methods with an average percentage difference of -1.3%. BRAB gives beam depths larger than the average beam depth by 39.1%, WRI gives beam depths smaller than the average beam depth by -15.3%, and WRI-TxASCE gives beam depths larger than the average beam depth by 20.0%.

(5) There is a strong similarity between the partial differential equations that govern both the unsaturated diffusion, and the consolidation phenomena. This dissertation proposes a new laboratory test (α-shrink test), that takes the advantage of this similarity to determine α in the laboratory in a similar way to c_v laboratory determination. The main advantage is that: c_v determination procedure is based on measuring soil sample volume changes with time. Consequently the conventional sophisticated suction measurements will be replaced with simple volume measurements to determine α. Moreover, the geotechnical practitioners are very familiar with the consolidation test, which will promote their acceptance and usage of this new technique. Procedure of α-shrink test was explained in details in Chapter IV.

(6) This dissertation proposes a new chart that estimates the coefficient of unsaturated diffusivity at field based on the cracked soil diffusion factor, F_{CrkDif}. The used technique for developing this chart may be considered as a first order approximation to this complicated problem. The technique simplifies the complicated micro/macro scale diffusion problem through intact soil and cracks network to a simple diffusion problem through a homogenous soil continuum with an equivalent (larger) value for the field coefficient of unsaturated diffusivity. The equivalent field coefficient of unsaturated diffusivity estimation shall be based on the bounding suction envelops, because designing the shallow foundation considers the extreme soil mound shapes, which are related to the bounding suction envelops.

(7) In extremely diffusive soils (i.e., α_{lab} value is very high), cracks networks do not significantly increase the overall soil mass diffusivity as the moisture can easily diffuse through the soil almost as easily as it does through cracks network. Consequently, cracked soil diffusion factor, F_{CrkDif} is small for highly diffusive soils. In very poorly diffusive soils (i.e., α_{lab} value is very low), the moisture takes very long time to diffuse either from the top soil surface or from cracks networks. Yet, the applied suction varies with time following a sinusoidal function. When the speed of suction front permeation becomes very slow relatively to the speed of surface suction changes, the suction front

penetration becomes very small, which results in a small cracked soil diffusion factor, F_{CrkDif}.

(8) A large scale laboratory test was carried out to verify the proposed new methods to determine the coefficient of unsaturated diffusivity at laboratory, α_{lab}, and to estimate the coefficient of unsaturated diffusivity at field, α_{field}. The large scale laboratory test was run to model the moisture diffusion in a 1.2 m diameter tank filled with 0.44 m homogeneous soil layer subjected to several wetting and drying cycles with two phases: uncovered phase-and covered phased. The uncovered phase consisted of six shrink-swell cycles that took 270 days, and the covered phase consisted of two shrink-swell cycles tha took 196 days. Cyclic wetting and drying cycles developed a steady crack network with a depth of active moisture changes of 0.32 m. The experiment was numerically simulated using ABAQUS / STANDARD; input parameters were measured in laboratory including the coefficient of unsaturated diffusivity at laboratory, α_{lab}, and the coefficient of unsaturated diffusivity at field, α_{field}. was estimated using the proposed chart Fig. 4.14. the ratio of the vertical strain to the volumetric strain was assumed as has been discussed in section 4.6.

(9) Very reasonable matching between the measured and predicted water content results was observed during the entire experiment. The average RMS values for all predicted and measured water content profiles were 0.974 % for the uncovered phase and 1.183 % for the covered phase.

(10) Strong matching between the measured and predicted average soil surface movements was observed during the uncovered phase, the RMS value was 0.511 mm. Local preferential moisture diffusion passes around the extension stems influenced the measured average movements at depths 100 and 220 mm inducing discrepancy between the measured and the predicted average movements at those depths.

(11) The proposed technique for the soil diffusion model consists of measuring the coefficient of unsaturated diffusivity at laboratory, α_{lab}, estimating the coefficient of unsaturated diffusivity at field, α_{field}, and assuming the coefficient of vertical to volumetric strain, *f*. Generally, the proposed technique succeeded to closely predict

water contents measurements and average soil surface movement measurements of this large scale long term laboratory experiment.

(12) This dissertation explains using the FAO 56-PM method to simulate a weightless cover performance for six cities in US that suffer significantly from shallow foundation problems on shrink-swell soils due to seasonal weather variations. These simulations provide us with more accurate weather site-specific parameters of such as the range of surface suction variations. The proposed weather-site specific parameters will be input parameters to the soil structure models.

(13) This dissertation recommends, for future work, to use actual representative soils at those cities, and the rest of US cities, to get more accurate suction change values. For the time being, it is recommended to use the maximum suction change values for design purposes as shown in Table 5.2.

(14) This dissertation proposes a closed form solution for the soil mound shape under the foundation slab, the new mound shape equation shows that the normalized mound shape is dependent on two main parameters: A dimensionless soil diffusion parameter, $\frac{\omega H^2}{2\alpha_{field}}$ and the diffusion domain aspect ratio, $\frac{L/2}{H}$. The curvature of the mound shape is dependent on both soil diffusion parameter and diffusion domain aspect ratio. Increasing any or both of those parameters increases the resistance to the moisture front diffusion, and increases the curvature of the mound shape. For the formally assumed mound equations, the mound exponent was an assumed constant value independent of both soil diffusion parameter and diffusion domain aspect ratio.

(15) The sensitivity study showed that the following factors influence the design of foundation slabs on grade on shrink-swell soils (factors are cited according their order of significancy starting from the most significant factor): slab stiffness, depth of active moisture zone, shrink-swell potential, slab length, soil surface suction change, imposed loads, soil stiffness, and many other minor factors. The sensitivity study recommended also reasonable values for parameters of minor significancy.

(16) This dissertation proposes a suction based design procedure as follows:

a) Determine the shrinkage limit, I_{sh} from the shrink test.

b) Determine the swell limit, I_{sw} from the swell test.

c) Determine the shrink-swell index, I_{SS} from the following equation:

$$I_{SS} = I_{sw} - I_{sh}$$

d) Estimate depth of active moisture zone H based on experience or available databases at the site location.

e) Estimate the suction change value at the soil surface for a free field, ΔU_0 in pF units based on experience, using Table 5.2, or by using available data bases at the site location, typical ranges of ΔU_0 : 0.8 to 1.5.

f) Determine the suction change value at the soil surface under the slab edge, ΔU_{edge} from the following equation:

$$\Delta U_{edge} \approx 0.5\, X\, \Delta U_0$$

g) Assume a beam depth (D), width (b), and spacing (S), then calculate the equivalent mat thickness, d_{eq} from the following equation:

$$S.\, d_{eq}^{\,3} = b.\, D^3$$

The previous equation was based on considering the concrete section moment of inertia, however this equation can be generalized to consider any section type as follows:

$$d_{eq} = \sqrt[3]{\frac{12I}{S}}$$

h) Calculate the applied load per unit beam length, q.

i) Knowing d_{eq}, I_{SS}, H, and ΔU_{edge}, find the equivalent cantilever length L_{eqv} and the unsupported length, L_{gap} from the provided L_{eqv} & L_{gap} design charts; note that: L_{eqv} is for both edge drop and edge lift cases, yet L_{gap} is only for edge drop case.

j) Knowing L/2H ratio, the slab length modification factor, F_{SL}

k) Calculate the corrected equivalent cantilever length, L'_{eqv} and the corrected unsupported length using the following equations:

$$L'_{eqv} = F_{SL}\, L_{eqv}$$

$$L'_{gap} = F_{SL}\, L_{gap}$$

l) Check for localized bearing capacity failure: The idealized equivalent cantilever length should not exceed a certain value after which, the contact pressure would induce a localized bearing capacity failure.

$$L'_{eqv\,\max} = \frac{L}{2}\left(1 - \frac{\frac{S}{S_L + S_s}\frac{q}{b}}{5.14 S_u}\right)$$

For edge drop case, S_u can be assumed to = 200 kPa, and for edge lift case, , S_u can be assumed to = 50 kPa

Hence,

$L'_{eqv} \le L'_{eqv\,\max}$ (for both edge drop and edge lift cases)

If not, use $L'_{eqv} = L'_{eqv\,\max}$

m) Knowing d_{eq}, I_{SS}, H, ΔU_{edge}, and L_{eqv} find $F_{\Delta max}$ and F_V from the provided $F_{\Delta max}$ and F_V design charts for both edge drop and edge lift cases.

n) Calculate the maximum deflection Δ_{max} (for both edge drop and edge lift cases) using the provided equation.

$$\Delta_{\max} = \frac{q_{service} L'^{4}_{eqv}}{F_{\Delta\max} E I_{cr}}$$

o) Check for maximum deflection (for both edge drop and edge lift cases)

$$\Delta_{\max allowable} = \frac{L}{480}$$

$$\Delta_{max} \le \Delta_{max\ allowable}$$

if not, increase the beam moment of inertia, recalculate d_{eq} and iterate steps m, n, & o until you meet the maximum deflection criteria.

p) Calculate the unsupported length deflection Δ_{gap} (only for both edge drop case) using the provided equation.

$$\Delta_{gap} = \frac{q_{service} L'^{4}_{gap}}{8EI}$$

q) Check for unsupported length deflection

$$\Delta_{gap\ allowable} = \frac{L'_{gap}}{200}$$

$$\Delta_{gap} \leq \Delta_{gap\ allowable}$$

if not, increase the beam moment of inertia, recalculate d_{eq} and iterate steps m, n, o, p,& q until you meet the unsupported length deflection criteria.

r) Calculate the maximum bending moments and maximum shearing forces M_{max} , and V_{max} (for both edge drop and edge lift cases) using the following equations.

$$M_{\max} = \frac{q_{ult} L'^{2}_{eqv}}{2}$$

$$V_{\max} = F_v q_{ult} L'_{eqv}$$

s) Choose reinforcement and calculate the ultimate bending moment and shearing forces, M_u and V_u for the beam section.

t) Check for maximum bending moments and maximum shearing forces M_{max} , and V_{max} (for both edge drop and edge lift cases).

$$M_{max} \leq \phi M_u$$

$$V_{max} \leq \phi\ V_u$$

if not, increase the beam moment of inertia and/ or reinforcements, recalculate d_{eq} and iterate steps m, n, o, p, q, r, s,&t until you meet the strength criteria.

(17) This dissertation proposes a water content based design procedure as follows:

a) Estimate depth of active moisture zone H based on experience or available databases at the site location.

b) Estimate the water content change value at the soil surface for a free field, Δw_0 based on experience or by using available data bases at the site location.

c) Determine the suction change value at the soil surface under the slab edge, Δw_{edge} from the following equation:

$$\Delta w_{edge} \approx 0.5\, X\, \Delta w_0$$

d) Assume a beam depth (D), width (b), and spacing (S), then calculate the equivalent mat thickness, d_{eq} from the following equation:

$$S.\, d_{eq}^{\,3} = b.\, D^3$$

The previous equation was based on considering the concrete section moment of inertia, however this equation can be generalized to consider any section type as follows:

$$d_{eq} = \sqrt[3]{\frac{12I}{S}}$$

e) Calculate the applied load per unit beam length, q.

f) Knowing d_{eq}, I_{SS}, H, and Δw_{edge}, find the equivalent cantilever length L_{eqv} and the unsupported length, L_{gap} from the provided L_{eqv} & L_{gap} design charts; note that: L_{eqv} is for both edge drop and edge lift cases, yet L_{gap} is only for edge drop case.

g) Knowing L/2H ratio, the slab length modification factor, F_{SL}

h) Calculate the corrected equivalent cantilever length, L'_{eqv} and the corrected unsupported length using the following equations:

$$L'_{eqv} = F_{SL}\, L_{eqv}$$

$$L'_{gap} = F_{SL}\, L_{gap}$$

i) Check for localized bearing capacity failure: The idealized equivalent cantilever length should not exceed a certain value after which, the contact pressure would induce a localized bearing capacity failure.

$$L'_{eqv\,\max} = \frac{L}{2}\left(1 - \frac{\frac{S}{S_L + S_s}\frac{q}{b}}{5.14 S_u}\right)$$

For edge drop case, S_u can be assumed to = 200 kPa, and for edge lift case, , S_u can be assumed to = 50 kPa

Hence,

$L'_{eqv} \le L'_{eqv\,\max}$ (for both edge drop and edge lift cases)

If not, use $L'_{eqv} = L'_{eqv\,\max}$

j) Knowing d_{eq}, I_{SS}, H, Δw_{edge}, and L_{eqv} find $F_{\Delta max}$ and F_V from the provided $F_{\Delta max}$ and F_V design charts for both edge drop and edge lift cases.

k) Calculate the maximum deflection Δ_{max} (for both edge drop and edge lift cases) using the provided equation.

$$\Delta_{\max} = \frac{q_{service} L'^{4}_{eqv}}{F_{\Delta \max} EI_{cr}}$$

l) Check for maximum deflection (for both edge drop and edge lift cases)

$$\Delta_{\max allowable} = \frac{L}{480}$$

$$\Delta_{max} \leq \Delta_{max\ allowable}$$

if not, increase the beam moment of inertia, recalculate d_{eq} and iterate steps j, k, & l until you meet the maximum deflection criteria.

m) Calculate the unsupported length deflection Δ_{gap} (only for both edge drop case) using the provided equation.

$$\Delta_{gap} = \frac{q_{service} L'^{4}_{gap}}{8EI_{cr}}$$

n) Check for unsupported length deflection

$$\Delta_{gap\ allowable} = \frac{L'_{gap}}{200}$$

$$\Delta_{gap} \leq \Delta_{gap\ allowable}$$

if not, increase the beam moment of inertia, recalculate d_{eq} and iterate steps j, k, l, m, & n until you meet the unsupported length deflection criteria.

o) Calculate the maximum bending moments and maximum shearing forces M_{max} , and V_{max} (for both edge drop and edge lift cases) using the following equations.

$$M_{\max} = \frac{q_{ult} L'^{2}_{eqv}}{2}$$

$$V_{\max} = F_v q_{ult} L'_{eqv}$$

p) Choose reinforcement and calculate the ultimate bending moment and shearing forces, M_u and V_u for the beam section.

q) Check for maximum bending moments and maximum shearing forces M_{max} , and V_{max} (for both edge drop and edge lift cases).

$$M_{max} \leq \phi M_u$$

$$V_{max} \leq \phi V_u$$

if not, increase the beam moment of inertia and/ or reinforcements, recalculate d_{eq} and iterate steps j, k, l, m, n, o, p, & q until you meet the strength criteria.

REFERENCES

Abdelmalak R., Briaud J.-L. (2006). "Comparison of beam depths for stiffened slabs on shrink-swell soils using WRI, PTI 2004 and AS 2870", *Proceedings of the Fourth International Conference on Unsaturated Soils*, Carefree Arizona, Volume 1, 347-353, ASCE Geotechnical Special Publication No. 147.

Aubeny, C. & Lytton, R. (2004). "Shallow slides in compacted high plasticity clay slopes," *ASCE Journal of Geotechnical and Geoenvironmental Engineering* 130(7), 717-727.

Australian Standard (AS2870) (1990), *Residential Slabs and Footings, Part 2: Guide to Design by Engineering Principles*, AS 2870.2 Standard House, Sydney NSW, Australia.

Australian Standard (AS2870) (1996), *Residential Slabs and Footings*, AS 2870 Standard House, Sydney NSW, Australia.

Bowles, J. E. (1996). *Foundation Analysis and Design;* fifth edition. The McGraw-Hill Company, Inc., New York.

Building Research Advisory Board (BRAB) (1968). "National Research Council Criteria for Selection and Design of Residential Slabs-on-Ground," U.S. National Academy of Sciences Publication 1571.

Bulut, R. (2001). "Finite element method analysis of slabs on elastic half space expansive soil foundations." Ph.D. dissertation, Department of Civil Engineering, Texas A&M University, College Station, TX.

Childs, E.C. (1969). *An Introduction to the Physical Basis of Soil Water Phenomena,* John Wiley & Sons Ltd., London.

Childs, E.C., and Collis-George, G.N. (1950). "The permeability of porous materials." *Proceedings, Royal Society of London, Series A*. 201, 392-405.

Durkee, D. B. (2000). "Active zone depth and edge moisture variation distance in expansive soils," Ph.D. dissertation, Department of Civil Engineering, Colorado State University, Fort Collins, CO.

Fraser, R. A., and Wardle, L. J. (1975). "The analysis of stiffened raft foundations on expansive soils," Symposium on recent Developments in the Analysis of Soil Behavior and their Application to Geotechnical Structure, University of New South Wales, Australia, July, pp. 89-98.

Gay, D. A. (1994). "Development of a predictive model for pavement roughness on expansive clay," Ph.D. dissertation, Department of Civil Engineering, Texas A&M University, College Station, TX.

Holland, J. E., Pitt, W. G., Lawrance, C. E., and Cimino, D. J. (Swinburne method) (1980). "The behavior and design of housing slabs on expansive soils," *Proceedings, 4th International Conference on Expansive Soils*, Denver, CO, 1, 448-468.

Jones, D. E. and Holtz, W. G., (1973). "Expansive soils - the hidden disaster." *Journal of Civil Engineering*, ASCE, New York, 43 (8), 49-51.

Knight, M. J. (1972). "Structural analysis of selected duplex soils" Ph.D. dissertation, Department of Geology, University of Melbourne, Melbourne, Australia.

Krohn, J. P. and Slosson, J. E. (1980). "Assessment of expansive soils in the United States." *Proc. 4th International Conference on Expansive Soils*, Denver, CO, 1, 596-608.

Laliberte, G. E., and Corey, A. T. (1967). "Hydraulic properties of disturbed and undisturbed soils." *Permeability and Capillary of Soils*. ASTM, 56-71.

Lytton, R. L. and Woodburn, J.A. (1973). "Design and performance of mate foundations on expansive clay," *Proceedings, 3rd International Conference on Expansive Soils*, Vol. 1, Israel Society of Soil Mechanics and Foundation Engineering, Haifa, Israel, 301-307.

Lytton, R. L. (1970). "Design criteria for residential slabs and grillage rafts on reactive clay," Report for Australian Commonwealth Scientific and Industrial Research Organization C.S.I.R.O., Melborne, Australia, November.

Lytton, R. L. (1972). "Design methods for concrete mats on unsaturated soils," *Proceedings 3rd Inter-American Conference on Materials Technology*, Rio de Janeiro, Brazil, 171-177.

Mitchell, P. W. (1979). ''The structural analysis of footings on expansive soils.'' *Research Report No. 1*, K. W. G. Smith and Assoc. Pty. Ltd., Newton, South Australia.

Mitchell, P. W. (1980). "The concepts defining the rate of swell in expansive soils," Proceedings, 4th International Conference on Expansive Soils, Vol. 1, Denver, CO, 106-116.

Naiser, D. D. (1997). "Procedures to predict differential soil movement for expansive soils," M.S. thesis, Department of Civil Engineering, Texas A&M University, College Station, TX.

Nelson, J., and Miller, D. (1992). *Expansive Soils: Problems and Practice in Foundation and Pavement Engineering*, John Wiley & Sons Ltd., New York.

Post-Tensioning Institute (PTI) (1996). Design and Construction of Post-Tensioned Slabs-on-Ground, 2nd Ed., Phoenix, AZ, USA,.

Post-Tensioning Institute (PTI) (2004). Design and Construction of Post-Tensioned Slabs-on-Ground, 3rd Ed., Phoenix, AZ, USA.

Poulos, D. (2000). "Foundation settlement analysis-practice versus research." Presented at the 8th Spencer J. Buchanan Lecture, Texas A&M University, College Station,TX.

Richards, B. G. (1965) "Measurement of the free energy of soil moisture by the psychrometric technique using thermistors," in Moisture Equilibrium and Moisture Changes in Soils Beneath Covered Area, A Symposium in print. Australia: Butterworths, 39-46.

Thornthwaite, C. W. (1948) "An approach toward a rational classification of climate," *Geographical Review*, 38, 55-94.

Walsh, P. and Cameron, D. (1997), *The Design of Residential Slabs and Footings*, Standards Association of Australia SAA HB 28-1997, [Homebush, NSW]: Standard Australia,

Walsh, P. F. (1974). "The design of residential slabs-on-ground", Commonwealth Scientific and Industrial Research Organization (C.S.I.R.O.) Division of Building Research, Technical Paper (2nd Series) 5, 25p.

Walsh, P. F. (1978). "To beam or not to beam," *Building Surveyor*, 2, 24-26

Walsh, P. F. (2005), personal communications (e-mail reply on Jan. 19th), University of Newcastle, School of Engineering, Australia.

Walsh, P. F. and Walsh, S. F., "Structure / reactive clay model for a microcomputer," Commonwealth Scientific and Industrial Research Organization (C.S.I.R.O.) Division of Building Research, Australia, DBR report R 86/9, 1986

Wire Reinforcement Institute (WRI) (1981). "Design of Slab-on- Ground Foundations," Findlay, Ohio, USA, August.

Wire Reinforcement Institute (WRI) (1996). "Design of Slab-on- Ground Foundations, An Update," Findlay, Ohio, USA, March,.

Woodburn, J. A., (1974). "Design of foundations on expansive clay soils; current design procedures and practice." *Report No. Z/48.* Industrial Research Institute of S. Australia.

Wray, W. K. (1978). "Development of a design procedure for residential and light commercial slabs-on-ground constructed over expansive soils," Ph.D. dissertation, Department of Civil Engineering, Texas A&M University, College Station, TX.

Wray, W. K. (1989). "Mitigation of damage to structures supported on expansive soils," Vols. I, II and III, Texas Tech University, National Science Foundation, Washington, D. C.

Zhang, X. (2004). "Consolidation theories for saturated-unsaturated soils and numerical simulation of residential buildings on expansive soils," Ph.D. dissertation, Department of Civil Engineering, Texas A&M University, College Station, TX.

APPENDIX A

COMPARISON OF BEAM DEPTHS FOR STIFFENED SLABS ON SHRINK-SWELL SOILS USING WRI, PTI 2004 AND AS 2870

Climate Parameters			Soil Properties				Slab Dim.		Beam Design Depth (m)			Average	% Difference from the average		
I_m	C_W	H_s (m)	γ_h	I_{pt}	LL%	PI%	L_L (m)	L_S (m)	PTI 2004	AS 2870	WRI	Depth (m)	PTI 2004	AS 2870	WRI
-16	17	3.3	0.028	0.0093	50	30	12	12	0.5	0.45	0.5	0.483	3.45	-6.90	3.45
-16	17	3.3	0.028	0.0093	50	30	24	24	0.7	0.45	0.55	0.567	23.53	-20.59	-2.94
-16	17	3.3	0.028	0.0093	50	30	24	12	0.6	0.45	0.55	0.533	12.50	-15.63	3.13
-16	17	3.3	0.077	0.0257	70	45	12	12	0.65	0.8	0.8	0.750	-13.33	6.67	6.67
-16	17	3.3	0.077	0.0257	70	45	24	24	0.9	0.45	0.85	0.733	22.73	-38.64	15.91
-16	17	3.3	0.077	0.0257	70	45	24	12	0.85	0.45	0.8	0.700	21.43	-35.71	14.29
-16	17	3.3	0.133	0.0443	90	60	12	12	0.7	1.1	0.85	0.883	-20.75	24.53	-3.77
-16	17	3.3	0.133	0.0443	90	60	24	24	1	1	0.95	0.983	1.69	1.69	-3.39
-16	17	3.3	0.133	0.0443	90	60	24	12	0.95	0.95	0.9	0.933	1.79	1.79	-3.57
0	21	2.4	0.028	0.0093	50	30	12	12	0.5	0.3	0.45	0.417	20.00	-28.00	8.00
0	21	2.4	0.028	0.0093	50	30	24	24	0.65	0.3	0.5	0.483	34.48	-37.93	3.45
0	21	2.4	0.028	0.0093	50	30	24	12	0.55	0.3	0.5	0.450	22.22	-33.33	11.11
0	21	2.4	0.077	0.0257	70	45	12	12	0.6	0.6	0.7	0.633	-5.26	-5.26	10.53
0	21	2.4	0.077	0.0257	70	45	24	24	0.85	0.3	0.75	0.633	34.21	-52.63	18.42
0	21	2.4	0.077	0.0257	70	45	24	12	0.8	0.3	0.75	0.617	29.73	-51.35	21.62
0	21	2.4	0.133	0.0443	90	60	12	12	0.7	0.95	0.8	0.817	-14.29	16.33	-2.04
0	21	2.4	0.133	0.0443	90	60	24	24	1.05	0.6	0.9	0.850	23.53	-29.41	5.88
0	21	2.4	0.133	0.0443	90	60	24	12	1	0.6	0.85	0.817	22.45	-26.53	4.08
18	25	1.8	0.028	0.0093	50	30	12	12	0.45	0.25	0.4	0.367	22.73	-31.82	9.09
18	25	1.8	0.028	0.0093	50	30	24	24	0.6	0.25	0.4	0.417	44.00	-40.00	-4.00
18	25	1.8	0.028	0.0093	50	30	24	12	0.5	0.25	0.4	0.383	30.43	-34.78	4.35
18	25	1.8	0.077	0.0257	70	45	12	12	0.6	0.5	0.65	0.583	2.86	-14.29	11.43
18	25	1.8	0.077	0.0257	70	45	24	24	0.9	0.5	0.7	0.700	28.57	-28.57	0.00
18	25	1.8	0.077	0.0257	70	45	24	12	0.8	0.5	0.65	0.650	23.08	-23.08	0.00
18	25	1.8	0.133	0.0443	90	60	12	12	0.75	0.75	0.75	0.750	0.00	0.00	0.00
18	25	1.8	0.133	0.0443	90	60	24	24	1.05	0.4	0.8	0.750	40.00	-46.67	6.67
18	25	1.8	0.133	0.0443	90	60	24	12	1	0.4	0.8	0.733	36.36	-45.45	9.09

APPENDIX B

INFLUENCE OF THE 2002 TEXAS SECTION OF ASCE RECOMMENDED PRACTICE ON THE BEAM DEPTHS FOR STIFFENED SLABS ON SHRINK-SWELL SOILS USING BRAB AND WRI

Design Input Data					Resulting Beam Design Depth (m)					
Climate	Soil Properties		Slab Dim.		BRAB	Beam D.	WRI	Beam D.		
C_W	LL%	PI%	L_L (m)	L_S (m)	Original	Tx ASCE	Original	Tx ASCE	PTI 2004	AS 2870
17	50	30	12	12	0.65	0.65	0.5	0.75	0.5	0.45
17	50	30	24	24	1.3	0.8	0.55	0.7	0.7	0.45
17	50	30	24	12	1.25	0.8	0.55	0.8	0.6	0.45
17	70	45	12	12	0.65	0.65	0.8	1.15	0.65	0.8
17	70	45	24	24	1.4	0.85	0.85	1.1	0.9	0.45
17	70	45	24	12	1.35	0.85	0.8	1.2	0.85	0.45
17	90	60	12	12	0.7	0.7	0.85	1.3	0.7	1.1
17	90	60	24	24	1.45	0.85	0.95	1.2	1	1
17	90	60	24	12	1.4	0.85	0.9	1.35	0.95	0.95
21	50	30	12	12	0.65	0.65	0.45	0.65	0.5	0.3
21	50	30	24	24	1.25	0.8	0.5	0.6	0.65	0.3
21	50	30	24	12	1.25	0.8	0.45	0.7	0.55	0.3
21	70	45	12	12	0.65	0.65	0.7	1.05	0.6	0.6
21	70	45	24	24	1.35	0.85	0.75	0.95	0.85	0.3
21	70	45	24	12	1.3	0.8	0.75	1.1	0.8	0.3
21	90	60	12	12	0.7	0.7	0.8	1.2	0.7	0.95
21	90	60	24	24	1.45	0.85	0.9	1.15	1.05	0.6
21	90	60	24	12	1.35	0.85	0.85	1.3	1	0.6
25	50	30	12	12	0.65	0.65	0.4	0.6	0.45	0.25
25	50	30	24	24	1.25	0.8	0.4	0.55	0.6	0.25
25	50	30	24	12	1.25	0.8	0.4	0.6	0.5	0.25
25	70	45	12	12	0.65	0.65	0.65	0.95	0.6	0.5
25	70	45	24	24	1.35	0.8	0.7	0.85	0.9	0.5
25	70	45	24	12	1.3	0.8	0.65	0.95	0.8	0.5
25	90	60	12	12	0.65	0.65	0.75	1.1	0.75	0.75
25	90	60	24	24	1.4	0.85	0.8	1.05	1.05	0.4
25	90	60	24	12	1.35	0.85	0.8	1.15	1	0.4

Comparing to the average of 6 design methods					Comparing to the average of 4 design methods				
$D_{ave\ 6}$ (m)	$\%\ \Delta_{BRAB,\ ave\ 6}$		$\%\ \Delta_{WRI,\ ave\ 6}$		$D_{ave\ 4}$ (m)	$\%\ \Delta_{BRAB,\ ave\ 4}$		$\%\ \Delta_{WRI,\ ave\ 4}$	
	Original	Tx ASCE	Original	Tx ASCE		Original	Tx ASCE	Original	Tx ASCE
0.58	11.43	11.43	-14.29	28.57	0.64	1.96	1.96	-21.57	17.65
0.75	73.33	6.67	-26.67	-6.67	0.84	55.22	-4.48	-34.33	-16.42
0.74	68.54	7.87	-25.84	7.87	0.85	47.06	-5.88	-35.29	-5.88
0.78	-17.02	-17.02	2.13	46.81	0.81	-20.00	-20.00	-1.54	41.54
0.93	51.35	-8.11	-8.11	18.92	1.05	33.33	-19.05	-19.05	4.76
0.92	47.27	-7.27	-12.73	30.91	1.05	28.57	-19.05	-23.81	14.29
0.89	-21.50	-21.50	-4.67	45.79	0.89	-21.13	-21.13	-4.23	46.48
1.08	34.88	-20.93	-11.63	11.63	1.11	30.34	-23.60	-14.61	7.87
1.07	31.25	-20.31	-15.63	26.56	1.13	24.44	-24.44	-20.00	20.00
0.53	21.88	21.88	-15.63	21.88	0.60	8.33	8.33	-25.00	8.33
0.68	82.93	17.07	-26.83	-12.20	0.79	58.73	1.59	-36.51	-23.81
0.68	85.19	18.52	-33.33	3.70	0.80	56.25	0.00	-43.75	-12.50
0.71	-8.24	-8.24	-1.18	48.24	0.76	-14.75	-14.75	-8.20	37.70
0.84	60.40	0.99	-10.89	12.87	0.98	38.46	-12.82	-23.08	-2.56
0.84	54.46	-4.95	-10.89	30.69	0.99	31.65	-18.99	-24.05	11.39
0.84	-16.83	-16.83	-4.95	42.57	0.85	-17.65	-17.65	-5.88	41.18
1.00	45.00	-15.00	-10.00	15.00	1.09	33.33	-21.84	-17.24	5.75
0.99	36.13	-14.29	-14.29	31.09	1.09	24.14	-21.84	-21.84	19.54
0.50	30.00	30.00	-20.00	20.00	0.58	13.04	13.04	-30.43	4.35
0.64	94.81	24.68	-37.66	-14.29	0.75	66.67	6.67	-46.67	-26.67
0.63	97.37	26.32	-36.84	-5.26	0.76	63.93	4.92	-47.54	-21.31
0.67	-2.50	-2.50	-2.50	42.50	0.73	-10.34	-10.34	-10.34	31.03
0.85	58.82	-5.88	-17.65	0.00	0.93	45.95	-13.51	-24.32	-8.11
0.83	56.00	-4.00	-22.00	14.00	0.93	40.54	-13.51	-29.73	2.70
0.78	-16.13	-16.13	-3.23	41.94	0.79	-17.46	-17.46	-4.76	39.68
0.93	51.35	-8.11	-13.51	13.51	1.03	36.59	-17.07	-21.95	2.44
0.93	45.95	-8.11	-13.51	24.32	1.04	30.12	-18.07	-22.89	10.84

APPENDIX C

DETERMINATION OF THE EQUIVALENT ALPHA COEFFICIENT FOR CRACKED SOIL

PRIMARY CRACKS SIMULATIONS

```
*HEADING
Determination of the equivalent Alpha coefficient for cracked soil (Primary Crack only)
*NODE
1,        0.,       -360.
21,       120.,   -360.
106,    0.,     0.
126,    120.,   0.
736,     0.,       360.
756,     120.,    360.
*NGEN, NSET=CONSTSUC
106,126
*NGEN, NSET=BOTTOM
1,21
*NGEN, NSET=TOP
736,756
*NFILL, NSET=ACTIVEZONE
CONSTSUC,TOP,30,21
*NFILL, NSET=DEEP,BIAS=1.5
BOTTOM,CONSTSUC,5,21
*NSET, NSET=SOILMASS, GENERATE
1,756
*NSET, NSET=LEFT, GENERATE
1,736,21
*NSET, NSET=RIGHT, GENERATE
21,756,21
*NSET, NSET=CRACK, GENERATE
295,736,21
```

```
*NSET, NSET=UNCRACK, GENERATE
1,274,21
*ELEMENT, TYPE=CPE4T
1, 1, 2, 23, 22
*ELGEN, ELSET=SOIL
1, 20, 1, 1, 35, 21,20
*SOLID SECTION,ELSET=SOIL,MATERIAL=SOIL
*MATERIAL, NAME=SOIL
*ELASTIC
2000, .4
*EXPANSION
1.E-7,
*DENSITY
1.6315,
*SPECIFIC HEAT
0.1,
*CONDUCTIVITY
2.34936,
*INITIAL CONDITIONS, TYPE=TEMPERATURE
SOILMASS,-3.5
*BOUNDARY
RIGHT,1,1,0.
LEFT,1,1,0.
BOTTOM,2,2,0.
**
*STEP,INC=1000
*COUPLED TEMPERATURE-DISPLACEMENT, DELTMX=0.05
5,365,,
```

```
*AMPLITUDE, NAME=SINCURVE, TIME=TOTAL TIME,
DEFINITION=PERIODIC
1,0.01721421,0.0,-3.5
0.,-1.0
*BOUNDARY
BOTTOM,11,11,-3.5
*BOUNDARY, AMPLITUDE=SINCURVE
TOP,11,11,1.
CRACK,11,11,1.
**
*NODE PRINT
 NT11
*END STEP
```

SECONDARY CRACKS SIMULATIONS

```
*HEADING
Determination of the equivalent Alpha coefficient for cracked soil (secondary Crack)
*NODE
1,        0.,       -360.
41,       120.,   -360.
206,    0.,     0.
246,    120.,   0.
1436,   0.,       360.
1476,   120.,    360.
*NGEN, NSET=CONSTSUC
206,246
*NGEN, NSET=BOTTOM
1,41
*NGEN, NSET=TOP
1436,1476
*NFILL, NSET=ACTIVEZONE
CONSTSUC,TOP,30,41
*NFILL, NSET=DEEP,BIAS=1.5
BOTTOM,CONSTSUC,5,41
*NSET, NSET=SOILMASS, GENERATE
1,1476
*NSET, NSET=LEFT, GENERATE
1,1436,41
*NSET, NSET=RIGHT, GENERATE
41,1476,41
*NSET, NSET=CRACK, GENERATE
616,1436,41
```

```
1046,1456,41
*NSET, NSET=UNCRACK, GENERATE
1,616,41
*ELEMENT, TYPE=CPE4T
1, 1, 2, 43, 42
*ELGEN, ELSET=SOIL
1, 40, 1, 1, 35, 41,40
*SOLID SECTION,ELSET=SOIL,MATERIAL=SOIL
*MATERIAL, NAME=SOIL
*ELASTIC
2000, .4
*EXPANSION
1.E-7,
*DENSITY
1.6315,
*SPECIFIC HEAT
0.1,
*CONDUCTIVITY
2.34936,
*INITIAL CONDITIONS, TYPE=TEMPERATURE
SOILMASS,-3.5
*BOUNDARY
RIGHT,1,1,0.
LEFT,1,1,0.
BOTTOM,2,2,0.
**
*STEP,INC=1000
*COUPLED TEMPERATURE-DISPLACEMENT, DELTMX=0.05
5,365,,
```

```
*AMPLITUDE, NAME=SINCURVE, TIME=TOTAL TIME,
DEFINITION=PERIODIC
1,0.01721421,0.0,-3.5
0.,-1.0
*BOUNDARY
BOTTOM,11,11,-3.5
*BOUNDARY, AMPLITUDE=SINCURVE
TOP,11,11,1.
CRACK,11,11,1.
**
*NODE PRINT
 NT11
*END STEP
```

TERTAIRY CRACKS SIMULATIONS (BETA = 0.5)

```
*HEADING
Determination of the equivalent Alpha coefficient for cracked soil (tertiary Crack_ Beta=0.5 )
*NODE
1,        0.,       -360.
81,       120.,   -360.
406,    0.,     0.
486,    120.,   0.
2836,   0.,       360.
2916,   120.,    360.
*NGEN, NSET=CONSTSUC
406,486
*NGEN, NSET=BOTTOM
1,81
*NGEN, NSET=TOP
2836,2916
*NFILL, NSET=ACTIVEZONE
CONSTSUC,TOP,30,81
*NFILL, NSET=DEEP,BIAS=1.5
BOTTOM,CONSTSUC,5,81
*NSET, NSET=SOILMASS, GENERATE
1,2916
*NSET, NSET=LEFT, GENERATE
1,2836,81
*NSET, NSET=RIGHT, GENERATE
81,2916,81
*NSET, NSET=CRACK, GENERATE
```

```
1621,2836,81
2532,2856,81
2228,2876,81
2572,2896,81
*NSET, NSET=UNCRACK, GENERATE
1,1216,81
*ELEMENT, TYPE=CPE4T
1, 1, 2, 83, 82
*ELGEN, ELSET=SOIL
1, 80, 1, 1, 35, 81,80
*SOLID SECTION,ELSET=SOIL,MATERIAL=SOIL
*MATERIAL, NAME=SOIL
*ELASTIC
2000, .4
*EXPANSION
1.E-7,
*DENSITY
1.6315,
*SPECIFIC HEAT
0.1,
*CONDUCTIVITY
14.09616000,
*INITIAL CONDITIONS, TYPE=TEMPERATURE
SOILMASS,-3.5
*BOUNDARY
RIGHT,1,1,0.
LEFT,1,1,0.
BOTTOM,2,2,0.
**
```

```
*STEP,INC=1000
*COUPLED TEMPERATURE-DISPLACEMENT, DELTMX=0.05
5,365,,
*AMPLITUDE, NAME=SINCURVE, TIME=TOTAL TIME,
DEFINITION=PERIODIC
1,0.01721421,0.0,-3.5
0.,-1.0
*BOUNDARY
BOTTOM,11,11,-3.5
*BOUNDARY, AMPLITUDE=SINCURVE
TOP,11,11,1.
CRACK,11,11,1.
**
*NODE PRINT
 NT11
*END STEP
```

TERTAIRY CRACKS SIMULATIONS (BETA = 0.667)

```
*HEADING
Determination of the equivalent Alpha coefficient for cracked soil (tertiary Crack)
*NODE
1,        0.,       -360.
81,       120.,   -360.
406,    0.,     0.
486,    120.,   0.
2836,   0.,       360.
2916,   120.,    360.
*NGEN, NSET=CONSTSUC
406,486
*NGEN, NSET=BOTTOM
1,81
*NGEN, NSET=TOP
2836,2916
*NFILL, NSET=ACTIVEZONE
CONSTSUC,TOP,30,81
*NFILL, NSET=DEEP,BIAS=1.5
BOTTOM,CONSTSUC,5,81
*NSET, NSET=SOILMASS, GENERATE
1,2916
*NSET, NSET=LEFT, GENERATE
1,2836,81
*NSET, NSET=RIGHT, GENERATE
81,2916,81
*NSET, NSET=CRACK, GENERATE
1216,2836,81
```

```
2451,2856,81
2066,2876,81
2491,2896,81
*NSET, NSET=UNCRACK, GENERATE
1,1216,81
*ELEMENT, TYPE=CPE4T
1, 1, 2, 83, 82
*ELGEN, ELSET=SOIL
1, 80, 1, 1, 35, 81,80
*SOLID SECTION,ELSET=SOIL,MATERIAL=SOIL
*MATERIAL, NAME=SOIL
*ELASTIC
2000, .4
*EXPANSION
1.E-7,
*DENSITY
1.6315,
*SPECIFIC HEAT
0.1,
*CONDUCTIVITY
4.228848,
*INITIAL CONDITIONS, TYPE=TEMPERATURE
SOILMASS,-3.5
*BOUNDARY
RIGHT,1,1,0.
LEFT,1,1,0.
BOTTOM,2,2,0.
**
*STEP,INC=1000
```

```
*COUPLED TEMPERATURE-DISPLACEMENT, DELTMX=0.05
5,365,,
*AMPLITUDE, NAME=SINCURVE, TIME=TOTAL TIME,
DEFINITION=PERIODIC
1,0.01721421,0.0,-3.5
0.,-1.0
*BOUNDARY
BOTTOM,11,11,-3.5
*BOUNDARY, AMPLITUDE=SINCURVE
TOP,11,11,1.
CRACK,11,11,1.
**
*NODE PRINT
 NT11
*END STEP
```

TERTAIRY CRACKS SIMULATIONS (BETA = 0.8)

```
*HEADING
Determination of the equivelent Alpha coefficient for cracked soil (tritary Crack_ Beta=0.8 )
*NODE
1,        0.,       -360.
81,       120.,   -360.
406,    0.,     0.
486,    120.,   0.
2836,   0.,       360.
2916,   120.,    360.
*NGEN, NSET=CONSTSUC
406,486
*NGEN, NSET=BOTTOM
1,81
*NGEN, NSET=TOP
2836,2916
*NFILL, NSET=ACTIVEZONE
CONSTSUC,TOP,30,81
*NFILL, NSET=DEEP,BIAS=1.5
BOTTOM,CONSTSUC,5,81
*NSET, NSET=SOILMASS, GENERATE
1,2916
*NSET, NSET=LEFT, GENERATE
1,2836,81
*NSET, NSET=RIGHT, GENERATE
81,2916,81
*NSET, NSET=CRACK, GENERATE
```

892,2836,81
2370,2856,81
1904,2876,81
2410,2896,81
*NSET, NSET=UNCRACK, GENERATE
1,1216,81
*ELEMENT, TYPE=CPE4T
1, 1, 2, 83, 82
*ELGEN, ELSET=SOIL
1, 80, 1, 1, 35, 81,80
*SOLID SECTION,ELSET=SOIL,MATERIAL=SOIL
*MATERIAL, NAME=SOIL
*ELASTIC
2000, .4
*EXPANSION
1.E-7,
*DENSITY
1.6315,
*SPECIFIC HEAT
0.1,
*CONDUCTIVITY
0.01409616,
*INITIAL CONDITIONS, TYPE=TEMPERATURE
SOILMASS,-3.5
*BOUNDARY
RIGHT,1,1,0.
LEFT,1,1,0.
BOTTOM,2,2,0.
**

```
*STEP,INC=1000
*COUPLED TEMPERATURE-DISPLACEMENT, DELTMX=0.05
5,365,,
*AMPLITUDE, NAME=SINCURVE, TIME=TOTAL TIME,
DEFINITION=PERIODIC
1,0.01721421,0.0,-3.5
0.,-1.0
*BOUNDARY
BOTTOM,11,11,-3.5
*BOUNDARY, AMPLITUDE=SINCURVE
TOP,11,11,1.
CRACK,11,11,1.
**
*NODE PRINT
 NT11
*END STEP
```

APPENDIX D

VERIFICATION OF THE PROPOSED MOISTURE DIFFUSION AND VOLUME CHANGE MODEL USING A LARGE SCALE LABORATORY TEST

UNCOVERED PHASE

```
*HEADING
Verification of the proposed moisture diffusion and volume change model using a large scale laboratory test (Phase I)
*NODE
1,        0.,       0.
61,       60.,    0.
2685,   0.,       44.0
2745,   60.0,    44.0
*NGEN, NSET=BOTTOM
1,61
*NGEN, NSET=TOP
2685,2745
*NGEN, NSET=CENTER
1,2685,61
*NGEN, NSET=OUT
61,2745,61
*NFILL, NSET=SOILMASS
BOTTOM,TOP,44,61
*ELEMENT, TYPE=CAX4T
1, 1, 2, 63, 62
*ELGEN, ELSET=SOILMASS
1, 60, 1, 1, 44, 61,60
*ELSET, ELSET=OUTSOIL, GENERATE
60, 2640, 60
*SOLID SECTION,ELSET=SOILMASS,MATERIAL=SOIL
*MATERIAL, NAME=SOIL
*ELASTIC
```

```
200000., .4
*EXPANSION
.1222,
*DENSITY
1.22,
*SPECIFIC HEAT
0.1,
*CONDUCTIVITY, DEPENDENCIES=1
0.0437, 1.
67.157,  100.
**
*INITIAL CONDITIONS, TYPE=TEMPERATURE
SOILMASS,-4.2163
**
*BOUNDARY
CENTER,1,1,0.
BOTTOM,2,2,0.
OUT,1,1,0.
**
*AMPLITUDE, NAME=CRACKFACTOR, TIME=TOTAL TIME, DEFINITION=TABULAR
0. , 1. , 7. ,19.15315256  , 20. , 25.61840569 , 35. , 32.95321382
51. , 34.4342813 , 66. , 35.56075421 , 270. , 35.56075421
*AMPLITUDE, NAME=ROOMSUCTION, TIME=TOTAL TIME, DEFINITION=TABULAR
0. , 0.001 , 7. , 0.001 , 8.0 , -5.5 , 20. , -5.5
20.001 , 0.001 , 35. , 0.001 , 36. , -5.5 , 51. , -5.5
51.001 , 0.001 , 66. , 0.001 , 67. , -5.5 , 84. , -5.5
84.001 , 0.001 , 101. , 0.001 , 102. , -5.5 , 122. , -5.5
```

```
122.001 , 0.001 , 158. , 0.001 , 159. , -5.5 , 179. , -5.5
179.001 , 0.001 , 204. , 0.001 , 205. , -5.5 , 254. , -5.5
254.001 , 0.001 , 270. , 0.001
**
**
*STEP,NAME=UNCOVERED, INC=10000
*COUPLED TEMPERATURE-DISPLACEMENT
2., 270. , ,
*FIELD, AMPLITUDE=CRACKFACTOR, VARIABLE=1
*BOUNDARY, AMPLITUDE=ROOMSUCTION
TOP,11,11,1.
**
*NODE PRINT
 NT11
*END STEP
```

COVERED PHASE

```
*HEADING
Verification of the proposed moisture diffusion and volume change model using a large scale laboratory test (Phase II)
*NODE
1,        0.,       0.
61,       60.,    0.
2685,   0.,       44.0
2745,   60.0,    44.0
*NGEN, NSET=BOTTOM
1,61
*NGEN, NSET=TOP
2685,2745
*NGEN, NSET=EXPOSED
2725,2745
*NGEN, NSET=CENTER
1,2685,61
*NGEN, NSET=OUT
61,2745,61
*NFILL, NSET=SOILMASS
BOTTOM,TOP,44,61
*ELEMENT, TYPE=CAX4T
1, 1, 2, 63, 62
*ELGEN, ELSET=SOILMASS
1, 60, 1, 1, 44, 61,60
*ELSET, ELSET=OUTSOIL, GENERATE
60, 2640, 60
*SOLID SECTION,ELSET=SOILMASS,MATERIAL=SOIL
```

```
*MATERIAL, NAME=SOIL
*ELASTIC
200000., .4
*EXPANSION
.1222,
*DENSITY
1.22,
*SPECIFIC HEAT
0.1,
*CONDUCTIVITY, DEPENDENCIES=1
0.0437, 1.
67.157,  100.
**
*INITIAL CONDITIONS, TYPE=TEMPERATURE
SOILMASS,-4.2163
**
*BOUNDARY
CENTER,1,1,0.
BOTTOM,2,2,0.
OUT,1,1,0.
**
*AMPLITUDE, NAME=CRACKFACTOR, TIME=TOTAL TIME, DEFINITION=TABULAR
0. , 1. , 7. ,19.15315256  , 20. , 25.61840569 , 35. , 32.95321382
51. , 34.4342813 , 66. , 35.56075421 , 466. , 35.56075421
*AMPLITUDE, NAME=ROOMSUCTION, TIME=TOTAL TIME, DEFINITION=TABULAR
0. , 0.001 , 7. , 0.001 , 8.0 , -5.5 , 20. , -5.5
20.001 , 0.001 , 35. , 0.001 , 36. , -5.5 , 51. , -5.5
```

```
51.001 , 0.001 , 66. , 0.001 , 67. , -5.5 , 84. , -5.5
84.001 , 0.001 , 101. , 0.001 , 102. , -5.5 , 122. , -5.5
122.001 , 0.001 , 158. , 0.001 , 159. , -5.5 , 179. , -5.5
179.001 , 0.001 , 204. , 0.001 , 205. , -5.5 , 254. , -5.5
254.001 , 0.001 , 270. , 0.001 , 271. , -5.5 , 302. , -5.5
302.001 , 0.001 , 340. , 0.001 , 341. , -5.5 , 402. , -5.5
402.001 , 0.001 , 466. , 0.001
**
**
*STEP,NAME=UNCOVERED, INC=10000
*COUPLED TEMPERATURE-DISPLACEMENT
2., 270. , ,
*FIELD, AMPLITUDE=CRACKFACTOR, VARIABLE=1
*BOUNDARY, AMPLITUDE=ROOMSUCTION
TOP,11,11,1.
*END STEP
**
*STEP,NAME=COVERED, INC=10000
*COUPLED TEMPERATURE-DISPLACEMENT
1., 196. , ,
*FIELD, AMPLITUDE=CRACKFACTOR, VARIABLE=1
*BOUNDARY, AMPLITUDE=ROOMSUCTION, OP=NEW
EXPOSED,11,11,1.
**
*NODE PRINT
 NT11
*END STEP
```

RESULTS

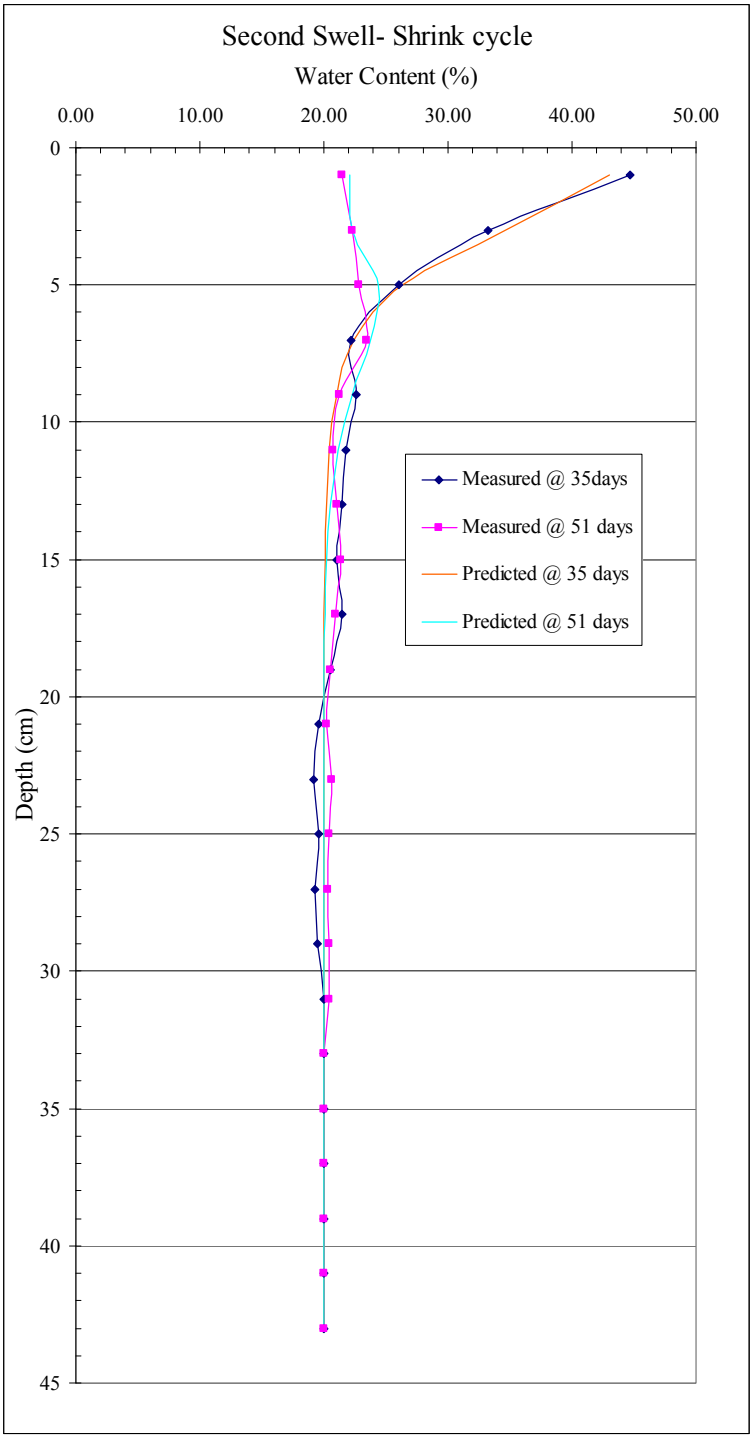

Fig. D.1. Water content results for second swell-shrink cycle (Uncovered phase)

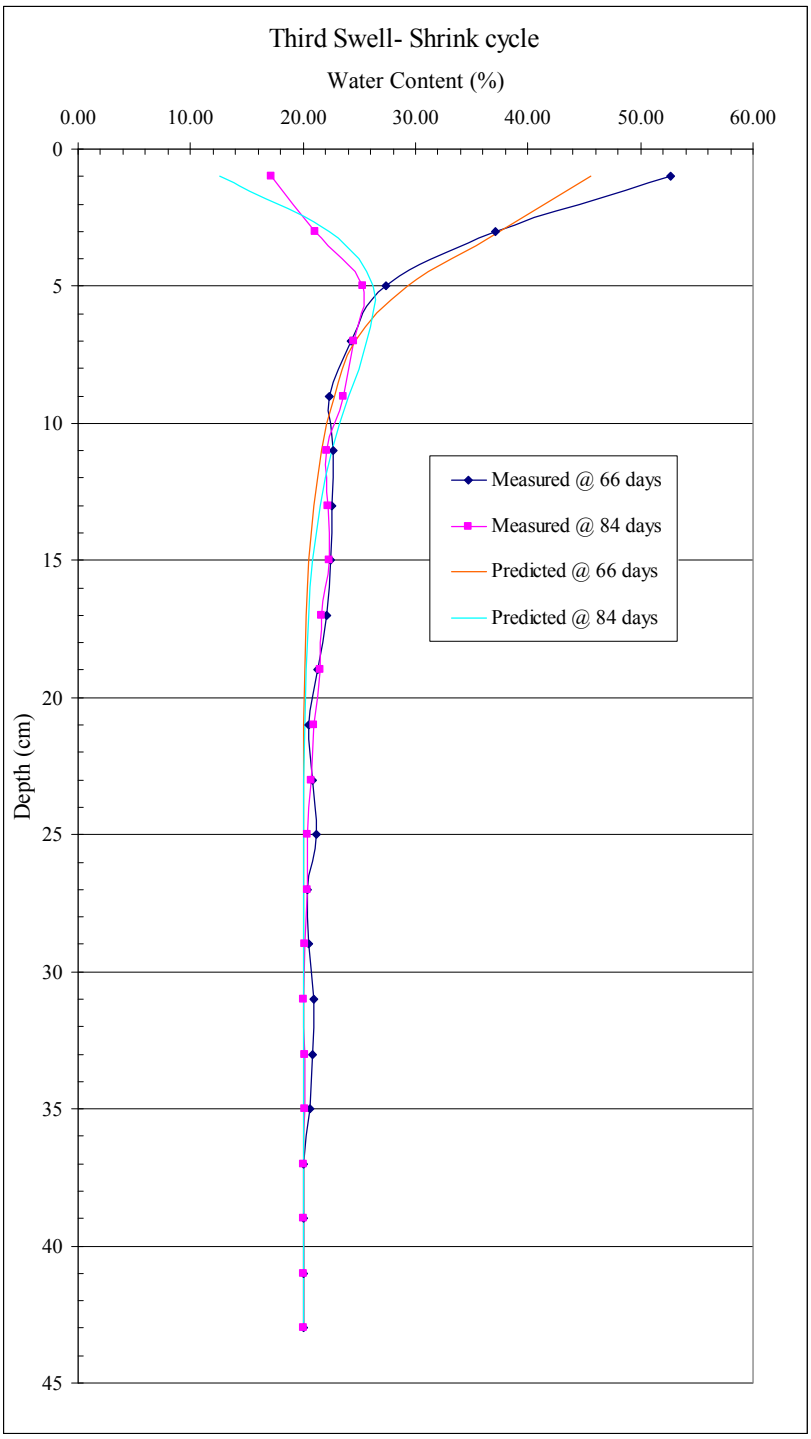

Fig. D.2. Water content results for third swell-shrink cycle (Uncovered phase)

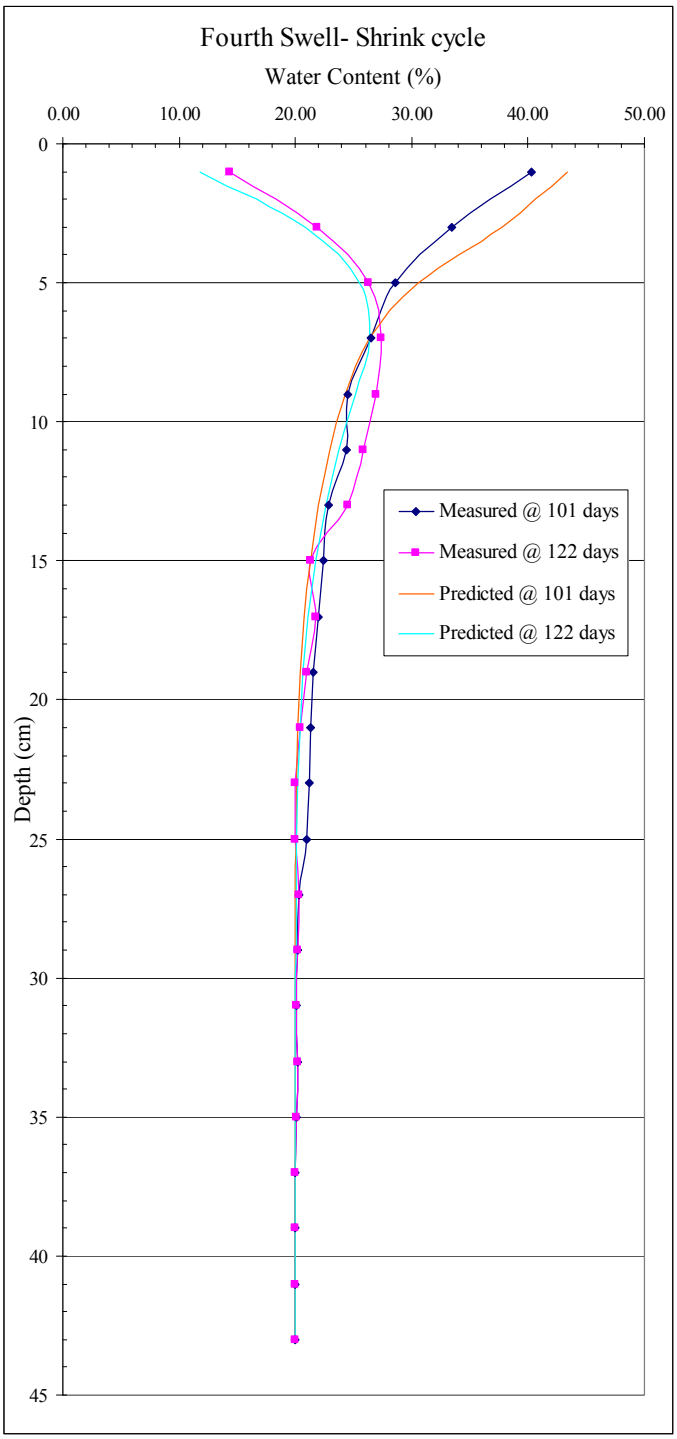

Fig. D.3. Water content results for fourth swell-shrink cycle (Uncovered phase)

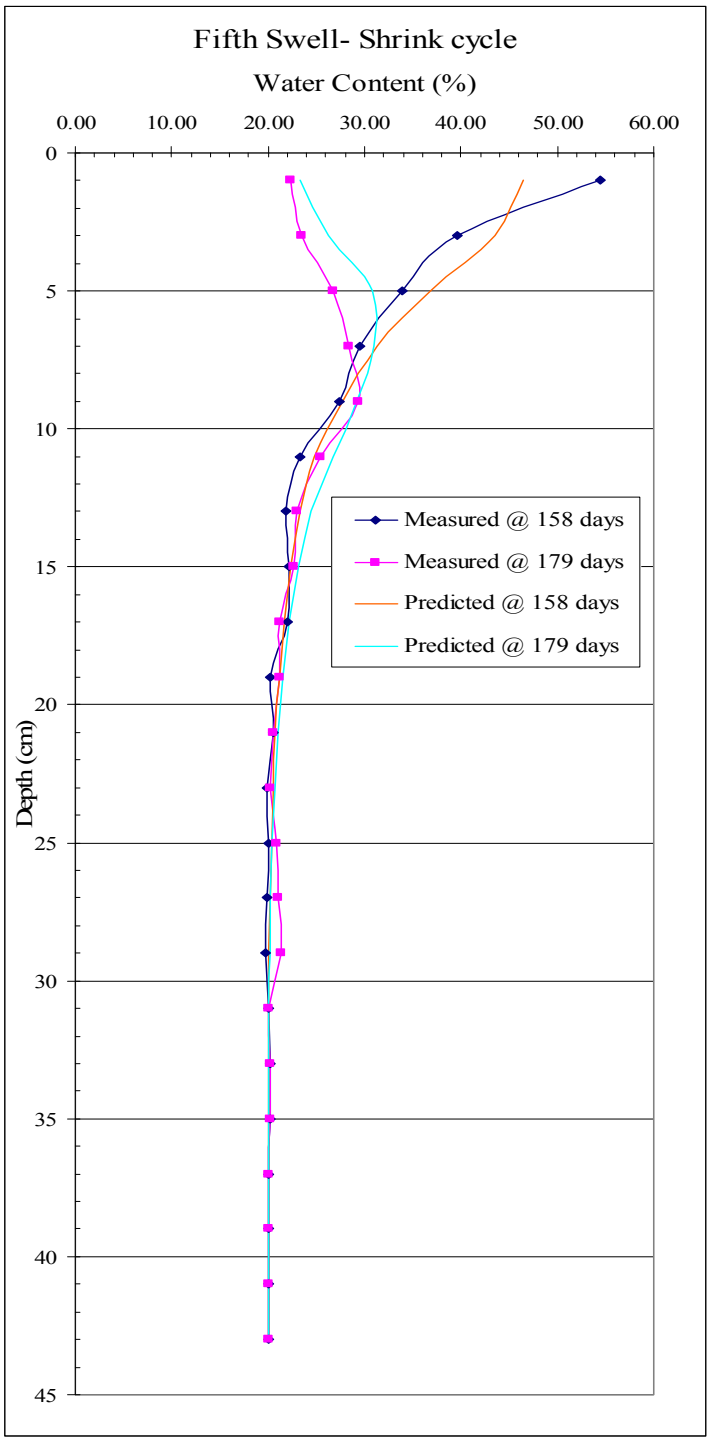

Fig. D.4. Water content results for fifth swell-shrink cycle (Uncovered phase)

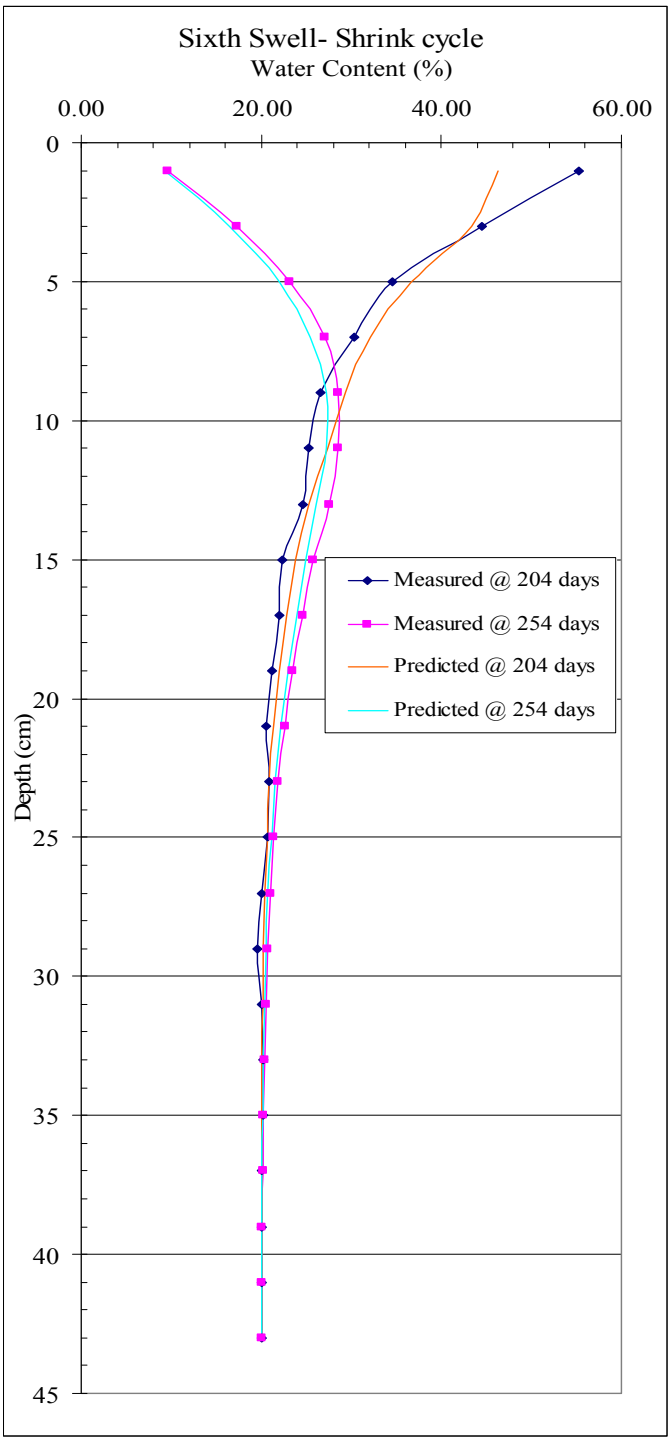

Fig. D.5. Water content results for sixth swell-shrink cycle (Uncovered phase)

Table D.1. Water content predicted results for six swell-shrink cycles (Uncovered phase)

Day#	7	20	35	51	66	84	101	122	158	179	204	254	270
End of	1st swell	1st shrink	2nd swell	2nd shrink	3rd swell	3rd shrink	4th swell	4th shrink	5th swell	5th shrink	6th swell	6th shrink	6th shrink
date	10/27/2004	11/9/2004	11/24/2004	12/10/2004	12/30/2004	1/17/2005	2/3/2005	2/24/2005	4/1/2005	4/22/2005	5/17/2005	7/6/2005	7/22/2005
time	12:15	12:15	12:15	12:50	14:05	15:15	15:07	16:07	15:00	18:30	12:40	13:40	12:00
R	37.5	37.5	25	37.5	37.5	37.5	37.5	37.5	25	37.5	25	25	37.5
theta	165	-15	-15	-45	135	135	-60	-60	-60	120	120	120	-50
Depth	**wc%**	**wc%**	**wc%**	**wc%**	**wc%**	**wc%**	**wc%**	**wc%**	**wc%**	**wc%**	**wc%**	**wc%**	**wc%**
1	38.12	11.86	43.03	22.13	45.52	12.54	43.39	11.85	46.45	23.24	46.32	9.22	45.37
3	27.79	19.36	34.61	22.33	37.50	22.29	37.72	20.87	43.60	26.17	43.37	16.52	36.39
5	21.73	21.54	26.35	24.43	29.31	26.17	30.56	25.49	36.89	30.80	36.64	22.03	28.75
7	20.34	21.16	22.40	23.71	24.65	25.70	26.40	26.38	31.26	30.98	32.06	25.38	25.78
9	20.06	20.54	21.01	22.25	22.74	24.05	24.25	25.16	27.69	29.24	29.40	27.20	25.68
11	20.01	20.20	20.46	21.17	21.65	22.55	22.96	23.77	24.78	26.67	27.34	27.24	25.79
13	20.00	20.06	20.21	20.55	20.94	21.51	21.98	22.58	23.34	24.48	25.23	26.12	25.48
15	20.00	20.01	20.09	20.25	20.50	20.87	21.25	21.72	22.39	23.09	23.87	24.97	24.81
17	20.00	20.00	20.03	20.11	20.25	20.48	20.75	21.11	21.69	22.13	22.79	23.89	23.98
19	20.00	20.00	20.01	20.04	20.12	20.25	20.44	20.69	21.16	21.48	21.97	22.95	23.14
21	20.00	20.00	20.00	20.01	20.05	20.13	20.24	20.41	20.78	21.00	21.37	22.17	22.39
23	20.00	20.00	20.00	20.00	20.03	20.06	20.12	20.24	20.50	20.67	20.94	21.57	21.78
25	20.00	20.00	20.00	20.00	20.01	20.03	20.07	20.14	20.31	20.44	20.63	21.12	21.29
27	20.00	20.00	20.00	20.00	20.00	20.01	20.03	20.07	20.20	20.28	20.42	20.79	20.92
29	20.00	20.00	20.00	20.00	20.00	20.00	20.01	20.04	20.12	20.18	20.28	20.54	20.65
31	20.00	20.00	20.00	20.00	20.00	20.00	20.00	20.01	20.07	20.11	20.17	20.37	20.45
33	20.00	20.00	20.00	20.00	20.00	20.00	20.00	20.01	20.04	20.07	20.11	20.25	20.31
35	20.00	20.00	20.00	20.00	20.00	20.00	20.00	20.00	20.03	20.04	20.07	20.16	20.21
37	20.00	20.00	20.00	20.00	20.00	20.00	20.00	20.00	20.01	20.03	20.04	20.11	20.14
39	20.00	20.00	20.00	20.00	20.00	20.00	20.00	20.00	20.00	20.01	20.03	20.07	20.09
41	20.00	20.00	20.00	20.00	20.00	20.00	20.00	20.00	20.00	20.00	20.01	20.05	20.07
43	20.00	20.00	20.00	20.00	20.00	20.00	20.00	20.00	20.00	20.00	20.01	20.04	20.06

Table D.2. Water content measured results for six swell-shrink cycles (Uncovered phase)

Day#	7	20	35	51	66	84	101	122	158	179	204	254	270	
End of	1st swell	1st shrink	2nd swell	2nd shrink	3rd swell	3rd shrink	4th swell	4th shrink	5th swell	5th shrink	6th swell	6th shrink	6th shrink	
date	10/27/2004	11/9/2004	11/24/2004	12/10/2004	12/30/2004	1/17/2005	2/3/2005	2/24/2005	4/1/2005	4/22/2005	5/17/2005	7/6/2005	7/22/2005	
time	12:15	12:15	12:15	12:50	14:05	15:15	15:07	16:07	15:00	18:30	12:40	13:40	12:00	
R	37.5	37.5	25	37.5	37.5	37.5	37.5	37.5	25	37.5	25	25	37.5	
theta	165	-15	-15	-45	135	135	-60	-60	-60	120	120	120	-50	
Depth	**wc%**	**wc%**	**wc%**	**wc%**	**wc%**	**wc%**	**wc%**	**wc%**	**wc%**	**wc%**	**wc%**	**wc%**	**wc%**	
1	45.38	12.00	44.65	21.50	52.65	17.23	40.24	14.30	54.44	22.30	55.22	9.58	56.30	
3	31.06	20.95	33.20	22.30	37.15	21.09	33.45	21.90	39.64	23.50	44.55	17.33	33.55	
5	24.37	21.59	26.00	22.80	27.31	25.30	28.64	26.31	33.90	26.78	34.55	23.17	29.44	
7	20.93	21.54	22.17	23.40	24.30	24.56	26.48	27.34	29.46	28.36	30.35	27.04	25.32	
9	20.37	21.00	22.56	21.30	22.33	23.60	24.50	26.89	27.40	29.30	26.61	28.57	24.84	
11	20.47	20.95	21.80	20.71	22.72	22.12	24.39	25.78	23.39	25.45	25.33	28.48	25.67	
13	19.67	21.10	21.50	21.07	22.57	22.26	22.87	24.53	21.90	23.02	24.56	27.58	24.08	
15	19.66	21.00	21.00	21.39	22.48	22.30	22.43	21.30	22.19	22.60	22.39	25.82	25.00	
17	20.63	20.90	21.50	20.90	22.13	21.65	21.96	21.76	22.02	21.14	22.04	24.60	25.19	
19	20.04	20.50	20.50	20.50	21.30	21.51	21.50	21.00	20.15	21.16	21.22	23.52	25.64	
21	20.00	20.30	19.63	20.20	20.53	20.90	21.30	20.45	20.51	20.57	20.53	22.63	23.61	
23	20.00	20.04	19.20	20.65	20.79	20.68	21.15	20.00	19.97	20.26	20.89	21.92	23.67	
25	20.00	20.37	19.55	20.42	21.20	20.35	20.97	20.00	20.03	20.83	20.70	21.39	23.69	
27	20.00	19.79	19.30	20.26	20.39	20.33	20.31	20.31	19.81	21.07	20.00	20.99	23.70	
29	20.00	20.00	19.49	20.39	20.44	20.20	20.20	20.20	19.74	21.38	19.51	20.69	23.44	
31	20.00	20.00	20.00	20.39	20.96	20.05	20.05	20.05	20.05	20.05	20.05	20.48	21.91	
33	20.00	20.00	20.00	20.00	20.84	20.16	20.16	20.16	20.16	20.16	20.16	20.32	20.10	
35	20.00	20.00	20.00	20.00	20.59	20.10	20.05	20.14	20.14	20.14	20.14	20.22	20.10	
37	20.00	20.00	20.00	20.00	20.00	20.00	20.00	20.00	20.00	20.00	20.00	20.14	20.00	
39	20.00	20.00	20.00	20.00	20.00	20.00	20.00	20.00	20.00	20.00	20.00	20.09	20.00	
41	20.00	20.00	20.00	20.00	20.00	20.00	20.00	20.00	20.00	20.00	20.00	20.07	20.00	
43	20.00	20.00	20.00	20.00	20.00	20.00	20.00	20.00	20.00	20.00	20.00	20.06	20.00	
RMS	0.950	0.571	0.786	0.587	1.013	0.711	1.230	0.824	1.270	1.340	1.107	0.766	1.509	0.974

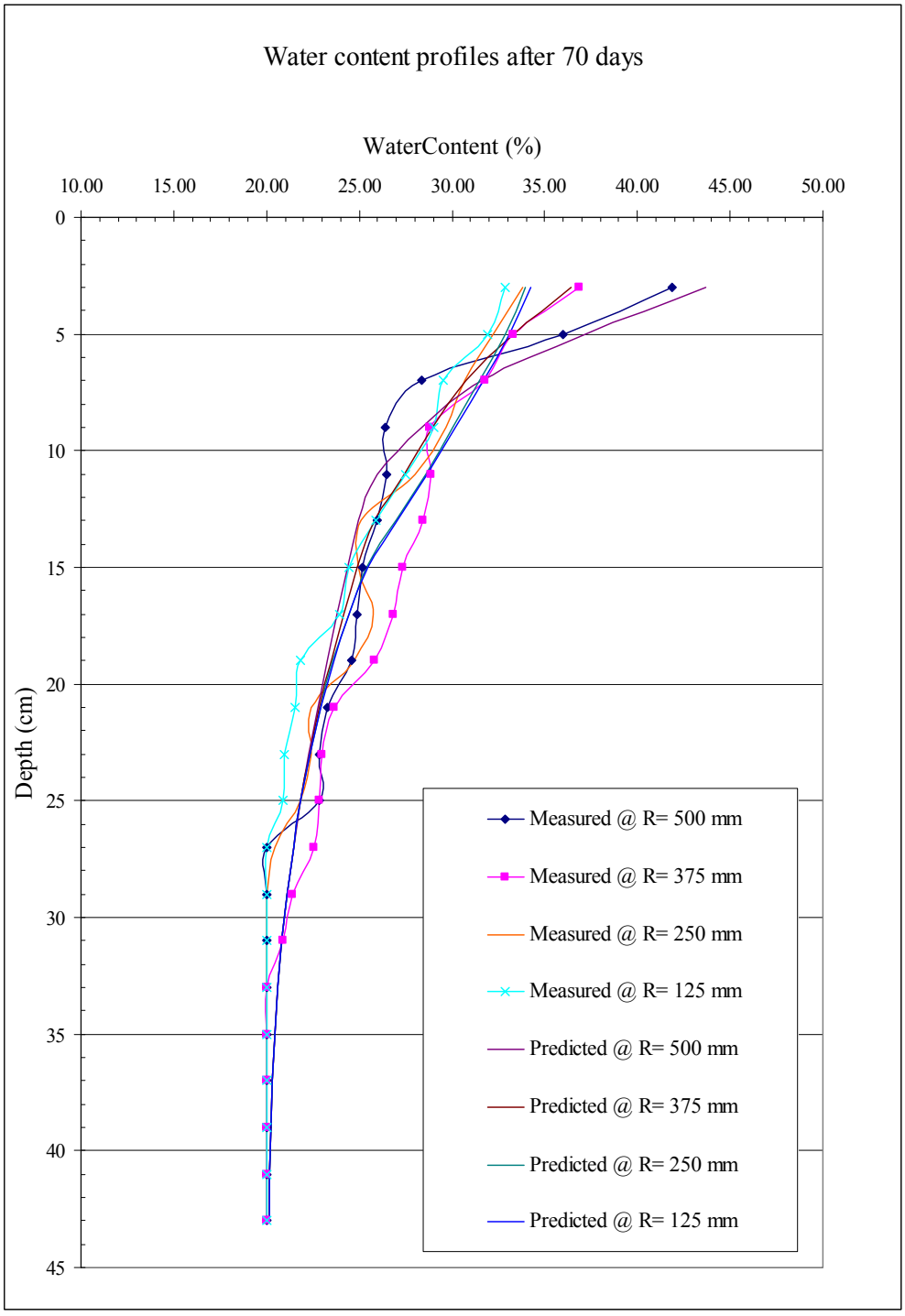

Fig. D.6. Water content measured and predicted results after 70 days (Covered phase)

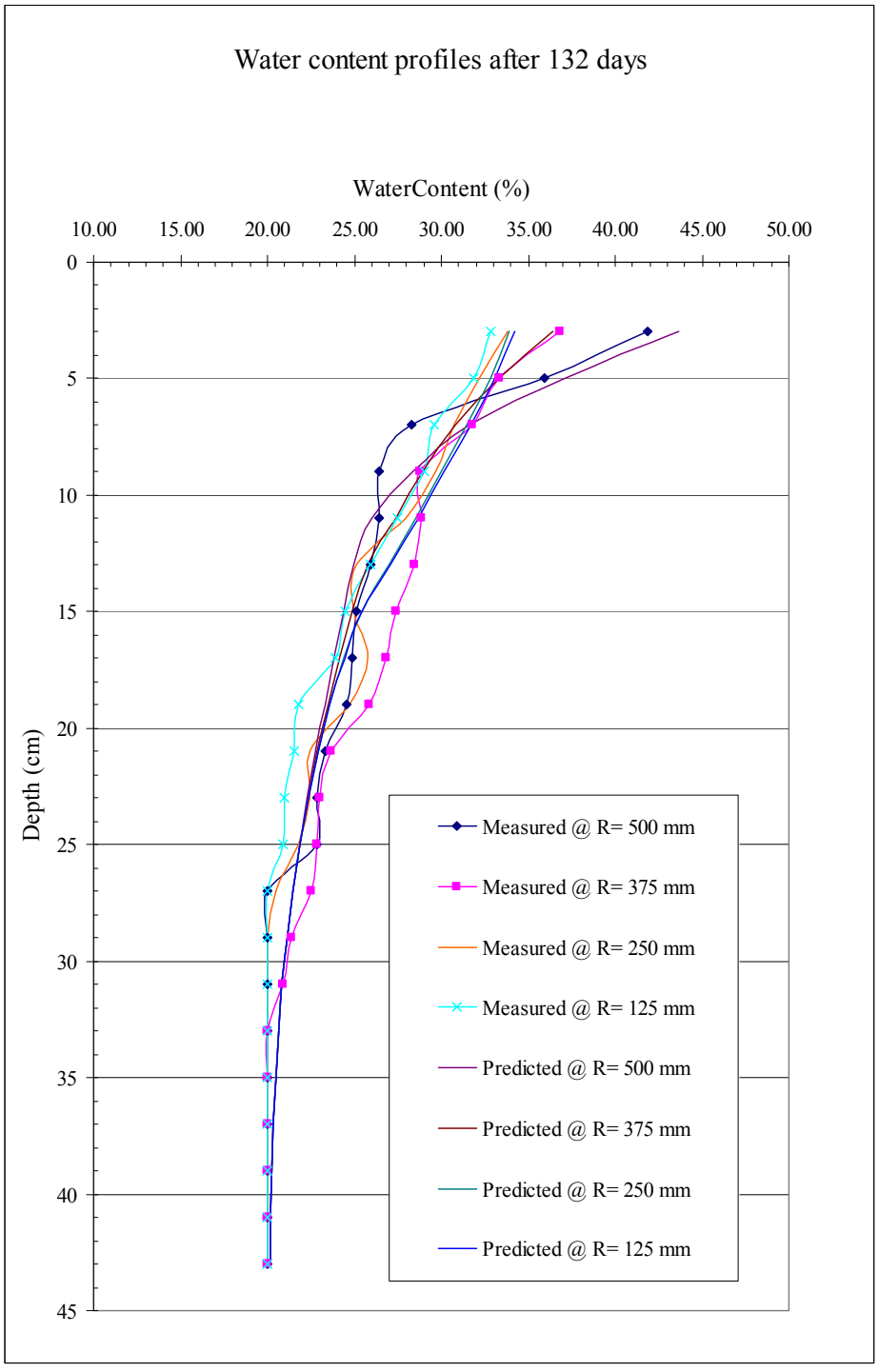

Fig. D.7. Water content measured and predicted results after 132 days (Covered phase)

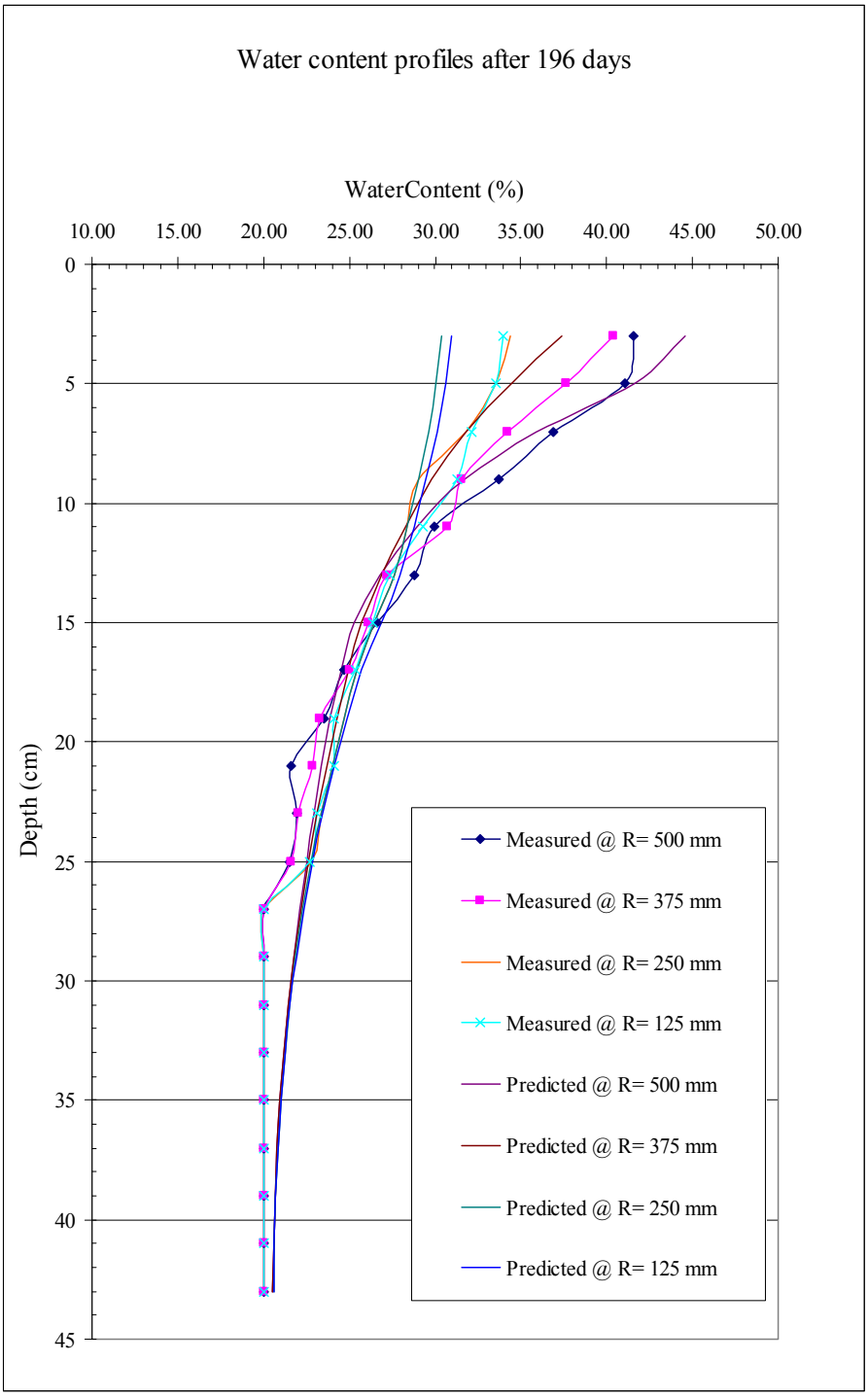

Fig. D.8. Water content measured and predicted results after 196 days (Covered phase)

Table D.3. Water content predicted results for two swell-shrink cycles (Covered phase)

Day#	0	32	32	32	32	70	70	70	70	132	132	132	132	196	196	196	196
End of		1st shrink	1sh shrink	1st shrink	1st shrink	1st swell	1st swell	1st swell	1st swell	2nd shrink	2nd shrink	2nd shrink	2nd shrink	2nd swell	2nd swell	2nd swell	2nd swell
date	7/22/2005	8/23/2005	8/24/2005	8/25/2005	8/26/2005	9/30/2005	9/30/2005	9/30/2005	9/30/2005	12/1/2005	12/1/2005	12/1/2005	12/1/2005	2/3/2006	2/3/2006	2/3/2006	2/3/2006
time	12:00	14:13	14:13	14:13	14:13	14:30	14:30	14:30	14:30	14:13	14:13	14:13	14:13	14:30	14:30	14:30	14:30
R	37.5	50	37.5	25	12.5	50	50	50	50	50	37.5	25	12.5	50	50	50	50
theta	-50	-30	-30	-30	-30	-60	-60	-60	-60								
Depth	**wc%**	**wc%**	**wc%**	**wc%**	**wc%**	**wc%**	**wc%**	**wc%**	**wc%**	**wc%**	**wc%**	**wc%**	**wc%**	**wc%**	**wc%**	**wc%**	**wc%**
1	45.37	9.67	29.97	38.27	38.30	46.47	38.99	34.53	34.85	8.59	23.37	32.14	32.48	46.82	39.81	30.58	31.12
3	36.39	17.26	30.44	36.63	36.65	43.65	36.41	33.93	34.23	14.93	24.88	31.86	32.19	44.58	37.43	30.40	30.94
5	28.75	22.41	30.28	34.01	34.03	37.15	33.30	32.86	33.11	19.97	26.76	31.34	31.66	41.65	34.43	30.07	30.60
7	25.78	25.02	29.35	31.31	31.32	31.63	30.77	31.49	31.69	23.45	27.97	30.64	30.92	35.87	31.83	29.62	30.10
9	25.68	25.80	28.10	29.07	29.08	28.38	28.92	30.02	30.16	25.38	28.17	29.76	30.02	31.74	29.83	29.05	29.49
11	25.79	25.65	26.58	27.19	27.19	25.98	27.40	28.56	28.68	26.15	27.84	28.80	29.03	28.98	28.31	28.36	28.77
13	25.48	25.16	25.40	25.55	25.56	24.97	25.81	26.96	27.07	25.93	26.91	27.77	27.96	26.81	26.89	27.60	27.98
15	24.81	24.55	24.63	24.68	24.68	24.36	24.91	25.41	25.46	25.33	25.73	26.28	26.51	25.29	25.66	26.43	26.87
17	23.98	23.91	23.94	23.95	23.95	23.82	24.14	24.41	24.45	24.60	24.87	25.18	25.30	24.49	24.93	25.47	25.70
19	23.14	23.27	23.27	23.28	23.28	23.30	23.47	23.61	23.62	23.87	24.07	24.30	24.39	23.90	24.29	24.71	24.89
21	22.39	22.64	22.64	22.64	22.64	22.78	22.86	22.92	22.92	23.21	23.37	23.54	23.61	23.40	23.69	24.00	24.14
23	21.78	22.07	22.08	22.08	22.08	22.29	22.32	22.34	22.34	22.65	22.77	22.88	22.92	22.94	23.14	23.37	23.46
25	21.29	21.59	21.59	21.59	21.59	21.83	21.84	21.86	21.86	22.16	22.24	22.33	22.36	22.50	22.64	22.80	22.87
27	20.92	21.19	21.19	21.19	21.19	21.44	21.45	21.45	21.45	21.76	21.81	21.87	21.89	22.11	22.20	22.31	22.36
29	20.65	20.87	20.87	20.87	20.87	21.11	21.11	21.11	21.11	21.41	21.45	21.48	21.49	21.74	21.81	21.88	21.91
31	20.45	20.63	20.63	20.63	20.63	20.83	20.83	20.83	20.83	21.13	21.15	21.16	21.17	21.44	21.48	21.53	21.55
33	20.31	20.45	20.45	20.45	20.45	20.62	20.62	20.62	20.62	20.89	20.90	20.91	20.91	21.17	21.21	21.24	21.25
35	20.21	20.31	20.31	20.31	20.31	20.46	20.46	20.46	20.46	20.71	20.71	20.72	20.72	20.97	20.98	21.00	21.01
37	20.14	20.22	20.22	20.22	20.22	20.33	20.33	20.33	20.33	20.56	20.56	20.56	20.56	20.80	20.81	20.83	20.83
39	20.09	20.16	20.16	20.16	20.16	20.25	20.25	20.25	20.25	20.45	20.45	20.45	20.46	20.69	20.69	20.70	20.70
41	20.07	20.12	20.12	20.12	20.12	20.20	20.20	20.20	20.20	20.38	20.38	20.38	20.38	20.61	20.61	20.62	20.62
43	20.06	20.11	20.11	20.11	20.11	20.17	20.17	20.17	20.17	20.34	20.34	20.34	20.34	20.56	20.56	20.57	20.57

Table D.4. Water content measured results for two swell-shrink cycles (Covered phase)

Day#	0	32	32	32	32	70	70	70	70	132	132	132	132	196	196	196	196	
End of		1st shrink	1sh shrink	1st shrink	1st shrink	1st swell	1st swell	1st swell	1st swell	2nd shrink	2nd shrink	2nd shrink	2nd shrink	2nd swell	2nd swell	2nd swell	2nd swell	
date	7/22/2005	8/23/2005	8/24/2005	8/25/2005	8/26/2005	9/30/2005	9/30/2005	9/30/2005	9/30/2005	12/1/2005	12/1/2005	12/1/2005	12/1/2005	2/3/2006	2/3/2006	2/3/2006	2/3/2006	
time	12:00	14:13	14:13	14:13	14:13	14:30	14:30	14:30	14:30	14:13	14:13	14:13	14:13	14:30	14:30	14:30	14:30	
R	37.5	50	37.5	25	12.5	50	50	50	50	50	37.5	25	12.5	50	50	50	50	
theta	-50	-30	-30	-30	-30	-60	-60	-60	-60									
Depth	**wc%**	**wc%**	**wc%**	**wc%**	**wc%**	**wc%**	**wc%**	**wc%**	**wc%**	**wc%**	**wc%**	**wc%**	**wc%**	**wc%**	**wc%**	**wc%**	**wc%**	
1	56.30	16.50				45.93												
3	33.55	20.03	28.71	36.77	33.68	41.89	36.83	33.83	32.87	16.40	26.33	35.54	35.99	41.58	40.43	34.40	33.94	
5	29.44	23.15	28.82	35.62	31.73	35.98	33.30	32.21	31.91	20.67	27.10	33.34	33.66	41.05	37.63	33.57	33.52	
7	25.32	23.84	29.65	33.77	29.80	28.33	31.80	30.72	29.56	26.56	27.97	31.00	32.42	36.87	34.22	31.76	32.10	
9	24.84	24.46	29.34	30.43	28.77	26.40	28.77	29.70	29.03	25.70	28.17	30.76	31.62	33.74	31.58	29.05	31.29	
11	25.67	24.87	27.30	27.08	27.12	26.46	28.84	28.01	27.51	27.33	27.84	29.80	30.03	29.98	30.68	28.36	29.28	
13	24.08	24.51	25.96	24.80	25.85	25.94	28.43	25.13	25.92	26.10	28.65	28.77	27.20	28.81	27.20	27.60	27.35	
15	25.00	23.86	24.14	23.75	22.75	25.14	27.37	24.96	24.45	26.23	27.43	26.78	26.35	26.59	26.13	26.43	26.39	
17	25.19	22.24	22.60	23.10	22.30	24.88	26.84	25.76	23.94	25.60	26.23	25.58	25.30	24.73	25.02	25.47	25.40	
19	25.64	21.76	21.39	22.94	21.54	24.58	25.83	24.73	21.80	23.45	25.46	24.40	24.39	23.50	23.26	24.71	24.12	
21	23.61	21.30	20.00	21.87	20.00	23.30	23.67	22.40	21.56	22.45	24.50	22.54	23.61	21.60	22.86	24.00	24.08	
23	23.67	20.45	20.00	20.00	20.00	22.84	23.00	22.43	20.97	22.14	22.13	21.88	22.92	21.94	22.01	23.37	23.10	
25	23.69	19.68	20.00	20.00	20.00	22.82	22.84	21.80	20.86	21.23	21.44	21.33	22.36	21.50	21.64	22.80	22.67	
27	23.70	20.00	20.00	20.00	20.00	20.00	22.54	20.46	20.00	20.00	20.00	20.00	20.00	20.00	20.00	20.00	20.00	
29	23.44	20.00	20.00	20.00	20.00	20.00	21.40	20.00	20.00	20.00	20.00	20.00	20.00	20.00	20.00	20.00	20.00	
31	21.91	20.00	20.00	20.00	20.00	20.00	20.87	20.00	20.00	20.00	20.00	20.00	20.00	20.00	20.00	20.00	20.00	
33	20.10	20.00	20.00	20.00	20.00	20.00	20.00	20.00	20.00	20.00	20.00	20.00	20.00	20.00	20.00	20.00	20.00	
35	20.10	20.00	20.00	20.00	20.00	20.00	20.00	20.00	20.00	20.00	20.00	20.00	20.00	20.00	20.00	20.00	20.00	
37	20.00	20.00	20.00	20.00	20.00	20.00	20.00	20.00	20.00	20.00	20.00	20.00	20.00	20.00	20.00	20.00	20.00	
39	20.00	20.00	20.00	20.00	20.00	20.00	20.00	20.00	20.00	20.00	20.00	20.00	20.00	20.00	20.00	20.00	20.00	
41	20.00	20.00	20.00	20.00	20.00	20.00	20.00	20.00	20.00	20.00	20.00	20.00	20.00	20.00	20.00	20.00	20.00	
43	20.00	20.00	20.00	20.00	20.00	20.00	20.00	20.00	20.00	20.00	20.00	20.00	20.00	20.00	20.00	20.00	20.00	
RMS	1.508	1.175	1.194	1.052	1.428	1.199	1.259	0.757	1.112	1.112	1.047	1.259	1.276	1.383	1.581	1.519	1.425	1.183

APPENDIX E

SOIL WEATHER INTERACTION ANALYSIS

APPENDIX E-1

SOIL WEATHER INTERACTION SIMULATIONS USING FAO 56 WEATHER MODEL

```
*HEADING
WEATHER-SOIL INTERACTION MODELLING USING FAO 56 WEATHER
MODEL AND SOIL WITH WEIGHTLESS COVER
*NODE
1,        -15.0,  -15.0
31,        0.,    -15.0
61,      15.0,  -15.0
1831,   -15.0,  0.
1861,   0.,     0.
1891,   15.0,   0.
*NSET,  NSET=TEDGE
1861
*NSET,  NSET=BEDGE
31
*NSET,  NSET=TLEFT
1831
*NSET,  NSET=BLEFT
1
*NSET,  NSET=TRIGHT
1891
*NSET,  NSET=BRIGHT
61
*NFILL, NSET=LEFT,BIAS=1.1
BLEFT,TLEFT,30,61
*NFILL, NSET=RIGHT,BIAS=1.1
```

```
BRIGHT,TRIGHT,30,61
*NFILL, NSET=EDGE,BIAS=1.1
BEDGE,TEDGE,30,61
*NFILL, NSET=COVERED,BIAS=1.1
LEFT,EDGE,30,1
*NFILL, NSET=UNCOVERED,BIAS=1.1
RIGHT,EDGE,30,-1
*ELSET,  ELSET=EXPOSED, GENERATE
1771, 1800,1
*NSET,  NSET=COVER, GENERATE
1831, 1861,1
*NSET,  NSET=FREESURF, GENERATE
1861, 1891,1
*NSET,  NSET=SOILMASS, GENERATE
1, 1891,1
*NSET,  NSET=BOTTOM, GENERATE
1, 61,1
**
*ELEMENT, TYPE=CPE4T
1, 1, 2, 63, 62
*ELGEN, ELSET=SOIL
1, 60, 1, 1, 30, 61,60
*SOLID SECTION,ELSET=SOIL,MATERIAL=SOIL
*MATERIAL, NAME=SOIL
*ELASTIC
2000, .4
*EXPANSION
1.E-7,
*DENSITY
```

```
11,
*SPECIFIC HEAT
0.35,
*CONDUCTIVITY
.02592,
*INITIAL CONDITIONS, TYPE=TEMPERATURE
SOILMASS,-3.1
```

APPENDIX E-2

RESULTING SUCTION ENVELOPS

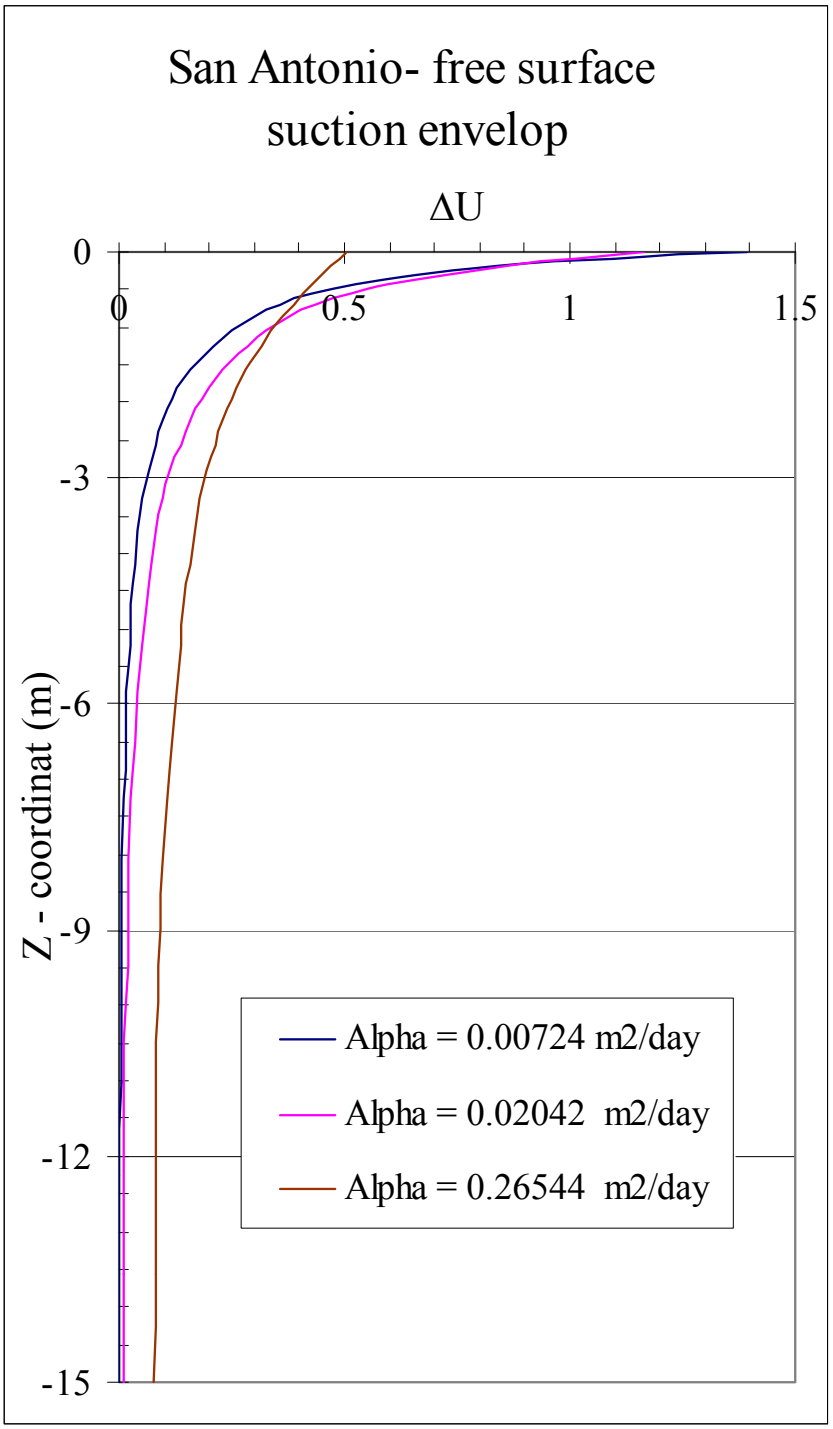

Fig. E.1. San Antonio, TX, free field suction envelops.

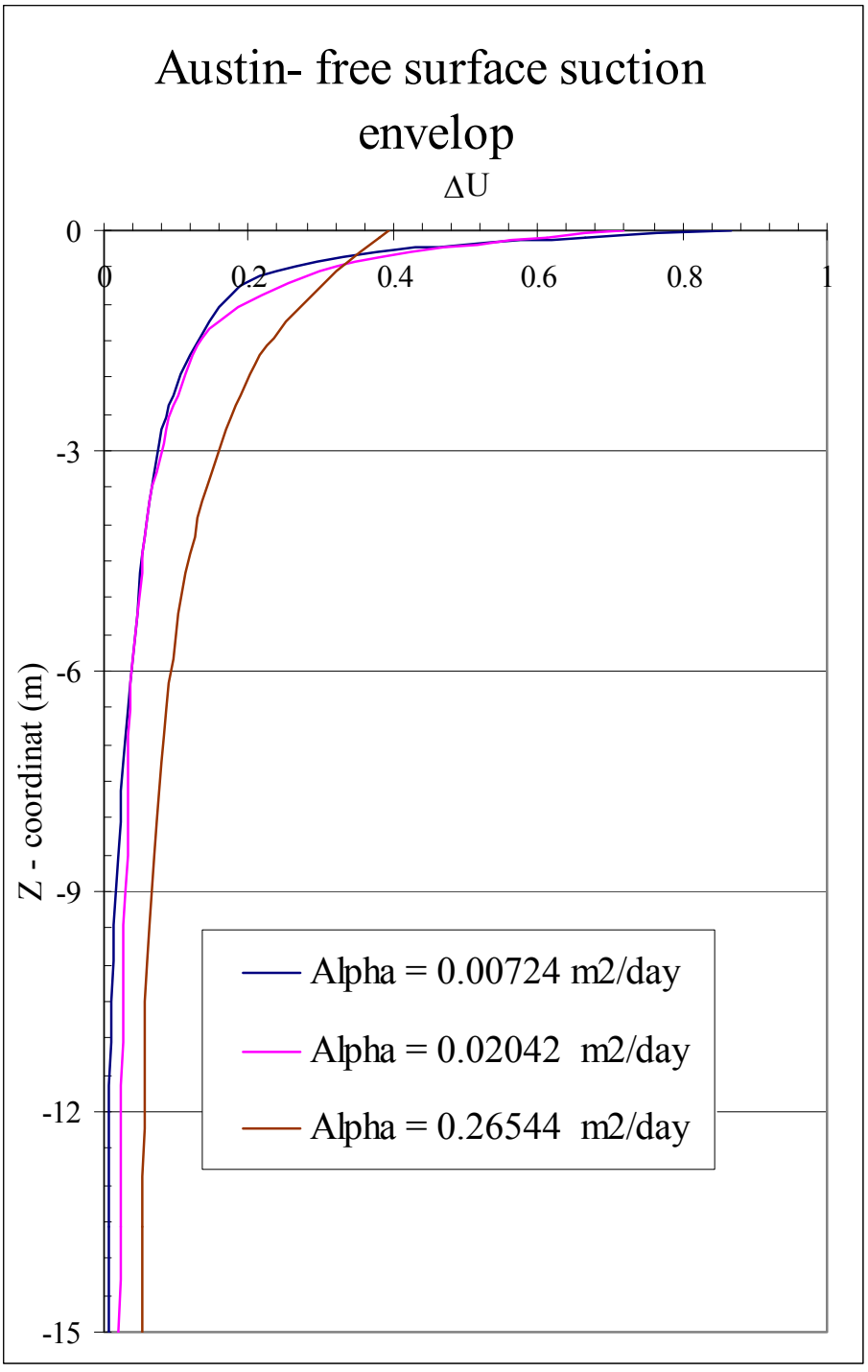

Fig. E.2. Austin, TX, free field suction envelops.

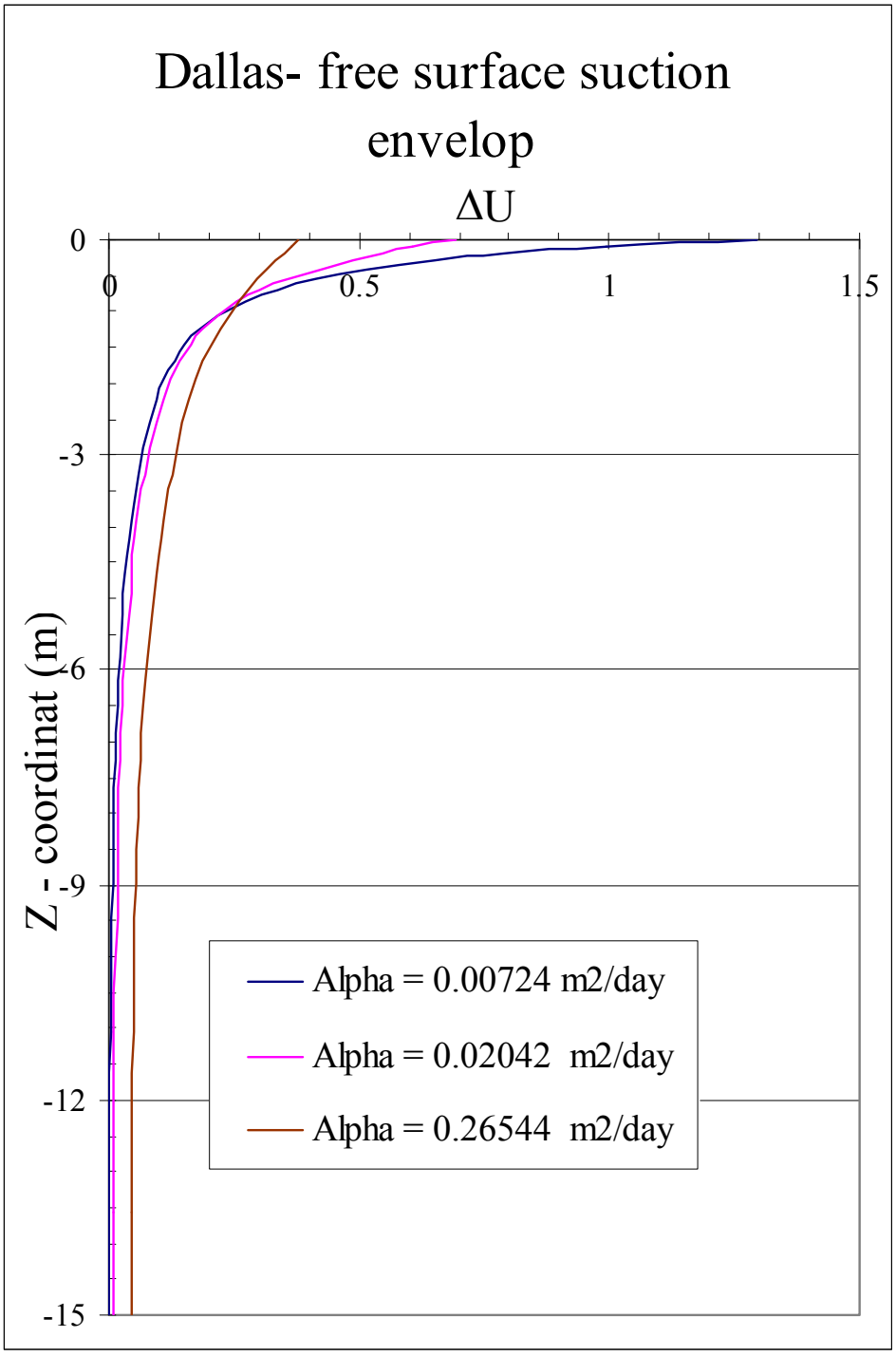

Fig. E.3. Dallas, TX, free field suction envelops.

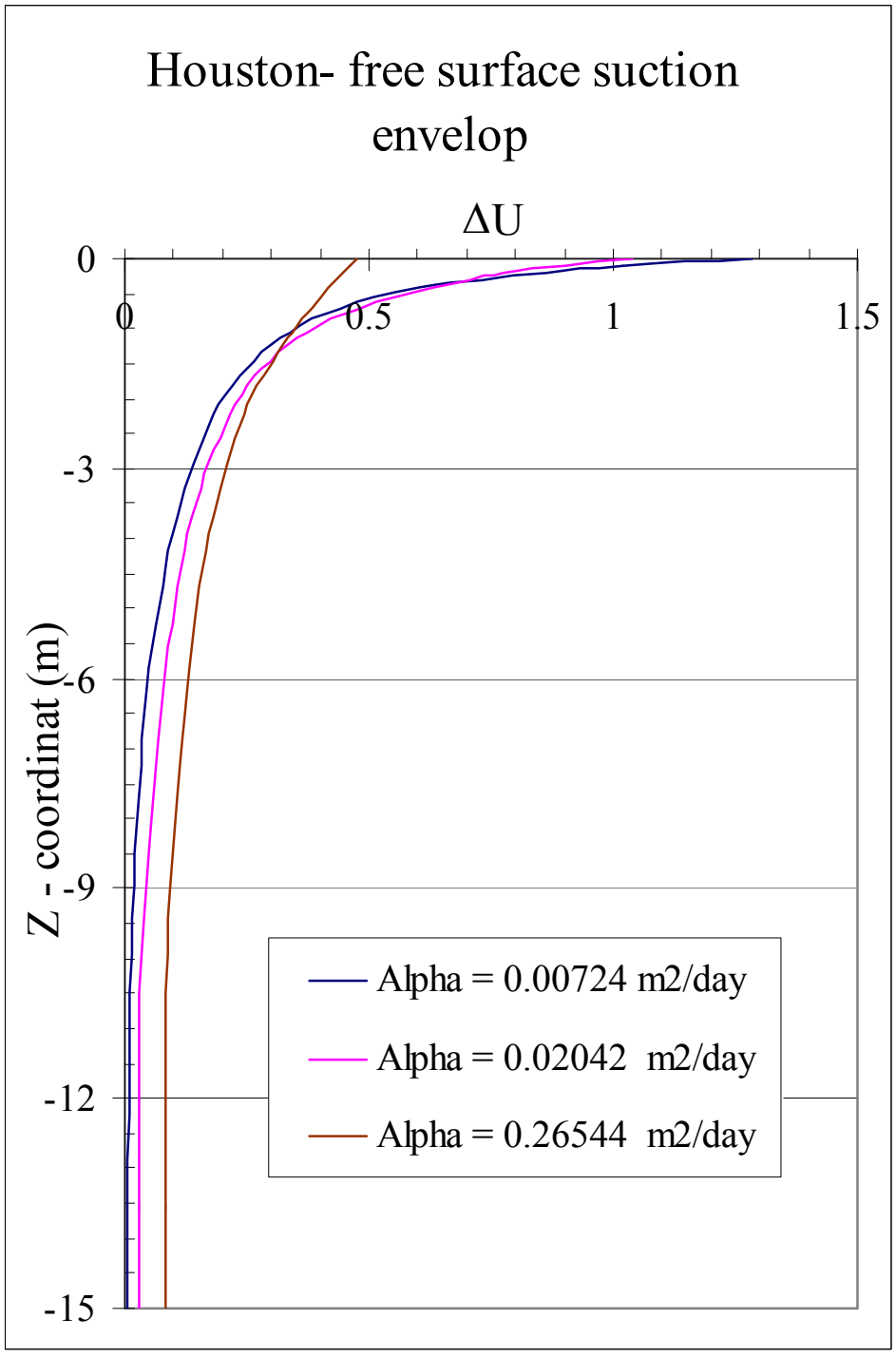

Fig. E.4. Houston, TX, free field suction envelops.

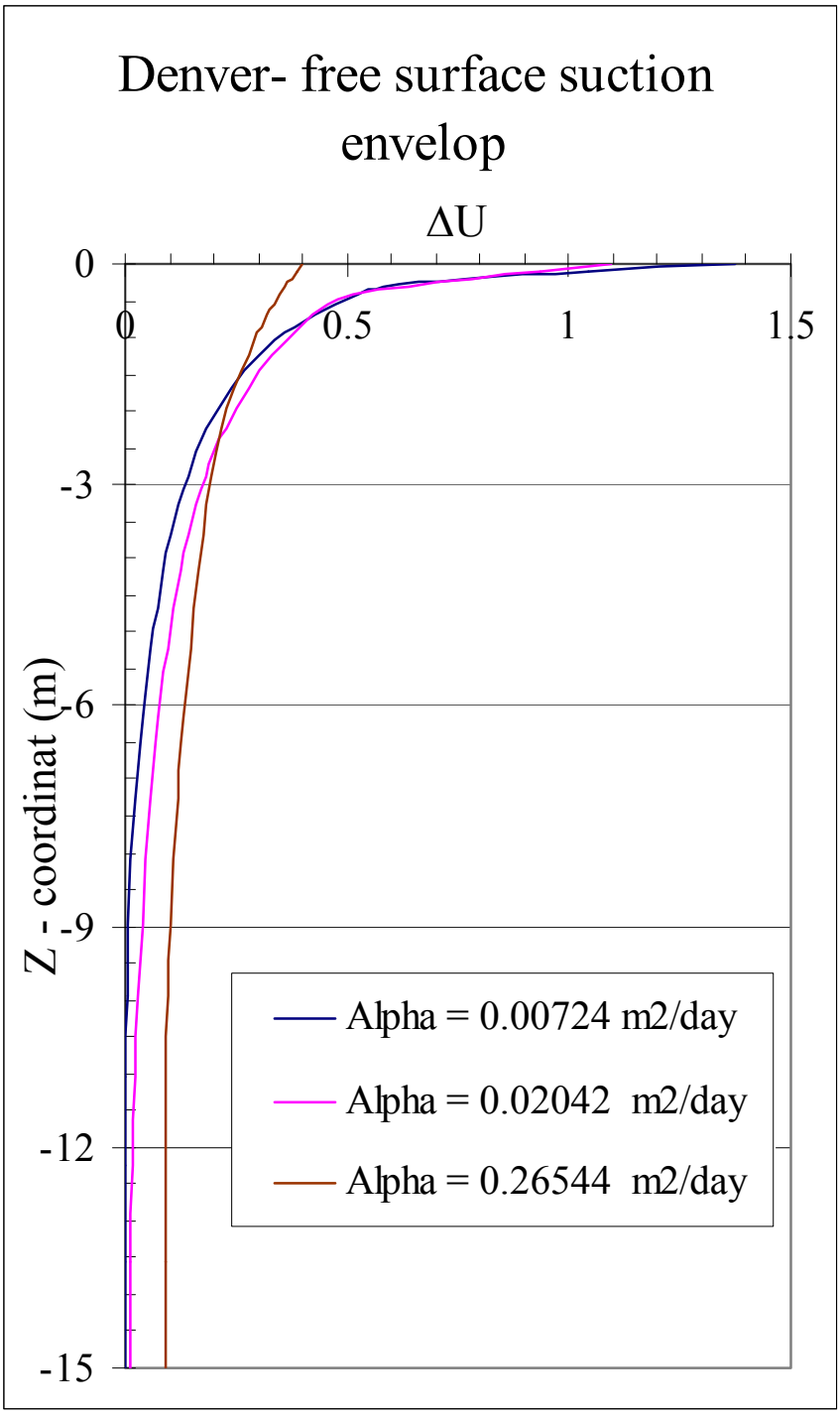

Fig. E.5. Denver, CO, free field suction envelops.

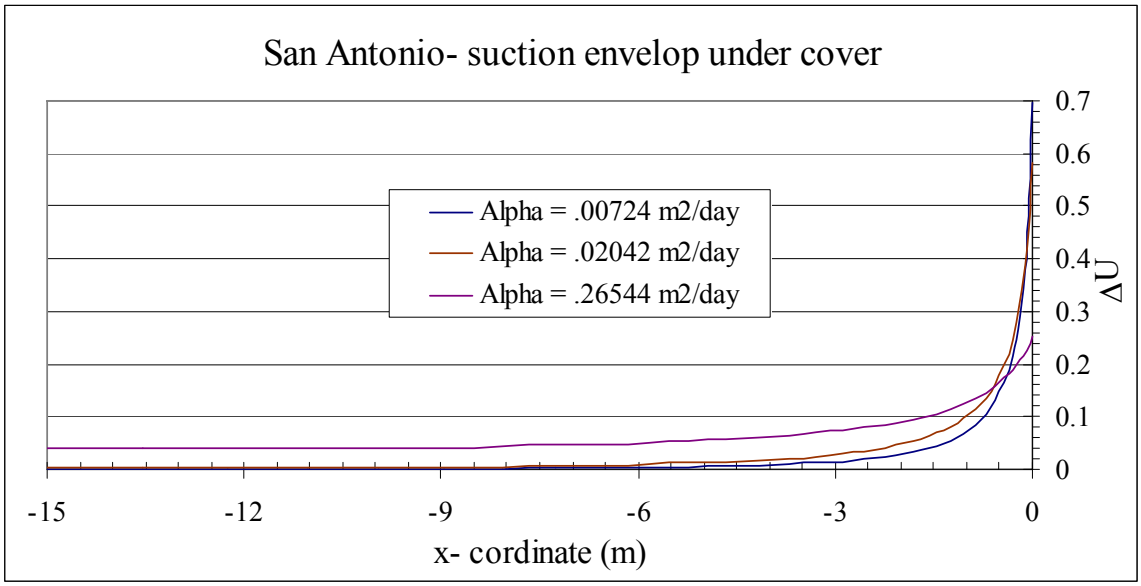

Fig. E.6. San Antonio, TX, suction envelops under cover.

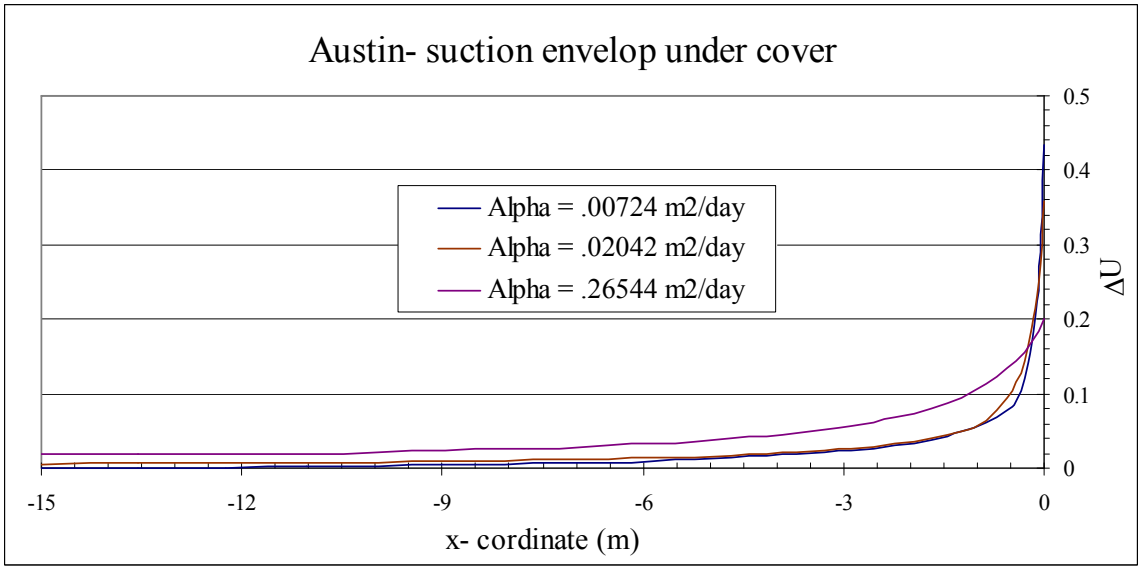

Fig. E.7. Austin, TX, suction envelops under cover.

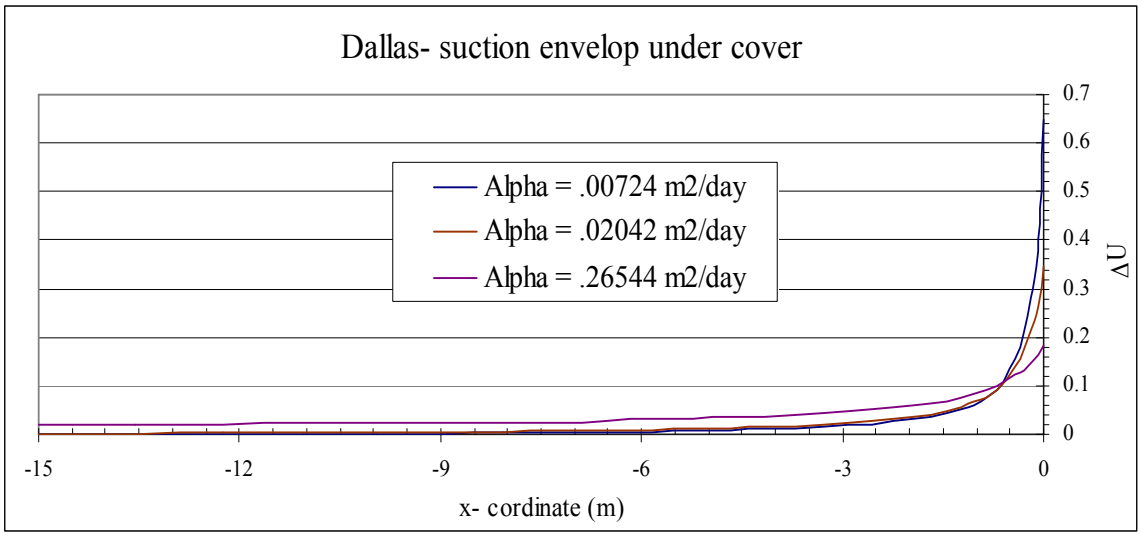

Fig. E.8. Dallas, TX, suction envelops under cover.

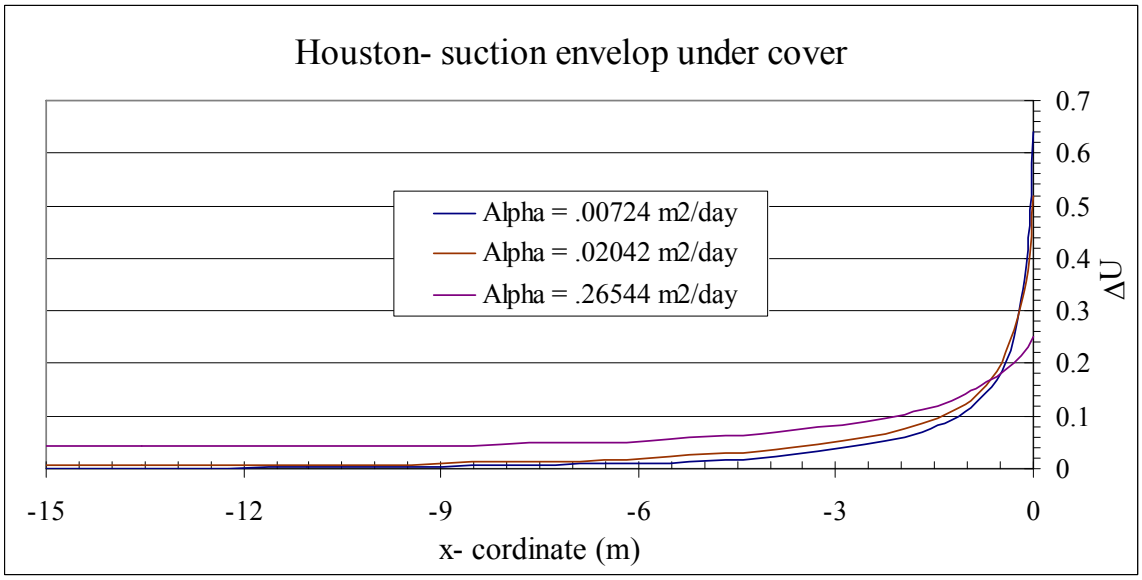

Fig. E.9. Houston, TX, suction envelops under cover.

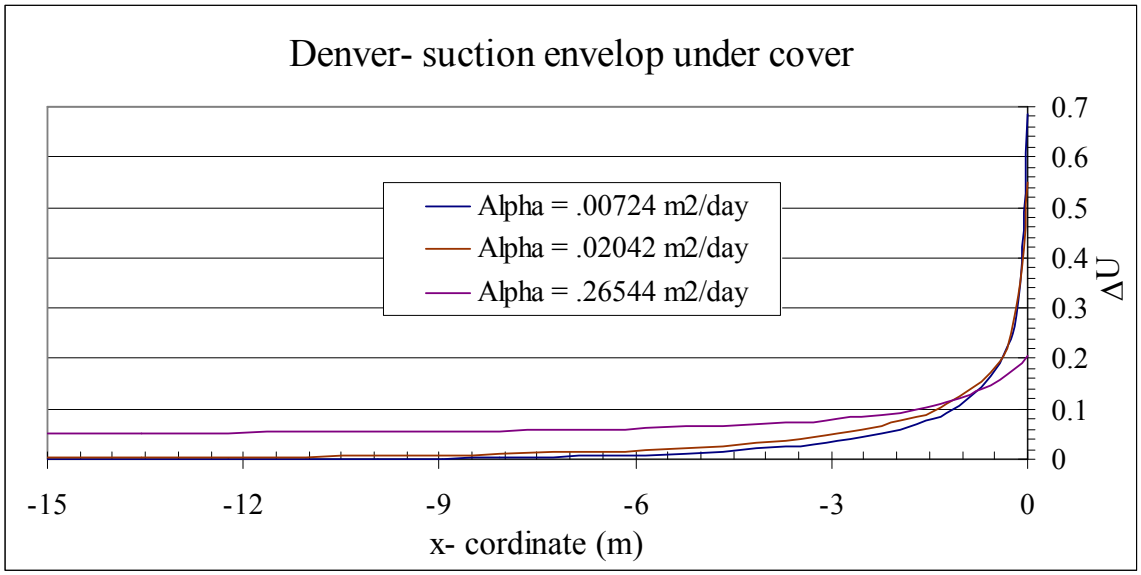

Fig. E.10. Denver, CO, suction envelops under cover.

APPENDIX F

SOIL STRUCTURE INTERACTION ANALYSIS

APPENDIX F.1

EXAMPLE INPUT FILE FOR SOIL STRUCTURE INTERACTION 2D SIMULATION OF FOUNDATION ON GRADE OF A SPECIFIC MOUND SHAPE (EDGE DROP CASE)

*HEADING

Soil Structure Interaction Model (SSIM) to 2D simulate foundation on grade of a specific mound shape (Edge Drop case)

*NODE

1, 0, 0.085

2, 0.2, 0.085

3, 0.4, 0.085

4, 0.6, 0.085

5, 0.8, 0.085

6, 1, 0.085

7, 1.2, 0.085

8, 1.4, 0.084

9, 1.6, 0.084

10, 1.8, 0.084

11, 2, 0.083

12, 2.2, 0.083

13, 2.4, 0.082

14, 2.6, 0.082

15, 2.8, 0.081

16, 3, 0.080

17, 3.2, 0.079

18, 3.4, 0.078

19, 3.6, 0.077

20, 3.8, 0.076

```
21,    4,     0.075
22,    4.2,   0.073
23,    4.4,   0.072
24,    4.6,   0.070
25,    4.8,   0.068
26,    5,     0.066
27,    5.2,   0.064
28,    5.4,   0.061
29,    5.6,   0.059
30,    5.8,   0.056
31,    6,     0.053
32,    6.2,   0.049
33,    6.4,   0.046
34,    6.6,   0.042
35,    6.8,   0.037
36,    7,     0.032
37,    7.2,   0.027
38,    7.4,   0.021
39,    7.6,   0.015
40,    7.8,   0.008
41,    0.0,   0.0
81,    8.0,   0.0
101,   24.0,  0.0
1566,  0.0,   -24.0
1606,  8.0,   -24.0
1626,  24.0,  -24.0
2001,  0.,    0.085
2041,  8.,    0.085
**
```

```
**
*NSET, NSET=N81
81
*NSET, NSET=N101
101
*NFILL, NSET=TOPCLEAR,BIAS=0.909091
N81,N101,20,1
*NGEN, NSET=TOPCOVERED
41,81
*NSET,  NSET=TOP
TOPCLEAR, TOPCOVERED
*NSET,  NSET=M, GENERATE
1, 40, 1
*NSET,  NSET=MOUND
M,81
*NSET, NSET=N1606
1606
*NSET, NSET=N1626
1626
*NFILL, NSET=BOTTOMCLEAR,BIAS=0.909091
N1606,N1626,20,1
*NGEN, NSET=BOTTOMCOVERED
1566,1606
*NSET,  NSET=BOTTOM
BOTTOMCLEAR, BOTTOMCOVERED
*NFILL, NSET=ORIGINALSOIL,BIAS=0.909091
TOP,BOTTOM,25,61
*NSET,  NSET=L, GENERATE
41, 1566, 61
```

```
*NSET,  NSET=LEFT
1, L
*NSET,  NSET=RIGHT, GENERATE
101, 1626, 61
*NGEN, NSET=FOUNDATION
2001,2041
**
**
*ELEMENT, TYPE=CPE3
40, 40, 80, 81
*ELEMENT, TYPE=CPE4
1, 1, 41, 42, 2
*ELEMENT, TYPE=CPE4
41, 41, 102, 103, 42
*ELGEN, ELSET=ORIGINALSOIL
41, 60, 1, 1, 25, 61,60
*ELGEN, ELSET=S
1, 39, 1, 1, 1
*ELSET, ELSET=MOUNDSOIL
S,40
*ELSET, ELSET=SOILMASS
MOUNDSOIL,ORIGINALSOIL
*ELEMENT, TYPE=B21
2001, 2001, 2002
*ELGEN, ELSET=BEAM
2001,40,1,1
**
**
*SOLID SECTION, ELSET=SOILMASS, MATERIAL=SOIL
```

```
*MATERIAL, NAME=SOIL
*ELASTIC
60000., .3
*DENSITY
18,
*BEAM GENERAL SECTION, ELSET=BEAM, DENSITY=25, SECTION=RECT
1.0, 0.3795447
0,0,-1
20000000., 8695652.
**
*INITIAL CONDITIONS, TYPE=STRESS, GEOSTATIC
SOILMASS, 0.0, 0.0, -12.0, 216, .42
*BOUNDARY
LEFT,1,1,0.
RIGHT,1,1,0.
BOTTOM,2,2,0.
2001,1,1,0.
2001,6,6,0.
**
**
*SURFACE, NAME=MOUNDSOIL, TYPE=ELEMENT
MOUNDSOIL,
*SURFACE, NAME=BEAM,TYPE=ELEMENT
BEAM, SNEG
*CONTACT PAIR, INTERACTION=GRATING
MOUNDSOIL, BEAM
*SURFACE INTERACTION, NAME=GRATING
*FRICTION,SLIP TOLERANCE=0.005, EXPONENTIAL DECAY
0.4,0.1,4.
```

```
*SURFACE BEHAVIOR, PRESSURE-OVERCLOSURE=HARD
**
**
*STEP,NLGEOM=YES, NAME=UNCOVERED
*STATIC
*DLOAD
BEAM,PY , -7.5
**
*NODE PRINT, NSET= MOUND
 U
*NODE PRINT, NSET= FOUNDATION
 U
*EL PRINT, ELSET=BEAM, POSITION=AVERAGED AT NODES
 SF, SM1
*END STEP
```

APPENDIX F.2

EXAMPLE INPUT FILE FOR SOIL STRUCTURE INTERACTION 2D SIMULATION OF FOUNDATION ON GRADE OF A SPECIFIC MOUND SHAPE (EDGE LIFT CASE)

*HEADING

Soil Structure Interaction Model (SSIM) to 2D simulate foundation on grade of a specific mound shape (Edge Lift case)

*NODE

142, 8.0, -0.042712

162, 24.0, -0.042712

102, 0., -0.042712

42, 0.2, -0.042702

43, 0.4, -0.042670

44, 0.6, -0.042618

45, 0.8, -0.042544

46, 1, -0.042449

47, 1.2, -0.042330

48, 1.4, -0.042187

49, 1.6, -0.042020

50, 1.8, -0.041826

51, 2, -0.041605

52, 2.2, -0.041353

53, 2.4, -0.041071

54, 2.6, -0.040754

55, 2.8, -0.040401

56, 3, -0.040009

57, 3.2, -0.039574

58, 3.4, -0.039094

59, 3.6, -0.038564
60, 3.8, -0.037980
61, 4, -0.037339
62, 4.2, -0.036634
63, 4.4, -0.035860
64, 4.6, -0.035013
65, 4.8, -0.034084
66, 5, -0.033068
67, 5.2, -0.031956
68, 5.4, -0.030741
69, 5.6, -0.029415
70, 5.8, -0.027967
71, 6, -0.026389
72, 6.2, -0.024669
73, 6.4, -0.022797
74, 6.6, -0.020761
75, 6.8, -0.018546
76, 7, -0.016140
77, 7.2, -0.013523
78, 7.4, -0.010673
79, 7.6, -0.007553
80, 7.8, -0.004089
81, 8.0, 0.000000
101, 24.0, 0.0
1566, 0.0, -24.0
1606, 8.0, -24.0
1626, 24.0, -24.0
2001, 0., 0.0
2041, 8., 0.0

```
**
**
*NSET, NSET=N81
81
*NSET, NSET=N101
101
*NFILL, NSET=TOPCLEAR,BIAS=0.909091
N81,N101,20,1
*NSET, NSET=N142
142
*NSET, NSET=N162
162
*NFILL, NSET=TOPRIGHT,BIAS=0.909091
N142,N162,20,1
*NGEN, NSET=TOPLEFT
102, 142
*NSET,  NSET=TOP
TOPRIGHT, TOPLEFT
*NSET,  NSET=M, GENERATE
42, 81, 1
*NSET,  NSET=MOUND
M,102
*NSET, NSET=N1606
1606
*NSET, NSET=N1626
1626
*NFILL, NSET=BOTTOMCLEAR,BIAS=0.909091
N1606,N1626,20,1
*NGEN, NSET=BOTTOMCOVERED
```

```
1566,1606
*NSET,  NSET=BOTTOM
BOTTOMCLEAR, BOTTOMCOVERED
*NFILL, NSET=ORIGINALSOIL,BIAS=0.909091
TOP,BOTTOM,24,61
*NSET,  NSET=LEFT, GENERATE
102, 1566, 61
*NSET,  NSET=RIGHT, GENERATE
101, 1626, 61
*NGEN, NSET=FOUNDATION
2001,2041
**
**
*ELEMENT, TYPE=CPE3
41, 102, 103, 42
*ELEMENT, TYPE=CPE4
42, 42,103, 104, 43
101, 102, 163, 164,103
*ELGEN, ELSET=ORIGINALSOIL
101, 60, 1, 1, 24, 61,60
*ELGEN, ELSET=S
42, 59, 1, 1, 1
*ELSET, ELSET=MOUNDSOIL
S,41
*ELSET, ELSET=SOILMASS
MOUNDSOIL,ORIGINALSOIL
*ELEMENT, TYPE=B21
2001, 2001, 2002
*ELGEN, ELSET=BEAM
```

```
2001,40,1,1
**
**
*SOLID SECTION, ELSET=SOILMASS, MATERIAL=SOIL
*MATERIAL, NAME=SOIL
*ELASTIC
15000., .3
*DENSITY
18,
*BEAM GENERAL SECTION, ELSET=BEAM, DENSITY=25, SECTION=RECT
1.0, 0.3795447
0,0,-1
20000000., 8695652.
**
*INITIAL CONDITIONS, TYPE=STRESS, GEOSTATIC
SOILMASS, 0.0, 0.0, -12.0, 216, .42
*BOUNDARY
LEFT,1,1,0.
RIGHT,1,1,0.
BOTTOM,2,2,0.
2001,1,1,0.
2001,6,6,0.
**
**
*SURFACE, NAME=MOUNDSOIL, TYPE=ELEMENT
MOUNDSOIL,
*SURFACE, NAME=BEAM,TYPE=ELEMENT
BEAM, SNEG
*CONTACT PAIR, INTERACTION=GRATING
```

```
MOUNDSOIL, BEAM
*SURFACE INTERACTION, NAME=GRATING
*FRICTION,SLIP TOLERANCE=0.005, EXPONENTIAL DECAY
0.4,0.1,4.
*SURFACE BEHAVIOR, PRESSURE-OVERCLOSURE=HARD
**
**
*STEP,NLGEOM=YES, NAME=UNCOVERED
*STATIC
*DLOAD
BEAM,PY , -7.5
**
*NODE PRINT, NSET= MOUND
 U
*NODE PRINT, NSET= FOUNDATION
 U
*EL PRINT, ELSET=BEAM, POSITION=AVERAGED AT NODES
 SF, SM1
*END STEP
```

VITA

Remon I. Abdelmalak received his B.S. degree from the Department of Civil Engineering at El-Minia University, El-Minia, Egypt in 1994 and his M.S. degree in geotechnical engineering at El-Minia University, El-Minia, Egypt in 2000. He worked as a lecturer assistant in the Department of Civil Engineering at El-Minia University, El-Minia, Egypt as a geotechnical engineer for seven years since 1995.

In 2004, he started his Ph.D. studies in the Department of Civil Engineering at Texas A&M University under the supervision of Dr. Jean-Louis Briaud. He worked as a research assistant in the Civil Engineering Department and received his degree in December 2007.

Remon is a citizen of Egypt. His mailing address is:

6100 Hillcroft Ave.
P.O. Box 740010
Houston, Texas 77274